CO_2-RESPONSIVE DRAW AGENTS FOR FORWARD OSMOSIS

by

Sarah N. Ellis

A thesis submitted to the Department of Chemistry

in conformity with the requirements for

the degree of Doctor of Philosophy

Queen's University

Kingston, Ontario, Canada

(September, 2021)

Abstract

Water purification is essential for modern human life. Without it we could not produce clean water, process wastewater or concentrate desired products. Unfortunately, standard water purification techniques are energy intensive, especially for concentrated feeds. Forward osmosis (FO) is a promising filtration method, with the ability to process concentrated feeds at lower energy costs than conventional methods.

FO operates by placing a concentrated “draw solution” opposite the water to be filtered (the feed), separated by a semipermeable membrane. The osmotic pressure (π) difference across the membrane causes water to flow from the feed to the draw solution. After filtration is complete the draw solute is removed, leaving behind clean water. While the initial filtration requires minimal energy, removing the draw solute from the clean water after filtration can be energy intensive due to the draw solutes’ high π. The efficiency of FO hinges on the nature of the draw solute.

An ideal draw solute must possess two seemingly contradictory properties: a high π state for efficient filtration and a low π state for easy draw solute removal post-filtration. CO_2-responsive materials are attractive draw solutes as they possess a high π under CO_2 (π_{CO2}) and a low π under air (π_{air}). The most successful draw solute reported to date, trimethylamine (TMA), exerts a very high π_{CO2} but is also flammable, malodorous and can cross the membrane.

This work investigated new CO_2-responsive materials which could be safe alternatives to TMA. Diverse CO_2-responsive materials were considered, including polymers, hydrogels and magnetic particles. In each case, materials were designed and synthesized, then their performance as a draw solute was assessed by measuring their π_{CO2} and π_{air} or their flux and recovery. Fluid draw agents outperformed solid draw agents due to improved mass transfer, and are easier to implement industrially.

Among all the draw solute studied, soluble poly(N,N-dimethylallylamine) (PDMAAm) showed the most promise due to its high π_{CO2} and low π_{air}. The use of PDMAAm's dual CO_2- and thermo-responsive character was found to facilitate its separation from water after filtration. Future work will study the performance of PDMAAm on larger scales for industrial use.

Statement to the Public

Water filtration is essential for modern human life. To avoid catastrophic damage to the environment and human health, water must be purified before it is used and before it is returned to the environment. Water filtration is used to produce potable water, process wastewater, and concentrate desired products in diverse industries (e.g., orange juice). However, conventional water purification methods such as distillation can have prohibitively high energy costs, especially if the solution to be filtered (the "feed") is concentrated.

Forward osmosis (FO) is a promising alterative water filtration technology which shows potential for low-energy treatment of concentrated feeds. FO is centered around osmosis, the natural movement of water from an area of low solute concentration through a semi-permeable membrane to an area of high solute concentration (e.g., the movement of water from the surface of skin into the body). In FO, water is extracted from the feed by osmosis; an extremely concentrated solution (the "draw solution") and the feed are separated by a semi-permeable membrane. The draw solution contains a high concentration of a "draw solute". Water flows from the feed (low concentration) through the membrane to the draw solution (high concentration) without the application of any energy, resulting in a concentrated feed and a diluted draw solution (Figure 1). After osmosis, the draw solute is separated from the water that passed through the membrane, resulting in a concentrated draw solution which can be recycled, and clean water. The nature of the draw solute is consequently very important to FO. A successful draw solute must be highly efficient at pulling water from the feed while remaining easily removed from water post-filtration. Unfortunately, conventional materials usually only possess one of these assets.

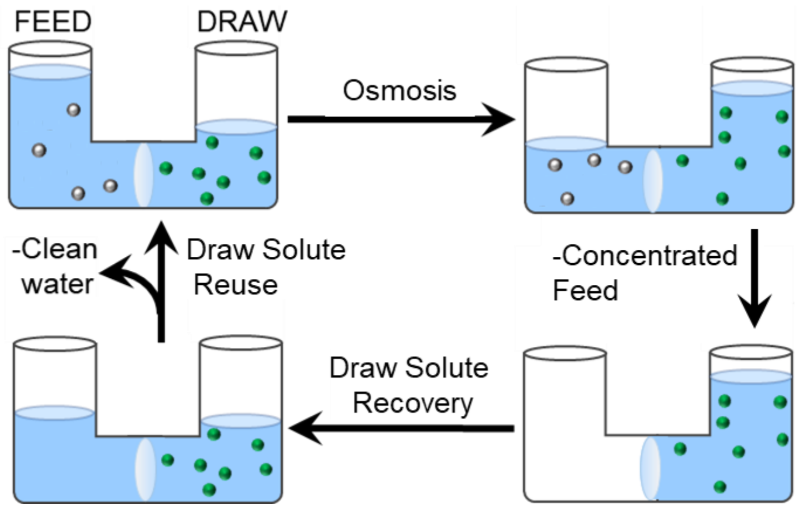

Figure 1. The FO process. Grey dots represent a dissolved material in the feed, while the green dots represent the draw solute.

While most materials have one fixed set of properties, "stimuli-responsive" materials can possess a different set of properties based on the application of a stimulus. Examples of stimuli-responsive materials include the dyes on thermochromic mugs which change colour in response to heat, and the compounds in plant stems which move flowers towards the sun in response to sunlight. "CO_2-responsive" draw solutes are highly water loving (making them excellent at filtration) in the presence of CO_2 but are less water loving (making them easily removed) under air (Figure 2). CO_2 can be added to these materials in the same way soda is carbonated. The CO_2 can be removed from these materials by applying mild heat. Consequently, CO_2-responsive materials are promising draw solutes. The most promising CO_2-responsive draw solute to date is flammable and possesses a strong odour and therefore cannot be used if the final product will be consumed by humans (e.g., drinking water or concentrated juice).

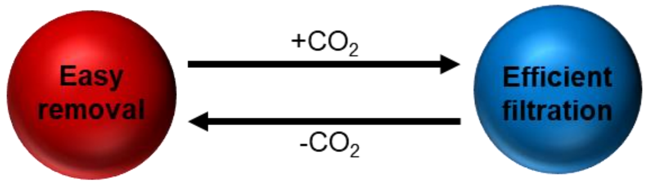

Figure 2. The two states of CO_2-responsive draw solutes

This work investigated a new generation of CO_2-respnsonive draw solutes which are less flammable and have no odour. A variety of CO_2-responsive materials were designed, synthesized, and tested for their potential as draw solutes. Diverse structures were considered including CO_2-repsonsive materials in long chains (polymers), in 3D networks (gels) and bound to magnetic particles. Several promising candidates were identified, which will be tested on larger scales in the future.

Acknowledgements

I have been extremely fortunate to work under the supervision of two stellar professors, Dr. Philip Jessop and Dr. Michael Cunningham. I cannot begin to express my thanks for the support and advice they have given me, as well as the endless hours they have dedicated to editing my work. You have both taught me so much, not only academically, but though your patience, kindness, and hard work.

I thank Dr. Mary Anne White for the faith she had in me as an undergraduate. I will never stop being appreciative for the guidance you gave me over the years that lead me to where I am today.

I thank Dr. Mark Obrovac and Dr. Tim Hatchard for the opportunities they gave at the very beginning of my career and for giving me a such a good foundation as a scientist and an employee.

I thank the many members of the Jessop lab who have helped me over the course of my time in grad school, especially Dr. Anna Riabtseva. I particularly thank Jaddie Ho, Lily Ellis and Devni Elamaldeniya for helping me during the writing process.

I thank the undergraduate students who have worked with me over the years: Sam Hargreaves, Anjini Datt, Dom Champagne-Hartley, McKenzie Madden and Megan Landsborough.

I thank the individuals who assisted me with equipment, including Dr. Sauriol (solid state NMR), Dr. Schatte (XRD), Dr. McEleney (electron microscopy) and the long-suffering Dr. Ying Zang (DSC, TGA, GPC).

I am very grateful to NSERC, the Government of Ontario, the Walter Sumner Foundation, and Queen's University, as well as Marie Mottashed and the family of William Neish for the financial assistance they provided through fellowships.

I thank GreenCentre Canada, Forward Water Technologies, Hatch, and Utilities Kingston for their material and intellectual support.

"More than cleverness we need kindness and gentleness."

-Charlie Chaplin

Statement of Originality

I hereby certify that all the work described within this thesis is the original work of the author. Any published (or unpublished) ideas and/or techniques from the work of others are fully acknowledged in accordance with the standard referencing practices. The contributions from collaborators are clearly noted below. All the work was performed under the supervision of Drs. Philip Jessop and Michael Cunningham.

Table 1.1 was developed in collaboration with Dr. Philip Jessop and McKenzie Madden and was first presented in McKenzie's B.Sc. honour's thesis.

In Chapter 2, the osmotic pressure measurements of PDMAAm at 30 and 35 wt. %, and the GPC measurements of PDMAAm were conducted by Dr. Anna Riabtseva, in addition to all viscosity measurements. The pK_{aH} measurements of l-PMEI, b-PMEI, and PDMAAm were conducted by Dom Champagne-Hartley.

In Chapter 3, all solid-state NMR spectra were obtained by Dr. Francoise Sauriol.

In Chapter 4, all TEM images were obtained by Dr. Kevin McEleney and the XRD spectrum was obtained by Dr. Gabriele Schatte.

Portions of this thesis have previously been published:

Section 1.2, 1.3.4.2, and Chapter 2 are based off of the following paper: S.N. Ellis, A. Riabtseva, R.R. Dykeman, S. Hargreaves, T. Robert, P. Champagne, M.F. Cunningham & P.G. Jessop, Nitrogen rich CO_2-responsive polymers as forward osmosis draw solutes, *Ind. Eng. Chem. Res.* **2019**. 58(50). 22579–2258. doi:10.1021/acs.iecr.9b04858.

Chapter 3 is based off the following paper: S.N. Ellis, M.F. Cunningham, & P.G. Jessop, A forward osmosis hydrogel draw agent that responds to both heat and CO_2, *Desal*. **2021**. 510 115074. https://doi.org/10.1016/J.DESAL.2021.115074.

Appendix B contains portions from the following patent: P.G. Jessop, M.F. Cunningham, P. Champagne, S.N. Ellis, R.R. Dykeman, C. Honeyman, A. Holland, T. Robert, B.P. Mudraboyina, Forming a Treated Switchable Polymer and Use Thereof in a Forward Osmosis System, 62/722,275, **2018**.

Sarah Ellis, June 2021

Table of Contents

Abstract ii
Statement to the Public iv
Acknowledgements vii
Statement of Originality ix
List of Figures xv
List of Tables xix
List of Abbreviations and Symbols xx
Chapter 1 Introduction 1
1.1 CO_2-Responsive Materials 1
1.1.1 Stimuli-Responsive Materials 1
1.1.2 The Chemistry of CO_2-Responsivity 2
1.1.3 CO_2-Responsive Polymers 6
1.2 Osmotic Pressure 7
1.2.1 Osmotic Pressure and Polymer Solutions 7
1.2.2 Measuring Osmotic Pressure 10
1.3 Forward Osmosis 13
1.3.1 Applications of Water Filtration 13
1.3.2 Conventional Methods 13
1.3.3 Forward Osmosis 17
1.3.3.1 Concentration Polarization 20
1.3.3.2 Membrane Fouling 21
1.3.3.3 Reverse Solute Flux 23
1.3.4 Draw Solutes 24
1.3.4.1 Small Molecule Non-Stimuli Responsive Draw Solutes 26
1.3.4.2 CO_2-Responsive Draw Agents 28
1.3.4.3 Polymers 33
1.3.4.4 Hydrogels 37
1.3.4.5 Magnetic Particles 43
1.4 Objectives 50
Chapter 2 CO_2-Responsive Polymers 51
2.1 Introduction 51

2.2 Materials and Methods........53
2.2.1 Materials........53
2.2.2 Characterization........54
2.2.3 Synthesis of CO_2-responsive polymers........56
2.2.3.1 l-PMEI........56
2.2.3.2 b-PMEI........58
2.2.3.3 PDMAAm........58
2.2.3.4 PDMAEMA........60
2.2.3.5 PDEAEMA........60
2.2.3.6 PDMAPMAm........60
2.3 Osmotic Pressure of CO_2-Responsive Polymers........61
2.3.1 Osmotic Pressures of Tertiary vs Primary and Secondary Amines........61
2.3.2 Effect of Oligomers on Osmotic Pressure........63
2.3.3 Osmotic Pressures of CO_2-Responsive Polymeric Draw Solutions........64
2.3.3.1 l-PMEI........64
2.3.3.2 b-PMEI........66
2.3.3.3 PDMAAm........67
2.3.3.4 Contribution of the Polymer Chain to the Total Osmotic Pressure........71
2.4 Basicity and Osmotic Pressure........73
2.5 Osmotic Pressure under CO_2 of Polymeric Draw Solutes at Reduced Temperatures........75
2.6 Conclusions........76
Chapter 3 CO_2- and Thermo-Responsive Gels........77
3.1 Introduction........77
3.2 Materials and Methods........78
3.2.1 Materials........78
3.2.2 Methods........79
3.2.2.1 Characterization........79
3.2.2.2 Synthesis of PDMAAm Gel........80
3.2.2.3 Procedure for FO........81
3.2.2.4 Procedure for Swelling Ratio........81
3.3 Results and Discussion........83
3.3.1 Gel Synthesis and Characterization........83
3.3.2 Responsivity........85
3.3.2.1 Thermo-Response........85

3.3.2.2 CO_2-Response ... 86
3.3.2.3 Combined CO_2- and Thermo-Response ... 88
3.3.3 Exploring the Relationship Between CO_2- and Thermo-responsiveness in Hydrogels 89
3.3.4 Performance of g-PDMAAm as a FO Draw Agent ... 92
3.4 Conclusions ... 96
Chapter 4 CO_2-Responsive Magnetic Particles ... 98
4.1 Introduction ... 98
4.2 Materials and Methods ... 100
4.2.1 Materials ... 100
4.2.2 Characterization ... 102
4.2.2.1 Polymers ... 102
4.2.2.2 Magnetite Nanoparticles ... 102
4.2.2.3 PDMAEMA-Magnetite Particles ... 103
4.2.2.4 Flux Characterization ... 103
4.2.3 Synthesis of Magnetite Nanoparticles ... 104
4.2.4 Synthesis of PDMAEMA-MNP Microgels ... 104
4.2.4.1 Synthesis of 2-Aminoethylmethacrylate Hydrochloride ... 104
4.2.4.2 Synthesis of P(DMAEMA-AEMA) ... 105
4.2.4.3 Synthesis of APTS functionalized magnetite ... 106
4.2.4.4 Synthesis of PDMAEMA-MNP Microgels ... 106
4.2.5 Synthesis of PDMAEMA-Functionalized MNP ... 107
4.2.5.1 Synthesis of ATRP Initiator ... 107
4.2.5.2 Grafting ATRP Initiator to Magnetite Nanoparticles ... 108
4.2.5.3 SI-Polymerization of DMAEMA from Magnetite Nanoparticles ... 108
4.3 Results and Discussion ... 108
4.3.1 Microgel Characterization ... 108
4.3.2 Microgel Stimuli-Responsivity ... 114
4.3.3 Nanoparticle Characterization ... 117
4.3.4 FO Performance ... 119
4.3.5 Critique of Insoluble Draw Agents ... 121
4.4 Conclusion ... 123
Chapter 5 Conclusions and Recommendations ... 124
5.1 Conclusions ... 124
5.2 Recommendations for Future Areas of Study ... 126

5.2.1 Soluble polymers 126
5.2.2 Gels 128
5.2.3 Magnetic Particles.. 128
References.. 130
Appendix A Instructions for Performing a DMO Measurement 166
Appendix B Soluble Polymer Supplementary Information 178
Appendix C Hydrogel Supplementary Information... 186
Appendix D Magnetic Particle Supplementary Information 194
Appendix E Alternative Applications of CO_2-Responsive Magnetic Microgels......................... 201

List of Figures

Figure 1.1 Equilibrium, and abundance with pH, of carbonate species in water under 1 bar of CO_2. The dashed line represents the pH of water under 1 bar of CO_2 at 25 °C. 3

Figure 1.2 CO_2-responsivity of different functional groups. Based on figure 1 from reference 11 with permission. pK_{aH} (pK_a of protonated amine) values obtained from reference 12,13, for R^{1-5} = alkyl. 4

Figure 1.3 The % protonation of organic bases with various pK_{aH} values vs. concentration in water in the absence of at 25 °C. Reproduced with permission from reference 7. 6

Figure 1.4 Structures and abbreviations of common CO_2-responsive polymers. Reproduced with permission from reference 26. 7

Figure 1.5 Images of membrane osmometers: a) an endosmometer, a predecessor to the modern DMO, and b) a modern DMO. Image a) was reproduced from reference 48. This image is in the public domain. 12

Figure 1.6 Relative energy consumption of common separation techniques. Reproduced from reference 58; this figure is in the public domain. 14

Figure 1.7 Water flux between solutions of different potential energies. The grey circles represent a contaminating solute while the green circles represent a draw solute. Draw solute recovery may be accomplished by diverse techniques (e.g., RO, decantation, magnetic separation). 18

Figure 1.8 Illustrations of concentration polarization. a) external concentration polarization with a symmetric membrane. b) active layer of asymmetric membrane facing the draw solution (PRO mode) c) active layer of asymmetric membrane facing the feed solution (FO mode). The curve lines illustrated the π change of the feed (F) and draw (D) solutions from the bulk (b) to the membrane surface (m). π_i denotes the effective osmotic pressure of the feed or draw after concentration polarization, and $\Delta\pi$ is the effective difference in osmotic pressure. This figure was reproduced with permission from reference 42. 21

Figure 1.9 Illustration of swelling ratio (SR) and water recovery (%R) used to describe draw agents. 38

Figure 1.10 Schematic of the magnetic field control FO module designed by Na et al. 2014 to maximize the π of the draw at the membrane surface and prevent magnetite draw agents from fouling the FO membrane. Reproduced with permission from reference 110. 45

Figure 2.1 The FO-UF process with CO_2-switchable polymers. The red lines represent a CO_2-switchable polymer ( ), the filled circles represent bicarbonate anions ( ), and the hollow circles ( ) represent the contaminating solutes in the feed. 51

Figure 2.2 Structures of soluble CO_2-switchable polymers studied in this work 53

Figure 2.3 Synthetic pathway for l-PMEI. 56

Figure 2.4 Synthetic pathway for b-PMEI. 58

Figure 2.5 Synthetic pathway for the synthesis of PDMAAm. 58

Figure 2.6 The effect of carbamate vs bicarbonate formation on the number of species in solution. 62

Figure 2.7 Osmotic pressures (gauge) in air (blue) and CO2 (red) for each of the tertiary amine polymer solutions in deionized water tested: (a) l-PMEI, (b) b-PMEI and (c) PDMAAm. The concentration (g/g) refers to the concentration of solutions prior to carbonation. The dotted trendlines are fitted 3rd order polynomial curves. 65

Figure 2.8 Dependence of kinematic viscosity on the concentration of aqueous solutions of PDMAAm under air or CO_2 at 25 °C. 69

Figure 2.9 a) Current and b) alternative synthetic pathway for PDMAAm. 70

Figure 2.10 Effect of CO_2 pressure on the % protonation of PDMAAm as a function of concentration. 71

Figure 2.11 Measured π_{CO2} (gauge pressure, red) and the concentration of bicarbonate (blue), for l-PMEI (solid lines) and PDMAAm (dashed lines). 72

Figure 2.12 Effect of pK_{aH} on the % protonation of an amine as a function of concentration. Assuming a molecular weight of 100 g/n, and 1 atm of CO_2. 74

Figure 3.1 Synthetic pathway for the crosslinking of g-PDMAAm. 84

Figure 3.2 Effect of temperature and atmosphere on the SR of g-PDMAAm. Gels were swollen in water under various atmospheres (air or CO_2 at 1 bar of absolute pressure) and temperatures (20-60 °C). To guide the eye, the CO_2 points are connected by a linear trendline while the air points are connected by a 3rd order polynominal curve. 87

Figure 3.3 Swelling ratios of g-PDMAAm obtained in water (under an atmosphere of air or water) or air (at 20 or 60 °C). 89

Figure 3.4 π_{air} (gauge) of soluble polymer solutions in water under air as a function of temperature for non-thermo-responsive PDADMAC (20 wt.%) and thermo-responsive soluble PDMAAm (17 wt.%, T_{cp}= ~28 °C) and PNIPAM (20 wt.%, LCST= 31-33 °C [227]) 92

Figure 3.5 FO performance of g-PDMAAm: a) initial flux with varying feed and draw solution concentrations; b) representative curve of flux and draw agent concentration vs time (30 wt.% g-PDMAAm draw vs. 3.5 % NaCl feed, red solid diamonds). The net concentration of the draw agent (blue filled circles), as well as the final concentration of the draw agent at the membrane surface (blue hollow circles) are shown... 94

Figure 3.6 Performance of g-PDMAAm draw agents over several cycles: a) swelling ratio and b) initial flux (hollow bar) and water recovery (solid bar) over several cycles (30 wt.% g-PDMAAm vs 1.75 wt.% NaCl). The line in a) was added to guide the eye. 96

Figure 4.1 Illustrations of the CO_2-responsive magnetic particles explored in this chapter: a) PDMAEMA microgels with embedded MNP and b) PDMAEMA functionalized MNP. Illustrations are not to scale. 100

Figure 4.2 Synthetic procedure for PDMAEMA-MNP microgels: a) grafting of APTS to MNP, b) synthesis of P(DMAEMA-AEMA), c) crosslinking reaction, d) illustration of microgel formation. 110

Figure 4.3 Characterization of PDMAEMA-MNP microgels and their precursors: a) IR spectrum and b) TGA thermogram.. 112

Figure 4.4 TGA thermograph of CO_2-responsive microgel particles before and after acid treatment. 114

Figure 4.5 Optical microscope images of PDMAEMA-MNP microgels in water a) under CO_2 at 20 °C, b) under air at 20°C and c) under air after exposure to 60 °C. 116

Figure 4.6 Size distribution of microgel particles in aqueous dispersions observed by optical microscopy, under CO_2 at 20 °C, after successive cycles (0-5) of carbonation (under an atmosphere of CO_2 at 20 °C) and decarbonation (under an atmosphere of air at 60 °C)............. 117

Figure 4.7 Synthesis of PDMAEMA-Fe_3O_4 nanoparticles 118

Figure 4.8 Characterization of PDMAEMA modified nanoparticles and their precursors: a) IR spectrum and b) TGA thermograms... 119

Figure 4.9 Radius of solid draw agents and osmotic pressure. Particles in closed packed configuration are illustrated by black lines. The regions of water affected by the particle surface are illustrated by dotted red lines. a) When particle size is small, the interparticle distance is small; all the bulk water is affected by the particles. b) When particles size increases, the volume of water between the particles increases; particles can no longer affect all the bulk water. Water unaffected by the particles is highlighted in yellow. 122

List of Tables

Table 1.1 Characteristics of VPO, FPO and DMO. 11

Table 1.2 Osmotic pressures of common water filtration feeds.* 16

Table 1.3 Pressure driven membrane separation techniques. 17

Table 1.4 Properties of classes of forward osmosis draw solutes. 25

Table 1.5 Properties of selected small molecule non-stimuli responsive FO draw solutes.† 27

Table 1.6 Properties of selected CO_2-responsive FO draw solutes.† 31

Table 1.7 Properties of selected polymeric FO draw solutes.† 35

Table 1.8 Properties of selected hydrogel FO draw agents.† 41

Table 1.9 Properties of selected FO magnetic particle draw agents.† 46

Table 2.1 Osmotic pressures under CO_2 of tertiary vs. primary/secondary amines polymers at 20 wt% loading in water. 62

Table 2.2 Effect of dialysis tubing MWCO on osmotic pressure of PDMAAm.† 63

Table 2.3 Calculated log P values† of studied polymers in their neutral form. 68

Table 2.4 Comparison of π_{CO2}^* of PtBAEMA and PDEAEMA. 75

Table 2.5 π_{CO2}^* of CO_2-responsive polymers at 20 wt.% with varying temperature. 76

Table 3.1 Comparison of selected CO_2- and thermo-responsive hydrogel draw agents from the literature. 95

List of Abbreviations and Symbols

%R	% water recovered
A	surface area of membrane
AAm	acrylamide
AEMA	aminoethylmethylmethacrylate
AIBN	2,2′-azobis(2-methylpropionitrile)
APTS	(3-Aminopropyl)triethoxysilane
ARGET	activators regenerated by electron transfer
ATR	attenuated total reflectance
ATRP	Atom transfer radical polymerization
BHT	butylated hydroxytoluene
BIBB	α-bromoisobutyryl bromide
b-PEI	branched poly(ethylenimine)
b-PMEI	branched poly(N-methylethylenimine)
C	concentration (molar)
c	concentration (weight/volume)
CHP	cyclohexylpiperidine
CTA	cellulose triacetate
d	density

Đ	dispersity
DEAEMA	2-(N,N-diethylamino)ethyl methacrylate
DI	deionized
DMA	N,N-dimethylacrylamide
DMAEMA	2-(N,N-dimethylamino)ethyl methacrylate
DMAPMAm	2-(N,N-dimethylamino)propyl methacrylamide
DMCA	N,N-dimethylcyclohexylamine
DMO	direct membrane osmometry
dn/dc	refractive index increment
DS	draw solution
DSC	differential scanning calorimetry
ECP	external concentration polarization
FO	forward osmosis
FPO	freezing point osmometry
FS	feed solution
FT	Fourier-transform
FTIR	Fourier-transform infrared spectroscopy
GPC	gel permeation chromatography
g-PDMAAm	poly(N,N-dimethylallylamine) gel
HMTETA	1,1,4,7,10,10-Hexamethyltriethylenetetramine
HPLC	high pressure liquid chromatography

ICP	internal concentration polarization
ICP-OES	inductively coupled plasma-optical emission spectrometry
IR	infrared
J_s	flux of solutes
J_w	flux of water
K^*_{a1}	combined K_a of CO_2 and carbonic acid
K_a	acid dissociation constant
K_{aH}	acid dissociation constant of the conjugate acid
K_H	Henry's constant
K_{hydr}	equilibrium constant of CO_2 hydration to carbonic acid
K_w	Auto-dissociation constant of water
LCST	lower critical solution temperature
LMH	L/m^2h
l-PEI	linear poly(ethylenimine)
l-PMEI	linear poly(N-methylethyleneimine)
MD	membrane distillation
MEA	monoethanolamine
MEMA	N-morpholine ethyl methacrylate
MF	microfiltration
M_n	molecular mass number
MNP	magnetic nanoparticle

M_w	molecular mass weight
MWCO	molecular weight cut off
N	mole fraction of solute
n	number of monomer units in chain
NF	nanofiltration
NIPAM	N-isopropylacrylamide
NMR	nuclear magnetic resonance
P	1-octanol/water partition coefficient
P(DMAEMA-AEMA)	poly((2-(N,N-dimethylamino)ethyl methacrylate)-2-aminoethyl methacrylate)
PAAm	poly(allylamine)
PDADMAC	poly(N,N-dimethylallylammoium chloride)
PDEAEMA	poly(2-(N,N-diethylamino)ethyl methacrylate)
PDMAAm	poly(N,N-dimethylallylamine)
PDMAEMA	poly(2-(N,N-dimethylamino)ethyl methacrylate)
PDMAPMAm	poly(2-(N,N-dimethylamino)propyl methacrylamide)
PEBMP	2-(phosphonooxy)ethyl 2-bromo-2-methylpropanoate
PEG	poly(ethylene glycol)
PEGDA	poly(ethylene glycol diacrylate)
PEI	poly(ethyleneimine)
PMEMA	poly(N-morpholine ethyl methacrylate)

PMMA	poly(methyl methacrylate)
PNIPAM	poly(N-isopropylacrylamide)
ppm	parts per million
PRO	pressure retarded osmosis
PS	polystyrene
PSA	poly(sodium acrylate)
PSS	poly(sodium styrene-4-sulfonate)
PtBAEMA	poly(2-(N-tert-butylamino)ethyl methacrylate)
QSR	ratio of swelling ratios
R	ideal gas constant
r	particle radius
RO	reverse osmosis
RSF	reverse solute flux
RT	room temperature
SA	sodium acrylate
SDS	sodium docecylsulfate
SHS	switchable hydrophilicity solvent
SI	surface initiated
$Sn(EH)_2$	tin(II) 2-ethylhexanoate
SR	swelling ratio
T	temperature

t	time
TDS	total dissolved solids
TEM	Transmittance electron microscopy
TGA	thermogravimetric analysis
TMA	trimethylamine
trDDM	tert-dodecylmercaptan
UF	ultrafiltration
UV	Ultraviolet
V	volume of 1 mole of water
V_o	molar volume of solvent
VPO	vapour pressure osmometry
VPTT	volume phase transition temperature
V_w	volume of water
W_R	water released
wt.%	weight percent of solute divided by total weight of solution
W_{WG}	weight of water in the swollen gel
XRD	x-ray diffraction
α	compressibility of solvent
π	osmotic pressure
π_{air}	osmotic pressure of a solution under air

$\pi_{bicarbonate}$	contribution of bicarbonate ions to the osmotic pressure of the solution under 1 bar of CO_2
π_{CO2}	osmotic pressure of a solution under 1 bar of CO_2
$\pi_{polymer}$	contribution of polymer chains (not including counterions) to the total osmotic pressure of the solution
χ_{ps}	free energy of interaction parameter between polymer and solvent

Chapter 1

Introduction

1.1 CO_2-Responsive Materials

1.1.1 Stimuli-Responsive Materials

While the properties of most chemicals are fixed (or vary only slightly with temperature and pressure), “stimuli-responsive” materials exhibit a wide variation of properties and performance based on the application of a trigger. One material can perform multiple tasks or exhibit different properties in different environments, potentially leading to lower energy consumption and material usage. Stimuli-responsive materials have been explored for use in diverse fields, including biomimetic materials, sensors, coatings and surfaces, pharmaceuticals, and chemical separations [1–3]. For example, drug delivery systems have been designed to release a drug from a stimuli-responsive polymer network based on the change in pH in a cell [4,5]. Common triggers include heat, pH, magnetism, light, humidity and electricity [1].

CO_2 has become a popular pH trigger in recent years, as it is a relatively safe, inexpensive, and abundant waste product which can be easily added to or removed from the system of interest [3]. While CO_2 in water is a weak acid, and therefore cannot cause a large change in pH like more conventional strong acids (e.g., hydrochloric acid), it has the unique advantage of being easily and completely removed from the system without leaving salts behind, which could build up over repeated switching cycles. CO_2-responsive materials can therefore be used multiple times without deterioration of properties or performance. In addition, the materials which respond to CO_2 are generally less expensive than those that respond to light, and less toxic than those that respond to voltage. CO_2-responsive systems are not restricted by the need to be conductive or transparent, like voltage- or light-triggered systems respectively. The use of CO_2 as a trigger therefore presents many advantages.

1.1.2 The Chemistry of CO_2-Responsivity

As a gas, CO_2 is relatively inert. Although CO_2 is non-polar, it exhibits significantly higher solubility in water compared to other non-polar gases such as N_2, CO or Ar [6]. This is due to the fact that when introduced into water, CO_2 forms a cascade of other species which increases its solubility in water [7]. The solubility of CO_2 in water is dependent on temperature and pressure and can be calculated given the Henry's law constant and the partial pressure (K_H = 0.342 M/MPa at 25 °C, 1 bar) [7,8]. The concentration of dissolved CO_2 increases with CO_2 pressure and decreases with temperature.

Upon exposure to water, CO_2 forms hydrates and carbonic acid. Carbonic acid is unstable at 25 °C (K_{hydr} = 0.0017 (unitless) at 25 °C, 1 bar), so CO_2 in water is predominantly in the form of hydrates [9]. Both hydrated CO_2 and carbonic acid are Brønsted acids which can dissociate in water to form bicarbonate; as it is difficult to separate the interactions of hydrated CO_2 and carbonic acid, a combined equilibrium constant is used (pK^*_{a1} = 6.36 at 25 °C, 1 bar) [7]. Note that this is significantly higher than that of carbonic acid, (pK_{a1} = 3.6), as hydrated CO_2 is a weaker acid. Bicarbonate can in turn dissociate to form carbonate (pK_{a2} = 10.3) (Figure 1.1). The concentration of CO_2 dissolved in pure water is approximately 0.03 M (25 °C, 1 bar), corresponding to a pH of approximately 3.94 (22 °C, 1 bar of CO_2) [10].

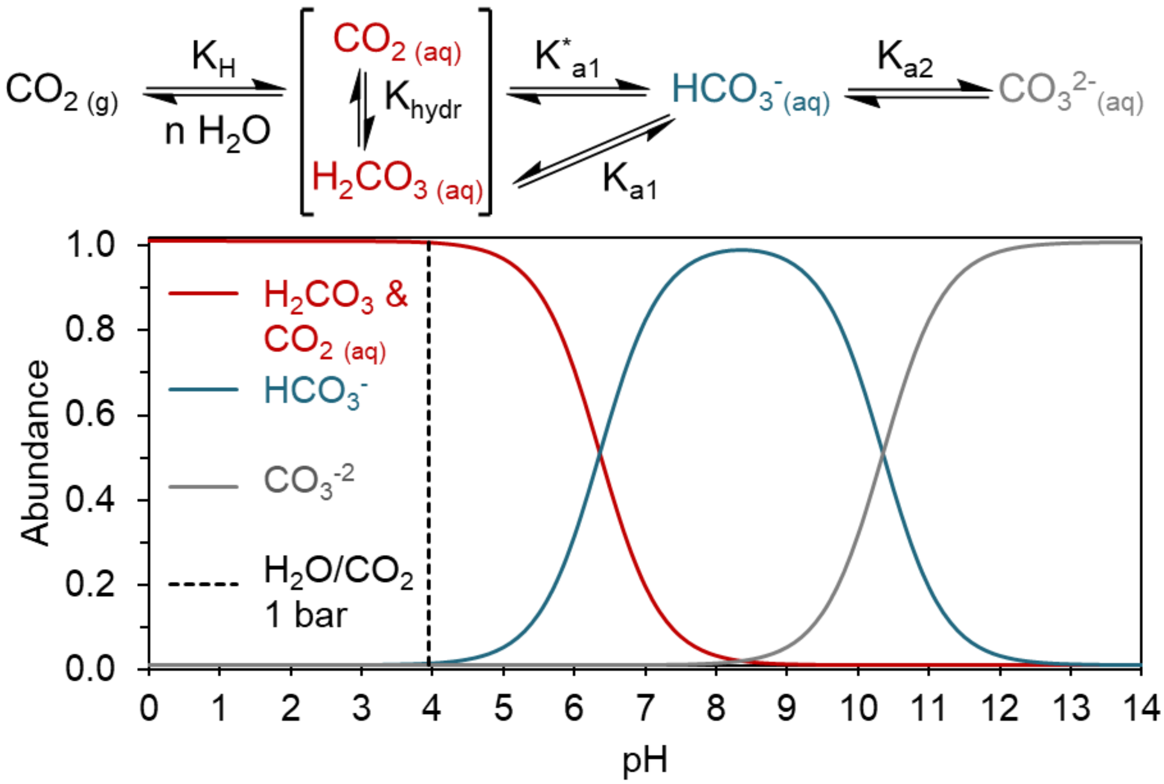

Figure 1.1 Equilibrium, and abundance with pH, of carbonate species in water under 1 bar of CO_2. The dashed line represents the pH of water under 1 bar of CO_2 at 25 °C.

Acidic hydrated CO_2 and carbonic acid can undergo acid-base reactions with bases. If the base is sufficiently weak, the reaction can be reversed by the removal of CO_2 (e.g., by applying heat or purging with a non-acidic gas) thereby returning the base to its original state. This is the basis for "CO_2-responsive" or "CO_2-switchable" chemistry. Switchable bases include amines, guanidines and amidines (Figure 1.2). Amines are generally preferred over guanidines and amidines as they are cheaper and more stable in water. Upon reaction with water, amines can form bicarbonate salts, carbamates, and carbamic acids. The nature and abundance of the product formed depends on the temperature and the structure of the base.

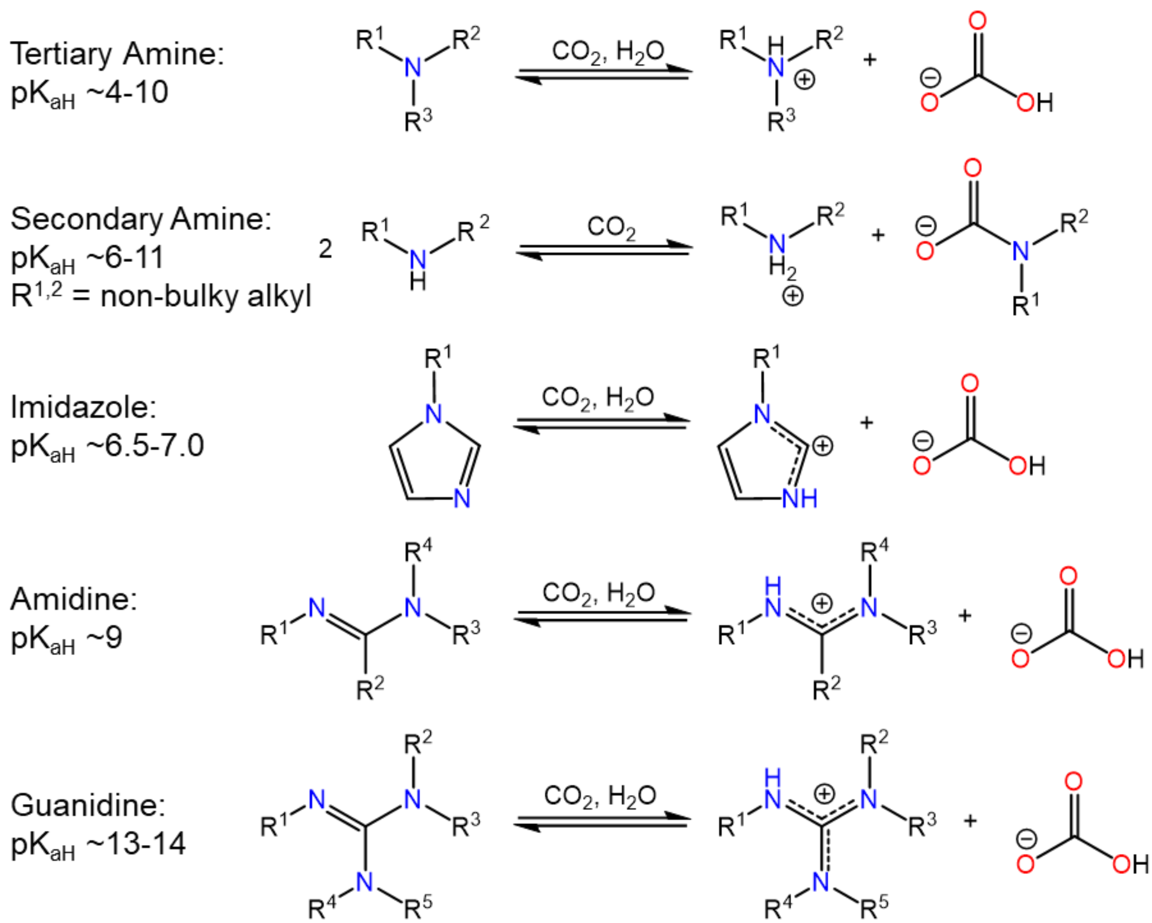

Figure 1.2 CO_2-responsivity of different functional groups. Based on figure 1 from reference 11 with permission. pK_{aH} (pK_a of protonated amine) values obtained from reference 12,13, for $R^{1\text{-}5}$ = alkyl.

Primary amines and sterically unhindered secondary amines form a mix of carbamates and bicarbonates in carbonated water, with carbamates being the major product. Bicarbonates are the major product when carbamate formation is disfavoured, in the case of tertiary amines or sterically hindered secondary amines. Carbamates are more thermodynamically stable than bicarbonates; they form more quickly but take more time and energy to revert to neutral amines than bicarbonates [14]. The preference for a carbamate or bicarbonate product depends on the application. Carbamates are used for applications requiring high thermal stability (e.g., carbon dioxide scrubbers and traps) [14–16], while bicarbonates are chosen for applications requiring faster reversals (e.g., paints [17]). In addition, carbamates and bicarbonates have different effects on the solution; upon carbonation of an aqueous solution of an amine, bicarbonate formation will increase the number of species in solution while carbamate formation will not. Tertiary amines are preferred for CO_2-responsive applications due to their easy reversal back to their uncharged state.

Tertiary amines in water can exhibit a dramatic swing in hydrophilicity and ionic strength between their neutral and carbonated states. CO_2-responsivity has been used to trigger changes in miscibility, solubility, viscosity, colour, fluorescence, osmotic pressure, stability of emulsions, and many more. It is generally desirable to have a large change of properties between air and CO_2 atmospheres, which requires a large change in the degree of protonation under air and CO_2. The percent protonation in carbonated water must be high (ideally >95%) and the percent protonation in uncarbonated water must be low (ideally <5%). The degree of protonation is dependent on the concentration or solubility of the neutral form in water, the presence of other species in solution, the partial pressure of CO_2 and temperature of the system as well as on the pK_{aH} (pK_a of the protonated amine) and concentration of the amine. The percent protonation decreases with concentration and increases with pK_{aH} (Figure 1.3). If the pK_{aH} of the amine is too high, the amine will be protonated even by uncarbonated water in air which decreases the magnitude of the property switch upon carbonation. As pK_{aH} increases, so does the energy required to decarbonate the amine. In addition, above pH 9 significant amounts of carbonate will be formed (Figure 1.1). If the pK_{aH} of the amine is too low (e.g., pyridines), the amine will not be protonated significantly by carbonated water, and the difference between the state under air and under CO_2 will be negligible. The preferred pK_{aH} values depend on the concentration; at high concentrations, the percent protonation is lower so higher pK_{aH} values are desired; at lower concentrations, the percent protonation is higher so lower pK_{aH} values are desired.

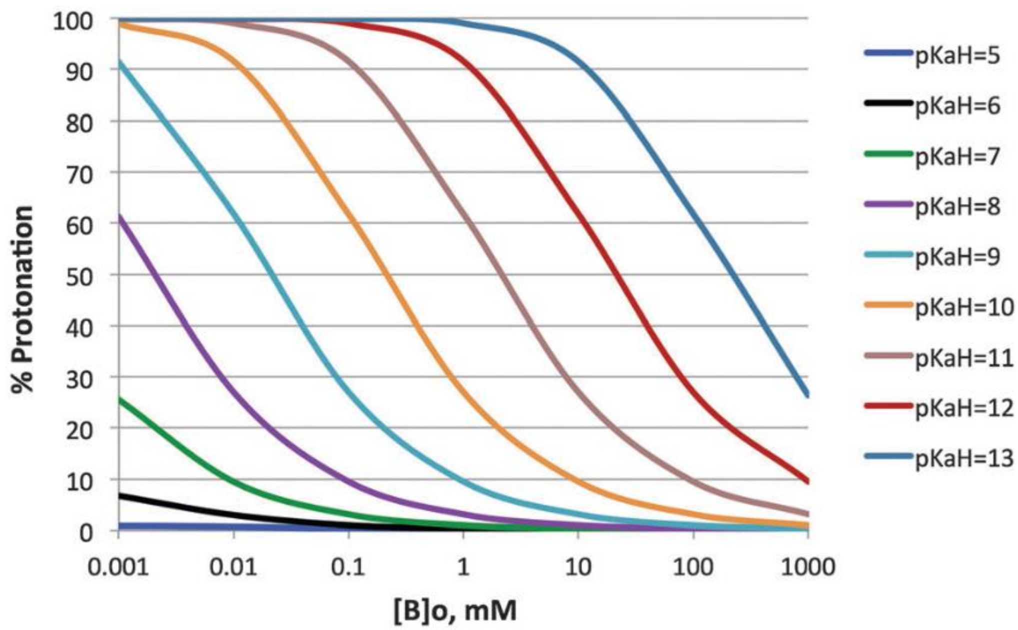

Figure 1.3 The % protonation of organic bases with various pK_{aH} values vs. concentration in water in the absence of at 25 °C. Reproduced with permission from reference 7.

1.1.3 CO_2-Responsive Polymers

The development of CO_2-switchable technology has led to research into a wide variety of potential applications of both academic and industrial interest including paints [17], latexes [18,19], Pickering emulsifiers [20,21], membranes [11,22], and drying agents [23]. Many of these technologies use CO_2-switchable polymers.

The magnitude of the change in properties can be enhanced by using diamines, or even polymeric amines. However, when using polymeric or polyamines, special consideration must be given to the pK_{aH} of the amine. If the carbon chain between two basic nitrogen atoms is small (less than 4 carbons) the pK_{aH} of an amine group will be reduced by the protonation of its neighbour. If the pK_{aH} values are significantly different, it is possible that not all of the amine groups in the molecule will be protonated by carbonated water [24]. While this effect is insignificant when the chain between the nitrogen atoms is longer than six carbons, the first and second pK_{aH} values of diamines will never be equal; the pK_{aH} values must differ by at least 0.6 units [24,25].

The complexity is further enhanced when considering polymers. Polymers exhibit a range of pK_{aH} values rather than one specific value. The average pK_{aH} of a polymeric amine is generally 1 pH unit less than that of its corresponding monomer [26].

There are relatively few commercially available CO_2-switchable polymers and monomers; the structures of the most commonly used CO_2-responsive polymers are shown in Figure 1.4. CO_2-switchable polymers have been made in the form of homopolymers and copolymers (e.g., statistical [27], block [28]), or various architectures (e.g., brush, star [29]), in diverse macroscopic structures (e.g., emulsions [18], gels [30]), and grafted to various surfaces (e.g., crystalline nanocellulose [21], metals [31], magnetite [32], silica [23]).

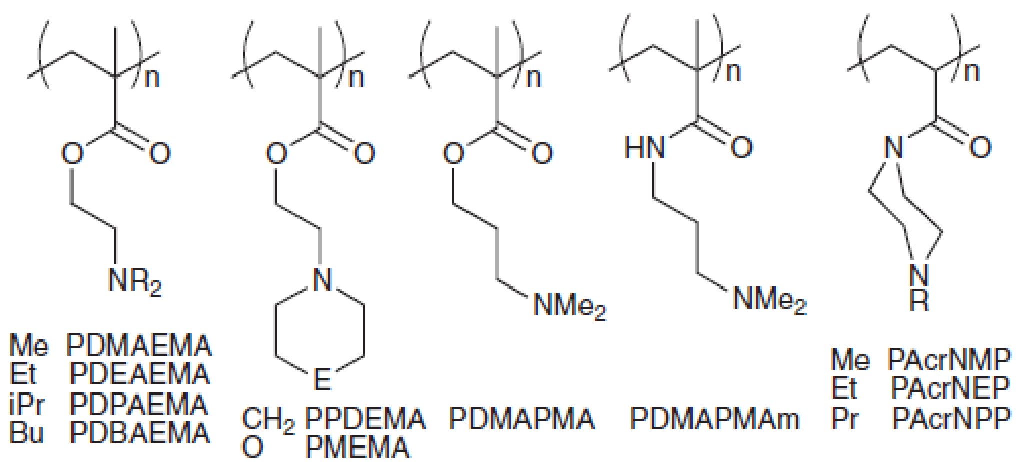

Figure 1.4 Structures and abbreviations of common CO_2-responsive polymers. Reproduced with permission from reference 26.

1.2 Osmotic Pressure

1.2.1 Osmotic Pressure and Polymer Solutions

Osmosis is the passive movement of water across a semipermeable membrane from a region of low solute concentration to a region of high solute concentration. Osmosis occurs because the water in the region of low solute concentration has a higher chemical potential than a region of high solute concentration. Water flows until the chemical potentials on either side of the membrane have equilibrated. Osmotic pressure (π) is the minimum pressure required to be applied to a solution to prevent osmosis. Swelling pressure (discussed in section 1.3.4.4) is akin to π, but for hydrogels rather than solutions. The π of an ideal solution can be calculated from the van't Hoff formula:

$$\pi = RTC \tag{1.1}$$

where R is the gas constant, T is the temperature and C is the total solute concentration. The van't Hoff equation assumes that π is directly proportional to the number of species in solution. However, this does not consider how different molecules interact with a given solvent or themselves in solution. For example, benzoic acid dimerizes in benzene, thereby reducing its interactions with the solvent and reducing the apparent number of species in solution [33]. Although equimolar NaCl and KCl solutions contain the same number of ions, the NaCl solution exerts a higher π than the KCl solution. This is because Na^+ has a higher charge density and has stronger interactions with water than K^+ [34,35]. Many equations have been developed in attempts to improve the van't Hoff formula.

The π of concentrated solutions can be calculated more accurately using the Lewis model:

$$\pi - \tfrac{1}{2}\alpha\pi^2 = -RT/V_o \ln(1-N) \tag{1.2}$$

where α is the compressibility of the solvent, V_o is the molar volume of the solvent, and N is the mole fraction of solute [36].

Changing the solute from a small molecule to a polymer adds another level of complexity. Concentrated polymer solutions are far from ideal. According to the van't Hoff equation, one polymer molecule would have the same π as one monomer molecule; however, this is not seen experimentally. The π of a polymer solution is a function of the number of chains present and the strength of the chain's interaction with water and itself. The π of polymer solutions can be calculated from the virial expansion:

$$\pi = RT\left(\frac{c}{M} + v\left(\frac{n}{M_w}\right)^2\left(\frac{c^2}{d^2}\right)\left(0.5 - \chi_{ps}\right) + v\left(\frac{n}{M_w}\right)^2\left(\frac{c^3}{3d^3}\right) + \cdots\right) \tag{1.3}$$

where M_w is the molecular weight of the monomeric unit, c is the polymer concentration (weight/volume), v is the volume of 1 mole of water, n is the number of monomer units in the chain, d is the density of the polymer, and χ_{ps} is a term relating to the strength of the interactions between the polymer and water [37]. However, given the number of terms in this equation and the difficulty in obtaining accurate values of each parameter, it is often not of practical use.

At a critical concentration, the polymer chains begin to overlap in solution. Polar aprotic polymers, such as those studied in this work, have more favourable polymer-water interactions than polymer-polymer interactions in solution. As the chains overlap at higher concentrations, they pull more water molecules to themselves to decrease the repulsion between chains. Therefore, π increases substantially above the critical concentration.

CO_2-responsive polymers are a further complication, as they are ionogens. Under air, the π of a CO_2-responsive polymer solution is also influenced by any hydroxide produced by reaction of the amine with water. If the polymer has an appropriate pK_{aH} value and the concentration is high, the percent protonation under air will be minimal [7], and the contribution from hydroxide can be neglected. The π_{air} is therefore expected to only be due to the neutral polymer chain:

$$\pi_{air} = \pi_{\text{uncharged polymer}} \tag{1.4}$$

Under CO_2, the π is affected by the bicarbonates in solution and the charged polymer chain:

$$\pi_{CO2} = \pi_{\text{bicarbonate}} + \pi_{\text{charged polymer}} \tag{1.5}$$

Both $\pi_{\text{bicarbonate}}$ and $\pi_{\text{charged polymer}}$ increase with concentration. The rate of $\pi_{\text{bicarbonate}}$ increase with concentration is expected to slow with increasing concentration, due to the decreasing percent protonation of the polymer. $\pi_{\text{charged polymer}}$ is expected to be greater than $\pi_{\text{uncharged polymer}}$ due to the polymer's increased hydrophilicity and hydrodynamic radius. In contrast to $\pi_{bicarbonate}$, $\pi_{charged\ polymer}$ increases with concentration following a polynomial function (see equation 1.3) and should increase substantially above the polymer's critical concentration.

1.2.2 Measuring Osmotic Pressure

In the literature, osmotic pressure is commonly obtained by freezing point osmometry (FPO), vapour pressure osmometry (VPO) and direct membrane osmometry (DMO), with FPO being the most frequently used technique. FPO and VPO do not measure π directly. Rather, FPO and VPO measure other colligative properties (freezing point and vapour pressure respectively) which are in turn used to calculate π via osmolality. Both methods rely on thermodynamic approximations which apply best to dilute, ideal solutions. Given that the solutions studied in this work are neither ideal nor dilute (and are consequently more difficult to model), the results obtained from these methods may be inaccurate [38]. In addition, these techniques may be unsuitable for carbonated solutions, as the concentration of CO_2 in solution changes when water is frozen or exposed to air. Furthermore, volatile amines can interact with the VPO sensor, making it difficult to obtain a reliable measurement [39]. π has also been determined using software [40], and from experimentally gathered fluxes [41,42]. These methods rely on their own calculations and assumptions to reach π, with varying degrees of accuracy, similar to FPO and VPO. By contrast, DMO measures π directly by measuring the pressure build up between a solution and a pure solvent, separated by a semipermeable membrane (Figure 1.5) [38,43]. DMO does not rely on any thermodynamic approximations or calculations. A limitation of DMO is the choice of membrane. Low molecular mass material (e.g., NaCl) can pass through the membrane which reduces the detected pressure. DMO successfully measures molecules as small as glucose [44].

DMO can measure very high pressures (ca. 120 bar), which is only limited by the equipment and the membrane. FPO can only measure π up to ca. 60 bar (4,000 mOsm/kg), although newer models may increase this limit [45]. Lines of best fit have been used to predict π at higher concentrations, but this assumes that the linear trend is maintained at these concentrations, which it often is not; this practice is consequently not recommended by many FPO manufacturers [46,47]. Important strengths and weaknesses of VPO, FPO and DMO are summarized in Table 1.1.

Table 1.1 Characteristics of VPO, FPO and DMO.

Property	VPO	FPO	DMO
π range/ bar	0-250	0-75	0-120*
Sample size/ mL	1-3	0.25	3-12
Temperature range	Variable	Fixed	Variable
Measurement time/ h	0.5-6	<0.1	0.5-8
Direct measurement of π	No	No	Yes

*Limited by instrumental and membrane constrains.

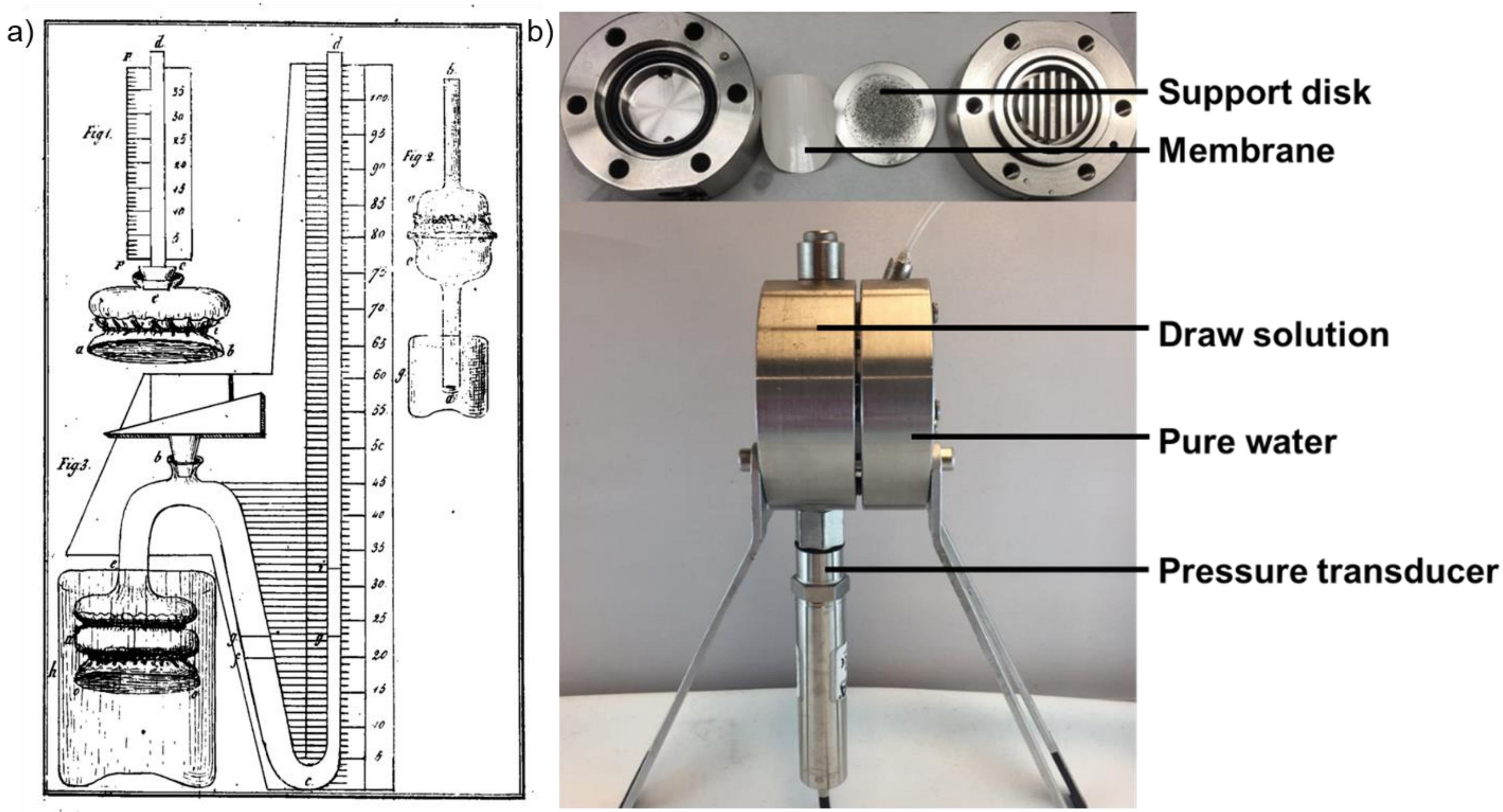

Figure 1.5 Images of membrane osmometers: a) an endosmometer, a predecessor to the modern DMO, and b) a modern DMO. Image a) was reproduced from reference 48. This image is in the public domain.

1.3 Forward Osmosis

1.3.1 Applications of Water Filtration

Water filtration technology is crucial to human life on earth. The demand for effective and energy efficient water filtration technology is rising with every passing year, due to the growing human population, climate change, resource depletion and increased industrialization. Water filtration is needed to produce clean water (e.g., for drinking [49,50] or agriculture [51]), concentrate desired products (e.g, food processing [52,53], recovering products prepared from biomass, mineral extraction [54]) and process wastewater (e.g., geothermal, oil and gas, textiles, mining) [55]. All these applications require the extraction of clean water from a feed solution, producing a concentrated feed, which may be the desired product in the case of food and beverage products, or may be a by-product in the case of water purification. While many different types of water filtration techniques exist, conventional methods still suffer from high energy costs or fail to deal with feeds with high π or fouling potential. To meet future demand and to facilitate the processing of complex and concentrated waste products, new water filtration technologies are required.

1.3.2 Conventional Methods

Chemical separations account for 10-15% of global energy use [56]. Examples of processes which require chemical separations include concentration of food products, isolation of desired products from a solution, processing of wastewater and desalination of ocean water. Diverse separation technologies exist. The characteristics of the feed (e.g., nature and concentration of solute) will determine which technology is best suited for its separation.

The simplest and most common separation techniques separate water from solutes by applying heat, such as distillation. Distillation can effectively separate water from even highly concentrated feeds. However, while advances have been made to distillation, including using solar and waste heat, the energetic and financial costs are still high [57,58]. Thermal techniques are inherently energetically costly as they require changing the phase and temperature of water (Figure 1.6). These changes are not trivial, as water has a higher heat capacity and enthalpy of vaporization than most liquids. Due to its high energy costs, distillation has been supplanted by membrane processes for water demineralization.

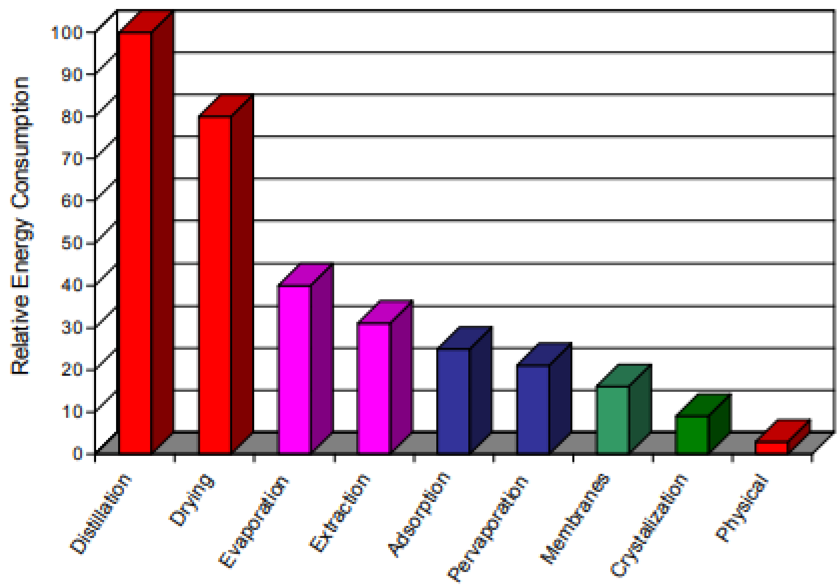

Figure 1.6 Relative energy consumption of common separation techniques. Reproduced from reference 58; this figure is in the public domain.

Membrane techniques separate solutes using a semipermeable membrane. Membranes separate primarily by size and polarity but can also select for other variables (e.g., charge). Material can be transferred across the membrane by various forces, such as osmotic pressure differentials, electric fields, temperature gradients, or pressure, the latter being the most common for demineralization. Membrane separations do not require changing the temperature of the solution to be filtered (the "feed"), and as a result, they generally use substantially less energy than thermal processes, and can be used to treat feeds containing temperature-sensitive materials (e.g., proteins, enzymes).

Reverse osmosis (RO) is the most widely used membrane separation technique; 69% of desalinated water produced globally was treated by RO [59]. As of 2019, there were 17,000 RO plants across the world, producing a total of 107 million m^3 of water every day [60]. In RO, high pressure is applied to the feed, overcoming its π, and forcing water through a semipermeable membrane, resulting in clean water (permeate) and concentrated brine. RO thus forces water to move in the energetically disfavored direction. The hydraulic pressure applied needs to be several times higher than the π of the feed solution, in order to maintain a higher pressure than the π of the final concentrated feed, to maintain a high flux of water (10-20 L/m^2h) and to overcome the resistance of the membrane. Typical RO water recovery ranges from 50-85%, (although this is highly dependant on the nature of the feed) [58]. Although RO has only been around for 50 years, research advances have made it energy efficient [58]. The efficiency of RO depends on the nature of the feed, operating conditions, and the nature of the membrane. The selectivity of RO is highly dependent on the membrane, which is an active area of research.

The high pressures used in RO lead to several limitations. Applying more pressure increases the volume of valuable permeate and decreases the volume of undesired brine but decreases the purity of the permeate and risks collapse or rupture of the membrane. High pressure also leads to high levels of membrane fouling, necessitating more pre-treatment steps and increasing the costs [61]. Furthermore, as there is an upper limit to the pressure than can be applied, there is also an upper limit to the salinity of feeds that can be processed. The maximum pressure that can be maintained in RO is ~120 bar, corresponding to a feed with total dissolved solids (TDS) of ~130 g/L [62]. π and TDS of common feeds are summarized in Table 1.2.

Table 1.2 Osmotic pressures of common water filtration feeds.*

Feed	TDS/ g/L	π/ bar
Pure water	0	0
Seawater [63]	ca. 35	26-28
Brackish water	0.5-35	0.4-26**
Brine	> 35	>27**
Geothermal wastewater [64]	314-160	120-240**
Textile wastewater	≥ 20 [65]	17-78
	3-5 [66]	-
	1.5-12 [67]	-
Raw municipal wastewater [68]	-	0.2
Flue gas desulfurization wastewater [15]	53	30
Apple juice [69]	150	22
Milk, skim [70,71]	8.9	7
Whey [70]	5.1-5.5	3.5-6.1

* Note that π and TDS values may vary significantly from the examples provided in this table depending on the source and treatment of the feed.

**Calculated value using reference 72

Membranes with slightly larger pores than RO membranes can be used; processes include nanofiltration (NF), microfiltration (MF), and ultrafiltration (UF) (Table 1.3). These membranes are used for chemical separations of larger molecular weight species, at lower energies and with higher fluxes than RO. They are often used commercially as pre-treatment steps before a finer filtration step such as RO [58,61,73].

Table 1.3 Pressure driven membrane separation techniques.

Technique	Pore Size [74]	Typically Used to Remove
RO	-	Ions, organics
NF	1-5 nm	Large ions, organics, macromolecules
UF	5-20 nm	Biological material
MF	0.05-1 μm	Large particulates, suspended solids

1.3.3 Forward Osmosis

Forward osmosis (FO) is a membrane separation method that utilizes π differences rather than hydraulic pressure to force water through a membrane. In FO, a feed solution is separated by a semipermeable membrane from a “draw solution”, which possesses a higher π than the feed. The draw solution contains a “draw solute” or “draw agent”. Water flows spontaneously from the side with lower π (feed) to the side with higher π (draw). Once filtration is terminated, the draw solute can be recovered and recycled, producing clean water (Figure 1.7) [9]. The rate at which water is filtered during FO is quantified by water flux (J_w), equal to the volume of water (V_w) transferred over a specific surface area of membrane (A) over a given time (t):

$$J_w=V_w/At \tag{1.6}$$

and has units of L/m^{2}h or LMH. Flux is primarily proportional to the π gradient, but is greatly influenced by concentration polarization, solution viscosity, the mass transfer coefficient of the draw solute, and the nature of the membrane [34,75,76]. These factors can reduce the flux by as much as 80% [77], and will be addressed in subsequent sections.

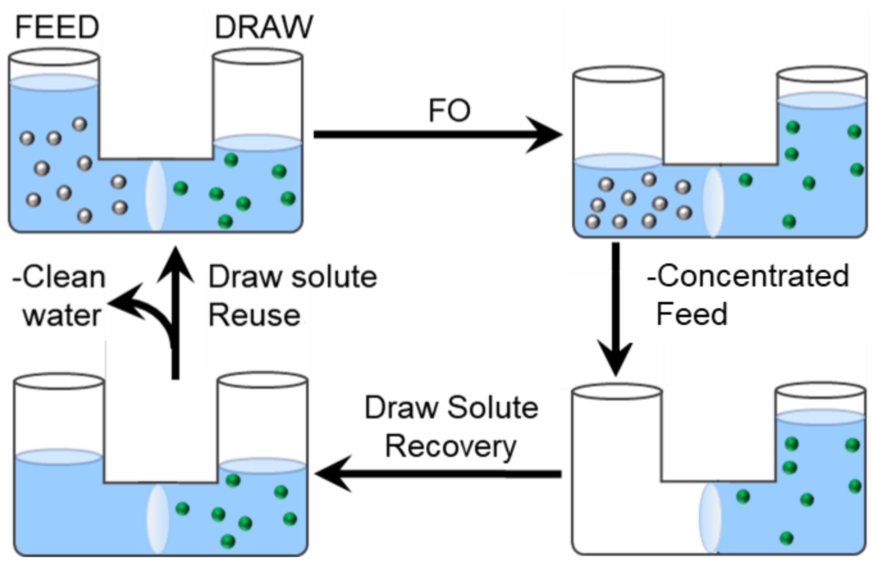

Figure 1.7 Water flux between solutions of different potential energies. The grey circles represent a contaminating solute while the green circles represent a draw solute. Draw solute recovery may be accomplished by diverse techniques (e.g., RO, decantation, magnetic separation).

While FO does not require external energy to pull water across the membrane, FO is not necessarily a low energy process [78]. While RO just separates the impurity from the water, FO involves an additional step (e.g., NF, RO, magnetic separation, phase separation) to recover the draw solution from the permeate. This step is energetically costly, as the draw solute has a higher π than the feed. It is therefore not possible for FO to consume less energy than RO if the draw solute is regenerated. The energy required to recirculate the draw solute must also be considered

[79]. However, if a stimuli-responsive draw solute is united with solar or waste heat to drive the regeneration step, FO has the potential to consume less electricity than RO, which could make FO a greener alternative [40,80,81]. In addition, waste heat (e.g., from a cement or power plant) is a cheaper source of energy than electricity, which could greatly reduce the costs of FO [82].

One key benefit of FO is that it may be used to clean highly concentrated wastewater streams that cannot be processed by RO, while consuming less energy than distillation. In addition, FO is less susceptible to membrane fouling than hydraulic pressure-based methods (e.g., RO, NF) [83]. As a result, feeds treated by FO may require less costly pre-treatments than RO. (Pretreatments can be responsible for up to 60% of the cost of treating oil and gas waste by RO [84]). FO may also exhibit higher rejection rates than RO [85], making it attractive for applications which require high purity products. With a high π draw solute, FO can extract more water from a given feed than RO, making the process more efficient, and reducing the volume of concentrated brine that needs to be disposed of after filtration. FO is being studied as an alternative filtration treatment for diverse applications including sea water and brine desalination [86], juice concentration [53], protein enrichment [87], and treatment of industrial process water [15] and raw sewage [55], as well as a pre-treatment for subsequent filtration steps [88]. FO is already a viable industrial technology; there are over two dozen companies which work on membranes, draw solutes and/or application development [89].

While FO is being successfully used industrially, there are still barriers to its further expansion, such as concentration polarization (section 1.3.3.1), membrane fouling (section 1.3.3.2), and reverse solute flux (section 1.3.3.3). These limitations can be resolved by further research on the nature of the draw solute and the membrane [90]. Few FO membranes are currently commercially available; there is currently much research being done to develop new and improved FO membranes [89]. Draw solutes will be discussed in detail in section 1.3.4.

1.3.3.1 Concentration Polarization

As flux occurs across the membrane, the feed solution is concentrated (raising its π) and the draw solution is diluted (decreasing its π). This produces concentration gradients, a phenomenon referred to as concentration polarization. Concentration polarization can occur within the membrane (internal concentration polarization (ICP)) or in the solution immediately next to the membrane (external concentration polarization (ECP)). Concentration polarization causes the effective $\Delta\pi$ across the membrane to decrease, which in turn decreases flux (Figure 1.8) [42,91].

ECP is accentuated by high viscosity solutions and poor mixing [92]. ECP can be greatly reduced by improving mixing and increasing the turbulence around the membrane. ICP is caused by poor draw solute mobility and mixing within the membrane, and consequently depends on the nature of the draw solute and membrane [93].

Most modern FO membranes are asymmetric, consisting of a thick, porous support layer which contributes to mechanical strength, and a thin, dense active layer which is responsible for selectivity. ICP primarily occurs within the support layer. For solutes to diffuse out of the membrane with greater ease, thinner support layers are desired, which are more porous and less tortuous. This must be balanced with maintaining high mechanical strength, water flux and selectivity [83]. The orientation of the membrane also has a significant influence on flux and ICP. The membrane can be placed with the active layer facing the feed solution (FO mode) or the draw solution (PRO (pressure retarded osmosis) mode). As the molecular weight of the draw solute increases, its diffusivity through the membrane decreases, resulting in enhanced ICP [75]. As a result, high molecular weight draw solutes will have significantly lower fluxes than a lower molecular weight draw solute with the same π. ICP is more difficult to counteract than ECP and is therefore often the primary cause of flux decline.

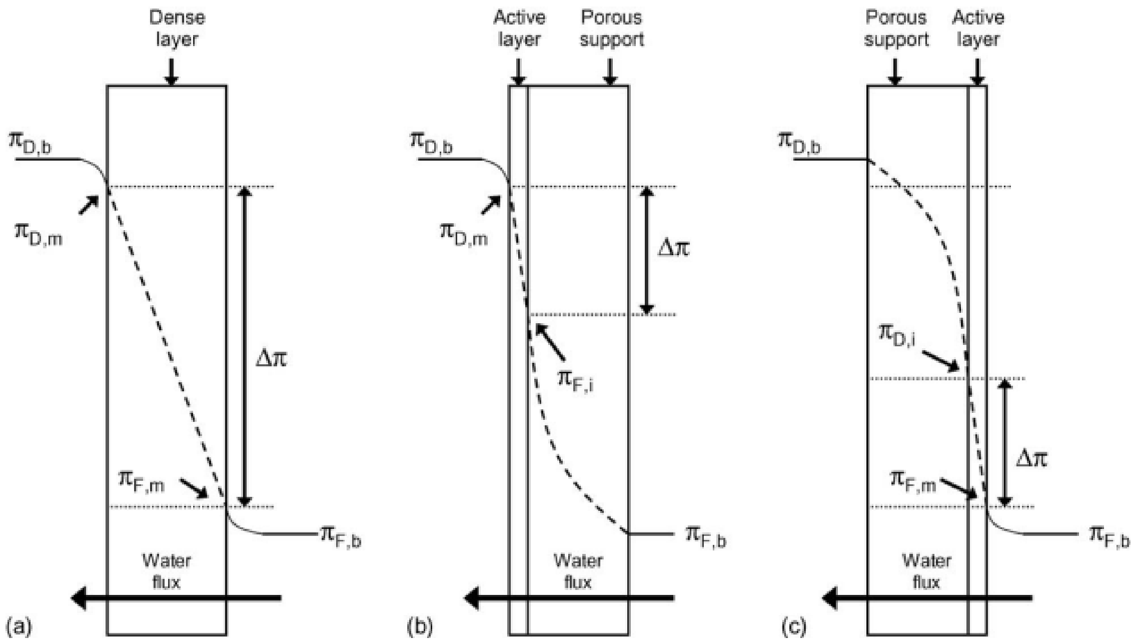

Figure 1.8 Illustrations of concentration polarization. a) external concentration polarization with a symmetric membrane. b) active layer of asymmetric membrane facing the draw solution (PRO mode) c) active layer of asymmetric membrane facing the feed solution (FO mode). The curve lines illustrated the π change of the feed (F) and draw (D) solutions from the bulk (b) to the membrane surface (m). π_i denotes the effective osmotic pressure of the feed or draw after concentration polarization, and Δπ is the effective difference in osmotic pressure. This figure was reproduced with permission from reference 42.

1.3.3.2 Membrane Fouling

Membrane fouling refers to the accumulation of degradative material (foulants) on or in a membrane during a membrane filtration process. Fouling can reduce the active surface area of the membrane, decrease flux, decrease selectivity, and increase maintenance time and costs [83,94]. Clogged pores can cause pressure to build up and if left unchecked, membrane fouling can affect the quality of the product [76]. Fouling can be caused by organic material (e.g., humics, sugars) [95–97], inorganic scaling (e.g., silica, calcium sulfate) [98], and biological material (e.g., algae, bacteria) [83,99].

As the feed solution is concentrated during filtration, material that has low solubility or is saturated in solution can precipitate, crystalize or polymerize to form very stable, low solubility species (e.g., gypsum, silicates) [98,100]. This can result in scaling on the membrane surface and clogged pores. Inorganic scaling can be avoided by using additives to prevent precipitation, and pre-treatment to reduce sedimentation [101].

Biological material can grow on the membrane and form biofilms. Biofoulants can be harder to avoid and combat than other foulants as they can proliferate very quickly [73,102]. The diversity of biofoulants and the intricate factors that govern their growth make them altogether more complex and consequently less well understood than crystallizations [83,103,104]. Biocides (e.g., chlorine, bleach) are often added to kill bacteria [105]. While chlorine is an effective and commonly used biocide, it can generate toxic halogenated by-products which remain in the water [102,106,107].

The major cause of fouling depends on the feed. For instance, seawater contains low levels of organics but higher levels of inorganics [63]. Fouling can also be synergistic; it has been reported that bacterial growth rates are higher when gypsum scaling is present [108]; calcium can crosslink alginate leading to accelerated fouling [109]. The draw solute can also effect fouling, especially if it has high reverse solute flux (see section 1.3.3.3) [81].

The nature of the membrane [110,111], FO operating conditions (e.g., temperature [112]), and cleaning procedures can reduce or reverse membrane fouling [83]. The design and orientation of the membrane can also influence fouling. Spiral wound membranes have higher fluxes due to higher surface areas, but likewise have higher fouling rates [113]. The support side of asymmetric FO membranes are generally more susceptible to fouling than the active layer, as they are more porous and have higher surface areas [114]. Designing membranes with reduced fouling propensity is a key area of research for improving FO [83].

Fouling in FO is distinctly different from that in pressure-based membrane processes. FO processes are generally less prone to fouling than RO [83], and FO membranes are more easily cleaned compared to RO membranes [115]. Some fouling can be reversed by physical methods (e.g., reverse cross flow, back flow) or chemical methods. Chemical methods can be more effective at eliminating fouling located within the membrane than physical methods, but generate more waste [116]. When using chemical methods, it is important to consider the chemical compatibility of the membrane.

1.3.3.3 Reverse Solute Flux

During FO, as in any membrane process, solute as well as water can pass through the semipermeable membrane. While solutes from both the feed and the draw can pass through the membrane, solute flux generally occurs predominantly in the energetically favoured direction, which in FO is from the draw to the feed. The movement of draw solute across the membrane to the feed is called reverse solute flux (RSF, J_s). The degree of RSF depends on the size, polarity, and charge of the draw solute, as well as the nature of the membrane. As the membrane is a relatively non-polar environment, neutral molecules generally have higher permeability than ions (e.g., $J_{NH3}>J_{NaCl}$) [117]. RSF decreases as molecular weight increases due to size exclusion [118]. RSF increases with J_w and solute concentration [111,119].

When RSF occurs, the π of the draw side is lowered and the π of the feed side is raised, which is detrimental to J_w. In addition, the draw solute may impart negative properties on the feed, such as toxicity or odor. If the concentrated feed will be ingested by humans, the tolerance for RSF is extremely low. Furthermore, RSF decreases the amount of draw solute that can be recovered and reused. It has been suggested that residual amine draw solute in the product water could be used to boost plant or algal growth [120].

Solute flux from the feed to the draw can also have negative consequences. For instance, if the draw solute is a CO_2-responsive amine, acids from the feed can cause the amines to become permanently charged, which will increase the energy cost of draw solute removal and decrease the life span of the draw solute.

1.3.4 Draw Solutes

The success of FO hinges on the nature of the draw solute. The development of new draw solutes is one of the key areas of research within the field of FO [40,77,121–123]. An ideal draw solute will have all the following properties: high J_w, easy and energy-efficient recycling, low viscosity, low RSF, and low membrane fouling. It should also be inexpensive, non-toxic, and possess long-term stability. To have a high J_w, a draw solute should have high π, low viscosity, and high diffusivity. Many of these variables are interrelated and can be difficult to separate from each other. For example, high draw solute concentrations lead to higher fluxes, but also can also lead to higher viscosities. Table 1.4 illustrates the diversity of draw solutes that have been reported in the literature, along with their major advantages and disadvantages.

Table 1.4 Properties of classes of forward osmosis draw solutes.

Classification	Example	Advantages	Disadvantages
Inorganic salts	NaCl [122,124]	High solubility Cheap High theoretical π	High RSF π of recycled draw solution limited by RO capacity
Consumables	Glucose [93] $(NH_4)_2HPO_4$ [125]	No removal Creates useful by-product	Cannot produce clean water Biofouling
Gases	Trimethylammonium bicarbonate [117]	Very high π	Toxicity Bad odour Flammability RSF
Polymers (non-responsive)	Poly(sodium aspartate) [126]	Low RSF Non-toxic	Energy intensive recovery High ICP Limited π Viscosity
Hydrogels	P(N-isopropylacrylamide) (PNIPAM) [127]	Low RSF Non-toxic	Rapid decline in J_w Very poor mass transfer Difficulties scaling up
Magnetic particles	Poly(ethylene glycol)diacid-coated magnetite nanoparticles [128]	Facilitated recovery Low RSF	Aggregation Particle decomposition Relatively expensive

1.3.4.1 Small Molecule Non-Stimuli Responsive Draw Solutes

Inorganic salts (e.g., NaCl, $MgCl_2$) were among the first draw solute candidates (Table 1.5) [34]. Advantages of these materials include their unmatched π (>1000 bar for $MgCl_2$) [40], low ICP and low costs. Disadvantages include high RSF and energy intensive recoveries. The use of small organic molecules such as sugars [93,129,130] and carboxylate salts [124] as draw solutes has been studied, but were found to have lower fluxes than inorganic salts. Impaired water (a natural source of water that has been contaminated and no longer meets water quality standards) has been used on a pilot scale to dilute seawater by FO before the saline water is desalinated by RO [131,132]. (Here the impaired water acts as the feed and the seawater act as the draw). This process decreases the energy required for desalination and leads to lower membrane fouling than direct RO of impaired water.

Several draw solutes are intended to not be removed post-filtration, as the diluted draw solution is used for another function. Nitrogenous salts (e.g., $NH_4H_2PO_4$) have been used as draw solutes, where the diluted draw solution is used as a fertilizer [125,133]. Sugars, such as glucose and fructose, have been used as draw solutes for portable water purification systems, producing potable water enriched with sugar [134,135]. This product has been commercialized by HTI and FTSH2O as portable hydration packs for use in lifeboats and survival gear [136]. While these draw solutes cannot be used to generate pure water, they have the potential to have extremely low energy costs, as draw solute recovery is the most energy intensive part of the FO process. However, the high levels of phosphorous and sugars may proliferate biofouling.

Table 1.5 Properties of selected small molecule non-stimuli responsive FO draw solutes.†

Draw Solute	π/bar	Separation Method	RSF/ g/m^2h	Flux‡/ L/m^2h	Draw solute in product water/ mg/L	Notes
NaCl [34]	42 at 50.8 g/L	RO	9.1	12.2	153.3	Precommercial by IDE technologies, Porifera
$MgCl_2$ [34]	42 at47.6 g/L	RO	5.6	9.72	82.6	
Sucrose [93]	27 at 1 M	NF	Negligible	12.9	-	
Sodium Acetate [124]	42 at 139 g/L	RO	3.55	10.4	185	
$(NH_4)_2HPO_4$ [125]	51.3 at 1 M	None	3.4	13.3 Feed= synthetic wastewater	-	Cannot produce pure water
Glucose [135]	56 at 2 M	None	-	-	-	Cannot produce pure water Commercialized by FTSH2O

†This table is designed to illustrate the range of draw solutes reported in the literature, and to make preliminary observations. Note that π values may vary between reports depending on the method used to measure it (e.g., DMO, FPO, VPO). FO data may vary depending on many variables including the membrane (type and orientation) and scale used.

‡Unless otherwise specified, Feed solution = deionized water

1.3.4.2 CO_2-Responsive Draw Agents

The key to reducing the energy consumption of FO is designing a draw solute that can generate a high J_w and yet can be easily removed from the permeate. The problem is that while many, diverse FO draw solutes have been designed, synthesized and tested [41,123,126,137–139], many fail to unite these two properties. Unfortunately, the properties that lead to high π usually make the draw solute more difficult to remove from the permeate. One way to unite these two apparently contradictory requirements is to use a stimuli-responsive draw solute that possesses a reversibly switchable π [140].

Since 2010, several patent applications have been filed on CO_2-switchable solutes that could control the osmotic pressures of their aqueous solutions [141,142]. These CO_2-responsive draw solutes are bicarbonate salts of tertiary amines. As long as an atmosphere of CO_2 is maintained, these solutions have high π and can therefore be used as draw agents for FO. Once the FO step is complete, removal of the CO_2 by heat and/or a flushing gas such as air causes the tertiary ammonium bicarbonate salt to decompose into a tertiary amine (equation 1.7, where "**B**" represents a CO_2-switchable material). The amine is then readily removed by evaporation for gaseous amines, decantation for liquid amines, NF or RO for soluble solid amines or filtration for insoluble solid amines.

$$\mathbf{B}_{(aq)} + nCO_{2\,(aq)} + nH_2O_{(l)} \rightleftharpoons H_n\mathbf{B}^{n+}{}_{(aq)} + nHCO_3^-{}_{(aq)} \qquad (1.7)$$

$$\text{Low } \pi \rightleftharpoons \text{High } \pi$$

Many of the most promising draw solutes reported in the literature to date are CO_2-responsive, including liquid amines (e.g., N,N-dimethylcyclohexylamine (DMCA) [120], 1-cyclohexylpiperidine (CHP) [84], monoethanolamine (MEA) [15]), polymeric amines (e.g., PDEAEMA [141] and PDMAEMA [143]), and gaseous amines (e.g., trimethylamine (TMA) [117]). The properties of CO_2-responsive draw solutes reported in the literature are summarized in Table 1.6. CO_2-responsive polymers and gels are discussed in detail in subsequent sections.

One of the most effective FO draw solutes tested to date is the bicarbonate salt of TMA. The osmotic pressure under CO_2 (π_{CO2}) of TMA is high, over 200 bar at 69 wt.%, and is easily removed after filtration by steam stripping. Compared to ammonia, which reports slightly higher J_w, TMA requires less energy to remove from water, is less prone to RSF, is less harmful to the membrane, and is easier to flare if there is a leak [117]. However, TMA it is not without disadvantages. TMA possesses an extremely pungent odour which can be sensed as low as 0.5 ppb [144]. Therefore, as small amounts of TMA may be present in the feed and recovered water, the applications of TMA as a draw solute are limited. In addition, although TMA is a naturally occurring amine present in many foods, prolonged exposure to concentrated TMA has negative health effects. TMA can cause severe damage to the skin, mucous membranes, eyes, liver, heart, and lungs, and can degrade in the liver to create trimethylamine N-oxide, a possible pathogen [144–146]. TMA is toxic to aquatic life in large quantities [145]. In addition, TMA is flammable both as a vapour and in solution and is corrosive [144,145]. In the case of accidental gaseous release, TMA can be flared, but combustion of TMA releases harmful carbon and nitrogen oxides [145].

Switchable hydrophilicity solvents (SHS) are liquid amines that are immiscible in water under air and miscible under CO_2. They are traditionally used as solvents to facilitate the separation of solutes and recycling of solvents [147,148]. SHSs have been used as draw solutes and have the unique ability to reject organic contaminants from the draw solution. SHSs are highly miscible with carbonated water, achieving high concentrations and π_{CO2}. The first reported SHS draw solute, DMCA, efficiently draws water from high π feeds, concentrating them by more than 90%, and shows energy requirements that are competitive with RO [120,149]. However, DMCA exhibits near quantitative RSF and shows limited membrane compatibility. In addition, DMCA needs to be heated to 95 °C, well above its flash point (42.2 °C), to remove CO_2. Once CO_2 is removed the subsequent RO step requires little energy, but trace amounts of DMCA are present in the recovered water. A second SHS draw solute, CHP, shows similar performance to DMCA, but exhibited a higher flash point and boiling point and improved membrane compatibility. CHP also decarbonates faster than DMCA and at lower temperatures (80 °C for CHP, 95 °C for DMCA) [84]. Despite these improvements, RSF is still a limitation of CHP.

MEA was proposed as a draw solute in a coupled FO-CO_2 capture process, with the goal of simultaneously reducing the CO_2 emissions and purifying the wastewater generated from fossil fuel based power plants [15]. A MEA aqueous solution is first used to scrub CO_2 from flue gas, forming MEA-carbamate; the carbonated MEA is then used as a draw solute in FO, using wastewater generated in the power plant as the feed; the draw solute and clean water are recovered using microdistillation (MD) (at 60 °C); finally, MEA and CO_2 are separated in a stripper (at 100-121 °C), regenerating the MEA. The high π_{CO2} and concentration (5 M) of the MEA-CO_2 draw solution resulted in high J_w from saline solutions. The draw solution also successfully concentrated real wastewater from a coal-fired power plant (π = 30 bar) by more than 75%; however, the fluxes were low despite feed pre-treatment, highlighting the degradative effects of concentration polarization and membrane fouling. MEA also exhibited substantial RSF, although these were lower than those of 5.0 M DMCA or 1.25 M ammonia. Small amounts of MEA was also transferred to the clean water during MD, which may be significant depending on the application. Due to the high temperatures required to separate the CO_2 and MEA (due to carbamate formation), this draw solute is likely too energy intensive for applications beyond coupled FO/CO_2-captured techniques.

Table 1.6 Properties of selected CO_2-responsive FO draw solutes.†

Class	Draw solute	π_{CO2}	Separation Method	RSF	Flux‡/ L/m^{2}h	Notes
Gels	PDMAEMA [150]	-	Purge with N_2; centrifugation	-	56 (after 2 min) DS: 50 wt.% FS: 2 wt.% NaCl	Very rapid decline in flux
Soluble Polymers	PDMAEMA, 4 kDa [143]	36 bar at 40 wt.% [151]	Inert gas+ heat (60 °C); decantation; UF 54.6 ppm DS in product water	ca. 0.19 g/m^{2}h	>2 DS: 60 wt.% FS: 0.6 M NaCl	No membrane fouling Water recovery >95% FO experiments done on small scale apparatus
Liquids	DMCA [120][84]	329 bar at 7.6 mol/kg	Heat (80 °C); liquid-liquid separation; RO 6 ppm DS in product water	1.8 wt.% (solubility limit)	11 DS: 5 mol/kg FS: 0.5 mol/kg NaCl	Corrodes CTA⁑ membrane Miscible up to 60.5 wt% Capability to concentrate seawater by 90%
	CHP [84]	>500 bar at 11.2 mol/kg	Heat (70 °C); liquid-liquid separation; RO	4 g/m^{2}h	8.5 DS: 5 mol/kg FS: 0.5 mol/kg NaCl	Improved membrane compatibility vs DMCA
	MEA [15]	-	Heat (60 °C) to remove H_2O, Heat (100 °C) to remove CO_2	10.3 mg/L	14.8 (45 °C) DS: 5M FS: 0.6 M NaCl	Cheap, commercially available High temperature regeneration
Gases	TMA	48.8 bar at	Steam stripping	0.1-0.2	33.4	Commercialized by

	[117,152]	1 M 200 bar at 69 wt.%	(60 °C)	mol/m^{2}h	FS: 1 M DS: DI water	Forward Water Technology
	Ammonia [117,153,154]	40.1 bar at 1 M 253 bar at 6 M	Steam stripping (60 °C)	ca. 0.3-0.7 mol/m^{2}h	35.6 FS: 1 M DS: DI water 23 DS: 6 M FS: 0.5 M NaCl	Commercialized by Oasys

†This table is designed to illustrate the range of draw solutes reported in the literature, and to make preliminary observations. Note that π values may vary between reports depending on the method used to measure it (e.g., DMO, FPO, VPO). FO data may vary depending on many variables including the membrane (type and orientation) and scale used.

‡ DS = draw solution, FS = feed solution, DI = deionized

*Obtained by extrapolation from dilute solutions

‡ CTA = cellulose triacetate

1.3.4.3 Polymers

Polymeric draw solutes have high molecular weights, which leads to a myriad of beneficial properties. Higher molecular weights lead to higher boiling points, which decreases flammability and odor. Polymers also have very low to no RSF, as they are too large to pass through the membrane pores [123]. In addition, polymers with a molecular weight greater than ca. 1000 Da cannot be absorbed through cellular membranes, leading to reduced toxicity [155,156]. (However, if ionic polymers do enter cells, they can cause osmotic shock and cell death.) Because of the negligible RSF, polymeric draw solutes have promising applications in areas which require high purity feeds, such as food products and pharmaceuticals. High molecular weights allow for the use of lower energy removal techniques, such as UF or NF.

However, possessing a high molecular weight can also lead to undesirable properties. In solution, high molecular weight materials generally have higher viscosities and lower mobilities, especially at higher concentrations, which increase concentration polarization and have an extremely adverse effect on J_w [75]. Highly viscous solutions also require more energy and pressure to push through piping and membrane modules [105]. High molecular weight leads to lower solubility which limits the π that can be reached; small molecules generally achieve their high π through very high concentrations (e.g., 69 wt.% for TMA-bicarbonate).

It is often reported that low molecular weight materials have higher π compared to high molecular weight materials [40]. However, this does not account for ionic or ionogenic polymers, which have high π as well as a high molecular weight. Despite this, no polymer can rival the high π of small species such as TMA or $MgCl_2$.

High molecular weights lend specific benefits to CO_2-responsive draw solutes. As RSF is predominantly due to the passage of uncharged molecules through the membrane [120], CO_2-responsive polymers are expected to have low RSF due to the fact that the sheer number of units decreases the probability of there being a chain that is completely uncharged, (in addition to steric factors). Moreover, as the draw solute is non-volatile, CO_2 can be removed by heat or even vacuum without risk of removing the draw solute, unlike gaseous and most liquid amines.

Only one soluble CO_2-responsive polymeric draw solute (PDMAEMA) has been reported to date outside of the Jessop group (see Table 1.7) [143]. PDMAEMA is a dual CO_2- and thermo-responsive draw solute. In this work, PDMAEMA produced low fluxes against 0.6 M NaCl (~ 2 LMH) although this may be partially attributed to the small sample size and poor mixing in the FO apparatus. PDMAEMA was recovered by heating above its LCST (~43 °C), decarbonating the solution and collapsing the polymer chains, followed by UF. CO_2-responsive polymers are discussed further in Chapter 2.

Numerous thermo-responsive polymers have been tested as draw solutes. Trevi Systems, founded in 2010, uses a thermo-responsive copolymer of ethylene and propylene oxides (M_w ca. 2 kDa, cloud point between 40-90 °C) as a draw solute, coupled with waste heat to assist recovery [105,157]. Viscosity was reported to be a problem in preliminary tests, specifically passing the viscous draw solution through the small fibers of the FO membrane module [105]. The Trevi polymer has been successfully tested on the pilot stage for a variety of feeds [157,158]. Many thermo-responsive draw solutes reported in the literature also possess a permanent charge, including: poly(tetrabutylphosphonium styrenesulfonate) [159], poly(([2-(methacryloyloxy) ethyl]trimethylammonium chloride) – (2-(2-methoxyethoxy)ethyl meth- acrylate)) [160], poly(4-vinylbenzyltributylammonium hexanesulfonate) [161], and poly(sodiumstyrene-4-sulfonate)-(N-isopropylacrylamide)) (SSS)-NIPAM) [162]. The properties of selected polymeric FO draw solutes are summarized in Table 1.7.

Table 1.7 Properties of selected polymeric FO draw solutes.†

Draw Solute	π	RSF	Flux‡/ L/m²h	DS in product water	Separation
poly(sodium aspartate), 1.3 kDa [126]	52 bar at 0.3 g/mL	ca. 4 g/m²h	31.8 DS: 0.3 g/mL FS: DI water	-	NF
PSA, 1.2 kDa [163]	ca. 44 bar at 0.72 g/mL	-	7 DS: 0.72 g/mL FS: 3.5 wt.% NaCl	Not detected	UF
Cationic starch [119]	12 bar at 30 wt.%, 40 °C	ca. 11.5 g/m²h	2.20 (45 °C) DS: 30 wt.% FS: 2 g/L NaCl	670 to 1090 mg/L	UF
PDMAEMA, 4 kDa [53, 72]	36 bar at 40 wt.%	ca. 60 mg/L	>2 DS: 0.6 g/g FS: 0.6 M NaCl	54.6 ppm	Inert gas + 60 °C; decantation & UF
Branched-PEI, pH=3, 0.8 Da [118]	35 bar at 25 wt.%	ca. 0.012 g/m²h	Ca. 6 DS: 5 wt.% FS: 2000 ppm NaCl	0.6% transferred	RO
Branched-PEI, pH=7, 25 kDa [43]	19 bar at 20 wt.%	-	11 DS: 20 wt.% FS: DI water	0.70 g/m²h	NF
P(tetrabutylphosphonium	43.5 bar at	0.14 g/m²h	6.12	0.49% transferred	60 °C;

styrenesulfonate), 2.1 kDa [159]	40 wt.%		DS: 20 wt.% FS: 2000 ppm NaCl		decantation
P(SSS-NIPAM) [162]	29 bar at 33 wt.%	2 g/m^{2}h	>3.5 DS: 33 wt.% FS: 0.6 M NaCl	negligible	50 °C; MD

†This table is designed to illustrate the range of draw solutes reported in the literature, and to make preliminary observations. Note that π values may vary between reports depending on the method used to measure it (e.g., DMO, FPO, VPO). FO data may vary depending on many variables including the membrane (type and orientation) and scale used.

‡DS = draw solution, FS = feed solution. Unless otherwise specified FO occurred, at room temperature.

1.3.4.4 Hydrogels

Hydrogels gained attention as draw agents due to their ease of recovery compared to small molecules. Tailored hydrogels can exhibit high swelling pressures, and due to their high molecular weight they are generally non-toxic and exhibit no RSF [164]. Swelling pressure can be defined analogously to osmotic pressure, as the minimum pressure required to be applied to a gel to prevent water from passing into the gel by osmosis [165]. A gel's maximum degree of swelling will be affected by the nature of the crosslinker and degree of crosslinking and porosity, in addition to factors which would affect a soluble polymer, such as interactions with the chains and water [165,166]. A dry gel expands by first absorbing small amounts of water by capillary action. Polar or charged groups inside the gel increase the J_w inside the gel. The expansion of the gel is limited by the elastic constrains of the polymer network [167].

Hydrogels are often characterized by their swelling ratio (SR), which describes how much water they can absorb, and the % water they can release (Figure 1.9). For a draw agent to be successful, the flux and percentage and rate of water released must be high. An extremely high SR (> ca. 100) is not necessary for a draw solute, as it is unlikely that in practical use the $\Delta\pi$ between the draw and the feed will be large enough to require the draw agent to absorb so much water.

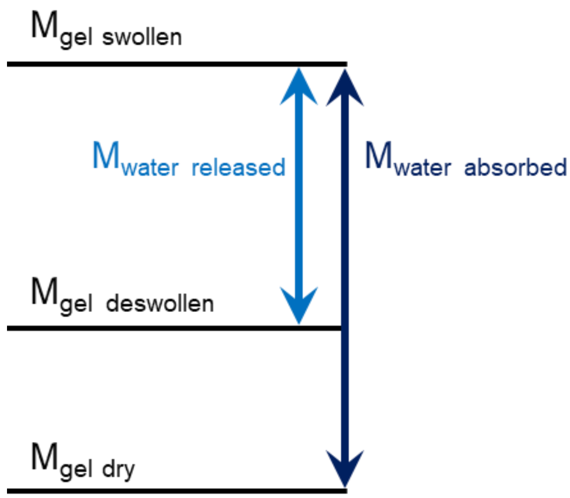

$$SR = \frac{M_{\text{gel swollen}} - M_{\text{gel dry}}}{M_{\text{gel dry}}}$$

$$\%\,R = \frac{M_{\text{water released}}}{M_{\text{water absorbed}}} \times 100$$

Figure 1.9 Illustration of swelling ratio (SR) and water recovery (%R) used to describe draw agents.

Many of the trends observed with small molecule draw agents apply to gels, such as that incorporating ionic groups increases J_w due to increased hydrophilicity and increased number of species in solution, but for the same reason decrease the amount of water recovered and increase the energy for recovery (see Table 1.8). As with other draw agents, stimuli-responsive hydrogels were considered as an alternative, specifically the thermo-responsive polymer poly(N-isopropylacrylamide) (PNIPAM). PNIPAM contracts above a threshold temperature (LCST= 32-34 °C), thereby expelling water and facilitating the recycling of the draw agent [168]. However, pure PNIPAM does not have a high π, and therefore produces low fluxes. In addition, as water is removed from a thermo-responsive hydrogel, a dry, dense layer forms on the gel's surface, making it difficult for liquid water to permeate out of the draw agent. Consequently, a significant portion of the water recovered from thermo-responsive material may be in the vapour rather than liquid phase [169].

In response, several researchers developed gels combining a highly absorptive, hydrophilic monomer and an easily removed, thermo-responsive monomer. Examples of such gels include: poly(NIPAM-SA) [87,168,170], poly(NIPAM-2-acrylamino-2-methylpropane sulfonic acid) [171], poly(NIPAM-itaconic acid) [172] and poly(NIPAM-acrylic acid) [173]. Some polymers (e.g., poly(butylhexylphosphonium styrenesulfonate)) possess a permanent charge and are thermo-responsive [137]. However, the hydrophilic component can limit the water released, and the thermo-responsive component does not contribute significantly to the π. Therefore, attempting to balance high flux and easy recovery using gels containing a thermo-responsive and a hydrophilic component usually result in a compromise between the two requirements rather than the material excelling at both.

Stimuli-responsive hydrogel draw agents have also been considered. Light-responsive hydrogels have also been synthesized by grafting P(NIPAM-SA) gels to light active surfaces (e.g., graphene) increased the water recovery, rate of water recovery and the flux compared to plain P(NIPAM-SA) gels [174,175]. Hydrogels which respond to electricity have been studied: hyaluronic acid/polyvinyl alcohol (HA/PVA) [176], and 2-acrylamido-2-methyl-1-propanesulfonic acid-DMAEMA gels [177], but both the fluxes and recoveries were low. Gels have been formed around magnetic particles, which are discussed in more detail in section 1.3.4.4.

The first CO_2-responsive hydrogel draw agents were reported in 2018; PDMAEMA and PDEAEMA microgels were made using various crosslinkers, with diameters of 200-250 nm under air [150]. High initial fluxes (56 LMH, 50% PDEAEMA slurry vs. 2 wt.% NaCl) were reported which quickly plateaued close to zero. The SR of the microgels was ca. 15 RSF. Product water purity was not reported. Intermediate water recoveries (50%) were obtained after purging with nitrogen followed by centrifugation at 12,000 rpm for 15 min. While being effective techniques, using nitrogen and centrifugation rather than heat decreases the energetic benefit of using a CO_2-responsive draw agent.

Disadvantages of hydrogels include low mass transport within the gel and poor contact with the membrane, resulting in low fluxes [164]. The inherent low mass transport in gels, even well-engineered ones, result in severe ECP which cannot be combated by the simple techniques used for liquid draw solutes. This may be a permanent limitation of hydrogel draw agents. In addition, many hydrogels reported in the literature have not been subjected to multiple cycles, so their ability to be reused is not known.

The size and structure of gels have been studied to improve their swelling and FO performance. Microgels have larger surface area: volume ratios than bulk gels, and therefore have higher response times and better contact with the membrane [170,178,179]. Incorporation of microfibers through the gel network has been shown to increase the response rate (both swelling and deswelling) by improving the mass transport of water [180]. However, both materials have more complex syntheses that bulk gels.

Hydrogel sheets which are fixed to the FO membrane have been explored, often consisting of a water drawing layer and a water releasing layer [181,182]. Such membranes are designed to be used in a continuous process, and commonly use solar heat to trigger the release of water. While such sheets are expected to have superior membrane coverage compared to microgels, they produced low fluxes. Moreover, it is unknown how repeated cycles of expansion and contraction will affect the physical properties of the gel and its contact with the membrane.

Table 1.8 Properties of selected hydrogel FO draw agents.†

Draw Agent	Separation	Flux‡/ L/m^2h	Water recovery	SR*
PDEAEMA microgel [150]	Purge with N_2, centrifugation	56, DS: 50 wt.% FS: 2 wt.% NaCl	50%	ca. 13.5
PDMAEMA microgel [150]	Purge with N_2, centrifugation	41 DS: 50 wt.% FS: 2 wt.% NaCl	44%	-
PNIPAM microgel [173]	Centrifugation at 40 °C	2 DS: dry gel FS: 2 wt.% NaCl	72.4%	1.3
P(NIPAM-SA) bulk gel [127]	3 MPa, 50 °C	0.55 DS: dry gel FS: 2 wt.% NaCl	17%	-
P($NIPAM_{92}$-AA_8) microgel [173]	Centrifugation at 40 °C	23.8 DS: dry gel FS: 2 wt.% NaCl	52%	ca. 10
P(NIPAM-itaconic acid) microgel [178]	Centrifugation at 40 °C	44.8 DS: dry gel FS: 2 wt.% NaCl	47.2%	-
P(NIPAM-DEAEMA) microgel [183]	Centrifugation at 40 °C	45.6 DS: dry gel	44.8%	-

		FS: 2 wt.% NaCl		
P(tributylhexylphosphonium p-styrenesulfonate) bulk gel [137]	60 °C	2 DS: dry gel FS: 2 wt.% NaCl	50%	3.8
P(NIPAM-SA) bulk gels- carbon particle composites [184]	Simulated sunlight (1 kW/m^2)	0.77 DS: dry gel FS: 2 wt.% NaCl	100%	138.6
Fe_3O_4@P(NIPAM-SA) bulk gel [169]	Magnetic field-induced heating (400.5 A)	1-1.6 DS: dry gel FS: 2 wt.% NaCl	53%	200-250
Multi-layer sheets P(NIPAM-SA) [182]	60 °C	0.25-0.30 DS: 2 wt.% FS: 2 wt.% NaCl	60-70%	ca. 150
PNIPAM/(polyvinyl alcohol) semi-interpenetrating network [168]	40 °C	0.23-0.24 DS: 58 wt.% FS: 2 wt.% NaCl	90-95%	60-70

†This table is designed to illustrate the range of draw solutes reported in the literature, and to make preliminary observations. Note that π values may vary between reports depending on the method used to measure it (e.g., DMO, FPO, VPO). FO data may vary depending on many variables including the membrane (type and orientation) and scale used.

‡DS = draw solution, FS = feed solution.

*Variable definitions of SR occur in the literature. Here SR is defined as in Figure 1.9.

1.3.4.5 Magnetic Particles

Many researchers have sought to facilitate the removal of draw agents post-filtration by using magnetic draw agents (Table 1.9). Ideally, these draw agents could be removed by simply applying a magnetic field and would have minimal RSF during the FO step due to their size. Magnetic draw agents are based on magnetite (Fe_3O_4) or, less commonly, maghemite (γ-Fe_2O_3) nanoparticles.

Unfunctionalized magnetite nanoparticles (MNP) are a poor draw solute. Magnetite has low π (2.4 bar, 45 wt.%) and dispersibility in water [185]. In addition, magnetite is brittle and is susceptible to corrosion, and oxidation to non-magnetic iron oxides [186,187]. Chemical degradation is enhanced by the high surface area of nanoparticles. Once magnetite loses its magnetic susceptibility, the draw agent can no longer be removed by application of a magnetic field, which removes its main benefit. Functionalizing the magnetite surface can help protect the magnetite from degradation and increase flux.

Preliminary reports of magnetic draw agents attempted to increase J_w by grafting hydrophilic materials on to the surface (e.g., citric acid, PEG, dextran, PSA) [128,188,189]. It has been reported that polymer bound to magnetic nanoparticles exert π several fold higher than the same amount of unbound, soluble polymer [35,188,190]. This phenomenon is ascribed to differences in polymer orientation in the bound and unbound states; an unbound polymer exist as a restrictive coil, while the bound polymer is forced to assume an extended, brush-like configuration which is more accessible to hydration [191]. While grafting hydrophilic materials on to the magnetite surface does improve J_w, it also decreases the amount of water that can be recovered and decreases the speed of the magnetite recovery [188]. As with other classes of draw agents, stimuli-responsive materials were considered to improve draw agents properties.

A stimuli-responsive coat on the magnetic particle will improve the amount of water recovered and the ease of draw agent recovery. In addition, if the magnetic particle possesses a state which is relatively hydrophobic, it may be recovered using a weaker magnetic field, which will reduce the chance of irreversible aggregation. Thermo-responsive PNIPAM-coated magnetite particles showed improved recovery, but still showed a low J_w due to PNIPAM's low hydrophilicity [192]. To increase J_w, PNIPAM was coupled with polyelectrolytes (e.g., PSA) [192]. While an improvement on previous attempts, these materials also failed to produce high fluxes.

Preliminary magnetic draw agents had electrolyte coats that were simply chemisorbed to the magnetite surface [110]. If the coating is not strongly bound to the magnetite surface, it can be removed over successive cycles, leading to increased aggregation and decreased flux [193,194]. When the coating is covalently bound to the surface, the particles show improved stability [138].

Aggregation is a recurring problem with magnetic draw agents. Aggregation decreases the draw agent's surface area and π, which leads to a decrease in J_w. Higher polymer loadings and charged groups can reduce aggregation [190]. Coating the magnetite surface with SiO_2 prior to further functionalization may impart further chemical resistance and reduce aggregation [195].

The size of the nanoparticle determines many of the draw agent's properties. Particles with smaller diameters and thicker coatings have higher π and respond to stimuli faster but are more challenging to recover [138]. Due to their large size (compared to inorganic salts), nanoparticles have low diffusivities which lead to higher ICP. However, magnetic draw agents with high fluxes have been reported (up to 30 LMH vs DI water, see Table 1.9) [196,197]. Both properties may be possible using a stimuli-responsive material. Nanoparticles also have unknown or hazardous effects on the human body [198].

Magnetic nanoparticles can clog pores in a membrane, especially if they are coated with a material which interacts strongly with the membrane (e.g., citric acid draw solutes and CTA membranes) [194,197,199]. Na et al. (2014) applied a magnetic field on either side of the FO membrane (Figure 1.10) to localize the particles close to the membrane and prevent them from embedding themselves in the support layer, which showed impressive improvements compared to a traditional FO apparatus. Applying a magnetic field can also risk inducing aggregation in the nanoparticles which would reduce surface area and π of the magnetic nanoparticles. However, this work highlights the unique and simple way the movement and position of magnetic draw agents can be manipulated.

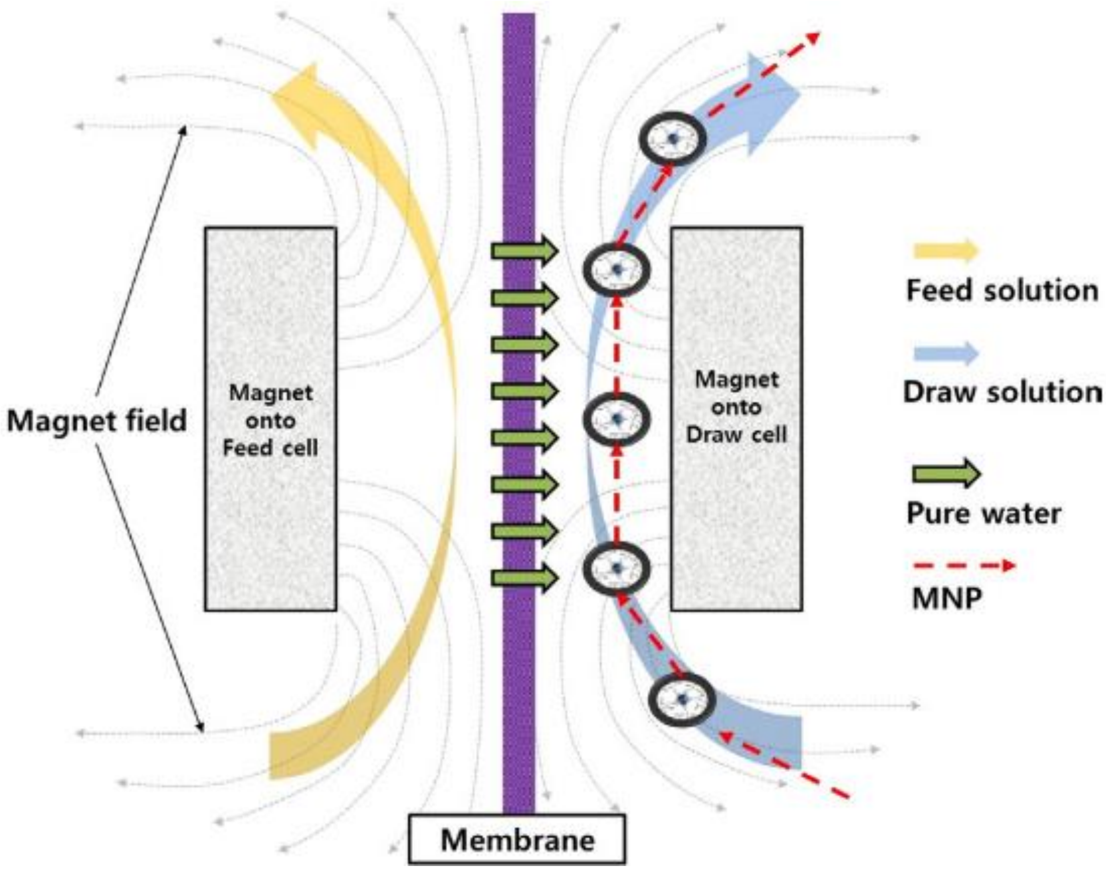

Figure 1.10 Schematic of the magnetic field control FO module designed by Na et al. 2014 to maximize the π of the draw at the membrane surface and prevent magnetite draw agents from fouling the FO membrane. Reproduced with permission from reference 110.

Table 1.9 Properties of selected FO magnetic particle draw agents.[†]

Draw Agent	Mass organic coating/ wt.%[‡]	π[*]	Flux/L/m^{2}h[**]	Recovery method
Fe_3O_4 nanoparticles	0	2.4 bar at 45 wt.% [185]	0.1 [200] DS: 2 wt.% FS: 1 wt.% NaCl	Magnetic field
SiO_2@MNP@PSA [138]	290	ca. 18 bar at 0.4 g/mL	-	Magnetic field
MNP@PSA [201]	37	9 bar at 7 wt.%	3.8 DS: 7 wt.% FS: DI water	Magnetic field
MNP@PSA [190]	60	11 bar at 0.078 wt.%	5.32 DS: 0.13 wt.% FS: DI water	Magnetic field
MNP@P(SA-NIPAM) [41]	76	25 bar at 0.067 w/v%	11.66 DS: 0.067 w/v% FS: DI water	Magnetic field + heat
MNP@PNIPAM-triethylene glycol [192]	38	-	ca. 1.6 DS:- FS: DI water	Not discussed
MNP@P(SSS-NIPAM) [202]	52.3	41 bar at 33	14.9	Magnetic field +

		wt.%	DS: 33 wt% FS: DI water 2.7 DS: 33 wt.% FS: seawater (1200 mOsm/kg NaCl)	70 °C; UF
MNP@P(NIPAM- sodium 2-acrylamido-2-methylpropane sulfonate) nanogel [203]	-	3.35 bar at 0.1 g/mL	0.65 DS: 0.1 g/mL FS: DI water	Magnetic field + 65 °C
MNP@Sodium citrate [110]	9.1	-	17.3 DS: 20 mg/L FS: DI water	Not discussed
MNP@Citric acid [197]	36.57	51 bar at 300 g/L	28.6 DS: 300 g/L FS: DI water 5 DS: 300 g/L FS: 3.5 wt.% NaCl	Not discussed
MNP@PEG$(COOH)_2$ [128]	23.6	74 bar at 0.065 M	13 DS: 0.13 M FS: DI water	Magnetic field (110V, 1.7 A)
MNP@Branched poly(deep eutectic solvent)* [204]	83.2	69 bar at 3.5 g/L	17.9 DS: 3.5 g/L	Magnetic field

			FS: DI water 8.5 DS: 3.5 g/L FS: 0.3 M NaCl	
MNP@Dextran [189]	78	-	ca. 3.6 DS: 0.5 M FS: DI water ca. 2.8 DS: 0.5 M FS: 2 g/L $MgSO_4$	Magnetic field
MNP@Pectin [200]	40	-	0.2 DS: 2 wt.% FS: 1 wt.% NaCl	Magnetic field
MNP@Gelatin [193]	52	1.5 bar at 27 g/L	1.54 DS: 27 g/L FS: DI water 0.62 DS: 27 g/L FS: 0.01 M NaCl	Magnetic field
MNP@SiO_2@Sodium alginate sulfate [205]	ca. 13	119 bar at 0.06 g/mL	12.8 DS: 0.06 g/mL FS: DI water 2.1	Magnetic field

DS: 0.06 g/mL

FS: 2 M NaCl

[†]This table is designed to illustrate the range of draw solutes reported in the literature, and to make preliminary observations. Note that π values may vary between reports depending on the method used to measure it (e.g., DMO, FPO, VPO). FO data may vary depending on many variables including the membrane (type and orientation) and scale used.

[‡]wt% = mass organic coating/mass magnetite x 100

[*] Note that FPOs have been used to measure the π of magnetite nanoparticles although this is not recommended by many manufactures.

[**]DS = draw solution, FS = feed solution, DI = deionized

[ǂ]deep eutectic solvent = branched polyglycerol-choline chloride

1.4 Objectives

The objective of this project was to develop CO_2-switchable draw solutes as an alternative to TMA. These draw solutes were designed with the following properties in mind: high water flux, easy removal from water, low viscosity, long term stability, low RSF, and low toxicity. Draw solutes in the form of polymers, gels, and polymer grafted magnetite particles were explored. The draw solutes were first synthesized and purified, then their fitness as a draw solute was assessed. Preliminary tests including measuring osmotic pressure, viscosity and FO performance were used to evaluate the diverse materials at the first stage of draw solute development.

Chapter 2

CO_2-Responsive Polymers

2.1 Introduction

CO_2-responsive materials are attractive FO draw solutes due to their ability to have a different π depending on the presence of CO_2. Although they have lower π than small molecule draw agents such as TMA, polymers are desirable draw solutes due to their greatly reduced RSF, odour and flammability. Such materials have promise for applications which require high purity products, such as the food and pharmaceutical industries [40]. The FO process with a CO_2-responsive polymer as a draw agent is illustrated in Figure 2.1. Ideally, solutions of these materials would have a low π_{air} to allow for easy filtration by UF separation from purified water, a high π_{CO2} to ensure high water flux from contaminated water, and low viscosity.

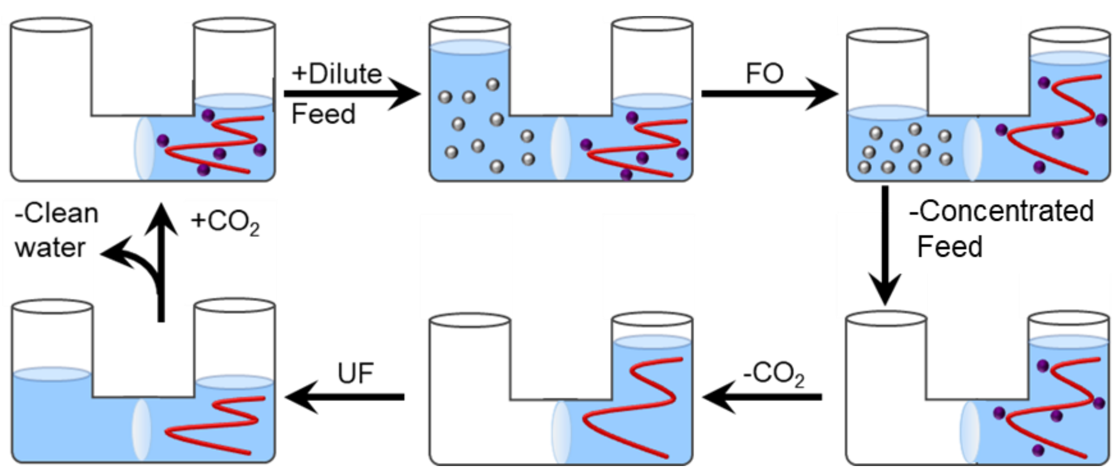

Figure 2.1 The FO-UF process with CO_2-switchable polymers. The red lines represent a CO_2-switchable polymer (▬), the filled circles represent bicarbonate anions (●), and the hollow circles (○) represent the contaminating solutes in the feed.

The Jessop and Cunningham groups previously considered CO_2-switchable polymeric draw solutes that are insoluble in water their neutral form (e.g., PDEAEMA), in an effort to facilitate the draw solute recycling; if the neutral polymer is insoluble in water, it can be removed by decantation rather than the more intensive filtration step (e.g., UF) required for soluble polymers. Although these insoluble polymers were more easily removed than soluble polymers, they either took long to redissolve in carbonated water (in the case of hard polymers), or were too difficult to handle (in the case of soft polymers). Future work focused on CO_2-switchable polymeric draw agents that remain water-soluble in their neutral form.

Water soluble CO_2-responsive polymers that are commercially available, or have commercially available monomers were tested (e.g., PDMAEMA, PDMAPMAm). Unfortunately, many of these polymers contain groups which hydrolyze over time. This produces small molecule amines which cannot be recovered by NF, and polymers which are no longer CO_2-responsive. Although this hydrolysis is very slow, hydrolysis is intolerable for a material that is designed to be reused multiple times. [206] In addition, all of these polymers had low π_{CO2}, and have relatively low solubilities in water which prevented high loadings.

The goal of this project was to synthesize CO_2-switchable polymeric draw solutes with high π_{CO2} while maintaining a low $\pi_{air.}$ It was hypothesized that the key to increasing the π_{CO2} exerted by a polymeric draw solute was to increase the number of bicarbonate anions present by increasing the number of protonatable nitrogen atoms per gram of polymer. The commercially available polymers have low nitrogen contents (8 wt.% for PDMAEMA), which be responsible for the low π_{CO2}. Increasing the nitrogen content was also expected to improve the polymer's solubility in water, which will further increase the number of bicarbonate anions present. This work investigated three potential CO_2-switchable polymers with high N:C ratios as FO draw solutes: linear poly(N-methylethyleneimine) (l-PMEI, 25 wt.% nitrogen), branched poly(N-methylethyleneimine) (b-PMEI, 25. wt.% nitrogen) and poly(N,N-dimethylallylamine)

(PDMAAm, 16 wt.% nitrogen) (Figure 2.2). One polymeric primary amine, poly(allylamine) (PAAm), and one polymer containing primary and secondary amines, branched poly(ethyleneimine) (b-PEI), were also evaluated for comparison.

In order to evaluate their potential as draw solutes, l-PMEI, b-PMEI and PDMAAm were synthesizes and rigorously purified, and their osmotic pressures were measured at various concentrations. The viscosity of the polymer solutions was also considered.

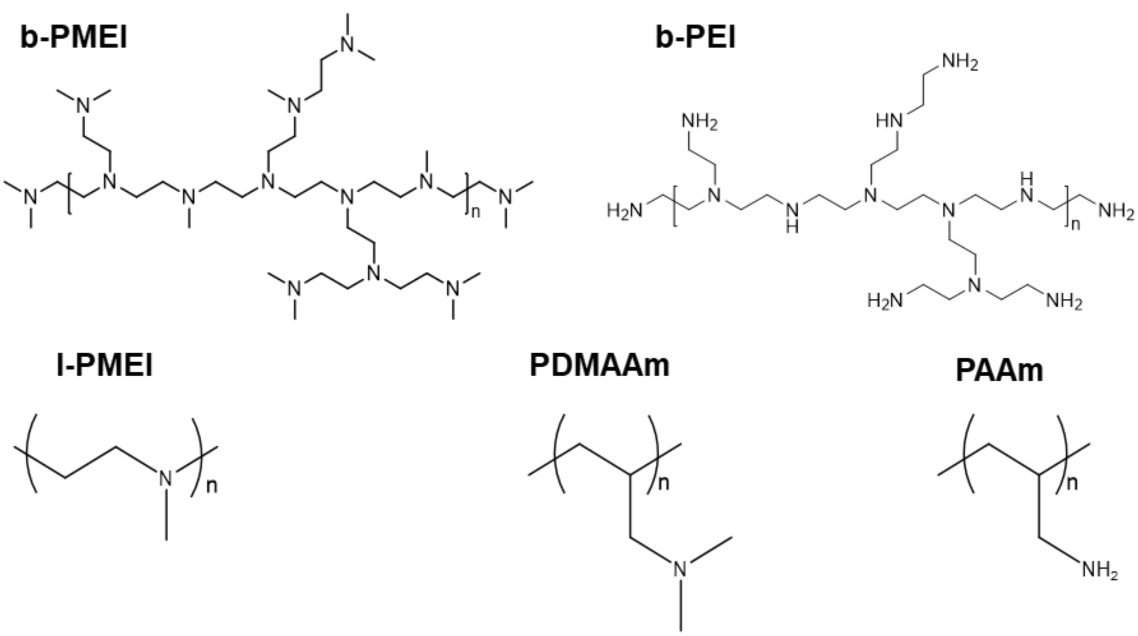

Figure 2.2 Structures of soluble CO_2-switchable polymers studied in this work

2.2 Materials and Methods

2.2.1 Materials

Chlorobenzene, 2-ethyl-2-oxazoline, methyltriflate, diisopropylamine, formaldehyde solution (37 % in water), sodium methoxide solution (35 %), chloroform, tert-dodecylmercaptan (trDDM), tetrahydrofuran, 4-methylmorpholine, lithium aluminum hydride powder, magnesium sulfate, and b-PEI were obtained from Millipore-Sigma and used as received. Poly(allylamine) (PAAm, 15 kDa) was obtained from PolyScience Inc. as a 15 wt. % solution. Poly(t-butylaminoethyl methacrylate) (PtBAEMA) (40 kDa) was obtained from Scientific Polymer Products, Inc. N,N-Dimethylacrylamide (DMA) was obtained from Millipore-Sigma, and was passed through an inhibitor removal column before use. 2,2′-Azobis(2-methylpropionitrile) (AIBN) was obtained from Millipore-Sigma and was recrystallized from ethanol before use. Diethyl ether, hexanes and methanol were obtained from ACP. Acetone, ethyl acetate, concentrated hydrochloric acid, and formic acid were obtained from Fisher Scientific. Sodium hydroxide pellets were obtained from Acros. Dialysis tubing (1 kDa, 3.5 kDa, and 10 kDa molecular weight cut off (MWCO)) was obtained from Thermo Scientific. Deionized water with a resistivity of 18.2 MΩ·cm was obtained from a Millipore Synergy system. CO_2 (Supercritical Chromatographic Grade, 99.998%, Praxair) was used as received.

2.2.2 Characterization

The polymers synthesized in this work were characterized by ^1H NMR spectroscopy, IR spectroscopy and GPC. ^1H NMR spectra were recorded at 298 K with a Bruker Avance 301 MHz NMR spectrometer. Fourier transform infrared (FTIR) spectra were collected on a Bruker Alpha FTIR base spectrometer using an ATR accessory over 500-4000 cm^{-1}.

IR spectroscopy was also used to monitor samples during carbonation. A Mettler Toledo ReactIR 15 IR spectrometer was used for these experiments over 600−2800 cm−1. Spectra were acquired every 1 min.

The GPC analysis of PDMAAm was performed using 0.3 wt. % LiBr and 0.3 M formic acid in HPLC grade water as the eluent. Samples were prepared at 1 mg/mL and passed through a 0.2 μm filter prior to injection. The samples were analysed on an Agilent triple detection GPC equipped with PSS NOVEMA Max Lux analytical and PSS NOVEMA Max Lux columns at 40 °C and 1 mL/min. The light scattering detector was calibrated using poly(2-vinylpyridine) standards. The dn/dc value (0.151) was measured by refractometry analysis using a Wyatt Optilab rEX refractive index detector.

The GPC analysis of poly(2-ethyl-2-oxazoline) (precursor to l-PMEI), was preformed using THF as the eluent. Samples were prepared at 4 mg/mL and passed through a 0.2 μm filter prior to injection. The samples were analyzed on a Waters 2695 separation module equipped with a Waters 410 differential refractometer and Waters Styragel HR (4.6 × 300 mm) 4, 3, 1 and 0.5 separation columns at 32 °C and 1 mL/min flow rate. The GPC was calibrated using PMMA monodisperse standards. Reported results are PMMA-equivalent molecular weights.

The GPC analysis of PDMAEMA, PDEAEMA and PDMAPMAm were preformed using 1mM LiBr in DMF as the eluent at 40 °C at 1 mL/min. A Viscotek GPCMax (4643) equipped one PSS GRAM 100 Å and two PSS GRAM 3000 Å columns. Polymers were detected with a Viscotek 302 differential refractive index detector. PMMA standards were used for calibration.

Kinematic viscosity was measured using a Cannon-Fenske type viscometer (tube size 200) at 25 °C. The pK_{aH} values of the polymers synthesized in this work were determined by titration. Polymer solutions were prepared at concentrations of 5-10 mg/mL and acidified to pH 3 with HCl. The solutions were stirred and titrated with 0.1 M NaOH solution to pH 12. The pH values were gathered using a Vernier pH sensor coupled to Logger Pro software.

The osmotic pressures of polymer solutions were measured at room temperature (23 ± 1 °C) using a DMO designed by Alessandro Grattoni [38], with Dow BW30 membranes. Detailed instructions for measuring π by DMO are provided in Appendix A. All reported π are gauge pressures. BW30 membranes are polyamide-thin film composites, with NaCl rejection of 99.5%, MWCO of ~100 Da and a pH range 2-11 (at 25 °C), suitable for brackish water [207]. The average error was 2% based on replicates. The polymers were rigorously lyophilized (using a Labconco FreeZone 6 Plus lyophilizer, 0.01 mbar, -60 °C) before taking the measurements to ensure that they were completely dry. Polymer solutions were carbonated at 1 atm by bubbling CO_2 through the solutions via a needle for a minimum of 5 h at room temperature.

2.2.3 Synthesis of CO_2-responsive polymers

2.2.3.1 l-PMEI

l-PMEI was synthesized in three steps: polymerization of 2-ethyl-2-oxazoline to form poly(2-ethyl-2-oxazoline), followed by hydrolysis of the amide bond to product l-PEI, followed by methylation of the secondary amine to produce l-PMEI (Figure 2.3). The procedure for the polymerization of 2-ethyl-2-oxazoline was based on reference 34.

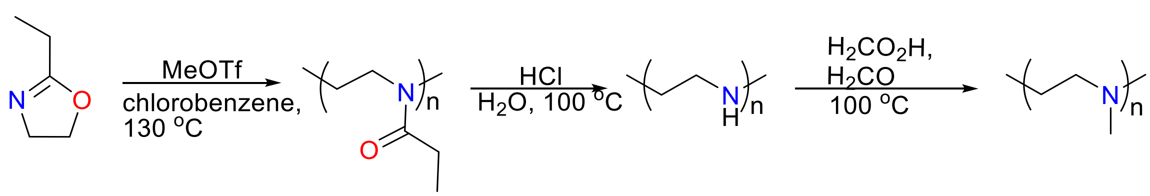

Figure 2.3 Synthetic pathway for l-PMEI.

To a flame dried 250 mL Schlenk flask was added chlorobenzene (120 mL) and 2-ethyl-2-oxazoline (30 mL). The solution was heated to 130 °C, and methyl triflate (80 µL) was added to the flask. The solution slowly turned from colourless to clear, dark orange. After 18 h, diisopropylamine (3 mL) was added, and the solution was stirred for an additional 4 h. The solution was cooled to room temperature, followed by dropwise precipitation in diethyl ether (cooled in an ice-water bath), yielding a yellow solid. The resulting poly(2-ethyl-2-oxazoline) was dried under vacuum.

Poly(2-ethyl-2-oxazoline) (25 g) was dissolved in concentrated hydrochloric acid (70 mL) in a 250 mL round-bottom flask. The resulting solution was refluxed for 18 h. The solution was dried under vacuum to dryness, producing linear poly(ethylenimine) as an orange solid.

The procedure for the methylation of l-PEI is based on reference 23. Linear poly(ethylenimine) (23 g) was added to a 500 mL round-bottomed flask equipped with a stir bar. The polymer was dissolved in formic acid (170 mL) and 37 % aqueous formaldehyde solution (160 mL). The solution was refluxed for 48 h. The volatiles were completely removed under vacuum followed by the addition of one equivalent of concentrated hydrochloric acid. The solution was stirred for 30 min, then all volatiles were completely removed under vacuum. The solid was dissolved in 20 wt. % sodium hydroxide solution (100 mL). The water was then removed under vacuum. The resulting poly(N-methylethylenimine) crude product was dissolved in chloroform (100 mL) and vacuum filtered to remove the salt by-product. The solvent was removed from the filtrate under vacuum.

The final linear poly(N-methylethenimine) product was purified by dialysis (3.5 kDa MWCO tubing) against MilliQ water. The polymer was dissolved in a minimal volume of water, placed in sealed dialysis tubing and immersed in 3.5 L of water. The water was exchanged ten times, after a minimum residence time of 4 h per exchange. The ^{1}H NMR spectrum matched the spectrum reported in reference 35 and is included in Appendix B. ^{1}H NMR (300 MHz, D_2O, δ ppm): 3.31 (4.0H, CH_2NCH_2), 2.49 (3.0H, CH_3N). GPC (THF): M_w = 25 kDa, M_n = 8.9 kDa, Đ = 2.8. pK_{aH} = 7.4 ± 0.2.

2.2.3.2 b-PMEI

b-PMEI was produced by methylating and dialysing commercial branched-PEI using the same procedure described above for linear-PEI (Figure 2.4).

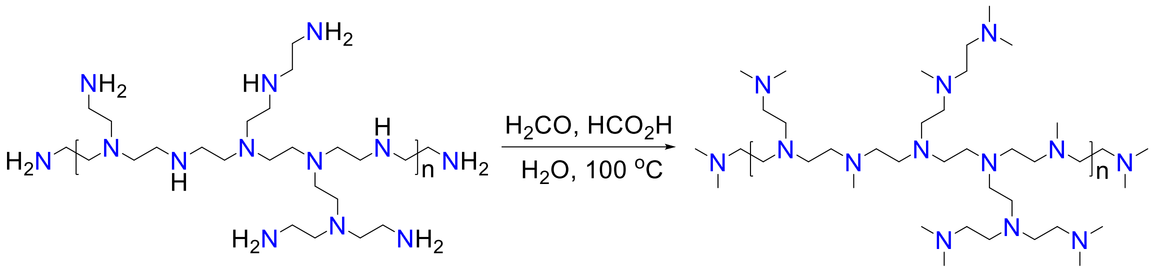

Figure 2.4 Synthetic pathway for b-PMEI.

The [1]H NMR spectrum matched the spectrum reported in reference [210] is included in Appendix B. [1]H NMR (300 MHz, $CDCl_3$, δ ppm): board multiplets: 3.4-2.9, 2.8-2.4, 2.4-2.0. Molecular weight (estimate based on data reported by manufacturer): M_w = 33 kDa, M_n = 13 kDa, Đ = 2.5, pK_{aH} = 7.6 ± 0.2.

2.2.3.3 PDMAAm

PDMAAm was synthesized in two steps: polymerizing DMAA to PDMAA, followed by the reduction of the amide to produce PDMAAm (Figure 2.5).

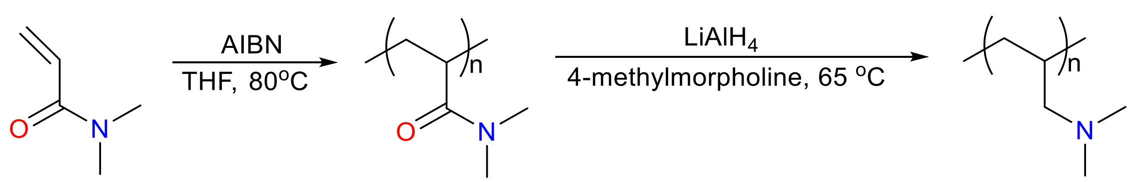

Figure 2.5 Synthetic pathway for the synthesis of PDMAAm.

DMA (20 ml), AIBN (0.428 g, 0.029 mol/l, 2.14 % per weight of monomer) and trDDM (1 wt. % relative to monomer) were dissolved in toluene (70 mL) and added to a 250 mL flame dried Schlenk flask. The mixture was purged with argon and heated to 70 °C, with stirring at 500 rpm. After 6 h, the flask was cooled to room temperature. The resulting polymer was purified from residual monomers by triple precipitation into hexanes and dried in a vacuum oven at 50 °C for 24 h.

A flame dried 500 mL three neck round-bottom flask was equipped with a stir bar. The three necks of the flask were connected to a condenser, a Schlenk line and a septum. The flask was evacuated and refilled with argon three times. Lithium aluminum hydride (pellets, 3.85 g) were added to the flask and dispersed in 4-methylmorpholine (80 mL). The mixture was heated to 65 °C. PDMA (10 g) was dissolved in 4-methylmorpholine (100 mL) in a 250 mL round-bottom flask. The PDMA solution was added dropwise to the $LiAlH_4$ solution by syringe via the septum, with strong stirring (>700 rpm). After 20 h, THF (35 mL) was added dropwise by syringe via the septum. After another 20 h, the flask was cooled in an ice bath and deionized water (4 mL) was added dropwise, followed by 15 wt. % sodium hydroxide solution (5 mL) and then more water (10 mL). The flask was warmed to room temperature and stirred until the precipitated polymer dissolved. Anhydrous magnesium sulfate was added until it clumped at the bottom of the flask. The solid phase was removed by gravity filtration and extracted twice with ethyl acetate. The solvent was removed from the filtrate under vacuum. The polymer was then re-dissolved in ethyl acetate, the solution centrifuged, and the supernatant transferred to a new flask and evaporated to dryness. The resulting poly(N,N-dimethylallylamine) was dissolved in water and purified by dialysis (3.5 kDa MWCO tubing). The ^{1}H NMR and IR spectra are included in Appendix B. ^{1}H NMR (300 MHz, D_2O, δ ppm): 2.20 (8.0H, $CH_2N(CH_3)_2$), 1.75-0.80 (3.0H, CH_2CH). GPC (water, 0.3 wt.% LiBr + 0.3 M formic acid): M_w = 12.4 kDa, M_n = 10.7 kDa, Đ = 1.2. pK_{aH} = 7.72 ± 0.06.

2.2.3.4 PDMAEMA

PDMAEMA was synthesized by free radical polymerization of DMAEMA. DMAEMA was passed through a column of basic alumina. A Schlenk flask was purged with argon three times. DMAEMA and THF (x3 volume of monomer) were added to the flask, which was heated to 65 °C with magnetic stirring (500 rpm). AIBN (1 mol% to monomer) was added to the flask, and the solution was stirred overnight. The solution was cooled to room temperature, then precipitated dropwise into ice-cold hexanes. The solid polymer was removed and dried under vacuum at 60 °C overnight. The ^{1}H NMR spectrum matched the spectrum reported in reference 211. ^{1}H NMR (300 MHz, $CDCl_3$, δ ppm): 4.05 (2.0H, $\mathit{CH_2}CO_2$), 2.55 (2.1H, $\mathit{CH_2}N$), 2.25 (6.0H, $(\mathit{CH_3})_2N$); 2.0-0.75 (5.0H, $\mathit{CH_2}C\mathit{CH_3}$). GPC (1 mM LiBr in DMF): M_n = 23 kDa, Đ = 1.5.

2.2.3.5 PDEAEMA

PDEAEMA was synthesized in the same way as PDMAEMA, with the substitution of DEAEMA for DMAEMA. The ^{1}H NMR spectrum matched the spectrum reported in reference 212. ^{1}H NMR (300 MHz, $CDCl_3$, δ ppm): 3.7 (1.7H, $\mathit{CH_2}CO_2$), 2.0-2.4 (6.6H, $\mathit{CH_2}N$), 1.2-1.6 (1.6H, $\mathit{CH_2}CCH_3$); 0.75-0.25 (9.0H, $CH_2C\mathit{CH_3}$, $CH_2(\mathit{CH_3})_2$). GPC (1 mM LiBr in DMF): M_n = 348 kDa, Đ = 1.8.

2.2.3.6 PDMAPMAm

PDMAPMAm was synthesized by free radical polymerization of DMAPMAm. DMAPMAm was passed through a column of basic alumina A Schlenk flask was purged with argon three times. DMAPMAm and toluene (x3 volume of monomer) were added to the flask, which was heated to 65 °C with magnetic stirring (500 rpm). AIBN (3 mol% to monomer) was added to the flask, and the solution was stirred overnight. The solution was cooled to room temperature, then precipitated dropwise into ice-cold hexanes. The solid polymer was removed and dried under vacuum at 60 °C overnight. The ^{1}H NMR spectrum matched the spectrum reported in reference 21. ^{1}H NMR (300 MHz, $CDCl_3$, δ ppm): 7.50 (0.8H OCN*H*), 3.45 (2.0H, CH_2CON), 2.4 (2.0H, $CH_2N(CH_3)_2$), 2.25 (6.0H, $N(CH_3)_2$, 1.8-0.75 (6.8H, CH_2CCH_3, $CONCH_2CH_2CH_2$-N). GPC (1 mM LiBr in DMF): M_w = 20 kDa, Đ = 4.0.

2.3 Osmotic Pressure of CO_2-Responsive Polymers

Before testing the osmotic pressures of carbonated solutions, carbonated water was placed in the osmometer to ensure that it did not contribute significantly to the osmotic pressure. No osmotic pressure was detected. This may be because the amount of CO_2 in carbonated water is relatively low (0.03 M (25 °C, 1 bar) [10]) or the CO_2 can pass through the membrane.

2.3.1 Osmotic Pressures of Tertiary vs Primary and Secondary Amines

The CO_2 switchable polymers studied in this work were designed to have a high π_{CO2}. In order to maximize the $\pi_{air:}$ π_{CO2}, this work focused on tertiary amines. Primary and unhindered secondary amines form carbamates in carbonated water in addition to bicarbonate salts [213]. It was expected that carbamate formation would not cause a large increase in osmotic pressure as it does not change the number of species in solution (Figure 2.6). This theory was confirmed by measuring the π_{CO2} of the primary and secondary amine precursors of the polymers studied in this work: (PAAm) for PDMAAm and b-PEI for b-PMEI (Table 2.1). It was revealed that the tertiary amine polymers have higher π_{CO2} than their primary and secondary counterparts. PAAm contains just primary amines while b-PEI contains 1:2:1 primary: secondary:tertiary amines. A higher proportion of the amines are expected to be protonated in b-PEI compared to PAAm. All the amines studied in this work were methylated to form tertiary amines, which will not form carbamates.

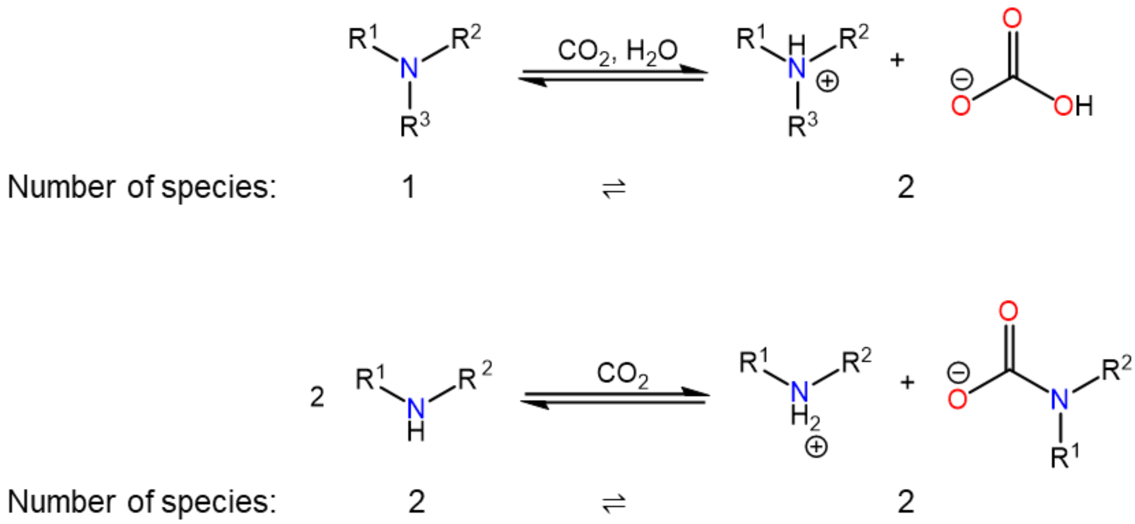

Figure 2.6 The effect of carbamate vs bicarbonate formation on the number of species in solution.

Table 2.1 Osmotic pressures under CO_2 of tertiary vs. primary/secondary amines polymers at 20 wt% loading in water.

Amine Degree	Polymer	$\pi_{CO2}{}^{*}$/bar
Primary	PAAm	3.6
Secondary	b-PEI	11.0
1:2:1 Primary: Secondary: Tertiary	b-PMEI	15.0
Tertiary	PDMAAm	19.5

* Gauge pressure

2.3.2 Effect of Oligomers on Osmotic Pressure

Dialysis was performed on each polymer sample to remove residual small molecules such as salts, monomers and oligomers. This was necessary as these species could artificially increase π_{air}. Low molecular weight chains amount to a small percentage of the total polymer content by mass but may represent a significant amount by number. Removing them can significantly reduce the π_{air}. This was highlighted by the difference in π_{air} of samples dialyzed with MWCO tubing.

Samples of PDMAAm were dialyzed with 1, 3.5, and 10 kDa MWCO dialysis tubing, and their π_{air} values were measured at 20 wt. % (Table 2.2). The π_{air} decreases with larger MWCO due to the greater removal of low molecular weight chains. Using a higher MWCO dialysis tubing for shorter periods of time was found to be more effective at reducing π_{air} than using smaller MWCO tubing for longer periods of time, but the solutions made with samples dialyzed with larger MWCO were noticeably more viscous. Based on these results, it is clear that the pressure, and therefore energy, required to remove a polymeric draw solute may be reduced by removing low M_w chains.

Table 2.2 Effect of dialysis tubing MWCO on osmotic pressure of PDMAAm.[†]

MWCO/ kDa	$\pi_{air,\ 20\ wt.\%}$ [*]/ bar
1	2.5
3.5	1.8
10	0.8

[†]All measurements were taken at 20 wt. % in deionized water. The dialysis time was the same for all three samples.

[*]Gauge pressure

2.3.3 Osmotic Pressures of CO_2-Responsive Polymeric Draw Solutions

2.3.3.1 l-PMEI

The relationship between osmotic pressure and l-PMEI concentration is presented in Figure 2.7.a. Note that the wt.% or weight fraction of polymer refers to the concentration of polymer in the uncarbonated state. The trend of π_{air} vs concentration of PMEI resembles that of PEI and PEG, reported previously [36,214]. The highest π_{CO2} measured in this work was 67 bar at 30 wt. %, which is high enough to be promising for desalination, being 2.5 times higher than the osmotic pressure of the common benchmark seawater (27 bar). Unfortunately, l-PMEI also exhibits high π_{air} (26 bar at 30 wt. %), making it likely too energy intensive to remove from clean water by UF. On average, the π_{CO2} is 2.5 times higher than the π_{air} at high loadings, an insufficient ratio for industrial applications.

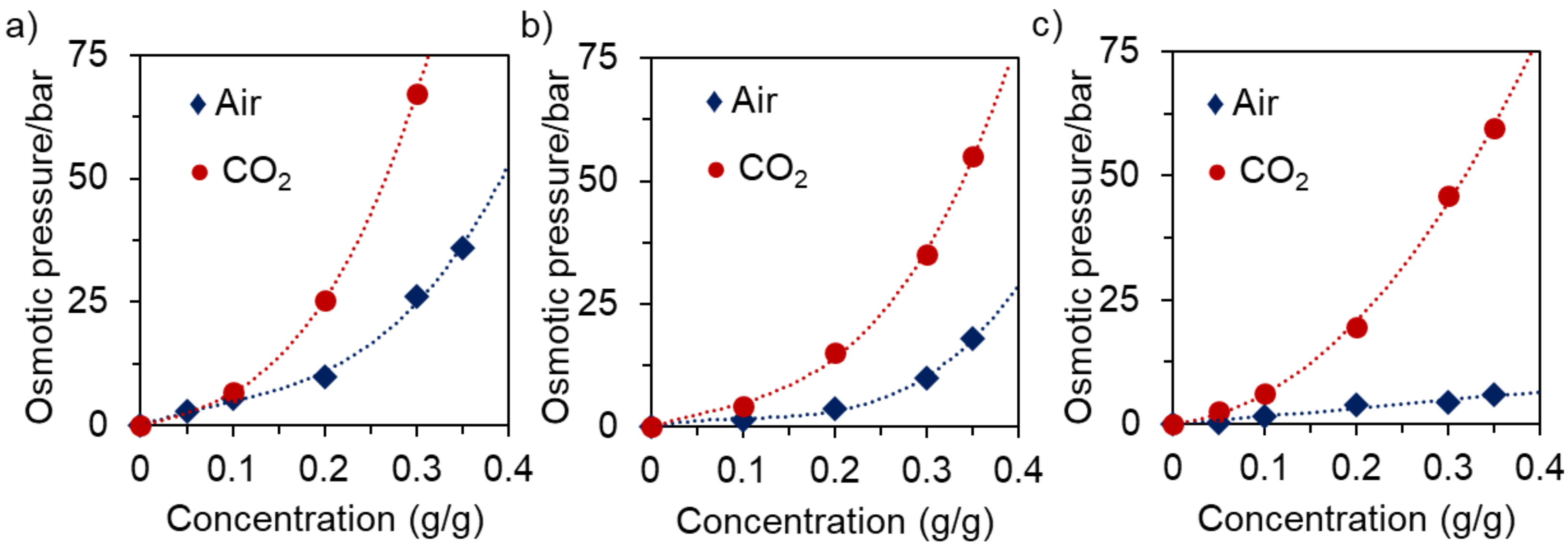

Figure 2.7 Osmotic pressures (gauge) in air (blue) and CO_2 (red) for each of the tertiary amine polymer solutions in deionized water tested: (a) l-PMEI, (b) b-PMEI and (c) PDMAAm. The concentration (g/g) refers to the concentration of solutions prior to carbonation. The dotted trendlines are fitted 3rd order polynomial curves.

2.3.3.2 b-PMEI

The relationship between osmotic pressure and b-PMEI concentration is presented in Figure 2.7.b. Branching was expected to reduce both the π_{air} and reduce the viscosity. In fact, branched-PMEI exhibited lower π_{air} and π_{CO2} than l-PMEI. On the other hand, the π_{CO2} : π_{air} for b-PMEI is 3.5, which is significantly higher than that of l-PMEI. The π_{air} remains high enough to be prohibitive for FO.

The difference in π_{air} and π_{CO2} between l- and b-PMEI could potentially be attributed to their different molecular weights, percent protonations, or structures. However, while the branched and linear PMEI had different molecular weights (M_w = 33 and 25 kDa respectively), both polymers also had large dispersities, making the difference less significant. Furthermore, previous work has shown that the effect of molecular weight on osmotic pressure becomes less significant with higher molecular weights. Given that l- and b-PMEI have similar pK_{aH} values, the difference in osmotic pressure is not due to different degrees of protonation. Rather, the difference in π_{air} and π_{CO2} may be attributed to differences in the polymer structures. Branching results in smaller hydrodynamic radii compared to their linear counterparts of the same molecular weight, resulting in lower π_{CO2} and π_{air} [36,215].

It is worth noting that the π_{CO2} values of b-PMEI reported in this work are 20-30 % lower than the osmotic pressure of protonated b-PEI reported in previous work [7,214]. A lower degree of protonation would result from using a weaker acid (hydrated CO_2) as opposed to the HCl used in previous work [7]. Unlike HCl, CO_2 can be used to switch the polymer between the protonated and neutral states without accumulating salts but has the disadvantage of achieving a lower degree of protonation of the polymeric amine.

2.3.3.3 PDMAAm

The relationship between osmotic pressure and PDMAAm concentration is presented in Figure 2.7.c. In contrast to the previous polymers, PDMAAm has an exceptionally low π_{air}, and high π_{CO2}:π_{air} of 10 between 30-35 wt. % loading in water. The π_{CO2}:π_{air} increases with polymer loading. At 35 wt.%, PDMAAm exhibited a π_{CO2} of 59.7 bar and a π_{air} of 6.0 bar. Preliminary FO tests with PDMAAm were performed and are discussed in Chapter 3. Briefly, a 30 wt.% PDMAAm draw solution produced an initial flux of 30 L/m^{2}h from a 1.75 wt.% NaCl feed solution (Appendix C, Figure C6), indicating that PDMAAM can produces high fluxes from concentrated feeds. Additionally, uncharged PDMAAm is thermo-responsive, which can facilitate the removal of the polymer from purified water [143]. The thermo-responsive behavior of PDMAAm is discussed further in Chapter 3.

The lower π_{air} exhibited by PDMAAm compared to l-PMEI may be caused by the polymer's percent protonation by water under air, its structure and/or its hydrophilicity. Although PDMAAm has fewer nitrogen atoms per gram of polymer compared to l-PMEI, the amines it contains are more basic, and consequently have a higher degree of protonation. However, the pK_{aH} values for PDMAAm, l-PMEI and b-PMEI are all relatively low (<8) and their concentrations are relatively high. The percent protonation of all polymers under air is calculated to be less than 1% at the concentrations studied in this work.

Differences in polymer structure may also be relevant; the nitrogen in PDMAAm is more accessible to protonation (being a pendant off the backbone) than the nitrogens in both l- and b-PMEI, which are hindered by the polymer backbone. Additionally, PDMAAm has a lower N:C ratio than PMEI (1:5 vs. 1:3 respectively) and is consequently less hydrophilic than PMEI. This decrease in hydrophilicity can be noted by the polymer's higher log P values (Table 2.3). This decreased hydrophilicity could lower the $\pi_{uncharged\ polymer}$, and therefore the π_{air} of PDMAAm compared to PMEI. This illustrates the balance that must be achieved in the N:C ratio; too low a ratio may give a low π_{CO2}, but too high a ratio risks an excessively high π_{air}.

Table 2.3 Calculated log P values† of studied polymers in their neutral form.

Polymer‡	Log P	Monomer	Log P
PEG	-0.11	EG	0.59
PMEI	2.01	MEI	1.18
PDMAAm	5.89	DMAAm	2.03

† LogP values were calculated using ALOPGS 2.1 software [215].

‡LogP values calculated for a decamer with methyl end groups.

One remaining limitation of PDMAAm as a draw solute is viscosity, which increases substantially above 25 wt. % (Figure 2.8 Dependence of kinematic viscosity on the concentration of aqueous solutions of PDMAAm under air or CO_2 at 25 °C.Figure 2.8). Low viscosity is an essential property of a draw solution [40]. High viscosities can reduce flux, increase concentration polarization, and increase the energy required to pump the draw solution through the FO apparatus. The viscosity of PDMAAm could be reduced by introducing a degree of branching [216] and/or reducing its molecular weight (currently 12.4 kDa). Reducing molecular weight leads to low viscosity but increased π and RSF. At this stage, no attempt was made to optimize the molecular weight of any of the polymers. The ethylene oxide-propylene oxide copolymer draw agent used by Trevi Systems has a molecular weight of ca. 2 kDa [217], indicating that there is significant room to reduce the molecular weight of PDMAAm. While reducing the molecular weight of PDMAAM will increase its π_{air}, its thermo-responsive properties can facilitate its removal (Responsivity 3.3.2).

In order to facilitate the study of PDMAAm on a larger scale a safer synthetic pathway is required. The PDMAAm described in this chapter was synthesized using lithium aluminum hydride, which is extremely pyrophoric, and would be difficult and hazardous to use on a large scale. The alternative pathway proposed in Figure 2.9 eliminates the use of flammable organic solvents or pyrophoric reagents. Full details of the synthesis can be found in Appendix B, and reference 52.

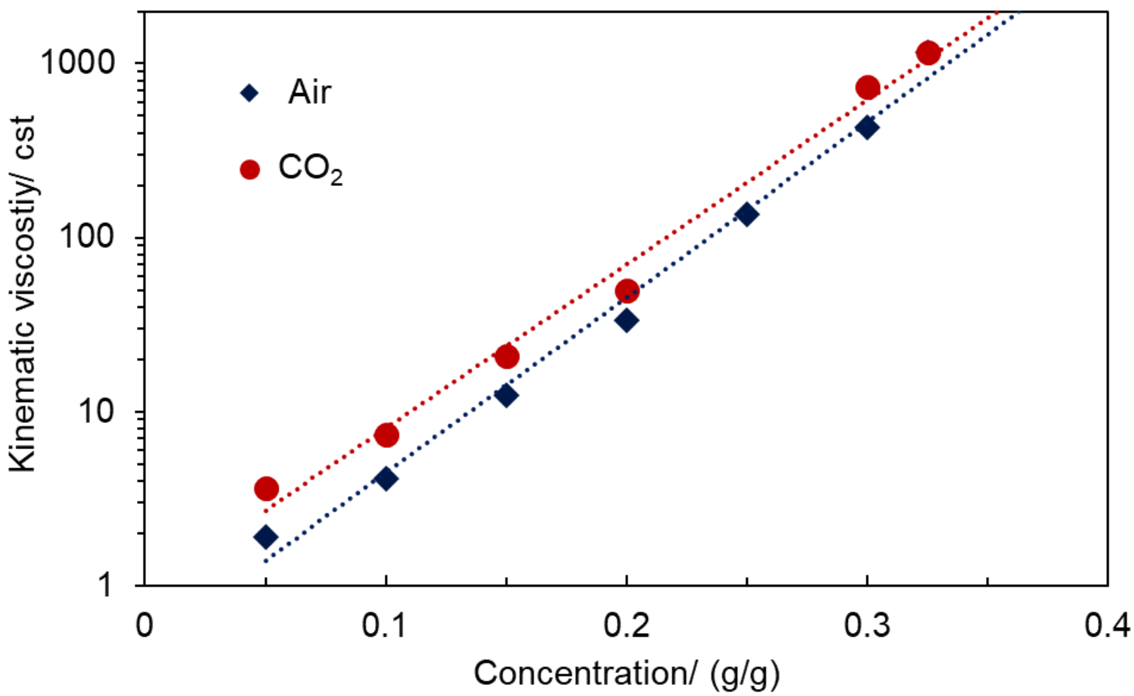

Figure 2.8 Dependence of kinematic viscosity on the concentration of aqueous solutions of PDMAAm under air or CO_2 at 25 °C.

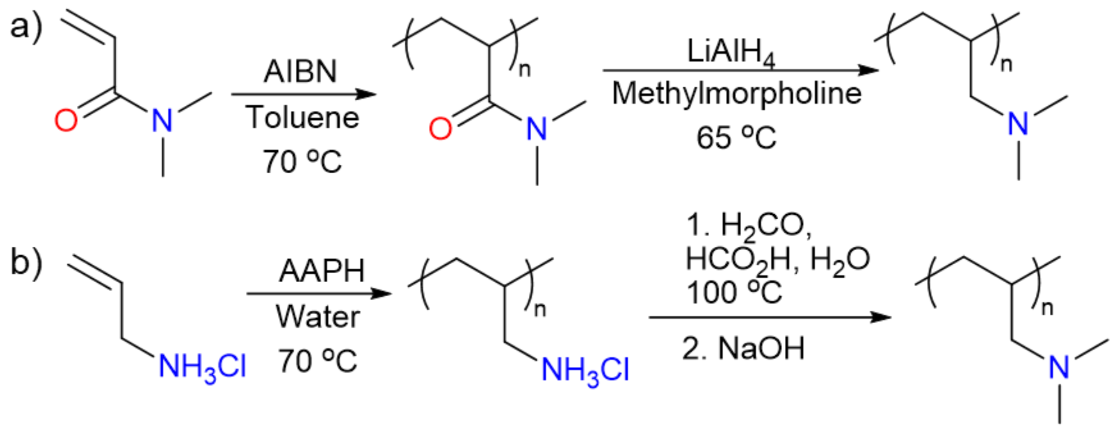

Figure 2.9 a) Current and b) alternative synthetic pathway for PDMAAm.

In addition to optimizing its molecular weight, the π_{CO2} of PDMAAm could be increased by applying a modest pressure of CO_2. The effect of CO_2 pressure on the percent protonation of PDMAAm is presented in Figure 2.10 (obtained using equations described in reference 7); at 20 wt.%, the precent protonation of PDMAAm increases by ca. 26% when the pressure is increased from 1 bar to 5 bar. Increasing percent protonation is expected to lead to an increase in π_{CO2}. The benefits of a higher π_{CO2} must be balanced with increased costs of a high-pressure FO apparatus.

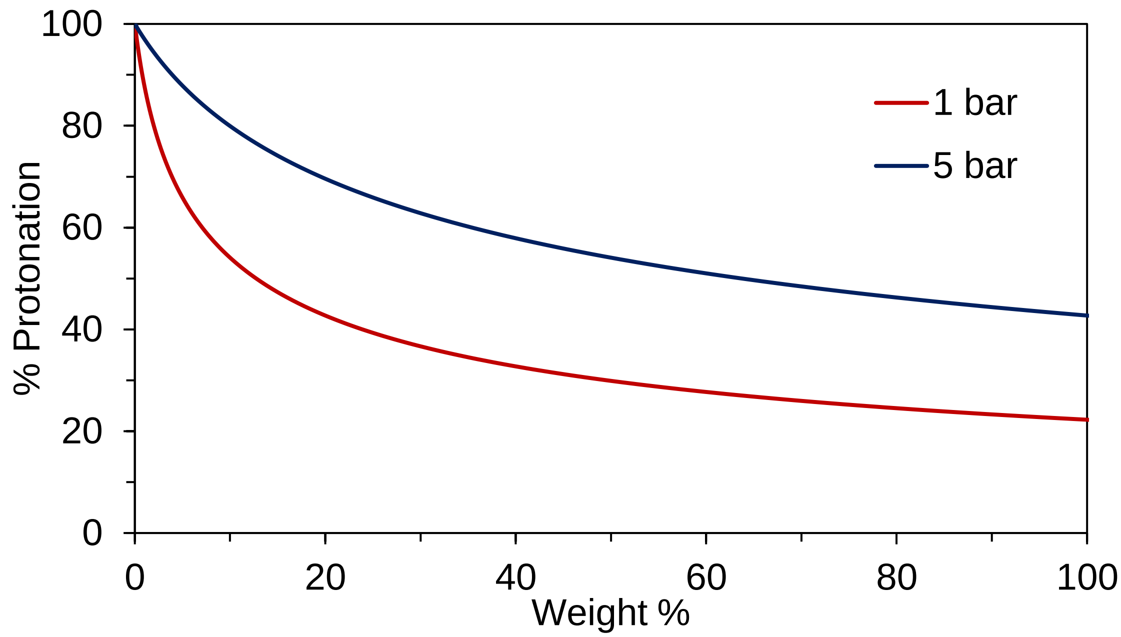

Figure 2.10 Effect of CO_2 pressure on the % protonation of PDMAAm as a function of concentration.

2.3.3.4 Contribution of the Polymer Chain to the Total Osmotic Pressure

In order for a draw solute to be practical and effective, a high π_{CO2} is essential. It is worth noting that as the concentration of the polymer increases (and consequently the pH of the solution), the percent protonation of the polymer will decrease. This phenomenon is illustrated in Figure 2.11 where the measured osmotic pressures of l-PMEI and PDMAAm are plotted alongside the bicarbonate concentration. It is clear that the osmotic pressure is not increasing proportionally with the bicarbonate concentration and must be therefore dominated by the protonated polymer chain.

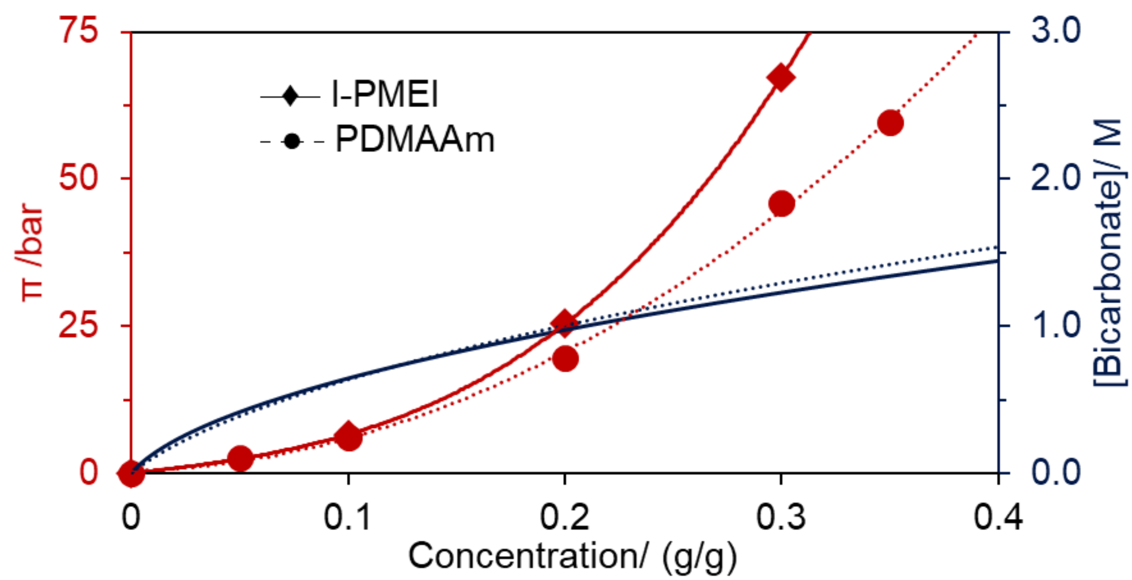

Figure 2.11 Measured π_{CO2} (gauge pressure, red) and the concentration of bicarbonate (blue), for l-PMEI (solid lines) and PDMAAm (dashed lines).

A rudimentary estimate of $\pi_{bicarbonate}$ can be calculated from the concentration of bicarbonate present [7], and the Lewis equation (equation 1.2) [36]. At all concentrations, the measured π_{CO2} is less than the calculated $\pi_{bicarbonate}$. Intriguingly, the observed pH values of the solutions were close or equal to the predicted pH values (see Appendix B, Table B1). This indicates that, while the number of bicarbonates predicted from theory are indeed being formed, those bicarbonate anions are not producing as high a π_{CO2} as expected. One possible explanation for this is that the bicarbonates may be engaged in intermolecular interactions, which would reduce the π_{CO2}. Examples of these interactions include strong ionic bonding between the bicarbonate and the cationic amine, bicarbonate hydrogen bonding with unprotonated amines, and bicarbonate dimerization. The latter is akin to the decreased osmotic pressure of benzoic acid in solution due to the dimerization of carboxylic acids units [33]. Dimerization and strong ionic attraction may be similarly enhanced within the relatively non-polar environment of the polymer coil. It is expected that this effect is enhanced with polymeric amines, as the amines are fixed close together by the polymer backbone.

2.4 Basicity and Osmotic Pressure

The polymers discussed so far have relatively low pK_{aH} values, the highest being PDMAAm at 7.72 ± 0.06. The percent protonation of an amine can be calculated using equations derived from the simultaneous acid-base equilibria, as outlined in reference 7. Using these equations, it was discovered that the percent protonation of b-PMEI, l-PMEI, and PDMAAm at the higher concentrations studied in this work (30-40 wt.%) are all relatively low (less than or equal to 50%). Higher degrees of protonation, and therefore osmotic pressures, could be reached if the polymers were more basic. However, a balance must be maintained in order to ensure the percent protonation under air remains low (Figure 2.12).

Figure 2.12 Effect of pK_{aH} on the % protonation of an amine as a function of concentration. Assuming a molecular weight of 100 g/n, and 1 atm of CO_2.

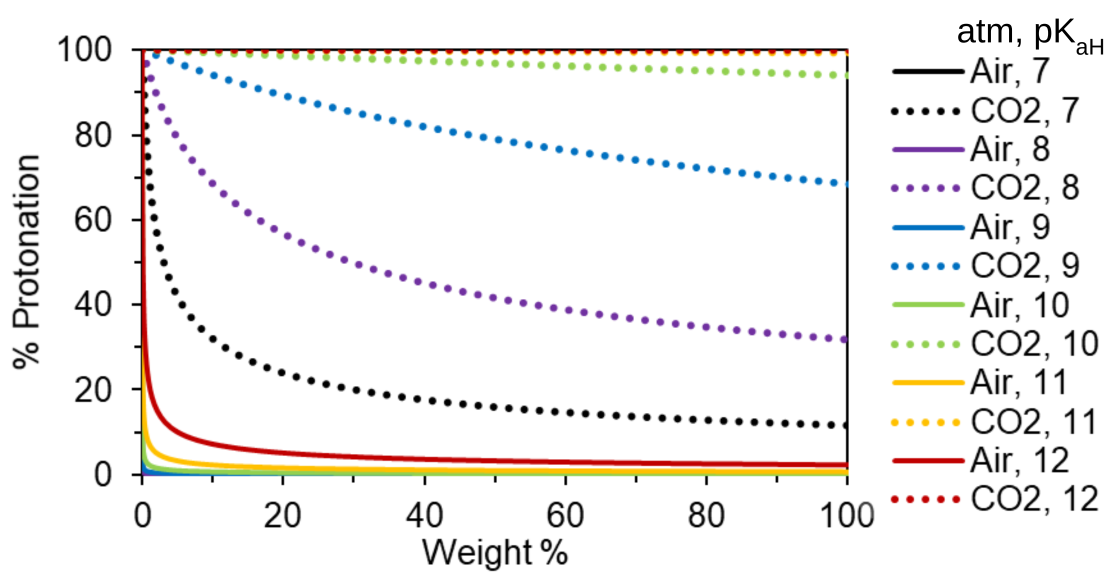

It was hypothesized that secondary amines, being more basic than tertiary amines, would have a higher degree of protonation, and therefore have a higher osmotic pressure. Bulky secondary amines will form bicarbonates rather than carbamates due to steric hinderance [16,147]. The osmotic pressure of PtBAEMA, a commercially available bulky secondary polymeric amine, was tested. Although the pK_{aH} of PtBAEMA has not been measured to date, the

pK_{aH} of its monomer tBAEMA is known to be 9.12 [218]. The pK_{aH} of PtBAEMA is therefore expected no lower than one unit less that of tBAEMA. The π_{CO2} of PtBAEMA at 20 wt.% is significantly lower than its tertiary amine isomer, PDEAEMA (Table 2.4). The difference between these two polymers may be due to the presence of the N-H bond in PtBAEMA, which can hydrogen bond more strongly with bicarbonates and decrease the π_{CO2}.

Table 2.4 Comparison of π_{CO2}^{*} of PtBAEMA and PDEAEMA.

Polymer	pK_{aH}	$\pi_{CO2,\ 20\ wt.\%}$ / bar	$\pi_{CO2,\ 30\ wt.\%}$/ bar
PtBAEMA	est. 8.1	6.5	11.1
PDEAEMA	6.9-7.5 [26]	14.8	-

* Gauge pressure

2.5 Osmotic Pressure under CO_2 of Polymeric Draw Solutes at Reduced Temperatures

In order for the draw solutes described in this chapter to be used industrially, their performance must be stable with temperature. It is known that the solubility of CO_2 in water decreases with increasing temperature, which would be undesirable for the FO process. The effect of lower temperatures is less clear; while the solubility of CO_2 in water and the pK_{aH} of the amine increases, the pK_{a1}^{*} of CO_2 decreases and pK_w increases. To explore the effect of temperature, the π_{CO2} of various CO_2-switchable polymer solutions were measured at 20 °C and 4 °C. The measurements at 4 °C were conducted in a cold room maintained at 4 °C. The solutions were carbonated in an ice-water bath, and the osmometer was cooled to 4 °C before the solution was injected into it. The π_{CO2} of the CO_2-switchable polymer solutions at 4 °C were found to be comparable to those measured at room temperature (Table 2.5). This demonstrates the robustness of the CO_2-switchable polymer draw solute system. Being able to operate at lower temperatures may be advantageous when processing feeds which are prone to spoilage (e.g., juices). The effect of temperature on π_{air} for thermo-responsive polymers will be discussed in section 3.3.3.

Table 2.5 π_{CO2}^{*} of CO_2-responsive polymers at 20 wt.% with varying temperature.

Polymer	pK_{aH}	$\pi_{air,\ 25\ °C}$	$\pi_{CO2,\ 25\ °C}$	$\pi_{CO2,\ 4\ °C}$
PDMAPMAm	8.8 [219]	2.5	13.6	13.5
PDMAEMA	7.4 [219]	1.2	11.5	11.4

* Gauge pressure

2.6 Conclusions

Polymeric draw solutes with high N:C ratios were synthesized, and their osmotic pressures were measured to evaluate their promise as FO draw solutes. We have shown that increasing the nitrogen content in CO_2-switchable polymers can produce π_{CO2} values exceeding 60 bar. The π_{air} can be reduced by removing short chains and other low molecular weight impurities. Preliminary results indicate that it is vital to balance the hydrophobicity of the polymer with a high number of protonatable amines, to maintain a high ratio of π_{CO2}: π_{air}. PDMAAm exhibits high π_{CO2} while maintaining low π_{air}. This polymer may prove to be an effective forward osmosis draw solute for feed streams which have medium to low osmotic pressures and require high purity products.

Chapter 3

CO_2- and Thermo-Responsive Gels

3.1 Introduction

Hydrogels have attracted attention as draw agents for forward osmosis due to their low toxicity, low reverse salt flux (draw solute crossing the membrane into the feed) and high capacity to absorb water. A diverse range of hydrogel draw agents have been reported in the literature (Table 1.8). However, hydrogel draw agents are limited by concentration polarization and trading off the apparently contradictory requirements of high flux during osmosis and facile water recovery during regeneration.

Hydrogels made from hydrophilic materials (e.g., PSA) produce high fluxes due to their high π, but consequently also require energy intensive methods to recover water from the draw agent post-filtration (e.g., mechanical or gas pressure) [127,170]. To facilitate their recovery, hydrophilic materials have been combined in a gel with more hydrophobic materials (e.g., PNIPAM) [41,87,220,221]. However, incorporation of the hydrophobic component resulted in a decrease in water flux. Rather than achieving both a high flux and easy recovery, combining a high π and low π material results in a compromise between the two competing requirements. In response, stimuli-responsive hydrogel draw agents have been designed which, upon application of a trigger (e.g., heat, pH, electricity, light), can switch between a hydrophilic state having a high π, and a hydrophobic state which is easily separated from water due to being hydrophobic or having a low π.

Thermo-responsive materials that absorb water below a specific temperature and release water above that temperature have been developed, and showed improved water recovery [168]. This temperature is referred to as the lower critical solution temperature (LCST) for soluble polymers, and volume phase transition temperature (VPTT) for gels. Common thermo-responsive draw agents (e.g., PNIPAM) do not produce sufficiently high fluxes alone due to their inadequate hydrophilicity [127,173].

CO_2-responsive draw solutes have been designed to produce a high π_{CO2} and a low π_{air}. CO_2-responsive PDMAEMA microgel draw agents produced high initial fluxes against saline feeds, but water was recovered from the microgels only by purging with nitrogen gas and centrifugation, both of which are costly on an industrial scale [150]. Superabsorbent CO_2-responsive hydrogels based on PMEMA have been synthesized, with a focus on producing very high swelling ratios (up to 800) [222]. However, the % of water release upon decarbonation was only 70%, and high swelling ratios do not guarantee high flux. Indeed, PMEMA is a very weak base (pK_{aH} = 4.9 [223]) and has a low π_{CO2} (1.2 bar at 20 wt.%, see Table C1, Appendix C); its ability to pull water across the membrane is expected to be low.

Combining CO_2-responsiveness with thermo-responsiveness in a single draw agent may enhance the difference between the water-absorbing and water-releasing states of the draw agent. Dual CO_2- and thermo-responsive PDMAEMA was used by Cai et al. as a dissolved draw agent, where the thermo-responsive property was used to facilitate the removal of the polymer [143]. In Chapter 2 PDMAAm was identified as a promising dual CO_2- and thermo-responsive dissolved draw agent, as it possesses a high π_{CO2} while maintaining a low π_{air}, even at high concentrations [52,224]. This chapter further explores the thermo-responsive properties of PDMAAm, and the performance of a PDMAAm hydrogel draw solute.

3.2 Materials and Methods

3.2.1 Materials

Poly(allylamine) (PAAm) (15 kDa, 15 wt.% aqueous solution) was obtained from PolySci Inc. Formaldehyde (37% aqueous solution), poly(diallyldimethylammonium chloride)

(PDADMAC) (typical molecular weight 400-500 kDa, 20 % solution), PNIPAM (M_w = ~40 kDa) and methanol (HPLC grade, >99.8) were obtained from Sigma-Aldrich and used as received. Formic acid (99%) was obtained from Alpha Aesar, hydrochloric acid (36.5-38.0% aqueous solution) was obtained from Fisher, and sodium hydroxide flakes (98%) were obtained from Acros Organics. All the water used in this study was deionized by a Synergy MilliQ system and had a resistivity of 18.2 MΩ/cm before exposure to air. Carbon dioxide (grade 3.0) and argon (grade 5.0) were obtained from Praxair. Dialysis tubing with a 3.5 kDa molecular weight cut off was obtained from VWR.

3.2.2 Methods

3.2.2.1 Characterization

IR spectra were obtained with an Agilent Technologies Cary 630 TRIR IR spectrometer with an ATR attachment from 600-4000 cm^{-1}. $^{13}C\{^1H\}$ NMR spectra were acquired using a 600.17 MHz Bruker Avance spectrometer in the solid state and using a 700.40 MHz Bruker spectrometer in solution. Gel fractions were obtained by Soxhlet extraction. Samples of gel (0.5-1 g) were extracted with methanol in glass fiber thimbles over one week. After extraction, the samples were dried under vacuum at 50 °C for 24 h.

The water content of the swollen gels was determined by TGA (TA Instruments, Q-500). Samples of gel were heated on platinum pans under a flow of argon (10 mL/min) from 25 °C to 120 °C at 10 °C/min followed by a 20 min isothermal step to completely remove water and carbon dioxide.

The thermal behaviour of soluble PDMAAm polymer was analysed by DSC (TA Instruments, Q-100). Solutions (3-8 mg) were hermetically sealed in aluminum pans, which were heated from 20 °C to 50 °C at 2 °C/min. The cloud point was taken from the onset temperature of the heating curve.

Osmotic pressures were measured using a DMO [38] with Dow BW30 RO membranes (purchased from Sterlitech). All reported π are gauge pressures. The final π was recorded after the pressure remained unchanged for 30 min. Measurements above 20 °C were obtained by placing the DMO in a temperature-controlled water bath (Canon Instrument Company CT-500 series II). Measurements below room temperature were obtained by placing the DMO in a refrigerator. Detailed instructions for measuring π by DMO are provided in Appendix A.

3.2.2.2 Synthesis of PDMAAm Gel

An aqueous solution of poly(allylamine) (PAAm, 15 wt.%) was stirred in a round bottom flask. Formic acid (2.0 equivalents) was added, immediately followed by formaldehyde (3.0 equivalents, 37 wt.% aqueous solution). The solution was heated at 100 °C for 1 day. Afterwards, the solution was cooled to room temperature, and dried under reduced pressure. The solid was dissolved in hydrochloric acid (1.1 equivalent, 0.1 M) solution, which was stirred for 10 min and then dried under reduced pressure. The resulting product was dispersed in water and then NaOH (10 wt.%) in water was added dropwise until the pH was 13. The solid gel was then washed with deionized water over a vacuum filter until the pH of the permeate was neutral. Residual salts and soluble polymer were separated from the gel by dialysis (3.5 kDa molecular weight cut off). The resulting gel was dried at 60 °C overnight then ground into a powder with a mortar and pestle. ATR IR (ν cm^{-1}): 2716-2950 (C-H stretch); 1453 (H-CH_2 bend); 1035, 1263 (C-N bend). ^{13}C $\{^1H\}$ NMR (600 MHz, solid state, δ ppm): 66 ($(CH_3)_2$-N); 44 (CH_2-N), 29-37 (CH_2-CH).

Uncrosslinked PDMAAm (M_w = 16 kDa, Đ = 1.2) was prepared as described in reference 224.

3.2.2.3 Procedure for FO

FTS H2O cellulose triacetate FO flat sheet membranes were obtained from Sterlitech. The membranes were cut into circular disks (2.5 cm diameter, 4.9 cm^2 surface area) and soaked in the feed solution for a minimum of 1 h prior to use. The draw agent was prepared by carbonating a gel containing a known amount of water (1 g total mass of swollen gel) overnight. FO tests were carried out using a glass u-tube apparatus (Appendix B, Figure B1). The draw side was kept under an atmosphere of CO_2. In this apparatus, the membrane is horizontal with the draw agent place on top of the membrane and the feed solution below, with the active side of the membrane facing the feed. The feed solution (50 mL) was continuously stirred at 700 rpm, and the top of the feed solution was kept approximately level with the membrane. The concentration of the feed solution was monitored using a conductivity probe that had been previously calibrated with NaCl standard solutions (Thermo Scientific Orion 013005MD). The volume lost by the feed was calculated from the change in concentration of the feed over time. Flux (equation 1.6) is defined as the volume of water (V, in L) transferred across a given area of membrane (A, in m^2) over a given amount of time (t, in h). Initial fluxes are reported after 2 min. Due to the small size of the apparatus the reported fluxes are not considered to be numerically representative of what will occur on a large scale, but rather are reported to indicate trends in time or between samples.

3.2.2.4 Procedure for Swelling Ratio

Swelling ratio (SR, equation 3.1) quantifies how much water a gel absorbed in one specific state (e.g., under air at 20 °C), and is defined as:

$$SR = {(M_{swollen} - M_{dry})}/{M_{dry}} \qquad 3.1$$

where $M_{swollen}$ is the mass of the swollen gel and M_{dry} is the mass of the dry gel. The change in swelling ratios (QSR, equation 3.2) compares the swelling ratios between two different states (e.g., under air at 20 °C vs under air at 60 °C):

$$QSR = {}^{SR_{state\ 1}}/_{SR_{state\ 2}} \tag{3.2}$$

To measure the SR, the masses of the swollen and dried gels were measured. Gels were swollen in excess water, and deswollen in air. To swell the gel, a known mass of deswollen PDMAAm gel (1-5 mg) was placed in a vial containing 20 mL deionized water under an atmosphere of either air or CO_2 and left to equilibrate for 4 h. For samples that were carbonated, the carbonation was achieved by bubbling CO_2 through the water via a needle for a minimum of 4 h. When the SR was measured at elevated temperatures, the vial containing the gel was first equilibrated at room temperature, then heated to the desired temperature and left to equilibrate again for 4 h. After equilibration was complete, the gel was removed from the excess water by gravity filtration and immediately weighed. Excess surface water was removed prior to weighing by lightly shaking the gel, and rolling it across dry filter paper.

To deswell the gel, the swollen gel was transferred to a glass fritted filter in air, which was placed in a glass jar (to limit evaporation). Depending on the method of deswelling, the jar was placed in an oven at 60 °C or simply left at room temperature. As the gel contracted, the released water passed through the frit and collected in the bottom of the jar. After the gel had fully contracted, the gel was recovered from the top of the frit and weighed, and the released water was recovered from the jar. The percent of water released (equation 3.3) is defined as the weight of water released (W_R) divided by the weight of water in the swollen gel (W_{WG}):

$$\%\ Water\ Released = {}^{W_R}/_{W_{WG}} \times 100 \tag{3.3}$$

3.3 Results and Discussion

3.3.1 Gel Synthesis and Characterization

The PDMAAm gel (g-PDMAAm) was synthesized via a one-pot methylation and crosslinking of PAAm (Figure 3.1). The methylation was achieved with an Eschweiler-Clarke reaction with formaldehyde and formic acid. Formaldehyde also serves as a crosslinking agent between primary amines, creating aminal linkages [225]. The successful completion of the methylation was verified by comparing the IR and $^{13}C\{^{1}H\}$ NMR spectra of g-PDMAAm to PAAm and soluble PDMAAm (Appendix C, Figure C2).

After the methylation, the broad N-H stretching peak at 3300 cm^{-1} in the IR spectrum disappeared, and all peaks sharpened due to the elimination of strong hydrogen bonding within the polymer (Appendix C, Figure C2.a). The IR spectra of g-PDMAAm and soluble PDMAAm show the same characteristic peaks, at the same intensities, notably the sharp C-N stretching peaks between 1260-1020 cm^{-1}. The $^{13}C\{^{1}H\}$ NMR spectra of the soluble polymer and gel PDMAAm show the same main peaks, including the appearance of the broad methyl peak at 66 ppm, indicative of methylation (Appendix C, Figure C2.b).

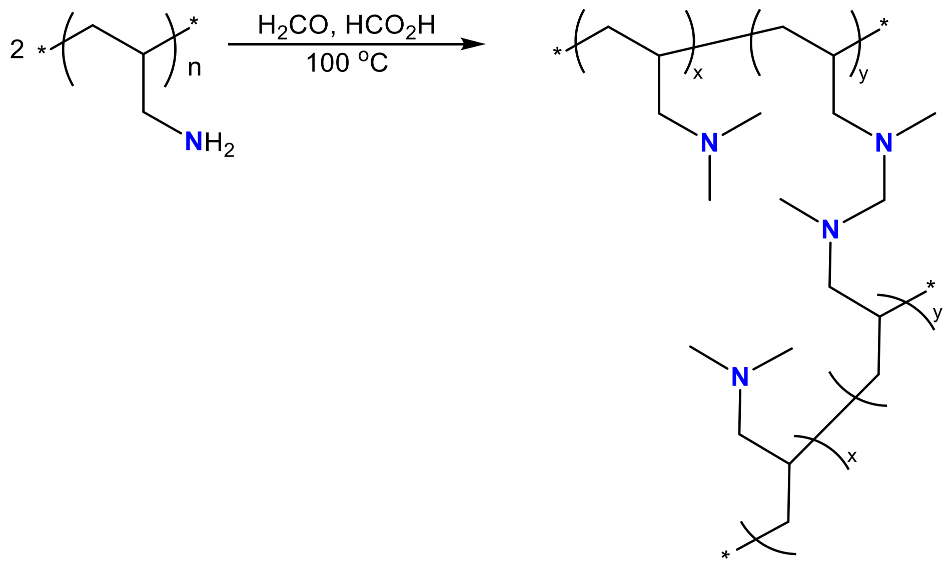

Figure 3.1 Synthetic pathway for the crosslinking of g-PDMAAm.

No attempt was made to control the degree of crosslinking in g-PDMAAm. In the simple procedure used in this work, the order and speed the reagents were added are key to producing a gel with a high swelling ratio rather than a soluble polymer. In future work, to achieve a desired degree of crosslinking, a targeted number of amines in PAAm could be protected by protonation with a stoichiometric amount formic acid. Upon addition of formaldehyde the unprotonated units would rapidly crosslink. This material could then be immediately methylated via the Eschweiler-Clarke reaction. Alternatively, PAAm gels could be produced by crosslinking during the polymerization of allylammonium chloride, followed by methylation to produce g-PDMAAm. This method would allow for higher control of the degree of crosslinking.

The soluble polymer fraction was extracted from the gel to ensure only crosslinked chains remained. The gel fraction was determined to be 98 wt.% via Soxhlet extraction, which demonstrates that the crosslinking was successful. The crosslink density could not be determined however, as this requires knowledge of the Flory polymer-solvent interaction parameter, which is not available in the published literature for this polymer with either water or carbonated water. Due to its low concentration the aminal linkage could not be detected by traditional characterization methods such as NMR or IR spectroscopy or elemental analysis. However, due to g-PDMAAm's large swelling capacity, it can be assumed that the degree of crosslinking is neither high enough to impede its performance as a draw agent, nor low enough to be detrimental to its physical and chemical stability, which is all that is required for its current purpose.

As the draw agent must be able to be reused many times, the gel must remain intact over multiple uses. Some aminals are not stable in acidic media [226]. Although the pH inside the gel will likely never be below 7, the gel will be exposed to carbonated water. The stability of g-PDMAAm in acid was investigated by soaking the gels in carbonated water for one week at room temperature. The water was evaporated and the gel fraction of the solid was found to be 99 wt.%, indicating that the crosslinks are resistant to degradation under the conditions the gel will be exposed to during the FO process.

3.3.2 Responsivity

3.3.2.1 Thermo-Response

The thermal behaviour of soluble PDMAAm in uncarbonated water was investigated by DSC (Appendix C, Figure C3). Above a specific temperature, the interactions between PDMAAm chains become more favourable than the interactions between PDMAAm and water. For a soluble polymer, this temperature is referred to as a cloud point and above it the polymer's solubility in water will decrease. For a gel, this temperature is referred to as a VPTT and above it the gel will contract. The cloud point is dependent many variables, such as the polymer concentration, molecular weight, salt concentration and pH. Although the LCST could not be determined (due to the high solution viscosity above 50 wt.%), the lowest cloud point detected was 23.9 °C at 50 wt.%. This is lower than the LCST of PNIPAM (31-33 °C) and PDMAEMA (32-53 °C) [211,227]. Carbonated PDMAAm, like other CO_2-responsive polymers (e.g., PDMAEMA [143]), does not exhibit thermo-responsive behaviour.

To study the thermo-responsive behaviour of g-PDMAAm isolated from its CO_2-responsive properties, g-PDMAAm was swollen in water at 20 °C and deswollen on a glass frit by heating to 60 °C, all under an atmosphere of air. In non-carbonated water at 20 °C, g-PDMAAm exhibits a SR of 74±7. Under these conditions, the amines have a low degree of protonation but the polymer retains a degree of hydrophilicity due to the polar amine groups. When the gel is warmed to 60 °C in water under an atmosphere of air, g-PDMAAm is above its VPTT, and rapidly adopts a contracted configuration with greatly reduced interactions with water. The SR in this state is consequently greatly reduced (SR = 0.04±0.01). Deswelling can be achieved even when the gel is heated in water rather than in air (SR = 2±1). Due to the dramatic degree of deswelling, there is a large change between the swollen and deswollen states produced using just heat as a trigger (QSR = 1850). However, as PDMAAm has a low π_{air} it will likely be unable to produce a high flux if used as a draw agent under air. It is therefore advisable to also take advantage of the CO_2-responsiveness [224].

The effect of temperature on the SR of g-PDMAAm under air was investigated further (lower line in **Figure 3.2**). The SR does not change significantly between 20-40 °C, then decreases from 50-60 °C until nearly all the water was expelled and the SR approaches 0.

3.3.2.2 CO_2-Response

To study the CO_2-responsive behaviour of g-PDMAAm unaffected by the thermo-responsive characteristics, g-PDMAAm was swollen in water under an atmosphere of CO_2 and deswollen on a glass frit by exposure to an atmosphere of air, at a constant temperature (20 °C).

In carbonated water at 20 °C, g-PDMAAm exhibits a SR of 198.5±0.5. Under these conditions, the amines in the gel are protonated by the carbonated water and the gel is consequently highly hydrophilic and the π within the gel has increased. The SR under CO_2 is not significantly affected by temperature (upper line in Figure 3.2). The protonated form of PDMAAm (both soluble polymer and gel) is not thermo-responsive. When deswollen on a glass frit under an atmosphere of air at 20 °C, the swelling ratio is reduced (SR = 65±8), but is still high as the polymer is still relatively hydrophilic in its neutral form. Consequently, when using just CO_2 as a trigger, the carbonated gel was able to absorb a large volume of water but the gel only releases two thirds of the water simply by removing the CO_2, resulting in a low QSR of 3. The deswollen gel still retains so much water that if it were recarbonated and reused as a draw agent, it would likely have a low π_{CO2} and consequently low flux.

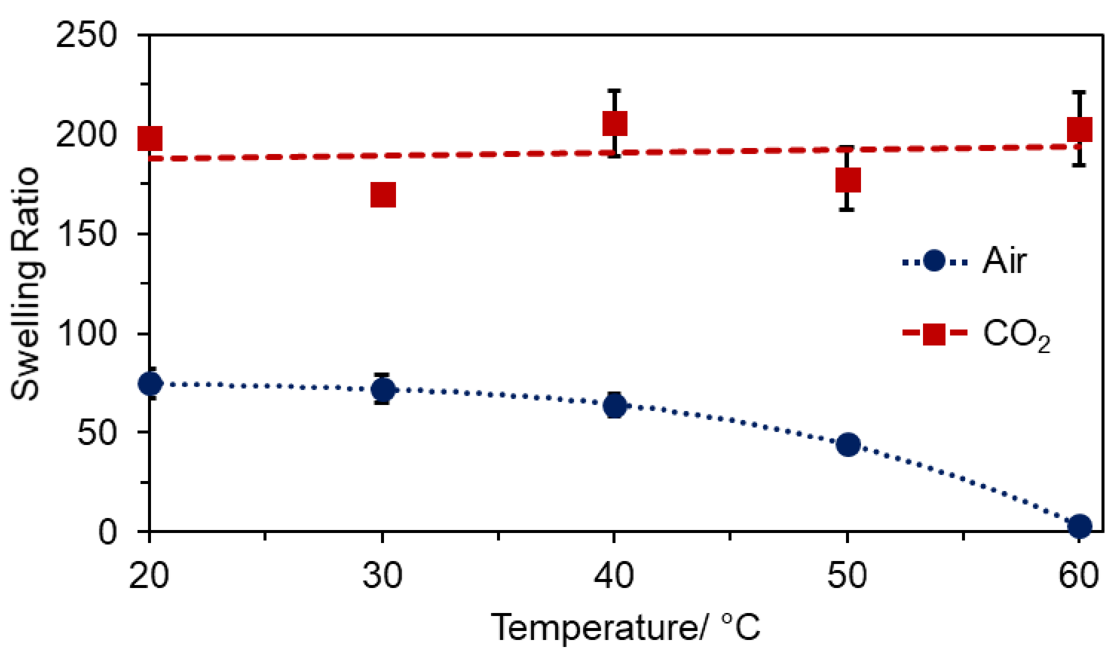

Figure 3.2 Effect of temperature and atmosphere on the SR of g-PDMAAm. Gels were swollen in water under various atmospheres (air or CO_2 at 1 bar of absolute pressure) and temperatures

(20-60 °C). To guide the eye, the CO_2 points are connected by a linear trendline while the air points are connected by a 3rd order polynominal curve.

3.3.2.3 Combined CO_2- and Thermo-Response

To study the combined effect of CO_2 and heat as triggers, g-PDMAAm was swollen in water under an atmosphere of CO_2 at 20 °C and deswollen on a glass frit under an atmosphere of air at 60 °C. When both CO_2 and heat are used as a trigger g-PDMAAm can both absorb and release large volumes of water (Figure 3.3). Using both stimuli unites the high water absortivity of a CO_2-responsive material and the easy recovery of a thermo-responsive material, resulting in an exceptionally high QSR of 4960. The charged, carbonated polymer is hydrophilic and exerts a high π_{CO2}, while the contracted polymer over its VPTT has reduced interactions with water and is able to release 99.9% of the water it as absorbed.

The rate of draw agent regeneration is an important metric of draw agent success. The rate of release of water from g-PDMAAm was explored by monitoring the amount of water released from carbonated g-PDMAAm over time. After 20 minutes of submersion in 60 °C water, the SR of g-PDMAAM carbonated at room temperature decreased by 68%.

Many gels reported in the literature combine a permanently hydrophilic monomer and a themo-responsive monomer to balance a high π and high water release [41,172,183]. However, the hydrophilic component can limit the water released, and the thermo-responsive component is often hydrophobic and does not greatly contribute to the π [228]. Using a dual responsive polymer such as PDMAAm ensures that the whole gel is contributing to both a high π_{CO2} and an easy recovery.

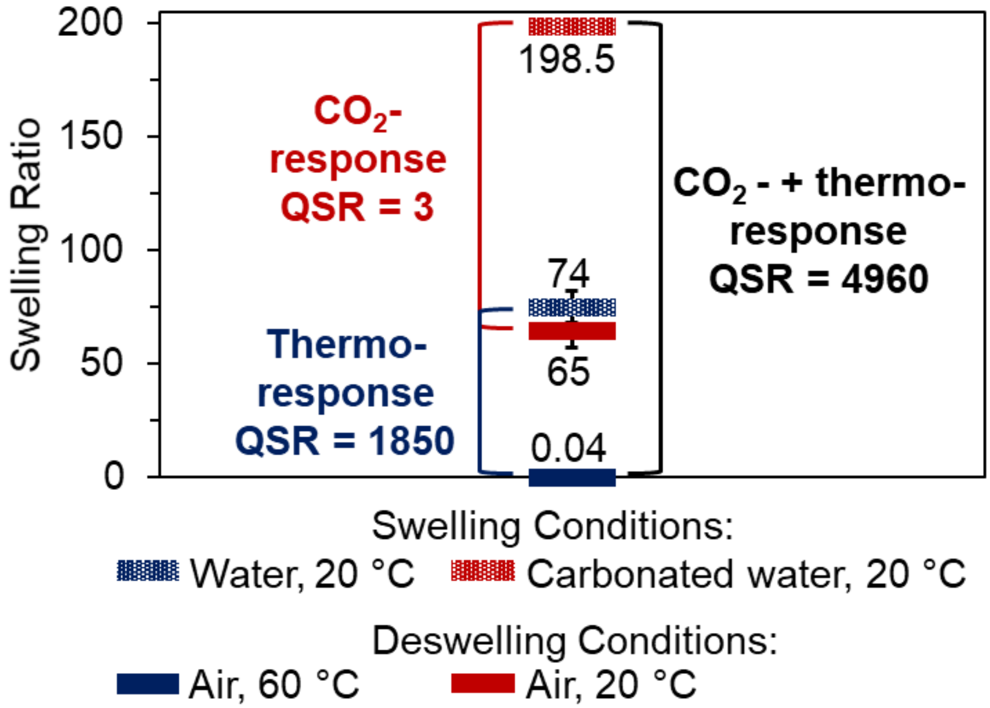

Figure 3.3 Swelling ratios of g-PDMAAm obtained in water (under an atmosphere of air or water) or air (at 20 or 60 °C).

The temperature required for the thermal trigger (ca. 60 °C) can be obtained as waste heat from industrial processes, thereby reducing the energy costs of the FO process. Furthermore, heat has already been proposed as a method to remove CO_2 from CO_2-responsive draw solutions post-filtration [84,120,224]. Therefore, no additional energy or steps needs to be added to regenerate the g-PDMAAm compared to other CO_2-responsive agents.

3.3.3 Exploring the Relationship Between CO_2- and Thermo-responsiveness in Hydrogels

Temperature can influence a dual CO_2- and thermo-responsive system not only via the cloud point/VPTT, but by influencing the degree of protonation of the amine under both air and CO_2. The differences in the properties of a CO_2-responsive material under air and CO_2 are due to the difference in the percent protonation in each state. A CO_2-responsive amine will be protonated to some degree in water, depending on its concentration, pK_{aH}, as well as the temperature and pressure. Increasing temperature affects the percent protonation of any amine under air by decreasing pK_w and pK_{aH}. When CO_2 is present, increasing temperature also decreases the solubility of CO_2 in water, and (to a lesser extent) decreases the effective pK_a of hydrated CO_2, which decreases the degree of protonation [7].

Temperature will further alter the percent protonation of a thermo-responsive amine by altering its concentration. Above its cloud point/VPTT, a hydrated thermo-responsive polymer contracts. As a CO_2-responsive polymer contracts, the amine becomes more concentrated within the polymer coil or gel network. When the amine becomes more concentrated, its percent protonation decreases, and with it the polymer's hydrophilicity. Thermo-responsivity can have a positive effect on CO_2-responsivity by increasing the difference in percent protonation, and thereby properties, between the two states.

For example, increasing temperature generally decreases the acceptable pK_{aH} range of a CO_2-responsive amine due to increased protonation under air [7]. Using a thermo-responsive material can allow for more basic (higher pK_{aH}) amines to be used at higher temperatures. In addition, at low concentrations, the percent protonation of a traditional amine may be high under air as well as CO_2, as was the case in reference 222. However, the percent protonation under air could be decreased by using a thermo-responsive amine at an elevated temperature.

Varying the temperature is expected to have a significant effect on the π of thermo-responsive materials, in addition to changes in the % protonation of the amine. To investigate this further, the π_{air} of thermo-responsive (soluble PDMAAm and PNIPAM) and non-thermo-responsive (PDADMAC) polymer solutions were measured with varying temperature (Figure 3.4). While soluble polymers rather than hydrogels were used (as the DMO can only measure liquid samples), the fundamental principles discussed here can be applied to both soluble and crosslinked polymers. The π_{air} of PDADMAC increases very slightly with temperature, as expected from the van't Hoff equation. Intriguingly, the π_{air} of PDMAAm decreases with temperature. Commonly used thermo-responsive material PNIPAM exhibited similar behaviour (Appendix C, Figure C4). For conventional materials, solute-water interactions (and therefore π) usually increase with temperature. The decrease in π_{air} with temperature observed with thermo-responsive PDMAAm and PNIPAM is likely due to decreased polymer-water interactions. π_{CO2} of CO_2-responsive polymers is not significantly affected by temperature (Appendix C, Table C1). A negative relationship between π and temperature has been previously noted for dextran, which is not considered to be thermo-responsive [229,230].

Decreasing π_{air} with increasing temperature has special significance for draw agents. The removal of the draw agent can be facilitated even by heating the draw agent below its cloud point, by the reduction in π_{air}. In some cases this may be more desirable than heating the draw solution above its cloud point, as the resulting solid polymer may have undesirable physical properties or take a long time to redisperse. While 17 wt.% PDMAAm at 25 °C exhibits a low π_{air} and is therefore already easily removed from water, the increase in π_{air} from 25 °C to 4 °C is significant (45%). This phenomenon may become more important at higher concentrations. It may also have more significance for other thermo-responsive draw agents which have higher π_{air} and LCSTs than PDMAAm (e.g., PDMAEMA, LCST = 32-53 °C) [211].

The temperature dependence of π should be considered when extrapolating the results of freezing point osmometry (FPO) to room temperature. As the temperature of the solution is by necessity changed during the FPO measurement, in some cases the osmotic pressure at the freezing point may differ from the results at room temperature. This may be especially problematic with new materials whose thermo-responsive properties have not been investigated. In addition, some materials, such as dextran, also have negative relationship between π and temperature, although they are not considered to be thermo-responsive [229,230]. Osmometry methods which take place at room temperature, such as DMO and vapour pressure osmometry, have an advantage over FPO in this regard.

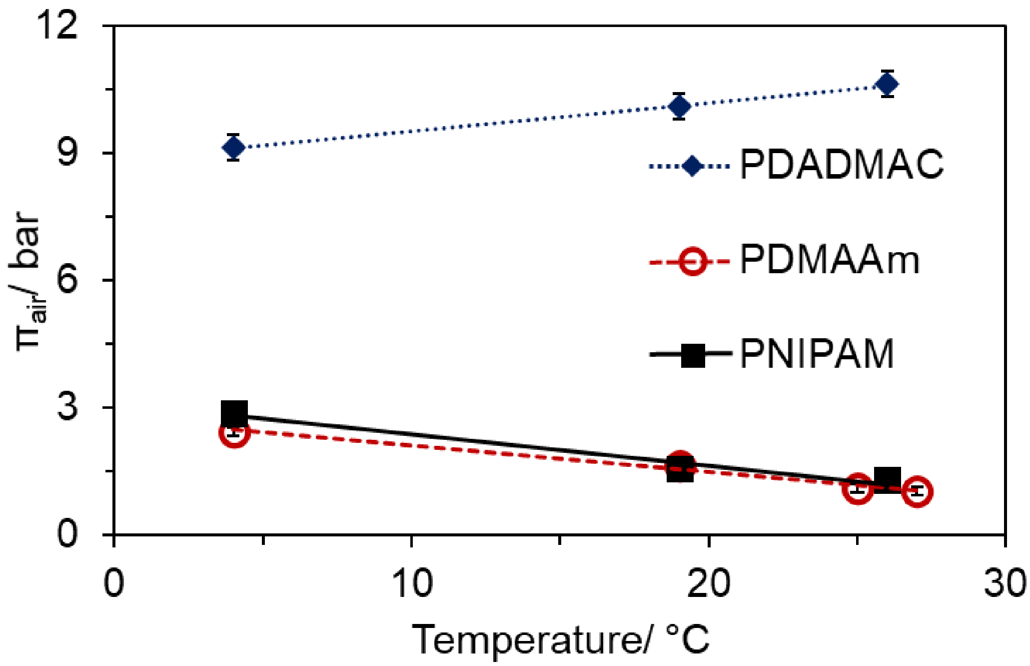

Figure 3.4 π_{air} (gauge) of soluble polymer solutions in water under air as a function of temperature for non-thermo-responsive PDADMAC (20 wt.%) and thermo-responsive soluble PDMAAm (17 wt.%, T_{cp} = ~28 °C) and PNIPAM (20 wt.%, LCST = 31-33 °C [227]) .

3.3.4 Performance of g-PDMAAm as a FO Draw Agent

The performance of g-PDMAAm as a draw agent was studied using a u-tube apparatus. Due to the small sample size used, the initial rates (after 2 min) are reported. As highlighted by Orme et al., making conclusions from the initial rates can be problematic [111]. It is therefore important to emphasize that although these experiments are an important starting point in the characterization of the performance of g-PDMAAm, they do not necessarily reflect how the gel will perform on a larger scale and on an apparatus specifically designed and optimized for hydrogel draw agents.

Pre-wetted g-PDMAAm was used a draw agent against NaCl feed solutions (1.75 or 3.5 wt.%) (see Figure 3.5.a). Samples of g-PDMAAm were swollen with a given amount of water (30 or 50 wt.% gel), then carbonated by exposure to 1 atm of CO_2 overnight. Swollen gels were springy and retained their shape. It was therefore challenging to ensure that the whole membrane was covered with gel, and the contact between them was firm. g-PDMAAm showed high initial fluxes, even against the more concentrated feed. Because the more concentrated feed (3.5 wt.% NaCl) had an initial π of ca. 27 bar, the pre-wetted g-PDMAAm must have a significantly greater π_{CO2}. The performance of g-PDMAAm compared to CO_2- and thermo-responsive gels reported in the literature is show in Table 3.1. g-PDMAAm is able to draw water from more concentrated feeds than mono-responsive gels in the literature and exhibits a significantly improved water recovery. Note that the flux of g-PDMAAm and its contact with the membrane could be improved by making microgels rather than a bulk gel [183].

The flux declines rapidly with time, as is common for small loadings of hydrogel in similar apparatuses (Figure 3.5.b, S9) [164]. This phenomenon is partially because the draw agent was not recirculated like liquid draw agents and because of the small samples used. As they are a solid material, the mass transfer of water within the gels is poor; within the first few minutes, the portion of the gel that is in contact with the membrane is quickly soaked with water, equilibrating its π with the feed resulting in a decrease in flux. The transport of water through the gel away from the membrane is slow, causing a concentration gradient to form within the gel, which limits the amount of gel that can participate in FO.

To further investigate the mass transfer within the gel draw agent, after an FO experiment of 1.75% NaCl vs 30 wt.% g-PDMAAm, a section of gel which was in contact with the membrane (no further than 2 mm away) was immediately removed and analyzed by TGA to determine the water content. The polymer composition close to the surface of the membrane was found to have decreased from 30 wt.% to ca. 14 wt.% (Appendix C, Figure C6), while the polymer composition of the gel sample used in the FO experiment as a whole decreased to just 25 wt.% (Figure 3.5.b). This indicates that gel further away from the membrane does not play an active role in the FO process during the period of high flux. While the π of a gel cannot be obtained by traditional methods (e.g., DMO or freezing point osmometry) which are designed for liquids, a rough estimate of the osmotic pressure inside the gel can be obtained by comparison to the π of the corresponding soluble polymer [150]. The π_{CO2} of 14 wt.% soluble PDMAAm (M_w = 16 kDa) and the 1.75 wt.% feed solution are very close (ca. 11 bar and 13 bar respectively) [224]. This suggests that the flux declined because the π_{CO2} of the draw agent at the membrane surface becomes equilibrated with the π of the feed solution. Indeed, the same mass of soluble PDMAAm outperforms g-PDMAAm in terms of initial flux and the equilibrium volume of water the draw can extract from the feed, partially due to its superior contact with the membrane and superior mass transfer within the draw. (Appendix C, Figure C7).

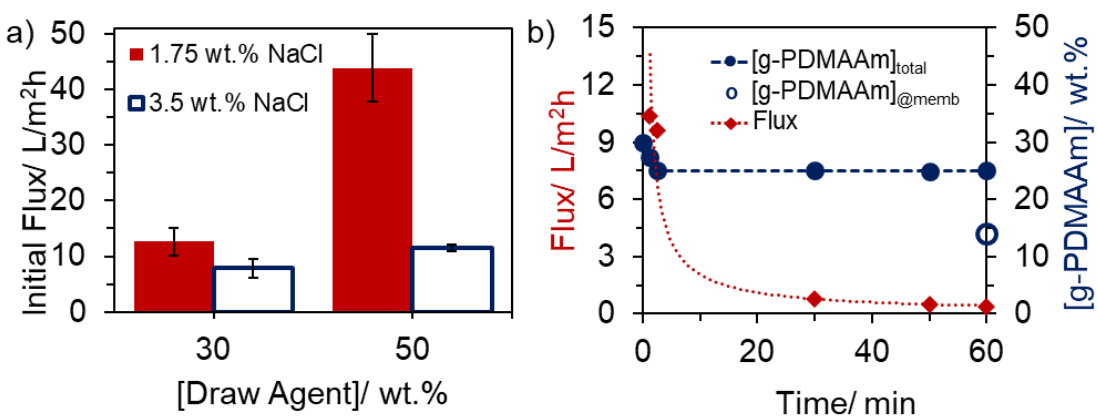

Figure 3.5 FO performance of g-PDMAAm in PRO mode: a) initial flux with varying feed and draw solution concentrations; b) representative curve of flux and draw agent concentration vs time (30 wt.% g-PDMAAm draw vs. 3.5 % NaCl feed, red solid diamonds). The net

concentration of the draw agent (blue filled circles), as well as the final concentration of the draw agent at the membrane surface (blue hollow circles) are shown.

Table 3.1 Comparison of selected CO_2- and thermo-responsive hydrogel draw agents from the literature.

Material	Trigger	FO Performance			
		Feed	Draw	Flux[a]/ LMH	Water Released/ %
P(DEAEMA-PEGDA)[b] microgel [150]	CO_2	0.2 % NaCl	0.1 g gel, 50% water	56	54-58
P(DEAEMA-NIPAM) microgel [183]	Heat	0.2 % NaCl	0.1 g dry gel	45.6	44.8
P($NIPAM_{95}$-AAm_5)[c] microgel [228]	Heat	0.2 % NaCl	0.1 g dry gel	24.7	78.7
PDMAAm bulk gel This work	CO_2 + heat	1.75% NaCl	1 g gel, 50% water	44	94[d]

[a] PRO mode, using apparatuses with not circulation on the draw side.

[b] DEAEMA = 2-(diethylamino) ethyl methacrylate, PEGDA = Poly(ethylene glycol diacrylate)

[c] AAm = acrylamide

[d] the wt% water released here is less than that in section 3.2.3 because the W_{WG} here was lower.

Consistent performance with multiple cycles is a key property of any draw agent. g-PDMAAm was subjected to various cycles of swelling and deswelling to explore its reusability (Figure 3.6). While the SR decreased after a few cycles from the initial value, this did not affect the performance of the gel as a draw agent. Neither the initial flux nor water recovery changed significantly over 10 cycles. If feeds with high π are used, the gel will likely never be swollen to its maximum extent (due to the lower $\Delta\pi$), so a slight decrease in the swelling ratio can be tolerated. It should be noted that to measure the SR the gels were deswelled to their maximum extent (almost to dryness), while as a draw agent the gels would only be deswelled back to their initial concentration. It is possible that drying the gels repeatedly decreases their swelling ability, or increases the time needed to return to the equilibrium value.

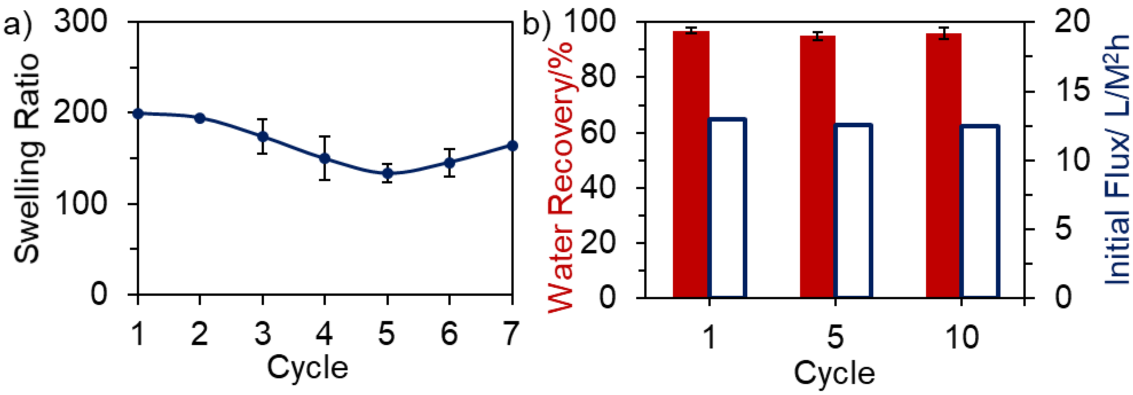

Figure 3.6 Performance of g-PDMAAm draw agents in PRO mode over several cycles: a) swelling ratio and b) initial flux (hollow bar) and water recovery (solid bar) over several cycles (30 wt.% g-PDMAAm vs 1.75 wt.% NaCl). The line in a) was added to guide the eye.

3.4 Conclusions

A dual responsive PDMAAm gel was synthesized by a one pot synthesis, and its performance as a draw agent was analyzed. The synergistic combination of CO_2- and thermo-responsiveness lead to an impressive QSR of 4960 when swelled in carbonated water, and the release up to 99.9 wt.% of absorbed water when exposed to mild heat. Thermo-responsivity can enhance properties of a CO_2-responsive draw agents by reducing the percent protonation, hydrophilicity and π_{air}. This leads to enhanced water recovery while maintaining a high flux. The

PDMAAm gel exhibited high initial fluxes from concentrated NaCl feeds and can be reused multiple times.

Chapter 4

CO_2-Responsive Magnetic Particles

4.1 Introduction

A successful draw agent must induce a high flux from concentrated feeds while remaining easily removed from water. However, the high π required to produce a high flux can make the draw agent difficult to remove. In response, many researchers have explored the use of magnetic nanoparticles as draw agents (generally using magnetite), which can be recovered by application of an external magnetic field.

In addition to their facilitated removal, magnetic particle draw agents have other advantages. Due to their size, magnetic particles generally have low RSF. By using a magnetic field, magnetic draw agents can be localized and concentrated at the membrane surface [110]. Polymer grafted magnetic particles reportedly exhibit higher π than the same free polymer, possibly due to the more extended orientation of the grafted polymer (which is more accessible to hydration), as opposed to a more constrictive coil adopted by a free polymer [190].

Magnetic particle draw agents are also accompanied by several severe drawbacks. Pure magnetite particles are prone to oxidation [231], suffer from aggregation [232], and have low dispersibility in water. The surfaces of magnetite particles are often modified to increase chemical resistance, reduce aggregation, and increase flux. However, the synthesis of functionalized magnetic particles is currently more expensive than traditional draw solutes (e.g., free polymers), which makes them less attractive and practical as draw solutes. The size of the particles may also present difficulties; while smaller particles have higher osmolalities, they are also more difficult to recover [233]. Magnetite particles can also foul the FO membrane (depending on their size and surface functionalization) by embedding themselves into membrane pores [110,194,197]. Depending on the size and functionalization of the magnetic particles, they may recover very slowly by application of a magnetic field alone, and require additional separation steps (e.g., UF) [140].

As pure magnetite nanoparticles exert a low π [185,200], magnetite has been functionalized with hydrophilic materials (e.g., PSA [138,190,201], citric acid [197], PEG [128], dextran [189], sodium alginate sulfate [205]) to improve flux. It is noteworthy that despite this, many magnetic particles fail to achieve significant fluxes against saline feeds (Table 1.9). Some magnetic nanoparticles functionalized with hydrophilic materials may be recovered from dispersions by application of a magnetic field [189,205]. However, when the hydrophilic particles are swollen with water after FO they often become increasingly difficult to completely recover with an external magnetic field [138].

Stimuli-responsive materials have been grafted to the surface of magnetite in an effort to achieve both high flux and easy draw agent removal. The stimuli-responsive coatings possess two states: one which excels at pulling water across the FO membrane and one which facilitates draw solute removal. In the former state the coating is generally hydrophilic, while in the latter state the coating is more hydrophobic, which triggers the release of water from the particles or cause the particles to aggregate. After osmosis, the magnetic particles are switched to the more hydrophobic state, which facilitates the particle removal via magnetic separation. One of the most common triggers for stimuli-responsive magnetic draw agents is heat.

Thermo-responsive materials with a LCST exhibit a sharp decline in the solubility above their cloud point. Thermo-responsive moieties (e.g., PNIPAM, LCST = 31-33 °C [227]) and hydrophilic moieties (e.g., PSA [41], triethylene glycol [192]) have been grafted to magnetic nanoparticles. Heating these particles above their cloud points triggers the release of absorbed water from the thermo-responsive coating and particle aggregation, which greatly facilitates the draw solute's removal. However, combining a hydrophilic and thermo-responsive material in a draw solute often results in a compromise between high flux and ease of removal, as discussed in detail in Chapter 3.

Although CO_2-responsive magnetite particles have been synthesized in the past [32,234–236], they have never been tested as FO draw agents. Incorporating CO_2-responsivity may lend similar benefits to magnetic draw agents as they have to polymers (Chapter 2) and hydrogels (Chapter 3). This chapter presents the first exploration of a CO_2-responsive magnetic FO draw agent. Two different structures were considered: PDMAEMA microgels containing dispersed magnetite nanoparticles (MNP) (Figure 4.1.a) and PDMAEMA-coated MNP (Figure 4.1.b).

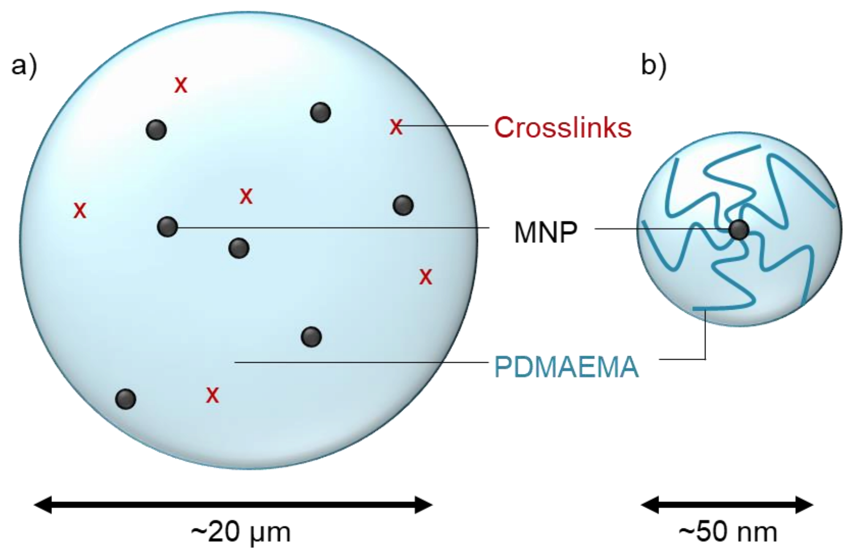

Figure 4.1 Illustrations of the CO_2-responsive magnetic particles explored in this chapter: a) PDMAEMA microgels with embedded MNP and b) PDMAEMA functionalized MNP. Illustrations are not to scale.

4.2 Materials and Methods

4.2.1 Materials

Ethylenediamine (≥99%), ethylenediamine dihydrochloride (98%), methanol (≥99.8%), methacrylic anhydride (94%, contains 2,000 ppm topanol A), 2-propanol (≥99.5%), iron(II) chloride tetrahydrate (≥99.0%), ammonia (≥ 25% in water), 3-(aminopropyl)triethoxysilane (APTS, 99%), glutaraldehyde (grade II, 25% in water), Tween® 80, Span® 80, Triton® X-100, chloroform (≥99.8%, contains ethanol as stabilizer), THF (≥99.0%, contains 250 ppm BHT as inhibitor), copper(II) bromide (99%), 1,1,4,7,10,10-hexamethyltriethylenetetramine (HMTETA, 97%), tin(II) 2-ethylhexanoate ($Sn(EH)_2$, 92.5-100.0%), ethylene glycol (anhydrous, 99.8%), phosphorus(V) oxychloride (99%) and α-bromoisobutyryl bromide (BIBB, 98%) were obtained from Sigma-Aldrich and used as received.

AIBN (>98%) was obtained from Sigma-Aldrich, and was recrystallized from methanol before use. DMAEMA (98%, containing 700-1000 ppm monomethyl ether hydroquinone as inhibitor) was obtained from Sigma-Aldrich. The inhibitor was removed by passing DMAEMA through a column of basic alumina before use. Dowex® 1x4 chloride form (200-400 mesh) ion-exchange resin was obtained from Sigma-Aldrich. The resin was converted to the hydroxide form by stirring in ca. 5 volume excess of 5 wt.% NaOH solution for 3 h, then washing with water until the pH of the permeate was neutral.

Sodium dodecyl sulfate (SDS, 95%) was obtained from T.J.Baker and was used as received. Iron(III) chloride hexahydrate (97-102%, as reported on the label) was obtained from Alfa Aesar and used as received. THF (anhydrous) was obtained from Millipore and used as received. Mazola brand canola oil was obtained from a grocery store and used as received. Concentrated hydrochloric acid (36.5-38.0%), DMF (99.9%) and DMSO (99.9%) were obtained from Fisher and used as received.

Dialysis tubing (3.5 kDa MWCO) was obtained from Thermo-Fisher. FTS H2O FO membranes (4.7 cm diameter disks) were obtained from Sterlitech. All water was obtained from a Synergy Millipore system (with a resistivity of 18.2 MΩ before contact with air). CO_2 (grade 3.0) and argon (grade 5.0) were obtained from Praxair.

During the draw agent synthesis, a RZR 50 Caframo overhead stirrer equipped with a 2-pronged (4.5 cm blade length) stir shaft was used to stir magnetic particles. Particles were dispersed using an ultrasonic bath (Fisher Scientific, FS30) and ultrasonic probe (Fisher Scientific, sonic dismembrator, Model 500). A 4x4x2 cm neodymium alloy magnet from DYIMAG (purchased from Amazon) was used to separate magnetic particles. Polymer solutions were dried using a Labconco FreeZone 6 Plus lyophilizer (0.01 mbar, -60 °C).

4.2.2 Characterization

4.2.2.1 Polymers

The polymers synthesized in this work were characterized by ^{1}H NMR spectroscopy, IR spectroscopy and GPC. ^{1}H NMR spectra were recorded at 298 K with a Bruker Avance 398 MHz NMR spectrometer. Fourier transform infrared (FTIR) spectra were collected on an Agilent Technologies Cary 630 FTIR base spectrometer using an ATR accessory over 400-4000 cm^{-1} for magnetite, and 600-4000 cm^{-1} for all other materials. The GPC analysis was performed on an Agilent GPC equipped with PSS NOVEMA Max Lux and PSS NOVEMA Max Lux analytical columns, and a light scattering detector (calibrated with poly(2-vinylpyridine) standards, 1,000,000-1,000 g/mol). Samples (2 mg/mL) were filtered with 0.2 μm syringe filters. Measurements were obtained at 40 °C with a flow rate of 1 mL/min using an acidic aqueous eluent (0.3 wt. % LiBr, 0.3 M formic acid in HPLC grade water).

4.2.2.2 Magnetite Nanoparticles

The crystal structure of the magnetite nanoparticles was confirmed by powder XRD using a Bruker AXS D8 Venture Duo diffractometer operating with Cu Kα radiation from 15-70°. The size of the particles was determined by TEM (Thermo Scientific Talos F200i) at an accelerating voltage of 200 kV. Particles were dispersed in water then cast on to Carbon type B coated 200 mesh Cu grids. Grids were dried under air at room temperature. A second grid was place on top of the sample loaded grid prior to insertion in the TEM. Particle size was measured manually using Micron 2.0 software, from a minimum of 50 particles.

4.2.2.3 PDMAEMA-Magnetite Particles

The compositions of all particles (microgel and nanoparticle) were determined by FTIR (as previously described) and TGA. TGA was conducted using a Texas Instrument Q500. The particles were analyzed using the following procedure: heating from room temperature to 120 °C at 20 °C/min; isothermal for 10 min; 120 °C to 900 °C at 20 °C/min; isothermal for 10 min.

The size of the microgels were measured by an optical microscopy using a Fisher Scientific Micromaster optical microscope. Particle sizes were measured manually using Micron 2.0 software, from an average of ca. 100 particles. TEM images were obtained as described in section 4.2.2.2.

4.2.2.4 Flux Characterization

The flux of the magnetic draw agents was determined using a glass U-tube apparatus (Appendix C, Figure C1). Feed solutions are placed below the membrane and draw solutions are placed above the membrane. Circular FTS H2O FO membranes (2.5 cm diameter) were soaked in the feed solution for 1 h prior to use, then placed in the U-tube apparatus, with the active side facing the feed. Flux (liters of water transferred from the feed to the draw per m^2 of membrane per hour, equation 1.6) was measured using the change in concentrated of the feed over time. The feed concentration was monitored over time using a conductivity probe (Thermo Scientific Orion

013005MD). NaCl concentrations were calculated from the observed conductivities using a calibration curve of the conductivity of NaCl standard solutions.

Draw agents were carbonated under 1 atm of CO_2 prior to use. Liquid draw solutions were carbonated by bubbling CO_2 through the solution for 4 h, while solid draw agents were exposed to 1 atm of CO_2 overnight. During the FO experiment, the draw side of the U-tube was kept under an atmosphere of CO_2. The duration of the FO experiments was 1 h.

4.2.3 Synthesis of Magnetite Nanoparticles

MNPs were synthesized via previously reported methods [237,238]. $FeCl_2·4H_2O$ (12 g) and $FeCl_3·6H_2O$ (24.3 g) were added to a round bottomed flask. The salts were dissolved in water (50 mL) under argon with magnetic stirring. The solution was heated to 70 °C, and ammonium hydroxide (25% aqueous solution, 40 mL) was added to the solution dropwise. The solution was stirred for 30 min, then cooled to room temperature. The black precipitate was recovered by applying a magnetic field and decanting the supernatant. The product was washed with water (3 x 50 mL) and stored as a wet slurry. Dry magnetite was obtained by removing the water in a vacuum oven at 60 °C overnight, then grinding the product into a fine powder with a mortar and pestle. The magnetic nanoparticles are used in the synthesis of the PDMAEMA-MNP microgels and the PDMAEMA-functionalized MNP.

4.2.4 Synthesis of PDMAEMA-MNP Microgels

4.2.4.1 Synthesis of 2-Aminoethylmethacrylate Hydrochloride

The synthesis of 2-aminoethylmethacrylate (AEMA) hydrochloride was based on previously reported methods [239,240]. Ethylenediamine (16 mL) and ethylenediammounium hydrochloride (30 g) were dissolved in water (100 mL), and magnetically stirred at room temperature for 1 h. Methanol (100 mL) was added, and the solution was cooled in an ice-water bath. Once the temperature had equilibrated, methacrylic anhydride (68 mL) in methanol (50 mL) was added dropwise to the solution over 30 min. The solution was stirred in the ice-water bath for 1 h, then warmed to room temperature and stirred for 30 min. Concentrated hydrochloric acid (40 mL) was added to the solution dropwise. The solution was stirred for another 1 h. The solvent was removed by rotary evaporation, and the crude product was washed with acetone. The precipitate was recrystallized from 2-propanol at 4 °C, and dried under vacuum at 45 °C. The ^{1}H NMR spectrum matched literature reports (Appendix D, Figure D5.iii) [240]. ^{1}H NMR (400 MHz, D_2O, ppm): 5.69 (0.97H, *H*CH=C), 5.42 (1.0 H, *H*CH=C), 3.59 (2.0H, OCNCH_2), 3.10 (2.0H, H_2CNH$_2$), 1.85 (3.0H, CH_3).

4.2.4.2 Synthesis of P(DMAEMA-AEMA)

A Schlenk flask was flame dried and purged with argon three times. Dry DMSO (27 mL) was added to the flask, followed by AEMA·HCl (1.5 g). The solution was mixed with a magnetic stir bar. After the AEMA·HCl was completely dissolved, DMAEMA (9 mL) was added to the flask. The solution was heated to 65 °C. Once the temperature had equilibrated, AIBN (52 mg) was added to the solution. The solution was stirred at 65 °C over night. The crude reaction mixture was dialyzed with 3.5 kDa MWCO tubing in 4 L of deionized water. The water was exchanged 5 times, with a minimum residence time of 4 h between exchanges. The polymer solution was passed through a column of hydroxide ion-exchange resin, then the solvent was removed by lyophilization, yielding pure polymer. ^{1}H NMR (400 MHz, D_2O, ppm): 4.07 (2.0H**,** H_2CCON), 3.58 (0.2H, CH_2CH$_2$NH$_3$Cl), 3.14 (0.2H, CH_2NH$_3$Cl), 2.65 (2.4H, CH_2N(CH$_3$)$_2$), 2.23 (6.0H, (CH_3)$_2$N), 1.83 (1.8H, CCH_2C), 0.92 (3.3H, CH_3C). GPC (water, 0.3 wt. % LiBr, 0.3 M formic acid): M_w = 41 kDa, Đ = 5.8.

4.2.4.3 Synthesis of APTS functionalized magnetite

APTS was grafted onto the magnetite nanoparticle surface following a procedure based on reference 241. Magnetite powder (0.5 g) was added to a 1:1 v:v solution of ethanol in water (100 mL total) and sonicated in an ultrasonic bath for 20 min. The solution was then mixed using an overhead stir shaft at 1000 rpm and APTS (2 mL) was added dropwise to the solution. The solution was then heated to 70 °C for 3 h. The solution was cooled to room temperature, and the particles were collected by applying a magnetic field and decanting the supernatant. The particles were washed with water (2 x 20 mL) followed by ethanol (2 x 20 mL). The particles were dried in a vacuum oven at 45 °C for 4 h, and ground into a fine powder with a mortar and pestle prior to use.

4.2.4.4 Synthesis of PDMAEMA-MNP Microgels

PDMAEMA-MNP microgels were synthesized via a method based on references 237,242, and 243. P(DMAEMA-AEMA) (1 g), SDS (1 mg) and PVP (3 mg) were dissolved in water (5.5 mL). APTS-functionalized magnetite (50 mg) was added to the solution. The dispersion was sonicated using an ultrasonic probe (55% max amplitude) for 20 min to ensure the magnetite was well dispersed. Span® 80 (2.4 mL), Tween® 80 (0.6 mL) and Triton X-100 (0.6 mL) were mixed into canola oil (60 mL). An emulsion was formed by mixing the organic phase and aqueous phase with an overhead stir shaft at 2000 rpm for 20 min. The speed was decreased to 450 rpm and glutaraldehyde (25 wt.% aqueous solution, 100 μL) was added dropwise to the emulsion. Stirring was continued for 2 min. The particles were sedimented by centrifugation (Thermo Scientific, IEC Medilite microcentrifuge) for 2 min, followed by washes with toluene (2 x 60 mL), ethanol (3 x 60 mL) and water (3 x 60 mL). After the final wash, the particles were redispersed in water by mixing for 20 min at 2000 rpm with an overhead stir shaft. The particles were stored as a slurry.

4.2.5 Synthesis of PDMAEMA-Functionalized MNP

4.2.5.1 Synthesis of ATRP Initiator

The ATRP initiator 2-(phosphonooxy)ethyl 2-bromo-2-methylpropanoate (PEBMP) was synthesized by the procedure described in reference 244. Anhydrous ethylene glycol (20 mL) was added to a Schlenk flask under argon. The flask was cooled in an ice-water bath, and the ethylene glycol was magnetically stirred at 500 rpm. BIBB (2 mL) was added dropwise to the ethylene glycol, then the solution was left to stir for 3 h. Water (10 mL) was added to the flask, and the product was extracted with chloroform (3 x 20 mL). The organic layer was dried with magnesium sulfate, which was subsequently removed by gravity filtration. The solvent was removed by rotary evaporation to yield 2-hydroxyethyl 2-bromo-2-methylpropanoate. The ^{1}H NMR spectrum matched literature reports [244]. ^{1}H NMR (400 MHz, $CHCl_3$, δ ppm): 4.25 (1.9H, CH_2OC), 3.81 (2.0H, CH_2OH), 3.05 (1.0H, O*H*), 1.91 (6.0H, $(CH_3)_2$).

Anhydrous THF (60 mL) and 2-hydroxyethyl 2-bromo-2-methylpropanoate (3.7 mL) were added to a Schlenk flask under argon. The flask was cooled in an ice-water bath, and the solution was magnetically stirred at 500 rpm. Phosphorus(V) oxychloride (2.5 mL) was added dropwise to the solution. After 1 h, the ice-water bath was removed, and the solution was left at room temperature for 3 h. Water (45 mL) was added to the flask, and the solution was extracted with chloroform (3 x 70 mL). The organic layer was dried with magnesium sulfate, which was subsequently removed by gravity filtration. The solvent was removed by rotary evaporation to yield PEBMP. The ^{1}H NMR and IR spectra (Figure 4.8.a) matched literature reports [244]. ^{1}H NMR (400 MHz, $CHCl_3$, δ ppm): 4.29 (2.5H, CH_2OC), 3.87 (2.0H, CH_2OP), 1.94 (6.0H, $(CH_3)_2$).

4.2.5.2 Grafting ATRP Initiator to Magnetite Nanoparticles

Anhydrous THF (10 mL), dry magnetite nanoparticles (0.2 g) and PEBMP (0.4 mL) were added to a 4 dram glass vial and sonicated in an ultrasonic bath for 45 min. The vial was shaken on a shaker plate overnight at 400 rpm. The particles were recovered by magnetic separation and washed with THF (3 x 20 mL). The particles were dried at room temperature under vacuum.

4.2.5.3 SI-Polymerization of DMAEMA from Magnetite Nanoparticles

Initiator-grafted magnetic particles (50 mg) were ground into a fine powder with a mortar and pestle and added to the 3-neck round bottom flask followed by DMAEMA (5 mL) and a solution of $CuBr_2$ (5 mg) and HMTETA (8.5 μL) in methanol (0.5 mL). The dispersion was sonicated using an ultrasonic bath for 5 min then the 3-neck flask was then equipped with an overhead stir shaft and an argon inlet. The third neck was used to add reagents and was sealed with a septum. The solution was then heated to 40 °C and stirred at 2000 rpm under a flow of argon. Once the solution reached the desired temperature, $Sn(EH)_2$ (500 μL) was added to the dispersion via syringe injection through the septum in the third neck. After 16 h, the reaction mixture was cooled to room temperature, and the dispersion was precipitated into cold hexanes (2 x 50 mL), followed by washing and magnetic separation with THF (2 x 20 mL) and water (2 x 20 mL). The particles were stored as a slurry in water.

4.3 Results and Discussion

4.3.1 Microgel Characterization

PDMAEMA microgels with embedded magnetite were synthesized using a method based on previous reports [237,242,243], by crosslinking water-in-oil emulsion droplets containing

PDMAEMA and MNP (Figure 4.2 and Appendix D, Figure D1). First, MNP and PDMAEMA were modified to contain primary amines which can react rapidly with glutaraldehyde crosslinkers at room temperature. Specifically, DMAEMA was copolymerized with a small fraction of AEMA, and MNP were functionalized with APTS. Amino-functionalized MNP were dispersed in an aqueous solution of P(DMAEMA-AEMA), which was then mixed with oil and surfactant to form a water-in-oil emulsion. Glutaraldehyde was added to the emulsion which crosslinked the primary amines in the polymer chains, and the magnetite surface, to form microgels of PDMAEMA with embedded MNP. Oil, surfactant and uncrosslinked polymer were removed by successive washes with toluene, ethanol and water.

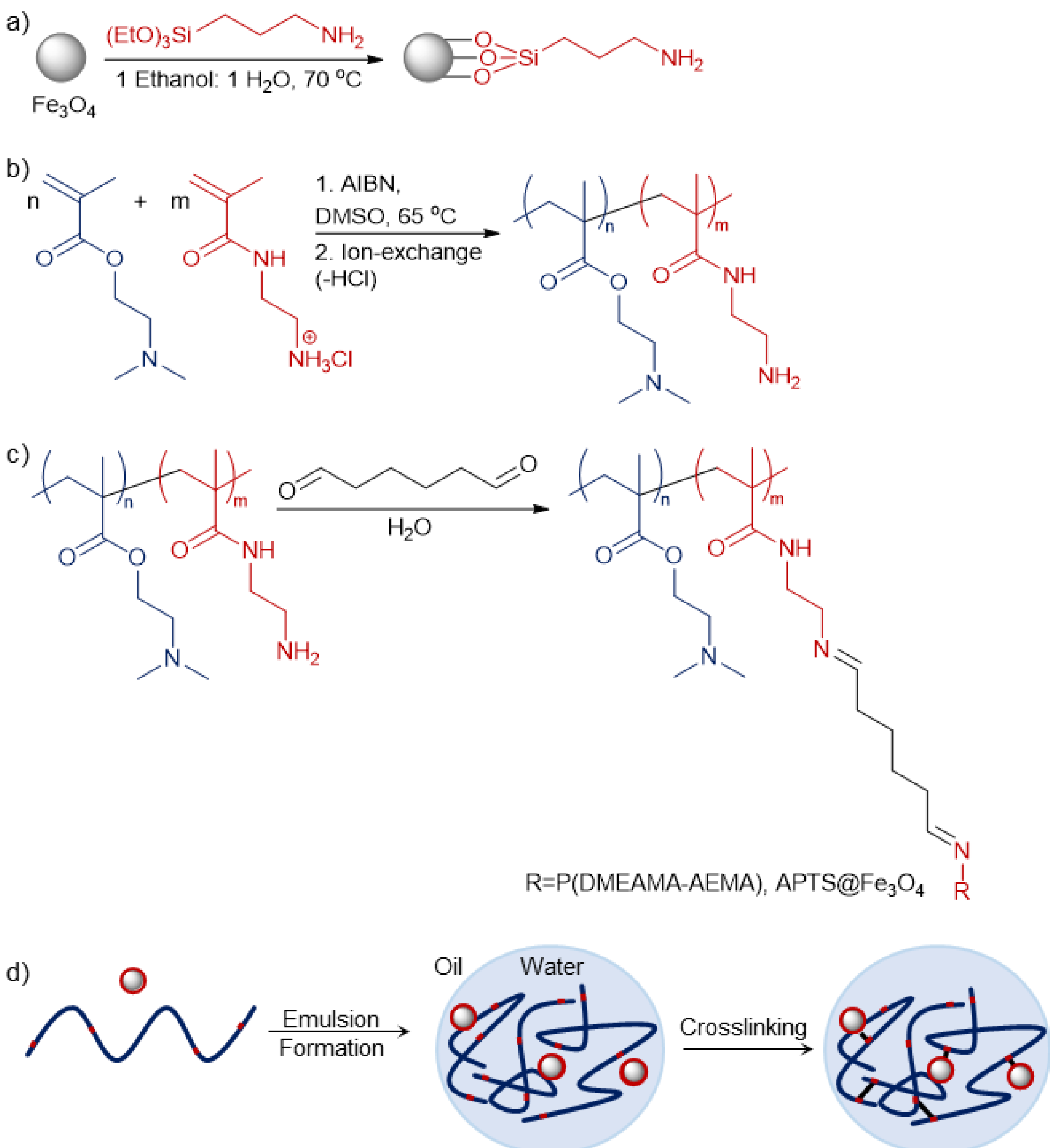

Figure 4.2 Synthetic procedure for PDMAEMA-MNP microgels: a) grafting of APTS to MNP, b) synthesis of P(DMAEMA-AEMA), c) crosslinking reaction, d) illustration of microgel formation.

The successful synthesis of magnetite was confirmed by powder XRD (Appendix D, Figure D3) [245,246]. The IR spectrum of the MNP showed the characteristic peak at 562 cm^{-1} indicative of Fe-O vibrations (Figure 4.3.a) [246,247]. The diameter of the individual MNP was determined to be 5-15 nm by TEM (Appendix D, Figure D4.a), in agreement with previous reports [248,249].

Successful grafting of APTS to the MNP was confirmed by IR spectroscopy, through the appearance of C-H stretches (2860-2925 cm^{-1}), N-H stretches (3000-3500 cm^{-1}), and overlapping C-N and Si-O stretches (1006-1207 cm^{-1}) (Figure 4.3.a) [246,250]. After grafting the MNP with APTS an additional 8 wt.% decline is observed between 200-700 °C by TGA, which is indicative of the decomposition of organics from the magnetite surface (Figure 4.3.b).

The successful purification of the DMAEMA-AEMA copolymer was confirmed by ^1H NMR spectroscopy, through the observation of the disappearance of the alkene monomer and DMSO peaks (5-6 ppm and 2.7 ppm respectively) (Appendix D, Figure D5). After polymerization, the peaks of the polymer were broad due to the increased molecular weight. The proportion of AEMA in the final polymer was determined by integration of the ^1H NMR CH_2NH_2 peak originating from AEMA to the CO_2CH_2 peak originating from DMAEMA (Appendix D, Figure D6). The molar ratio of AEMA to DMAEMA in the final polymer was determined to be 9:91 (slightly lower than the theoretical ratio of 15:85). The presence of AEMA in the copolymer can also be seen in the IR spectra, through the shifted carbonyl stretching peak at 1650 cm^{-1} (Appendix D, Figure D7).

Mixing the aqueous phase containing P(DMAEMA-AEMA) and dispersed APTS-functionalized MNP into the oil phase produced an emulsion, with droplets ranging from 5-30 μm in diameter (Appendix D, Figure D8). The polymer in the emulsion was crosslinked into a microgel upon addition of glutaraldehyde. The dialdehyde rapidly reacts with primary amines to form a Schiff base. This reaction can occur between AEMA units in P(DMAEMA-AEMA) which crosslinks the polymer into a microgel, and between AEMA and ATPS-functionalized MNP which covalently anchors the MNP into the microgel.

After crosslinking, the IR spectrum of the isolated magnetic microgels matches that of P(DMAEMA-AEMA) (Figure 4.3.a). The composition of the particles was determined to be 9.8 wt.% magnetite by TGA (Figure 4.3.b). The size of the particles in neutral water at 20 °C was determined to be 9±4 μm by optical microscopy.

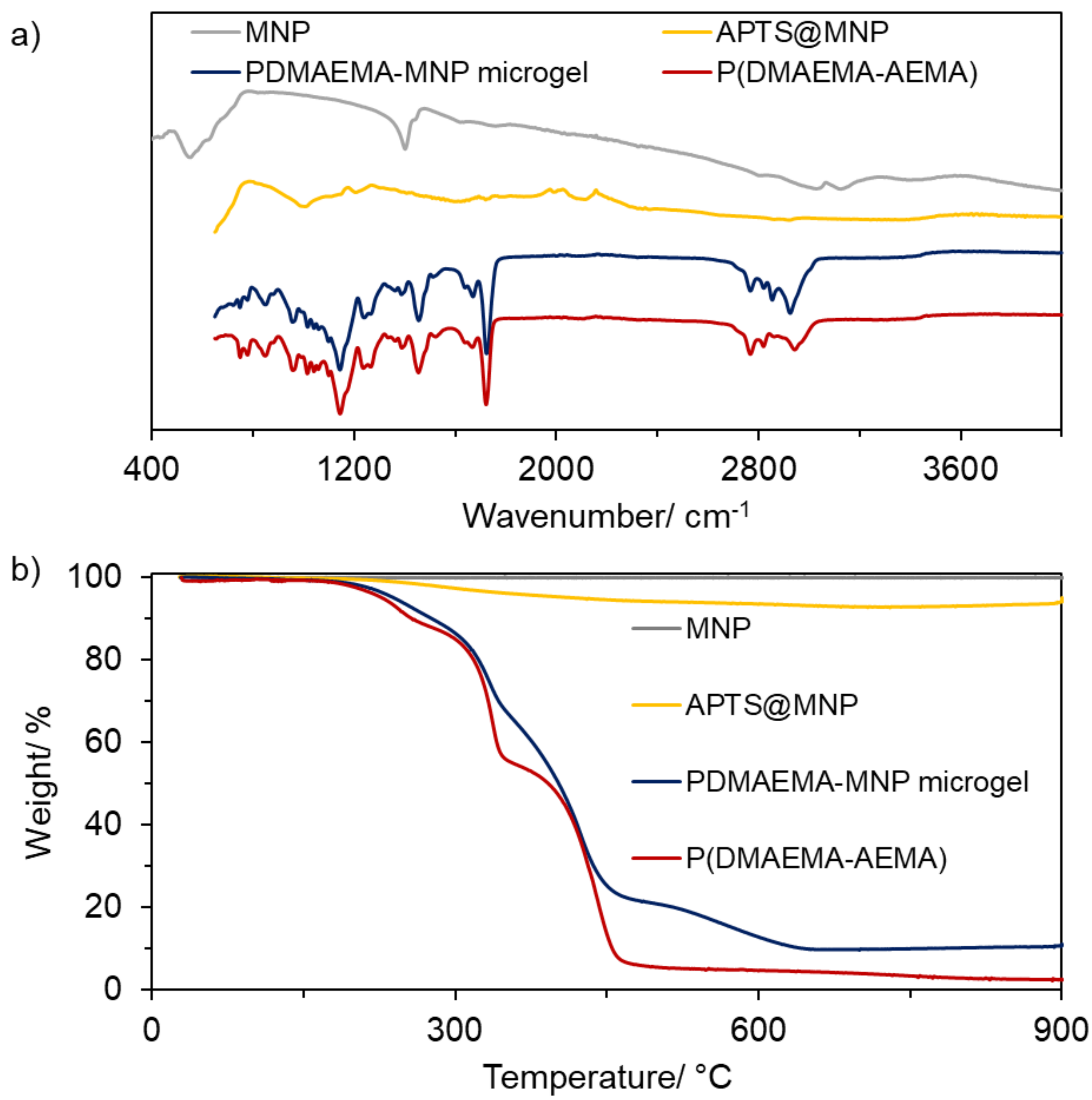

Figure 4.3 Characterization of PDMAEMA-MNP microgels and their precursors: a) IR spectrum and b) TGA thermogram.

It was essential to covalently bind the MNP within the polymer network so they would not migrate out of CO_2-responsive hydrogel when it was swollen under CO_2. To determine if APTS functionalization successfully anchored the MNP within the microgel, PDMAEMA-MNP microgels were exposed to an acidic solution (HCl, pH 1) for 16 h. (NB, the particles used in this study contained 5 wt.% magnetite. These particles were made following the same procedure as described in section 4.2.4.4, but with half the mass of magnetite). The particles were subsequently treated with base then washed three times with water. Microgels made with APTS-functionalized magnetite showed a slight (3.6 wt.%) increase in MNP content (Figure 4.4). If MNP were migrating out of the gel in acidic conditions, the wt.% after heating to 900 °C would decrease after treatment with HCl. The increase in MNP content in the microgel may be due to the migration of uncrosslinked P(DMAEMA-AEMA) out of the microgel. Note that degree of hydrolysis of the ester groups in PDMAEMA is expected to be negligible at pH 1 after 16 h [251]. This test also demonstrated that the APTS and polymer coating increases the chemical resistance of the magnetite, as bare magnetite oxidizes rapidly at pH 1.

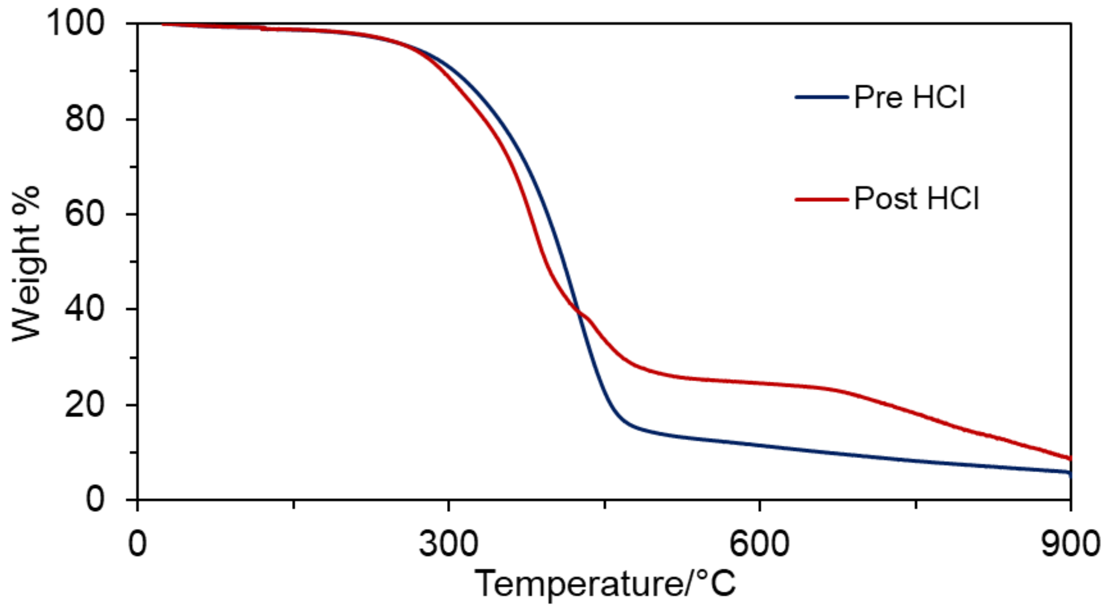

Figure 4.4 TGA thermograph of CO_2-responsive microgel particles before and after acid treatment.

4.3.2 Microgel Stimuli-Responsivity

In water, PDMAEMA is both CO_2- and thermo-responsive (LCST = 32-53 °C [211]). The effects of both triggers were explored separately. The CO_2-responsivity of the PDMAEMA-MNP microgels was explored by exposing dilute aqueous dispersions of the particles to different atmospheres (CO_2 and air) at a constant temperature of 20 °C. Under air at 20 °C, the PDMAEMA-MNP microgels have a diameter of 18±8 μm and exist in small aggregates. Upon exposure to CO_2 (at 20 °C) the diameter of the microgels increases to 50±10 μm, which corresponds to a 17-fold increase in volume (Figure 4.5.a,b). The gels expand upon exposure to CO_2 due to the increased hydrophilicity and π inside the gel caused by the generation of bicarbonate salts.

The thermo-responsivity of the PDMAEMA-MNP microgels was explored by exposing dilute aqueous dispersion of microgels to various temperatures (20 and 60 °C) under a constant atmosphere of air. As temperature increased from 20 °C to 60 °C, the microgels contract and form large aggregates (Figure 4.5.b,c). Above their VPTT, intramolecular polymer interactions become more favourable than polymer-water interactions, resulting in a decrease in particle size. The formation of aggregates is reversed upon application of CO_2 or lowering the temperature and rapidly mixing the dispersion.

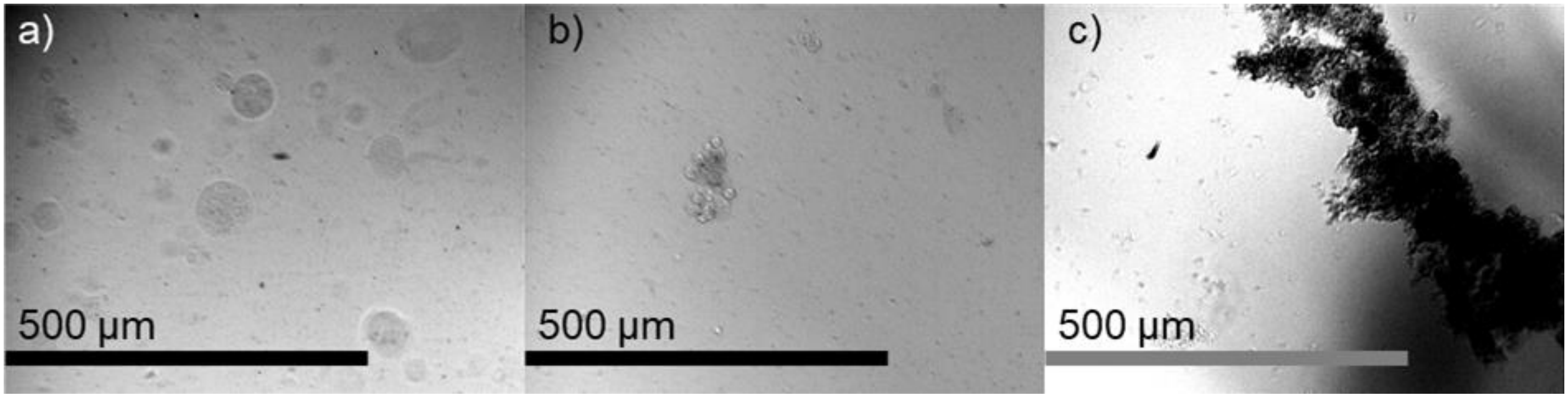

Figure 4.5 Optical microscope images of PDMAEMA-MNP microgels in water a) under CO_2 at 20 °C, b) under air at 20°C and c) under air after exposure to 60 °C.

To explore the performance of the microgels with repeated use, the microgels were subject to 5 cycles of carbonation (under an atmosphere of CO_2 at 20 °C) followed by decarbonation (under an atmosphere of air at 60 °C). After the 2nd cycle, some sediment was observed. However, the overall size distribution remained relatively unchanged (Figure 4.6).

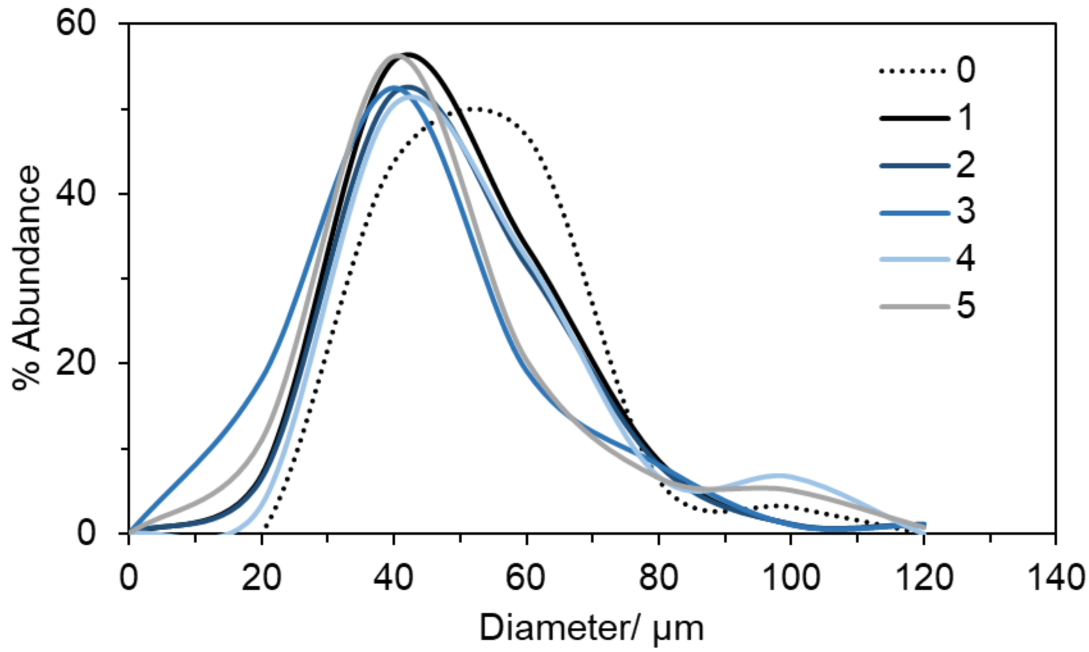

Figure 4.6 Size distribution of microgel particles in aqueous dispersions observed by optical microscopy, under CO_2 at 20 °C, after successive cycles (0-5) of carbonation (under an atmosphere of CO_2 at 20 °C) and decarbonation (under an atmosphere of air at 60 °C).

4.3.3 Nanoparticle Characterization

PDMAEMA-functionalized MNP were synthesized by polymerizing DMAEMA from the MNP surface via surface initiated-Activator ReGenerated by Electron Transfer (SI-ARGET) atom transfer radical polymerization (ATRP) (Figure 4.7). ARGET was used as it is more tolerant to air than traditional ATRP, which facilitates scale up and the use of mechanical stirring.

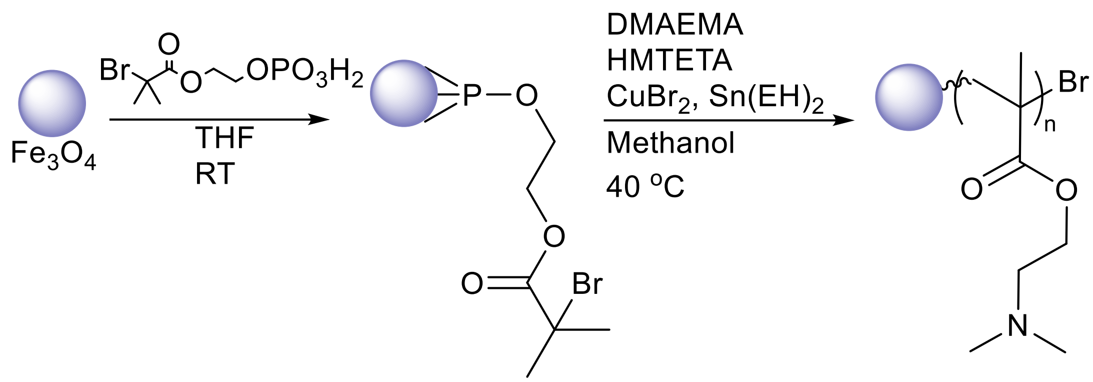

Figure 4.7 Synthesis of PDMAEMA-Fe_3O_4 nanoparticles

PEBMP was selected as the ATRP initiator as it results in increased grafting density compared to more common alternatives such as BIBB [244]. The grafting of PEBMP on the MNP surface was confirmed by the appearance of the aliphatic C-H (2917-3077 cm^{-1}), C=O (1732 cm^{-1}), P=O (1274 cm^{-1}) and P-O (1021 cm^{-1}) stretches in the IR spectrum (Figure 4.8.a). The amount of initiator on the surface was determined to be 13 wt.% by TGA (Figure 4.8.b). The high amount of grafted initiator is consistent with previous reports [244,252].

After polymerization, the IR spectrum of PDMAEMA-functionalized MNP matches that of PDMAEMA (Figure 4.8). The loading of polymer was determined to be 34 wt.% by TGA. As magnetite is significantly denser than PDMAEMA (5.175 g/mL [186] vs 1.32 g/mL [253]) the volumetric ratio of PDMAEMA in the nanoparticle (0.4 MNP: 1 PDMAEMA) is significantly higher than the weight ratio (1 MNP: 1.6 PDMAEMA). The volume of the PDMAEMA coating will be further increased in solution, when the PDMAEMA is swollen with water. The PDMAEMA coating can be visualized by TEM (Appendix D, Figure D4.b). The PDMAEMA layer can be seen to expand upon protonation with glycolic acid (Appendix D, Figure D4.c). The stimuli-responsivity of the nanoparticles could not be measured due to instrumental limitations.

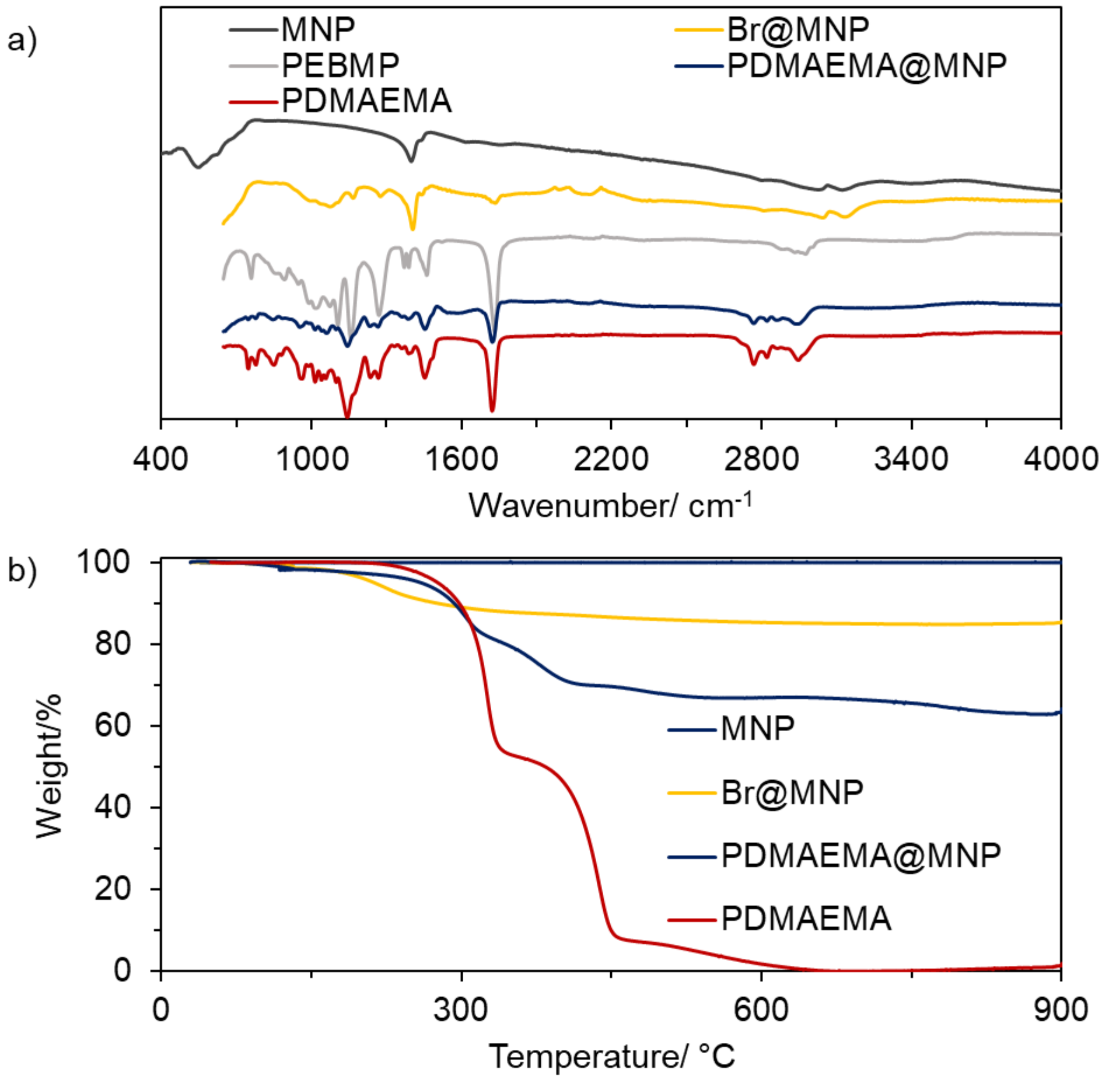

Figure 4.8 Characterization of PDMAEMA modified nanoparticles and their precursors: a) IR spectrum and b) TGA thermograms.

4.3.4 FO Performance

The FO performance of the magnetic microgels and nanoparticles were assessed using the U-tube apparatus that had been employed to measure fluxes in Chapter 3 (Appendix C, Figure C1). Various concentrations of draw agent and feed solution were used. Microgels were used in concentrations of 1, 3, 30 and 50 wt.% prior to carbonation. Nanoparticles were used in concentrations of 1 and 8 wt.% prior to carbonation. Feed solutions of 3.5, 1.75, 0.2, and 0.1 wt.% NaCl were used.

None of the draw agents tested were able to pull a detectable amount of water across the FO membrane in 1 h, even against dilute feeds. Higher concentrations of draw agents were initially employed (30-50 wt.% of the microgels, and 8 wt.% for the nanoparticles), as π increases with concentration. None of these draw agents produced a significant flux, even against dilute feeds. It was hypothesized that the poor results may be due to poor physical properties arising from the high concentration of draw agent. At high concentrations, the microgels were a solid, and it was consequently difficult to achieve complete and intimate coverage of the membrane. The solid nature of the draw solute could also lead to decreased mass transfer and therefore decreased carbonation within the microgel. While the nanoparticle dispersions were a fluid at all concentrations explored, the dispersions become viscous at high concentrations, which could also lead to decreased rates of carbonation. In addition, the aggregation of magnetic nanoparticles is expected to be severe at high concentrations, which could decrease the surface area and therefore lower the π of the draw agent. Lower draw agent concentrations were therefore considered.

Draw agents of lower concentrations (1, 3 wt.% for microgels, 1 wt.% for nanoparticles) were used in FO experiments against dilute feeds (0.2, 0.1 wt.% NaCl). Note that although these concentrations are low, magnetic draw agents with similar concentrations have been reported to exert fluxes from dilute feeds (Table 1.9). At low concentrations, the microgels had a consistency of a wet paste, and the nanoparticle dispersions were less viscous. The improved consistency facilitated the loading of the microgels on to the membrane and improved the contact between the draw agent and the membrane. However, none of the dilute draw agents produced a significant positive flux against any feed, even 0.1 wt.% NaCl, which has a predicted π of just ca. 0.7 bar. The poor FO performance may be due to the dilute draw agents' low π_{CO2}. Further optimization of the draw concentration and balancing physical properties and π_{CO2} maybe be required to produce positive flux results.

While the magnetic particles discussed in this chapter did not prove to be successful draw agents, they may have more success in other applications. The microgels have the added advantage of being easily removed under CO_2 as well as air, which may prove useful for in other fields. Alternative applications of the PDMAEMA-MNP microgels are discussed in Appendix E.

4.3.5 Critique of Insoluble Draw Agents

Insoluble draw agents, such as gels and particles, attracted attention due to their ease of removal and low RSF. Dozens of papers have been published on the subject, with varying degrees of success. However, insoluble materials possess several inherent properties which limit their potential as draw agents.

Due to their larger size (and often higher density), solid draw agents cannot achieve high loadings in water. Increasing the concentration will either decrease the fluidity of the dispersion (in the case of some microgels) or result in sedimentation (in the case of dense particles). Significant loadings of draw solute are essential to produce a high π.

As the particle size of the solid draw agent increases, other problems arise. Even if a high concentration of draw agent can be achieved, as the particle size grows, so does the maximum interparticle distance (Figure 4.9). For example, as the particle radius (r) increases from 0.5 μm to 100 μm, the maximum interparticle distance (approximately equal to 0.15 x r) increases from 0.07 μm to 15 μm. As the draw agent can only affect the chemical potential of water within a certain distance of its surface, at a critical particle radius there will be water between the particles which is unaffected by the particles and will have the same chemical potential as bulk water. As the particle radius grows further (e.g., bulk gels), ECP and contact with the membrane must also be addressed, as discussed in Chapter 3.

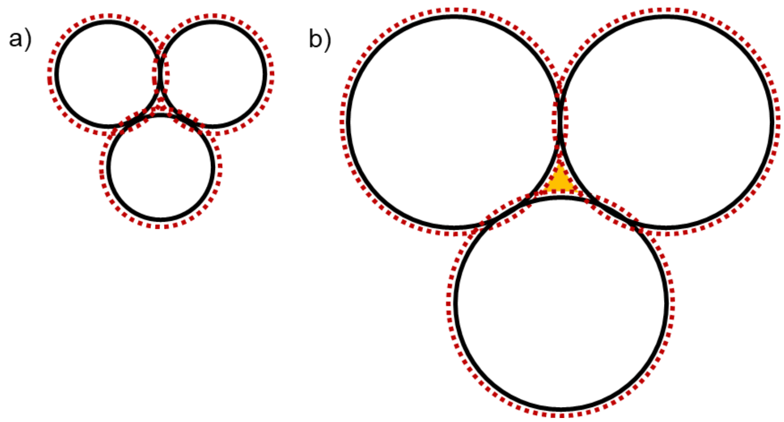

Figure 4.9 Radius of solid draw agents and osmotic pressure. Particles in closed packed configuration are illustrated by black lines. The regions of water affected by the particle surface are illustrated by dotted red lines. a) When particle size is small, the interparticle distance is small; all the bulk water is affected by the particles. b) When particles size increases, the volume of water between the particles increases; particles can no longer affect all the bulk water. Water unaffected by the particles is highlighted in yellow.

The use of insoluble draw agents also presents mechanical challenges. Conventional osmometers are designed to measure the π of solutions, which makes characterizing insoluble draw agents difficult. In addition, conventional FO apparatuses are designed for fluids, not solids. The use of insoluble draw agents would involve a significant redesigned of the traditional FO apparatus. For example, the draw agent must either be stationary, or a method must be developed to cycle solid material away from the membrane. These changes are not trivial.

Barring future improvements, as it currently stands the benefits provided by solid draw agents are outweighed by their limitations. Furthermore, the benefits offered by solid draw agents can all be provided for by modern soluble draw agents, which can be more easily incorporated into industrial FO apparatuses.

4.4 Conclusion

The use of thermo-and CO_2-responsive magnetic particles as FO draw solutes was explored. Two types of particles were synthesized: PDMAEMA-functionalized MNP, and PDMAEMA microgels with embedded MNP. Both the magnetic microgels and nanoparticles failed to produce significant fluxes, even against dilute feeds. Their poor FO performance, in combination with other problems common to insoluble draw agents, make them unlikely successors to TMA as a high-performance draw agent. The ease of recovery of the magnetic microgel particles may lead to their successful use in other fields.

Chapter 5

Conclusions and Recommendations

5.1 Conclusions

This thesis presented an in-depth study of CO_2-responsive forward osmosis draw solutes. Forward osmosis has the potential to revolutionize the field of water purification by reducing the energy required to filter concentrated feeds and facilitating the filtration of feeds with high fouling propensity. Prior to this work, the only viable CO_2-responsive draw solute was TMA, which has excellent FO performance but is limited by its odour and safety hazards. This work sought to find safe alternatives to TMA, while maintaining excellent FO performance. Several different CO_2-responsive materials were studied in this thesis: soluble polymers, magnetic particles, and hydrogels.

CO_2- and thermo-responsive PDMAAm hydrogels were synthesized via a simple one pot-synthesis. PDMAAm hydrogels displayed high swelling ratios, were able to expel >99% of absorbed water and exhibited high initial fluxes on a small scale. However, the gels were severely limited by poor mass transfer and ECP which could restrict their use as a draw agent. FO performance may be improved by using a new FO apparatus which circulates the gel while maintaining firm contact between the gel and membrane. However, this requires a large investment of time and capital which is unappealing as superior draw solutes exist.

Two CO_2-responsive magnetic draw agents were considered: PDMAEMA microgels with embedded magnetite nanoparticles and PDMAEMA grafted magnetic nanoparticles. Neither draw agent produced significant fluxes, even against dilute feeds. The advantages of using a magnetic draw agent were outweighed by their numerous disadvantages, including reduced chemical compatibility, more complex and costly synthesis, and decreased loading in water.

Although these materials were not proven to be successful in this preliminary study, future work and optimization may result in more success.

While the hydrogels and magnetic particles did not show great promise as draw agents in this work, it was essential to explore the potential of these less conventional draw agents, if only to eliminate them from contention. Exploring frontiers is important, even if they do not prove to be successful.

Among all the draw solutes studied in this work, soluble polymers are the most promising candidates to replace TMA. These polymers are relatively inexpensive to synthesize and would be easy to substitute from TMA as they can be used in traditional apparatuses and use conventional methods of recovery (e.g., UF). Among the polymers studied, PDMAAm displayed the best properties; concentrated PDMAAm solutions produced high π_{CO2} while maintaining a low π_{air}. PDMAAm was discovered to have thermo-responsive behaviour in water which could further facilitate the draw solution's regeneration. Preliminary FO results demonstrated that concentrated PDMAAm solutions can produce high fluxes from concentrated feed solutions. An alternative synthetic route for PDMAAm was developed to facilitate its production on a large scale by avoiding the use of pyrophoric reagents and minimizing the use of flammable organic solvents.

Further work has been done in the Jessop group to increase the π_{CO2} of PDMAAm and decrease its viscosity [216]. The FO performance of PDMAAm on a large scale is being investigated by Forward Water Technologies. The introduction of PDMAAm as a draw solute could expand the range of feeds that can currently be processed by CO_2-responsive FO to include feeds with high purify requirements, which currently cannot be done with TMA. It is hoped that the technology first explored in this work will continue to be developed, and will one day lead to more wastewater being properly disposed of, resulting in less damage to the environment and human health.

5.2 Recommendations for Future Areas of Study

5.2.1 Soluble polymers

While this work identified a promising draw solute candidate in PDMAAm, much more work remains to be done before it can be used industrially. Initially, further exploration of the role of the structure of PDMAAm is required. This includes optimization of the molecular weight and dispersity while considering their effect on viscosity, π_{air} and RSF. The use (and viability) of controlled radical polymerization should be considered when optimizing the dispersity. The synthesis of PDMAAm should also be examined in depth, to decrease its environmental impact and cost.

Although the π_{air}, π_{CO2}, and small-scale FO results of concentrated PDMAAm solutions are positive and mark an important first step in assessing draw solute ability, many other key draw solute metrics have not yet been explored. The performance of PDMAAm on a large-scale FO apparatus must be assessed. The flux versus a range of feeds, RSF, optimal temperature and membrane compatibility must be studied. The use of slight CO_2 pressures (≤5 bar) to increase the percent protonation of the amines should also be investigated; the benefits of the additional π_{CO2} must be balanced with increased equipment and operation costs. The recycling of PDMAAm must also be studied, including the dewater flux by NF, rate and percentage of decarbonation, rate of recarbonation, as well as the purity of the product water. The use of solar or waste heat for draw solute decarbonation and separation must be studied; this is essential to reduce the electric power consumption of FO, and to make it competitive with traditional methods. In addition, the use of the thermo-responsive properties of PDMAAm during draw solute separation should be investigated. The effect of using ionized water (e.g., municipal tap water) (as opposed to deionized water) as the draw solution solvent on the LCST must also be considered. Finally, the energy consumed by the whole FO process using PDMAAm as a draw solute must be quantified and compared to other draw solutes and conventional water filtration techniques to determine whether PDMAAm's performance is competitive.

The anti-bacterial properties of PDMAAm should be investigated. The anti-bacterial properties of cationic amines have been extensively studied, including PEI [254] and PDMAEMA [255,256]. PDMAAm may exhibit the same properties when protonated. Bacterial fouling can cause membranes to fail with catastrophic results, such as when they are used to produce potable water for rural communities with limited water supplies [107,257]. While using an anti-bacterial draw likely could not inhibit fouling on the feed side, it has the potential to increase the lifespan of the membrane. The pH of the uncarbonated draw solution is likely high enough to prevent bacterial growth.

Although PDMAAm is an excellent draw solute candidate, it was discovered from a relatively small pool of contestants. Screening of more polymers could lead to a draw solute with improved properties. Further work could include investigating the placement of the nitrogen within the polymer- for example, poly(N-methylbutylenimine), which is an isomer of PDMAAm. In addition, finding a polymer with an optimal pK_{aH} could also increase the π_{CO2}.

Finally, the polymers examined in this work could be substituted for small molecule amines used in other CO_2-responsive applications, such as switchable water [258,259]. Polymeric amines may be an improvement over small molecules due to their larger change in ionic strength and reduced flammability. Using CO_2- and thermo-responsive polymers, such as PDMAAm, may lead to enhanced amine separation and improved phase separation (as discussed in Chapter 3). CO_2- and thermo-responsive small molecules (e.g., morpholine derivatives [260]) have not yet been unexplored in depth and therefore also merit further study.

5.2.2 Gels

Insoluble materials such as gels are a newer class of draw agent and have been investigated less than liquid or soluble draw agents. Using insoluble draw agents consequently requires more research, and proof of concept experiments. Before investing further time studying hydrogel draw agents, the feasibility of using any gel draw agent on a large scale should be investigated in depth. Considerations must include ensuring that there is good contact between the gel and the membrane, that high fluxes can be maintained for extended periods of time, and that the gels may be incorporated into a continuous process.

If gels draw solutes are deemed to be industrially practical, many more FO parameters remain to be investigated, as with the soluble draw agents. Future experiments should include further review of the reuse performance and mechanical properties, as well as the rates of carbonation, decarbonation, and water release. The form of the PDMAAm gel (bulk versus microgel) should also be explored. If the CO_2- and thermo-responsive gels do not prove to be successful as draw solutes, there are a variety of other applications which could benefit from a material which has a high capacity to absorb water and release it at accessible temperatures (e.g., drying agents, pet litter, personal hygiene products, gels with slow water release for agriculture).

5.2.3 Magnetic Particles

While the magnetic particle draw agents explored in this work did not produce high fluxes, other magnetic draw agents have proved to be effective in the literature. Therefore, it is likely that further optimization of the system is required, including the nature of the CO_2-responsive polymer, the carbonation process, and the concentration of the draw agent.

One area where magnetic particles have a unique advantage over other draw agents is the use of induction heating. By using induction heating as opposed to conduction heating, the magnetic particles may be heated directly (and rapidly), rather than heating the solution around it. Induction heating has been used in the past to dewater magnetic particles with thermo-responsive coatings, and could be used to accelerate the removal of CO_2 from carbonated draw agents [169,261]. This may be particularly useful if amines with higher enthalpies of protonation were used.

The particles used in this work may also have use in applications aside from FO. Potential examples include as scavengers for water contaminants (e.g., metals [29,262], dyes [263]), Pickering emulsifiers [264] or catalysts (which may also benefit from localized heating via induction) [20]). Incorporation of magnetic particles may also have use in other CO_2-responsive systems. In many cases, the CO_2-responsive materials need to be removed after use (e.g., SHS, switchable water). These materials rely on the properties of the uncarbonated state facilitating their separation. However, the change in properties under air and CO_2 is often not sufficient (e.g., PMEI as discussed in Chapter 2). Using magnetic nanoparticles could ease the removal of such CO_2 responsive materials. In addition, the use of induction heating may facilitate the decarbonation of carbamates, which requires high temperatures.

References

[1] M. Wei, Y. Gao, X. Li, M.J. Serpe, Stimuli-responsive polymers and their applications, Polym. Chem. 8 (2017) 127–143. https://doi.org/10.1039/c6py01585a.

[2] Y. Kotsuchibashi, M. Ebara, T. Aoyagi, R. Narain, Recent advances in dual temperature responsive block copolymers and their potential as biomedical applications, Polymers (Basel). 8 (2016). https://doi.org/10.3390/polym8110380.

[3] P.G. Jessop, M.F. Cunningham, CO_2-switchable materials, 1st ed., Royal Society of Chemistry, London, 2021.

[4] T. Yildirim, A. Traeger, E. Preussger, S. Stumpf, C. Fritzsche, S. Hoeppener, S. Schubert, U.S. Schubert, Dual Responsive Nanoparticles from a RAFT Copolymer Library for the Controlled Delivery of Doxorubicin, Macromolecules. 49 (2016) 3856–38368. https://doi.org/10.1021/acs.macromol.5b02603.

[5] N. Vijayakameswara Rao, H. Ko, J. Lee, J.H. Park, Recent progress and advances in stimuli-responsive polymers for cancer therapy, Front. Bioeng. Biotechnol. 6 (2018). https://doi.org/10.3389/fbioe.2018.00110.

[6] E. ToolBox, Solubility of Gases in Water, (2008). https://www.engineeringtoolbox.com/gases-solubility-water-d_1148.html (accessed April 27, 2020).

[7] A.K. Alshamrani, J.R. Vanderveen, P.G. Jessop, A guide to the selection of switchable functional groups for CO_2-switchable compounds, Phys. Chem. Chem. Phys. 18 (2016) 19276–19288. https://doi.org/10.1039/C6CP03302D.

[8] A. Stefánsson, P. Bénézeth, J. Schott, Carbonic acid ionization and the stability of sodium bicarbonate and carbonate ion pairs to 200°C - A potentiometric and spectrophotometric

study, Geochim. Cosmochim. Acta. 120 (2013) 600–611. https://doi.org/10.1016/j.gca.2013.04.023.

[9] C. Housecroft, A. Sharpe, Inorganic Chemistry, 5th ed., Pearson Higher Ed., 2012.

[10] C. Roosen, M. Ansorge-Schumacher, T. Mang, W. Leitner, L. Greiner, Gaining pH-control in water/carbon dioxide biphasic systems, Green Chem. 9 (2007) 455–45. https://doi.org/10.1039/b613345b.

[11] L. Dong, Y. Zhao, CO_2-switchable membranes: Structures, functions, and separation applications in aqueous medium, J. Mater. Chem. A. 8 (2020) 16738–16746. https://doi.org/10.1039/d0ta04835f.

[12] H.J. Reich, Bordwell pKa Table (water), Org. Chem. Data. (2001). https://organicchemistrydata.org/hansreich/resources/pka/#pka_general (accessed January 26, 2021).

[13] R. Williams, pKa Data compiled by R.Williams, Res. Psu.Edu/Brpgroup/PKa_compilation.Pdf. (2011). https://organicchemistrydata.org/hansreich/resources/pka/pka_data/pka-compilation-williams.pdf (accessed January 26, 2021).

[14] X. Wang, N.G. Akhmedov, Y. Duan, B. Li, Nuclear magnetic resonance studies of CO_2 absorption and desorption in aqueous sodium salt of alanine, Energy and Fuels. 29 (2015) 3780–3784. https://doi.org/10.1021/acs.energyfuels.5b00535.

[15] G. Gwak, D.I. Kim, J. Kim, M. Zhan, S. Hong, An integrated system for CO_2 capture and water treatment by forward osmosis driven by an amine-based draw solution, J. Memb. Sci. 581 (2019) 9–17. https://doi.org/10.1016/j.memsci.2019.03.036.

[16] F. Bougie, M.C. Iliuta, Sterically hindered amine-based absorbents for the removal of CO_2

from gas streams, J. Chem. Eng. Data. 57 (2012) 635–669. https://doi.org/10.1021/je200731v.

[17] J. Ho, B. Mudraboyina, C. Spence-Elder, R. Resendes, M.F. Cunningham, P.G. Jessop, Water-borne coatings that share the mechanism of action of oil-based coatings, Green Chem. 20 (2018) 1899–1905. https://doi.org/10.1039/c8gc00130h.

[18] X. Su, M.F. Cunningham, P.G. Jessop, Use of a switchable hydrophobic associative polymer to create an aqueous solution of CO_2 -switchable viscosity, Polym. Chem. 5 (2014) 940–944. https://doi.org/10.1039/C3PY01382K.

[19] X. Su, P.G. Jessop, M.F. Cunningham, Surfactant-Free Polymerization Forming Switchable Latexes That Can Be Aggregated and Redispersed by CO_2 Removal and Then Readdition, (2012). https://doi.org/10.1021/ma202547c.

[20] J. Tang, X. Zhou, S. Cao, L. Zhu, L. Xi, J. Wang, Pickering Interfacial Catalysts with CO_2 and Magnetic Dual Response for Fast Recovering in Biphasic Reaction, ACS Appl. Mater. Interfaces. 11 (2019) 16156–16163. https://doi.org/10.1021/acsami.9b00821.

[21] J. Glasing, P.G. Jessop, P. Champagne, M.F. Cunningham, Graft-modified cellulose nanocrystals as CO_2-switchable Pickering emulsifiers, Polym. Chem. 9 (2018) 3864–3872. https://doi.org/10.1039/c8py00417j.

[22] A. Rezaee Shirin-Abadi, M. Gorji, S. Rezaee, P.G. Jessop, M.F. Cunningham, CO_2-Switchable-hydrophilicity membrane (CO_2-SHM) triggered by electric potential: faster switching time along with efficient oil/water separation, Chem. Commun. 54 (2018) 8478–8481. https://doi.org/10.1039/c8cc04266g.

[23] K.J. Boniface, R.R. Dykeman, A. Cormier, H.-B. Wang, S.M. Mercer, G. Liu, M.F. Cunningham, P.G. Jessop, CO2-switchable drying agents, Cite This Green Chem. 18 (2016) 208. https://doi.org/10.1039/c5gc01201e.

[24] S.M. Mercer, T. Robert, D. V. Dixon, C.-S. Chen, Z. Ghoshouni, J.R. Harjani, S. Jahangiri, G.H. Peslherbe, P.G. Jessop, Design, synthesis, and solution behaviour of small polyamines as switchable water additives, Green Chem. 14 (2012) 832. https://doi.org/10.1039/c2gc16240g.

[25] G.M. Ullmann, Relations between protonation constants and titration curves in polyprotic acids: A critical view, J. Phys. Chem. B. 107 (2003) 1263–1271. https://doi.org/10.1021/jp026454v.

[26] M.F. Cunningham, P.G. Jessop, An introduction to the principles and fundamentals of CO_2-switchable polymers and polymer colloids, Eur. Polym. J. 76 (2016) 208–215. https://doi.org/10.1016/j.eurpolymj.2016.01.036.

[27] C. Zhang, M. Maric, C. Zhang, M. Maric, Synthesis of Stimuli-responsive, Water-soluble Poly[2-(dimethylamino)ethyl methacrylate/styrene] Statistical Copolymers by Nitroxide Mediated Polymerization, Polymers (Basel). 3 (2011) 1398–1422. https://doi.org/10.3390/polym3031398.

[28] C. Pietsch, U. Mansfeld, C. Guerrero-Sanchez, S. Hoeppener, A. Vollrath, M. Wagner, R. Hoogenboom, S. Saubern, S.H. Thang, C.R. Becer, J. Chiefari, U.S. Schubert, Thermo-induced self-assembly of responsive poly(DMAEMA-b-DEGMA) block copolymers into multi- and unilamellar vesicles, Macromolecules. 45 (2012) 9292–9302. https://doi.org/10.1021/ma301867h.

[29] Y. Bai, Y.N. Liang, X. Hu, An eco-friendly approach for heavy metal adsorbent regeneration using CO_2-responsive molecular octopus, Chemosphere. 185 (2017) 1157–1163. https://doi.org/10.1016/j.chemosphere.2017.07.086.

[30] L. Hu, L.Y. Chu, M. Yang, H.D. Wang, C. Hui Niu, Preparation and characterization of novel cationic pH-responsive poly(N, N′-dimethylamino ethyl methacrylate) microgels, J.

Colloid Interface Sci. 311 (2007) 110–117. https://doi.org/10.1016/j.jcis.2007.02.063.

[31] H. Liu, X. Yuan, J. Ho, M.F. Cunningham, R.D. Oleschuk, P.G. Jessop, A CO_2-switchable surface on aluminium, Appl. Surf. Sci. 525 (2020) 146630. https://doi.org/10.1016/j.apsusc.2020.146630.

[32] T. Liu, B. Liu, X. Fu, S. Sun, W. Liu, G. Bian, Y. Qi, X. Yang, Synthesis of multifunctional microspheres having polymer brush with magnetism, fluorescence, and pH-responsiveness, Colloid Polym. Sci. 293 (2015) 809–816. https://doi.org/10.1007/s00396-014-3469-4.

[33] K.R. Harris, P.J. Dunlop, Osmotic coefficient data for the system benzene-benzoic acid at 25.degree., J. Phys. Chem. 71 (2005) 483–486. https://doi.org/10.1021/j100862a004.

[34] A. Achilli, T.Y. Cath, A.E. Childress, Selection of inorganic-based draw solutions for forward osmosis applications, J. Memb. Sci. 364 (2010) 233–241. https://doi.org/10.1016/j.memsci.2010.08.010.

[35] J.D. Roach, M.M. Bondaruk, Z. Burney, Nonideal Solution Behavior in Forward Osmosis Processes Using Magnetic Nanoparticles, in: Osmotically Driven Membr. Process. - Approach, Dev. Curr. Status, InTech, 2018. https://doi.org/10.5772/intechopen.72474.

[36] G.N. Lewis, The osmotic pressure of concentrated solutions, and the laws of the perfect solution, J. Am. Chem. Soc. 30 (1908) 668–683. https://doi.org/10.1021/ja01947a002.

[37] C.J. Van Oss, K. Arnold, S. Ohki, R.J. Good, K. Gawrisch, Interfacial tension and the osmotic pressure of solutions of polar polymers, J. Macromol. Sci. Part A - Chem. 27 (1990) 563–580. https://doi.org/10.1080/00222339009349643.

[38] A. Grattoni, G. Canavese, F.M. Montevecchi, M. Ferrari, Fast membrane osmometer as alternative to freezing point and vapor pressure osmometry, Anal. Chem. 80 (2008) 2617–

2622. https://doi.org/10.1021/ac7023987.

[39] M. Madden, S.N. Ellis, A. Riabtseva, A.D. Wilson, M.F. Cunningham, P.G. Jessop, Comparison of Vapour Pressure Osmometry, Freezing Point Osmometry and Direct Membrane Osmometry for the Determination of Osmotic Pressure of Aqueous Solutions (UNPUBLISHED), 2021.

[40] D.L. Shaffer, J.R. Werber, H. Jaramillo, S. Lin, M. Elimelech, Forward osmosis: Where are we now?, Desalination. 356 (2015) 271–284. https://doi.org/10.1016/j.desal.2014.10.031.

[41] P. Dey, E.L. Izake, Mixed Polymer-Coated Magnetic Nanoparticles as Forward Osmosis Draw Agents of Tuned Hydrophilicity, Chem. - A Eur. J. 22 (2016) 11253–11260. https://doi.org/10.1002/chem.201600144.

[42] J.R. Mccutcheon, M. Elimelech, Influence of concentrative and dilutive internal concentration polarization on flux behavior in forward osmosis, J. Memb. Sci. 284 (2006) 237–247. https://doi.org/10.1016/j.memsci.2006.07.049.

[43] M. Cho, S.H. Lee, D. Lee, D.P. Chen, I.C. Kim, M.S. Diallo, Osmotically driven membrane processes: Exploring the potential of branched polyethyleneimine as draw solute using porous FO membranes with NF separation layers, J. Memb. Sci. 511 (2016) 278–288. https://doi.org/10.1016/j.memsci.2016.02.041.

[44] N. Hiroshi, N. Mitsutoshi, W. Atsuo, I. Shin-ichi, N. Shin-ichi, K. Shoji, Development of a New Type of Membrane Osmometer, J. Chem. Eng. Japan. 25 (1992) 269–274.

[45] Advanced Instruments, The Advanced Osmometer Model 3250 User's Guide, Norwood, MA, 2003. https://ca.vwr.com/assetsvc/asset/en_CA/id/15963129/contents (accessed June 11, 2020).

[46] Gonotec, User Guide Cryoscopic Osmometer OSMOMAT auto, 2006. www.gonotec.com (accessed June 8, 2020).

[47] Knauer, K-7400 Freezing Point Osmometer Instructions, Berlin, 2020. www.knauer.net (accessed June 10, 2020).

[48] H. Dutrochet, Nouvelles observations sur l'endosmose et l'exosmose, et sur la cause de ce double phénomène, Ann. Chim. Phys. 35 (1827) 393–400. http://www.bibnum.education.fr/sciencesdelavie/biologie/nouvelles-observations-sur-l-endosmose-et-l-exosmose-et-sur-la-cause-de-ce- (accessed May 18, 2021).

[49] D. Talbot, Desalination out of Desperation, MIT Technol. Rev. (2014). https://www.technologyreview.com/s/533446/desalination-out-of-desperation/ (accessed October 20, 2016).

[50] UNESCO, Managin Water under Uncertainty and Risk, Report 4, Paris, 2012.

[51] P. Drechsel, M. Qadir, D. Wichelns, Wastewater: Economic asset in an urbanizing world, Wastewater Econ. Asset an Urban. World. (2015) 1–282. https://doi.org/10.1007/978-94-017-9545-6.

[52] P.G. Jessop, M.F. Cunningham, P. Champagne, S.N. Ellis, R.R. Dykeman, C. Honeyman, A. Holland, T. Robert, B.P. Mudraboyina, Forming a Treated Switchable Polymer and Use Thereof in a Forward Osmosis System, 62/722,275, 2018.

[53] Y. Hu, Z. Liu, N. Wang, X. An, Z. Zhou, Continuous juice concentration by integrating forward osmosis with membrane distillation using potassium sorbate preservative as a draw solute, J. Memb. Sci. 573 (2018) 192–199. https://doi.org/10.1016/j.memsci.2018.12.010.

[54] S. Murodjon, X. Yu, M. Li, J. Duo, T. Deng, Lithium Recovery from Brines Including

Seawater, Salt Lake Brine, Underground Water and Geothermal Water, in: Thermodyn. Energy Eng. [Working Title], IntechOpen, 2020. https://doi.org/10.5772/intechopen.90371.

[55] M. Xie, L.D. Nghiem, W.E. Price, M. Elimelech, A forward osmosis-membrane distillation hybrid process for direct sewer mining: System performance and limitations, Environ. Sci. Technol. 47 (2013) 13486–13493. https://doi.org/10.1021/es404056e.

[56] U.S. Department of Energy, Materials for separation technologies: energy and emission reduction opportunities, (2005).

[57] A. Ali, R.A. Tufa, F. Macedonio, E. Curcio, E. Drioli, Membrane technology in renewable-energy-driven desalination, Renew. Sustain. Energy Rev. 81 (2018) 1–21. https://doi.org/10.1016/j.rser.2017.07.047.

[58] M. Qasim, M. Badrelzaman, N.N. Darwish, N.A. Darwish, N. Hilal, Reverse osmosis desalination: A state-of-the-art review, Desalination. 459 (2019) 59–104. https://doi.org/10.1016/j.desal.2019.02.008.

[59] M. Simon, Desalination Is Booming. But What About All That Toxic Brine? | WIRED, Wired. (2019). https://www.wired.com/story/desalination-is-booming-but-what-about-all-that-toxic-brine/ (accessed May 25, 2021).

[60] IDA, Internation Desalination Association, Desalin. Water Reuse by Numbers. (2019).

[61] P.S. Goh, W.J. Lau, M.H.D. Othman, A.F. Ismail, Membrane fouling in desalination and its mitigation strategies, Desalination. 425 (2018) 130–155. https://doi.org/10.1016/j.desal.2017.10.018.

[62] Saltworks, Applying Ultra-High Pressure Reverse Osmosis in Brine Management, Saltworkstech.Com. (2019). https://www.saltworkstech.com/articles/applying-ultra-high-

pressure-reverse-osmosis-in-brine-management/ (accessed March 19, 2021).

[63] DuPont, Water Chemistry and Pretreatment Feedwater Type and Analysis, 2020.

[64] H.T. Madsen, T.B. Hansen, T. Nakao, S. Goda, E.G. Søgaard, Combined geothermal heat and pressure retarded osmosis as a new green power system, Energy Convers. Manag. 226 (2020) 113504. https://doi.org/10.1016/j.enconman.2020.113504.

[65] M. Sheldon, E.Z. Jingxi, D. De Jager, R. Augustine, J. Korenak, C. Helix-Nielsen, I. Petrinic, Potential of dyes as draw solutions in forward osmosis for the south african textile industry, Water SA. 44 (2018) 258–268. https://doi.org/10.4314/wsa.v44i2.11.

[66] J. Hussain, I. Hussain, M. Arif, CHARACTERIZATION OF TEXTILE WASTEWATER, 2004.

[67] D.A. Yaseen, · M Scholz, Textile dye wastewater characteristics and constituents of synthetic effluents: a critical review, Int. J. Environ. Sci. Technol. 16 (2019) 1193–1226. https://doi.org/10.1007/s13762-018-2130-z.

[68] Y. Sun, J. Tian, Z. Zhao, W. Shi, D. Liu, F. Cui, Membrane fouling of forward osmosis (FO) membrane for municipal wastewater treatment: A comparison between direct FO and OMBR, (2016). https://doi.org/10.1016/j.watres.2016.08.039.

[69] V.A. Timkin, V.A. Lazarev, Determination of the Osmotic Pressure of Multicomponent Solutions in the Food Industry, Pet. Chem. 55 (2015) 301–307. https://link-springer-com.proxy.queensu.ca/content/pdf/10.1134/S0965544114090011.pdf (accessed May 12, 2021).

[70] J. Hiddink, R. De Boer, P.F.C. Nooy, Reverse Osmosis of Dairy Liquids, n.d. https://doi.org/10.3168/jds.S0022-0302(80)82915-8.

[71] U. Kulozik, H. Kesssler, Permeation Rate During Reverse Osmosis of Milk Influenced by

Osmotic Pressure and Deposit Formation, J. Food Sci. 53 (1988) 1377–1383. https://doi.org/10.1111/j.1365-2621.1988.tb09281.x.

[72] Lenntech, Osmotic Pressure Calculation, Lenntech.Com. (2021). https://www.lenntech.com/calculators/osmotic/osmotic-pressure.htm (accessed May 21, 2021).

[73] T.F. Speth, A.M. Gusses, R. Scott Summers, Evaluation of nanofiltration pretreatments for flux loss control, Desalination. 130 (2000) 31–44. https://doi.org/10.1016/S0011-9164(00)00072-2.

[74] H.K. Shon, S. Phuntsho, D.S. Chaudhary, S. Vigneswaran, J. Cho, Nanofiltration for water and wastewater treatment-a mini review, Drink. Water Eng. Sci. 6 (2013) 47–53. https://doi.org/10.5194/dwes-6-47-2013.

[75] M. Yasukawa, Y. Tanaka, T. Takahashi, M. Shibuya, S. Mishima, H. Matsuyama, Effect of molecular weight of draw solute on water permeation in forward osmosis process, Ind. Eng. Chem. Res. 54 (2015) 8239–8246. https://doi.org/10.1021/acs.iecr.5b01960.

[76] Q. She, R. Wang, A.G. Fane, C.Y. Tang, Membrane fouling in osmotically driven membrane processes: A review, J. Memb. Sci. 499 (2016) 201–233. https://doi.org/10.1016/j.memsci.2015.10.040.

[77] Q. Ge, M. Ling, T.S. Chung, Draw solutions for forward osmosis processes: Developments, challenges, and prospects for the future, J. Memb. Sci. 442 (2013) 225–237. https://doi.org/10.1016/j.memsci.2013.03.046.

[78] R.K. McGovern, J.H. Lienhard V, On the potential of forward osmosis to energetically outperform reverse osmosis desalination, J. Memb. Sci. 469 (2014) 245–250. https://doi.org/10.1016/j.memsci.2014.05.061.

[79] S. Zou, H. Yuan, A. Childress, Z. He, Energy Consumption by Recirculation: A Missing Parameter When Evaluating Forward Osmosis, Environ. Sci. Technol. 50 (2016) 6827–6829. https://doi.org/10.1021/acs.est.6b02849.

[80] R.L. McGinnis, M. Elimelech, Energy requirements of ammonia-carbon dioxide forward osmosis desalination, Desalination. 207 (2007) 370–382. https://doi.org/10.1016/j.desal.2006.08.012.

[81] S. Lee, C. Boo, M. Elimelech, S. Hong, Comparison of fouling behavior in forward osmosis (FO) and reverse osmosis (RO), J. Memb. Sci. 365 (2010) 34–39. https://doi.org/10.1016/j.memsci.2010.08.036.

[82] Trevi Systems, Technology | Trevi Systems Inc, (2019). https://www.trevisystems.com/technology- (accessed May 22, 2020).

[83] Y. Chun, D. Mulcahy, L. Zou, I.S. Kim, A short review of membrane fouling in forward osmosis processes, Membranes (Basel). 7 (2017) 30. https://doi.org/10.3390/membranes7020030.

[84] C.J. Orme, A.D. Wilson, 1-Cyclohexylpiperidine as a thermolytic draw solute for osmotically driven membrane processes, Desalination. 371 (2015) 126–133. https://doi.org/10.1016/j.desal.2015.05.024.

[85] C.Y. Tang, Q. She, W.C.L. Lay, R. Wang, A.G. Fane, Coupled effects of internal concentration polarization and fouling on flux behavior of forward osmosis membranes during humic acid filtration, J. Memb. Sci. 354 (2010) 123–133. https://doi.org/10.1016/j.memsci.2010.02.059.

[86] V. Yangali-Quintanilla, Z. Li, R. Valladares, Q. Li, G. Amy, Indirect desalination of Red Sea water with forward osmosis and low pressure reverse osmosis for water reuse, Desalination. 280 (2011) 160–166. https://doi.org/10.1016/j.desal.2011.06.066.

[87] N. Gawande, A.A. Mungray, Superabsorbent polymer (SAP) hydrogels for protein enrichment, Sep. Purif. Technol. 150 (2015) 86–94. https://doi.org/10.1016/j.seppur.2015.04.024.

[88] Modern Water, Forward Osmosis : Desalination, (2012). https://www.modernwater.com/desalination-systems/forward-osmosis-desalination (accessed May 22, 2020).

[89] W.A. Suwaileh, N. Pathak, H. Shon, N. Hilal, Forward osmosis membranes and processes: A comprehensive review od research trends and future outlook, Desalination. 485 (2020) 114455–114476.

[90] P.S. Goh, A.F. Ismail, B.C. Ng, M.S. Abdullah, Recent progresses of forward osmosis membranes formulation and design for wastewater treatment, Water (Switzerland). 11 (2019) 2043. https://doi.org/10.3390/w11102043.

[91] K. Jamal, M.A. Khan, M. Kamil, Mathematical modeling of reverse osmosis systems, Desalination. 160 (2004) 29–42. https://doi.org/10.1016/S0011-9164(04)90015-X.

[92] Y. Cai, X.M. Hu, A critical review on draw solutes development for forward osmosis, Desalination. 391 (2016) 16–29. https://doi.org/10.1016/j.desal.2016.03.021.

[93] J. Su, T.-S. Chung, B.J. Helmer, J.S. De Wit, Enhanced double-skinned FO membranes with inner dense layer for wastewater treatment and macromolecule recycle using Sucrose as draw solute, J. Memb. Sci. 396 (2012) 92–100. https://doi.org/10.1016/j.memsci.2012.01.001.

[94] X. Huang, M. Leal, Q. Li, Degradation of natural organic matter by TiO2 photocatalytic oxidation and its effect on fouling of low-pressure membranes, Water Res. 42 (2008) 1142–1150. https://doi.org/10.1016/j.watres.2007.08.030.

[95] H.K. Shon, S. Vigneswaran, I.S. Kim, J. Cho, H.H. Ngo, Fouling of ultrafiltration membrane by effluent organic matter: A detailed characterization using different organic fractions in wastewater, J. Memb. Sci. 278 (2006) 232–238. https://doi.org/10.1016/j.memsci.2005.11.006.

[96] W. Yuan, A.L. Zydney, Humic Acid Fouling during Ultrafiltration, Environ. Sci. Technol. 34 (2000) 5043–5050. https://doi.org/10.1021/es0012366.

[97] C. Jarusutthirak, G. Amy, J.P. Croué, Fouling characteristics of wastewater effluent organic matter (EfOM) isolates on NF and UF membranes, Desalination. 145 (2002) 247–255. https://doi.org/10.1016/S0011-9164(02)00419-8.

[98] B. Mi, M. Elimelech, Silica scaling and scaling reversibility in forward osmosis, Desalination. 312 (2013) 75–81. https://doi.org/10.1016/j.desal.2012.08.034.

[99] M. Herzberg, M. Elimelech, Biofouling of reverse osmosis membranes: Role of biofilm-enhanced osmotic pressure, J. Memb. Sci. 295 (2007) 11–20. https://doi.org/10.1016/j.memsci.2007.02.024.

[100] B. Mi, M. Elimelech, Gypsum Scaling and Cleaning in Forward Osmosis: Measurements and Mechanisms, Environ. Sci. Technol. 44 (2010) 2022–2028. https://doi.org/10.1021/es903623r.

[101] Saltworks, Reverse Osmosis Brine Treatment: Minimize Volume & Cost, (2019). https://www.saltworkstech.com/articles/reverse-osmosis-brine-treatment-minimize-volume-cost/ (accessed March 18, 2021).

[102] H.C. Flemming, G. Schaule, T. Griebe, J. Schmitt, A. Tamachkiarowa, Biofouling - The Achilles heel of membrane processes, Desalination. 113 (1997) 215–225. https://doi.org/10.1016/S0011-9164(97)00132-X.

[103] C. Dreszer, A.D. Wexler, S. Drusová, T. Overdijk, A. Zwijnenburg, H.C. Flemming, J.C. Kruithof, J.S. Vrouwenvelder, In-situ biofilm characterization in membrane systems using Optical Coherence Tomography: Formation, structure, detachment and impact of flux change, Water Res. 67 (2014) 243–254. https://doi.org/10.1016/j.watres.2014.09.006.

[104] J.M. Veza, M. Ortiz, J.J. Sadhwani, J.E. Gonzalez, F.J. Santana, Measurement of biofouling in seawater: some practical tests, Desalination. 220 (2008) 326–334. https://doi.org/10.1016/j.desal.2007.01.037.

[105] S. Mancuso, G. Carmignani, J. Webley, Trevi Systems' Forward Osmosis Pilot at Orange County Water District, Petaluma, CA, USA, 2019. www.trevisystems.com (accessed May 22, 2020).

[106] S.H. Kim, S.-Y. Kwak, B.-H. Sohn, T.H. Park, Design of TiO 2 nanoparticle self-assembled aromatic polyamide thin-film-composite (TFC) membrane as an approach to solve biofouling problem, 2003.

[107] J. Barrera, Attawapiskat declares state of emergency over water quality | CBC News, CBC. (2019). https://www.cbc.ca/news/indigenous/attawapiskat-water-quality-emergency-1.5204652 (accessed May 8, 2020).

[108] Y. Liu, B. Mi, Combined fouling of forward osmosis membranes: Synergistic foulant interaction and direct observation of fouling layer formation, J. Memb. Sci. 407 (2012) 136–144. https://doi.org/10.1016/j.memsci.2012.03.028.

[109] B. Mi, M. Elimelech, Chemical and physical aspects of organic fouling of forward osmosis membranes, J. Memb. Sci. 320 (2008) 292–302. https://doi.org/10.1016/j.memsci.2008.04.036.

[110] Y. Na, S. Yang, S. Lee, Evaluation of citrate-coated magnetic nanoparticles as draw solute for forward osmosis, Desalination. 347 (2014) 34–42.

https://doi.org/10.1016/j.desal.2014.04.032.

[111] C.J. Orme, A.D. Wilson, 1-Cyclohexylpiperidine as a thermolytic draw solute for osmotically driven membrane processes, Desalination. 371 (2015) 126–133. https://doi.org/10.1016/j.desal.2015.05.024.

[112] S. Zhao, L. Zou, Effects of working temperature on separation performance, membrane scaling and cleaning in forward osmosis desalination, Desalination. 278 (2011) 157–164. https://doi.org/10.1016/j.desal.2011.05.018.

[113] H. Zhou, D.W. Smith, Advanced technologies in water and wastewater treatment, J. Environ. Eng. Sci. 1 (2002) 247–264. https://doi.org/10.1139/s02-020.

[114] V. Parida, H.Y. Ng, Forward osmosis organic fouling: Effects of organic loading, calcium and membrane orientation, Desalination. 312 (2013) 88–98. https://doi.org/10.1016/j.desal.2012.04.029.

[115] B. Mi, M. Elimelech, Organic fouling of forward osmosis membranes: Fouling reversibility and cleaning without chemical reagents, J. Memb. Sci. 348 (2010) 337–345. https://doi.org/10.1016/j.memsci.2009.11.021.

[116] C. Riziero Martinetti, A.E. Childress, Y. Cath, High recovery of concentrated RO brines using forward osmosis and membrane distillation, J. Memb. Sci. 331 (2009) 31–39. https://doi.org/10.1016/j.memsci.2009.01.003.

[117] C. Boo, Y.F. Khalil, M. Elimelech, Performance evaluation of trimethylamine-carbon dioxide thermolytic draw solution for engineered osmosis, J. Memb. Sci. 473 (2015) 302–309. https://doi.org/10.1016/j.memsci.2014.09.026.

[118] B.M. Jun, T.P.N. Nguyen, S.H. Ahn, I.C. Kim, Y.N. Kwon, The application of polyethyleneimine draw solution in a combined forward osmosis/nanofiltration system, J.

Appl. Polym. Sci. 132 (2015) 1–9. https://doi.org/10.1002/app.42198.

[119] S. Laohaprapanon, Y.J. Fu, C.C. Hu, S.J. You, H.A. Tsai, W.S. Hung, K.R. Lee, J.Y. Lai, Evaluation of a natural polymer-based cationic polyelectrolyte as a draw solute in forward osmosis, Desalination. 421 (2017) 72–78. https://doi.org/10.1016/j.desal.2017.04.027.

[120] M.L. Stone, C. Rae, F.F. Stewart, A.D. Wilson, Switchable polarity solvents as draw solutes for forward osmosis, Desalination. 312 (2013) 124–129. https://doi.org/10.1016/j.desal.2012.07.034.

[121] H. Luo, Q. Wang, T.C. Zhang, T. Tao, A. Zhou, L. Chen, X. Bie, A review on the recovery methods of draw solutes in forward osmosis, J. Water Process Eng. 4 (2014) 212–223. https://doi.org/10.1016/j.jwpe.2014.10.006.

[122] Y. Cai, X.M. Hu, A critical review on draw solutes development for forward osmosis, Desalination. 391 (2016) 16–29. https://doi.org/10.1016/j.desal.2016.03.021.

[123] H.K. Shon, L. Chekli, S. Phuntsho, J. Kim, J. Cho, Draw Solutes in Forward Osmosis Processes, Forw. Osmosis. (2015) 85–113. https://doi.org/10.1061/9780784414071.ch05.

[124] K.S. Bowden, A. Achilli, A.E. Childress, Organic ionic salt draw solutions for osmotic membrane bioreactors, Bioresour. Technol. 122 (2012) 207–216. https://doi.org/10.1016/j.biortech.2012.06.026.

[125] L. Chekli, Y. Kim, S. Phuntsho, S. Li, N. Ghaffour, H.K. Leiknes, TorOve, Shon, Evaluation of fertilizer-drawn forward osmosis for sustainable agriculture and water reuse in arid regions, J. Environ. . 187 (2017) 137–145. https://ac.els-cdn.com/S0301479716308970/1-s2.0-S0301479716308970-main.pdf?_tid=33ee1ccc-0cdb-11e8-b034-00000aab0f26&acdnat=1518099804_9bde063cb3862da4977a85f05237afc1 (accessed February 8, 2018).

[126] G. Gwak, B. Jung, S. Han, S. Hong, Evaluation of poly (aspartic acid sodium salt) as a draw solute for forward osmosis, Water Res. 80 (2015) 294–305. https://doi.org/10.1016/j.watres.2015.04.041.

[127] D. Li, X. Zhang, J. Yao, G.P. Simon, H. Wang, Stimuli-responsive polymer hydrogels as a new class of draw agent for forward osmosis desalination, Chem. Commun. 47 (2011) 1710–1712. https://doi.org/10.1039/c0cc04701e.

[128] Q. Ge, J. Su, T.-S. Chung, G. Amy, Hydrophilic Superparamagnetic Nanoparticles: Synthesis, Characterization, and Performance in Forward Osmosis Processes, Ind. Eng. Chem. Res. 50 (2011) 382–388. https://doi.org/10.1021/ie101013w.

[129] H.Y. Ng, W. Tang, Forward (Direct) Osmosis: A Novel and Prospective Process for Brine Control, Water Environ. Found. 2006 (2014) 4345–4352. https://doi.org/10.2175/193864706783778952.

[130] K.B. Petrotos, P. Quantick, H. Petropakis, A study of the direct osmotic concentration of tomato juice in tubular membrane - Module configuration. I. The effect of certain basic process parameters on the process performance, J. Memb. Sci. 150 (1998) 99–110. https://doi.org/10.1016/S0376-7388(98)00216-6.

[131] T.Y. Cath, N.T. Hancock, C.D. Lundin, C. Hoppe-Jones, J.E. Drewes, A multi-barrier osmotic dilution process for simultaneous desalination and purification of impaired water, J. Memb. Sci. 362 (2010) 417–426. https://doi.org/10.1016/j.memsci.2010.06.056.

[132] N.T. Hancock, N.D. Black, T.Y. Cath, A comparative life cycle assessment of hybrid osmotic dilution desalination and established seawater desalination and wastewater reclamation processes, Water Res. 46 (2012) 1145–1154. https://doi.org/10.1016/j.watres.2011.12.004.

[133] S. Phuntsho, F. Lotfi, S. Hong, D.L. Shaffer, M. Elimelech, H.K. Shon, Membrane scaling

and flux decline during fertiliser-drawn forward osmosis desalination of brackish groundwater, Water Res. 57 (2014) 172–182. https://doi.org/10.1016/j.watres.2014.03.034.

[134] K. Stache, Apparatus for transforming seawater, brackish water, polluted water, or the like into a nutrious drink by means of osmosis, US4879030A, 1989. https://patents.google.com/patent/US4879030A/en (accessed May 28, 2020).

[135] R.E. Kravath, J.A. Davis, Desalination of sea water by direct osmosis, Desalination. 16 (1975) 151–155. https://doi.org/10.1016/S0011-9164(00)82089-5.

[136] FTSH2O, Personal Hydration, Forw. Osmosis Solut. Ind. Appl. (2017). http://ftsh2o.com/products/personal-hydration/ (accessed May 28, 2020).

[137] Y. Cai, R. Wang, W.B. Krantz, A.G. Fane, X. ‘Matthew’ Hu, Exploration of using thermally responsive polyionic liquid hydrogels as draw agents in forward osmosis, RSC Adv. 5 (2015) 97143–97150. https://doi.org/10.1039/C5RA19018E.

[138] Y. Mino, D. Ogawa, H. Matsuyama, Functional magnetic particles providing osmotic pressure as reusable draw solutes in forward osmosis membrane process, Adv. Powder Technol. 27 (2016) 2136–2144. https://doi.org/10.1016/j.apt.2016.08.001.

[139] M. Yu, H. Zhang, F. Yang, Supplementary Information-A study of a ferric-lactate complex as draw solute in forward osmosis, Chem. Eng. J. 314 (2017) 132–138. https://ac.els-cdn.com/S1385894716318721/1-s2.0-S1385894716318721-main.pdf?_tid=8ef3c876-0c39-11e8-a5b3-00000aacb361&acdnat=1518030379_d47465e4e30b740bfd8d2c7d669fccd3 (accessed February 8, 2018).

[140] D. Zhao, S. Chen, C.X. Guo, Q. Zhao, X. Lu, Multi-functional forward osmosis draw solutes for seawater desalination, in: Chinese J. Chem. Eng., 2016: pp. 23–30.

https://doi.org/10.1016/j.cjche.2015.06.018.

[141] P.G. Jessop, S.M. Mercer, T. Robert, T.J. Clark, B.E. Mariampillai, R. Resendes, S. Brown, Systems and methods for use of water with switchable ionic strength, US 2014/0076810 A1, 2012. https://patentimages.storage.googleapis.com/52/f7/99/a5540b43183f97/US20140076810A1.pdf (accessed March 7, 2018).

[142] M. Ikeda, K. Miyamoto, Draw Solution for Forward Osmosis Process, US 10,087,089 B2, 2018. https://patentimages.storage.googleapis.com/8c/09/7d/293a7e9e8f79ff/US10087089.pdf (accessed March 22, 2019).

[143] Y. Cai, W. Shen, R. Wang, W.B. Krantz, A.G. Fane, X. Hu, CO_2 switchable dual responsive polymers as draw solutes for forward osmosis desalination, Chem. Commun. 49 (2013) 8377. https://doi.org/10.1039/c3cc43289k.

[144] Environmetal Protection Agency, Acute Exposure Guidline Levels for Trimethylamine, 2006. https://www.epa.gov/sites/production/files/2014-08/documents/trimethylamine_interim_ornl_jun_2008c.pdf (accessed January 3, 2020).

[145] Sigma-Aldrich, Trimethylamine Safty Data Sheet, Oakville, Canada, 2019. https://www.sigmaaldrich.com/MSDS/MSDS/DisplayMSDSPage.do?country=CA&language=en&productNumber=92251&brand=ALDRICH&PageToGoToURL=https%3A%2F%2Fwww.sigmaaldrich.com%2Fcatalog%2Fsearch%3Fterm%3DTrimethylamine%26interface%3DAll%26N%3D0%26mode%3Dpartialmax%26.

[146] M.T. Velasquez, A. Ramezani, A. Manal, D.S. Raj, Trimethylamine N-oxide: The good, the bad and the unknown, Toxins (Basel). 8 (2016) 326–337. https://doi.org/10.3390/toxins8110326.

[147] J.R. Vanderveen, J. Durelle, P.G. Jessop, Design and evaluation of switchable-hydrophilicity solvents, Green Chem. 16 (2014) 1187–1197. https://doi.org/10.1039/c3gc42164c.

[148] K.J. Viner, H.M. Roy, R. Lee, O. He, P. Champagne, P.G. Jessop, Transesterification of soybean oil using a switchable-hydrophilicity solvent, 2-(dibutylamino)ethanol, Green Chem. 21 (2019) 4786–4791. https://doi.org/10.1039/c9gc00241c.

[149] D.S. Wendt, C.J. Orme, G.L. Mines, A.D. Wilson, Energy requirements of the switchable polarity solvent forward osmosis (SPS-FO) water purification process, Desalination. 374 (2015) 81–91. https://doi.org/10.1016/j.desal.2015.07.012.

[150] H. Rabiee, B. Jin, S. Yun, S. Dai, Gas-responsive cationic microgels for forward osmosis desalination, Chem. Eng. J. 347 (2018) 424–431. https://doi.org/10.1016/j.cej.2018.04.148.

[151] S. Sharpe, Use of Switchable Polymers and Polyamines for Switchable FO. B. Sc. Thesis., Queen’s, 2015.

[152] R. Dykeman, M.F. Cunningham, P.G. Jessop, Meausring the osmotic pressure of TMA by DMO, Unpubl. Rep. (2015).

[153] J.R. McCutcheon, R.L. McGinnis, M. Elimelech, Desalination by ammonia-carbon dioxide forward osmosis: Influence of draw and feed solution concentrations on process performance, J. Memb. Sci. 278 (2006) 114–123. https://doi.org/10.1016/j.memsci.2005.10.048.

[154] J.R. McCutcheon, R.L. McGinnis, M. Elimelech, A novel ammonia-carbon dioxide forward (direct) osmosis desalination process, Desalination. 174 (2005) 1–11. https://doi.org/10.1016/j.desal.2004.11.002.

[155] J.D. Bos, M.M.H.M. Meinardi, The 500 Dalton rule for the skin penetration of chemical compounds and drugs, Exp. Dermatol. 9 (2000) 165–169. https://doi.org/10.1034/j.1600-0625.2000.009003165.x.

[156] P. Matsson, J. Kihlberg, How Big Is Too Big for Cell Permeability?, J. Med. Chem. 60 (2017) 1662–1664. https://doi.org/10.1021/acs.jmedchem.7b00237.

[157] M. Ahmed, R. Kumar, B. Garudachari, J.P. Thomas, Assessment of pilot scale forward osmosis system for Arabian Gulf seawater desalination using polyelectrolyte draw solution, Desalin. Water Treat. 157 (2019) 342–348. https://doi.org/10.5004/dwt.2019.24267.

[158] M. Ahmed, Y. Al-Wazzan, R. Kumar, B. Garudachari, J.P. Thomas, A comparative study of two different forward osmosis membranes tested using pilot-plant system for arabian gulf seawater desalination, Desalin. Water Treat. 176 (2020) 252–259. https://doi.org/10.5004/dwt.2020.25526.

[159] J.J. Kim, H. Kang, Y.S. Choi, Y.A. Yu, J.C. Lee, Thermo-responsive oligomeric poly(tetrabutylphosphonium styrenesulfonate)s as draw solutes for forward osmosis (FO) applications, Desalination. 381 (2016) 84–94. https://doi.org/10.1016/j.desal.2015.11.013.

[160] J. joo Kim, J.S. Chung, H. Kang, Y.A. Yu, W.J. Choi, H.J. Kim, J.C. Lee, Thermo-responsive copolymers with ionic group as novel draw solutes for forward osmosis processes, Macromol. Res. 22 (2014) 963–970. https://doi.org/10.1007/s13233-014-2142-6.

[161] C. Ju, C. Park, T. Kim, S. Kang, H. Kang, Thermo-responsive draw solute for forward osmosis process; Poly(ionic liquid) having lower critical solution temperature characteristics, RSC Adv. 9 (2019) 29493–29501. https://doi.org/10.1039/c9ra04020j.

[162] D. Zhao, P. Wang, Q. Zhao, N. Chen, X. Lu, Thermoresponsive copolymer-based draw

solution for seawater desalination in a combined process of forward osmosis and membrane distillation, Desalination. 348 (2014) 26–32. https://doi.org/10.1016/j.desal.2014.06.009.

[163] Q. Ge, J. Su, G.L. Amy, T.-S. Chung, Exploration of polyelectrolytes as draw solutes in forward osmosis processes, Water Res. 46 (2012) 1318–1326. https://doi.org/10.1016/j.watres.2011.12.043.

[164] J. Wang, S. Gao, J. Tian, F. Cui, W. Shi, Recent developments and future challenges of hydrogels as draw solutes in forward osmosis process, Water (Switzerland). 12 (2020) 1–20. https://doi.org/10.3390/w12030692.

[165] S. Zhao, Osmotic pressure versus swelling pressure: Comment on "bifunctional polymer hydrogel layers as forward osmosis draw agents for continuous production of fresh water using solar energy," Environ. Sci. Technol. 48 (2014) 4212–4213. https://doi.org/10.1021/es5006994.

[166] H. Wang, J. Wei, G.P. Simon, Response to Osmotic pressure versus swelling pressure: Comment on "bifunctional polymer hydrogel layers as forward osmosis draw agents for continuous production of fresh water using solar energy," Environ. Sci. Technol. 48 (2014) 4214–4215. https://doi.org/10.1021/es5011016.

[167] H. Wang, J. Wei, G.P. Simon, Response to Osmotic pressure versus swelling pressure: Comment on "bifunctional polymer hydrogel layers as forward osmosis draw agents for continuous production of fresh water using solar energy," Environ. Sci. Technol. 48 (2014) 4214–4215. https://doi.org/10.1021/es5011016.

[168] Y. Cai, W. Shen, S.L. Loo, W.B. Krantz, R. Wang, A.G. Fane, X. Hu, Towards temperature driven forward osmosis desalination using Semi-IPN hydrogels as reversible draw agents, Water Res. 47 (2013) 3773–3781.

https://doi.org/10.1016/j.watres.2013.04.034.

[169] A. Razmjou, M.R. Barati, G.P. Simon, K. Suzuki, H. Wang, Fast deswelling of nanocomposite polymer hydrogels via magnetic field-induced heating for emerging FO desalination, Environ. Sci. Technol. 47 (2013) 6297–6305. https://doi.org/10.1021/es4005152.

[170] A. Razmjou, G.P. Simon, H. Wang, Effect of particle size on the performance of forward osmosis desalination by stimuli-responsive polymer hydrogels as a draw agent, Chem. Eng. J. 215–216 (2013) 913–920. https://doi.org/10.1016/j.cej.2012.11.088.

[171] H. Luo, Q. Wang, T. Tao, T.C. Zhang, A. Zhou, Performance of strong ionic hydrogels based on 2-acrylamido-2-methylpropane sulfonate as draw agents for forward osmosis, J. Environ. Eng. (United States). 140 (2014) 04014044. https://doi.org/10.1061/(ASCE)EE.1943-7870.0000875.

[172] Y. Hartanto, M. Zargar, H. Wang, B. Jin, S. Dai, Thermoresponsive Acidic Microgels as Functional Draw Agents for Forward Osmosis Desalination, Environ. Sci. Technol. 50 (2016) 4221–4228. https://doi.org/10.1021/acs.est.5b04123.

[173] Y. Hartanto, S. Yun, B. Jin, S. Dai, Functionalized thermo-responsive microgels for high performance forward osmosis desalination, Water Res. 70 (2015) 385–393. https://doi.org/10.1016/j.watres.2014.12.023.

[174] Y. Zeng, L. Qiu, K. Wang, J. Yao, D. Li, G.P. Simon, R. Wang, H. Wang, Significantly enhanced water flux in forward osmosis desalination with polymer-graphene composite hydrogels as a draw agent, RSC Adv. 3 (2013) 887–894. https://doi.org/10.1039/c2ra22173j.

[175] D. Li, X. Zhang, J. Yao, Y. Zeng, G.P. Simon, H. Wang, Composite polymer hydrogels as draw agents in forward osmosis and solar dewatering, Soft Matter. 7 (2011) 10048–10056.

https://doi.org/10.1039/c1sm06043k.

[176] H. Zhang, J. Li, H. Cui, H. Li, F. Yang, Forward osmosis using electric-responsive polymer hydrogels as draw agents: Influence of freezing-thawing cycles, voltage, feed solutions on process performance, Chem. Eng. J. 259 (2015) 814–819. https://doi.org/10.1016/j.cej.2014.08.065.

[177] H. Cui, H. Zhang, M. Yu, F. Yang, Performance evaluation of electric-responsive hydrogels as draw agent in forward osmosis desalination, Desalination. 426 (2018) 118–126. https://doi.org/10.1016/j.desal.2017.10.045.

[178] Y. Hartanto, M. Zargar, H. Wang, B. Jin, S. Dai, Thermoresponsive Acidic Microgels as Functional Draw Agents for Forward Osmosis Desalination, Environ. Sci. Technol. 50 (2016) 4221–4228. https://doi.org/10.1021/acs.est.5b04123.

[179] Y. Hartanto, S. Yun, B. Jin, S. Dai, Functionalized thermo-responsive microgels for high performance forward osmosis desalination, Water Res. 70 (2015) 385–393. https://doi.org/10.1016/j.watres.2014.12.023.

[180] R. Ou, H. Zhang, G.P. Simon, H. Wang, Microfiber-polymer hydrogel monolith as forward osmosis draw agent, J. Memb. Sci. 510 (2016) 426–436. https://doi.org/10.1016/j.memsci.2016.03.031.

[181] A. Razmjou, Q. Liu, G.P. Simon, H. Wang, Bifunctional Polymer Hydrogel Layers As Forward Osmosis Draw Agents for Continuous Production of Fresh Water Using Solar Energy, Environ. Sci. Technol. 47 (2013) 32. https://doi.org/10.1021/es403266y.

[182] J. Zeng, S. Cui, Q. Wang, R. Chen, Multi-layer temperature-responsive hydrogel for forward-osmosis desalination with high permeable flux and fast water release, Desalination. 459 (2019) 105–113. https://doi.org/10.1016/j.desal.2019.02.002.

[183] Y. Hartanto, M. Zargar, X. Cui, Y. Shen, B. Jin, S. Dai, Thermoresponsive cationic copolymer microgels as high performance draw agents in forward osmosis desalination, J. Memb. Sci. 518 (2016) 273–281. https://doi.org/10.1016/j.memsci.2016.07.018.

[184] D. Li, X. Zhang, J. Yao, Y. Zeng, G.P. Simon, H. Wang, Composite polymer hydrogels as draw agents in forward osmosis and solar dewatering, Soft Matter. 7 (2011) 10048–10056. https://doi.org/10.1039/c1sm06043k.

[185] L. Liu, S. Adham, J. Oppenheimer, M. Kumar, Dewatering reverse osmosis concentrate using forward osmosis, in: 2007 Membr. Technol. Conf. Expo. Proc., Alexandria, VA, 2007: pp. 1–45.

[186] Hudson Institute of Mineralogy, Magnetite, MitDat. (2021). https://www.mindat.org/min-2538.html (accessed February 24, 2021).

[187] J. Wallyn, N. Anton, T.F. Vandamme, Synthesis, principles, and properties of magnetite nanoparticles for in vivo imaging applications—A review, Pharmaceutics. 11 (2019) 601. https://doi.org/10.3390/pharmaceutics11110601.

[188] M.M. Ling, K.Y. Wang, T.S. Chung, Highly water-soluble magnetic nanoparticles as novel draw solutes in forward osmosis for water reuse, Ind. Eng. Chem. Res. 49 (2010) 5869–5876. https://doi.org/10.1021/ie100438x.

[189] H. Bai, Z. Liu, D.D. Sun, Highly water soluble and recovered dextran coated Fe3O4 magnetic nanoparticles for brackish water desalination, Sep. Purif. Technol. 81 (2011) 392–399. https://doi.org/10.1016/j.seppur.2011.08.007.

[190] P. Dey, E.L. Izake, Magnetic nanoparticles boosting the osmotic efficiency of a polymeric FO draw agent: Effect of polymer conformation, Desalination. 373 (2015) 79–85. https://doi.org/10.1016/j.desal.2015.07.010.

[191] O. Tirosh, Y. Barenholz, J. Katzhendler, A. Priev, Hydration of polyethylene glycol-grafted liposomes, Biophys. J. 74 (1998) 1371–1379. https://doi.org/10.1016/S0006-3495(98)77849-X.

[192] M.M. Ling, T.S. Chung, X. Lu, Facile synthesis of thermosensitive magnetic nanoparticles as “smart” draw solutes in forward osmosis, Chem. Commun. 47 (2011) 10788–10790. https://doi.org/10.1039/c1cc13944d.

[193] F. Azadi, A. Karimi-Jashni, M.M. Zerafat, Desalination of brackish water by gelatin-coated magnetite nanoparticles as a novel draw solute in forward osmosis process, Environ. Technol. (United Kingdom). (2020). https://doi.org/10.1080/09593330.2020.1717642.

[194] I. Ban, S. Markuš, S. Gyergyek, M. Drofenik, J. Korenak, C. Helix-Nielsen, I. Petrinić, Synthesis of poly-sodium-acrylate (PSA)-coated magnetic nanoparticles for use in forward osmosis draw solutions, Nanomaterials. 9 (2019). https://doi.org/10.3390/nano9091238.

[195] F.N. Al-Deen, J. Ho, C. Selomulya, C. Ma, R. Coppel, Superparamagnetic nanoparticles for effective delivery of malaria DNA vaccine, Langmuir. 27 (2011) 3703–3712. https://doi.org/10.1021/la104479c.

[196] Q. Ge, L. Yang, J. Cai, W. Xu, Q. Chen, M. Liu, Hydroacid magnetic nanoparticles in forward osmosis for seawater desalination and efficient regeneration via integrated magnetic and membrane separations, J. Memb. Sci. 520 (2016) 550–559. https://doi.org/10.1016/j.memsci.2016.07.033.

[197] Manal-Mounir, R. Eglal, H. Gadallah, A.A. Azab, H.M. Ali, Comparative study for the preparation of superparamagnetic-citric coated magnetic nanoparticle and fodesalination application, ARPN J. Eng. Appl. Sci. 13 (2018) 1150–1162. www.arpnjournals.com (accessed November 21, 2019).

[198] Government of Canada, Engineered nanoparticles: Health and safety considerations - Canada.ca, Employ. Soc. Dev. Canada. (2019). https://www.canada.ca/en/employment-social-development/services/health-safety/reports/engineered-nanoparticles.html (accessed March 18, 2021).

[199] Y. Na, S. Yang, S. Lee, Evaluation of citrate-coated magnetic nanoparticles as draw solute for forward osmosis, Desalination. 347 (2014) 34–42. https://doi.org/10.1016/j.desal.2014.04.032.

[200] O.A. Attallah, M.A. Al-Ghobashy, M. Nebsen, R. El-Kholy, M.Y. Salem, Assessment of pectin-coated magnetite nanoparticles in low-energy water desalination applications, Environ. Sci. Pollut. Res. 25 (2018) 18476–18483. https://doi.org/10.1007/s11356-018-2060-9.

[201] I. Ban, S. Markuš, S. Gyergyek, M. Drofenik, J. Korenak, C. Helix-Nielsen, I. Petrinić, Synthesis of Poly-Sodium-Acrylate (PSA)-Coated Magnetic Nanoparticles for Use in Forward Osmosis Draw Solutions, Nanomaterials. 9 (2019) 1238. https://doi.org/10.3390/nano9091238.

[202] Q. Zhao, N. Chen, D. Zhao, X. Lu, Thermoresponsive Magnetic Nanoparticles for Seawater Desalination, ACS Appl. Mater. Interfaces. 5 (2013) 11453−11461. https://doi.org/10.1021/am403719s.

[203] A. Zhou, H. Luo, Q. Wang, L. Chen, T.C. Zhang, T. Tao, Magnetic thermoresponsive ionic nanogels as novel draw agents in forward osmosis, RSC Adv. 5 (2015) 15359–15365. https://doi.org/10.1039/c4ra12102c.

[204] Y. Bide, S. Shokrollahzadeh, Toward tailoring of a new draw solute for forward osmosis process: Branched poly (deep eutectic solvent)-decorated magnetic nanoparticles, J. Mol. Liq. 320 (2020) 114409. https://doi.org/10.1016/j.molliq.2020.114409.

[205] F. Khazaie, S. Shokrollahzadeh, Y. Bide, S. Sheshmani, A.S. Shahvelayati, Forward osmosis using highly water dispersible sodium alginate sulfate coated-Fe3O4 nanoparticles as innovative draw solution for water desalination, Process Saf. Environ. Prot. 146 (2021) 789–799. https://doi.org/10.1016/j.psep.2020.12.010.

[206] P. van de Wetering, N.J. Zuidam, M.J. van Steenbergen, O.A.G.J. van der Houwen, W.J.M. Underberg, W.E. Hennink, A Mechanistic Study of the Hydrolytic Stability of Poly(2-(dimethylamino)ethyl methacrylate), Macromolecules. 31 (1998) 8063–8068. https://doi.org/10.1021/ma980689g.

[207] Sterlitech, Reverse Osmosis (RO) Membranes - Flat Sheet Membranes | Sterlitec, Sterlitech Flat Sheet Membr. (2019). https://www.sterlitech.com/reverse-osmosis-ro-membrane.html?designation=BW30 (accessed May 8, 2020).

[208] Q. Liu, M. Konas, J.S. Riffle, Investigations of 2-Ethyl-2-oxazoline Polymerizations in Chlorobenzene, Macromolecules. 26 (1993) 5572–5576. https://doi.org/10.1021/ma00073a007.

[209] R. Tanaka, M. Koike, T. Tsutsui, T. Tanaka, Linear poly(n-methylethylenmine) and related polymers, J. Polym. Sci. Polym. Lett. Ed. 16 (1978) 13–19. https://doi.org/10.1002/pol.1978.130160103.

[210] F.I. Yepez Castillo, Poly(ethylenimine)-based electrolytes for batteries and fuel cells: synthesis, modification, and characterization, University of Oklahoma, 2009. https://search-proquest-com.proxy.queensu.ca/docview/304971668?pq-origsite=gscholar&fromopenview=true (accessed February 20, 2021).

[211] J.Y. Zheng, M.J. Tan, P. Thoniyot, X.J. Loh, Unusual thermogelling behaviour of poly[2-(dimethylamino)ethyl methacrylate] (PDMAEMA)-based polymers polymerized in bulk, RSC Adv. 5 (2015) 62314–62318. https://doi.org/10.1039/c5ra12816a.

[212] D.R. Bhandari, Homogenously-Catalysed Coupling Reactions in Switchable Solvents, Queen’s, 2019.

[213] N.P. Money, Osmotic Pressure of Aqueous Polyethylene Glycols 1 Relationship between Molecular Weight and Vapor Pressure Deficit, Plant Physiol. 91 (1989) 766–769. https://doi.org/10.1104/pp.91.2.766.

[214] A. Striolo, Osmotic second virial coefficient for linear and star poly(ethylene oxide), Polymer (Guildf). 42 (2002) 4773–4775. https://doi.org/10.1016/s0032-3861(00)00649-2.

[215] I. V. Tetko, J. Gasteiger, R. Todeschini, A. Mauri, D. Livingstone, P. Ertl, V.A. Palyulin, E. V. Radchenko, N.S. Zefirov, A.S. Makarenko, V.Y. Tanchuk, V. V Prokopenko, Virtual computational chemistry laboratory- design and description, J. Comput. Aid. Mol. Des. 19 (2005) 453–463.

[216] A. Riabtseva, S.N. Ellis, P. Champagne, P.G. Jessop, M.F. Cunningham, CO_2-responsive branched polymers for forward osmosis applications: the effect of branching on draw solute properties, Ind. Eng. Chem. Res. Accepted. (2021).

[217] O.A. Attallah, M.A. Al-Ghobashy, M. Nebsen, R. El-Kholy, M.Y. Salem, Assessment of pectin-coated magnetite nanoparticles in low-energy water desalination applications, Environ. Sci. Pollut. Res. 25 (2018) 18476–18483. https://doi.org/10.1007/s11356-018-2060-9.

[218] S. Lenoir, C. Pagnoulle, M. Galleni, P. Compère, R. Jérôme, C. Detrembleur, Polyolefin matrixes with permanent antibacterial activity: Preparation, antibacterial activity, and action mode of the active species, Biomacromolecules. 7 (2006) 2291–2296. https://doi.org/10.1021/bm050850c.

[219] P. Van De Wetering, E.E. Moret, N.M.E. Schuurmans-Nieuwenbroek, M.J. Van Steenbergen, W.E. Hennink, Structure-activity relationships of water-soluble cationic

methacrylate/methacrylamide polymers for nonviral gene delivery, Bioconjug. Chem. 10 (1999) 589–597. https://doi.org/10.1021/bc980148w.

[220] A. Zhou, H. Luo, Q. Wang, L. Chen, T.C. Zhang, T. Tao, Magnetic thermoresponsive ionic nanogels as novel draw agents in forward osmosis, RSC Adv. 5 (2015) 15359–15365. https://doi.org/10.1039/c4ra12102c.

[221] A. Razmjou, M.R. Barati, G.P. Simon, K. Suzuki, H. Wang, Fast Deswelling of Nanocomposite Polymer Hydrogels via Magnetic Field-Induced Heating for Emerging FO Desalination, Environ. Sci. Technol. 47 (2013) 26. https://doi.org/10.1021/es4005152.

[222] R.D. Jansen-Van Vuuren, G. Drechsler Vilela, M. Ramezani, P.H. Gilbert, D. Watson, N. Mullins, A.K. Lucas, A.J. Giacomin, M.F. Cunningham, P.G. Jessop, CO_2-Responsive Superabsorbent Hydrogels Capable of >90% Dewatering When Immersed in Water, ACS Appl. Polym. Mater. (2021). https://doi.org/10.1021/acsapm.1c00136.

[223] V. Bütün, S.P. Armes, N.C. Billingham, Synthesis and aqueous solution properties of near-monodisperse tertiary amine methacrylate homopolymers and diblock copolymers, Polymer (Guildf). 42 (2001) 5993–6008. https://doi.org/10.1016/S0032-3861(01)00066-0.

[224] S.N. Ellis, A. Riabtseva, R.R. Dykeman, S. Hargreaves, T. Robert, P. Champagne, M.F. Cunningham, P.G. Jessop, Nitrogen Rich CO_2-Responsive Polymers as Forward Osmosis Draw Solutes, Ind. Eng. Chem. Res. 58 (2019) 22579–22586. https://doi.org/10.1021/acs.iecr.9b04858.

[225] E.A. Hoffman, B.L. Frey, L.M. Smith, D.T. Auble, Formaldehyde crosslinking: A tool for the study of chromatin complexes, J. Biol. Chem. 290 (2015) 26404–26411. https://doi.org/10.1074/jbc.R115.651679.

[226] E. Sawatzky, A. Drakopoulos, M. Rölz, C. Sotriffer, B. Engels, M. Decker, Experimental and theoretical investigations into the stability of cyclic aminals, Beilstein J. Org. Chem.

12 (2016) 2280–2292. https://doi.org/10.3762/bjoc.12.221.

[227] K. Jain, R. Vedarajan, M. Watanabe, M. Ishikiriyama, N. Matsumi, Tunable LCST behavior of poly(N-isopropylacrylamide/ionic liquid) copolymers, Polym. Chem. 6 (2015) 6819–6825. https://doi.org/10.1039/c5py00998g.

[228] Y. Hartanto, M. Zargar, X. Cui, B. Jin, S. Dai, Non-ionic copolymer microgels as high-performance draw materials for forward osmosis desalination, J. Memb. Sci. 572 (2019) 480–488. https://doi.org/10.1016/j.memsci.2018.11.042.

[229] H.Y. Shi, L.M. Zhang, Phase-transition and aggregation characteristics of a thermoresponsive dextran derivative in aqueous solutions, Carbohydr. Res. 341 (2006) 2414–2419. https://doi.org/10.1016/j.carres.2006.06.015.

[230] H. Vink, Precision measurements of osmotic pressure in concentrated polymer solutions, Eur. Polym. J. 7 (1971) 1411–1419. https://doi.org/10.1016/0014-3057(71)90035-8.

[231] M. Yamaura, R.L. Camilo, L.C. Sampaio, M.A. Macêdo, M. Nakamura, H.E. Toma, Preparation and characterization of (3-aminopropyl)triethoxysilane-coated magnetite nanoparticles, J. Magn. Magn. Mater. 279 (2004) 210–217. https://doi.org/10.1016/j.jmmm.2004.01.094.

[232] H. Deng, X. Li, Q. Peng, X. Wang, J. Chen, Y. Li, Monodisperse Magnetic Single-Crystal Ferrite Microspheres, Angew. Chemie. 117 (2005) 2842–2845. https://doi.org/10.1002/ange.200462551.

[233] M.M. Ling, K.Y. Wang, T. Chung, Highly Water-Soluble Magnetic Nanoparticles as Novel Draw Solutes in Forward Osmosis for Water Reuse, Ind. Eng. Chem. Res. 49 (2010) 5869–5876.

[234] L. Zhou, J. Yuan, W. Yuan, X. Sui, S. Wu, Z. Li, D. Shen, Synthesis, characterization, and

controllable drug release of pH-sensitive hybrid magnetic nanoparticles, J. Magn. Magn. Mater. 321 (2009) 2799–2804. https://doi.org/10.1016/j.jmmm.2009.04.020.

[235] L. Zhou, Z. Cai, J. Yuan, Y. Kang, W. Yuan, D. Shen, Multifunctional hybrid magnetite nanoparticles with pH-responsivity, superparamagnetism and fluorescence, Polym. Int. 60 (2011) 1303–1308. https://doi.org/10.1002/pi.3081.

[236] H. Che, M. Huo, L. Peng, Q. Ye, J. Guo, K. Wang, Y. Wei, J. Yuan, CO_2-switchable drug release from magneto-polymeric nanohybrids, Polym. Chem. 6 (2015) 2319–2326. https://doi.org/10.1039/c4py01800a.

[237] M. Hamoudeh, A. Al Faraj, E. Canet-Soulas, F. Bessueille, D. Léonard, H. Fessi, Elaboration of PLLA-based superparamagnetic nanoparticles: Characterization, magnetic behaviour study and in vitro relaxivity evaluation, Int. J. Pharm. 338 (2007) 248–257. https://doi.org/10.1016/j.ijpharm.2007.01.023.

[238] A. Mukhopadhyay, N. Joshi, K. Chattopadhyay, G. De, A facile synthesis of PEG-coated magnetite (Fe 3O 4) nanoparticles and their prevention of the reduction of cytochrome C, ACS Appl. Mater. Interfaces. 4 (2012) 142–149. https://doi.org/10.1021/am201166m.

[239] B.E. Holbein, M.T.C. Ang, D.V. Palaskar, G. Satyanarayana, G. Mahandru, S.V.B. Reddy, S. Ali, Polymeric metal chelating compositions and methods of preparing same for controlling growth and activities of living cells and organisms, (2018). https://patentscope.wipo.int/search/en/detail.jsf?docId=WO2018035613&tab=PCTDESCRIPTION (accessed July 29, 2019).

[240] U.D. Hemraz, K.A. Campbell, J.S. Burdick, K. Ckless, Y. Boluk, R. Sunasee, Cationic poly(2-aminoethylmethacrylate) and polyN-(2-aminoethylmethacrylamide) modified cellulose nanocrystals: Synthesis, characterization, and cytotoxicity, Biomacromolecules. 16 (2015) 319–325. https://doi.org/10.1021/bm501516r.

[241] Y. Liu, Y. Li, X.M. Li, T. He, Kinetics of (3-aminopropyl)triethoxylsilane (aptes) silanization of superparamagnetic iron oxide nanoparticles, Langmuir. 29 (2013) 15275–15282. https://doi.org/10.1021/la403269u.

[242] D. Muller-Schulte, Magnetic Polymer Particles on the Basis of Polyvinylalcohol Process For the Production and Use, US 2001/0014468 A1, 2001.

[243] M. Hamoudeh, H. Fessi, Preparation, characterization and surface study of poly-epsilon caprolactone magnetic microparticles, J. Colloid Interface Sci. 300 (2006) 584–590. https://doi.org/10.1016/j.jcis.2006.04.024.

[244] K. Babu, R. Dhamodharan, Grafting of poly(methyl methacrylate) brushes from magnetite nanoparticles using a phosphonic acid based initiator by Ambient Temperature Atom Transfer Radical Polymerization (ATATRP), Nanoscale Res. Lett. 3 (2008) 109–117. https://doi.org/10.1007/s11671-008-9121-9.

[245] Y. Pei, Q. Han, L. Tang, L. Zhao, L. Wu, Fabrication and characterisation of hydrophobic magnetite composite nanoparticles for oil/water separation, Mater. Technol. 31 (2016) 38–43. https://doi.org/10.1179/1753555715Y.0000000024.

[246] A.H. Gemeay, B.E. Keshta, R.G. El-Sharkawy, A.B. Zaki, Chemical insight into the adsorption of reactive wool dyes onto amine-functionalized magnetite/silica core-shell from industrial wastewaters, Environ. Sci. Pollut. Res. 27 (2020) 32341–32358. https://doi.org/10.1007/s11356-019-06530-y.

[247] S.D. Abkenar, M. Khoobi, R. Tarasi, M. Hosseini, A. Shafiee, M.R. Ganjali, Fast Removal of Methylene Blue from Aqueous Solution Using Magnetic-Modified Fe3O4 Nanoparticles, J. Environ. Eng. 141 (2015) 04014049. https://doi.org/10.1061/(ASCE)EE.1943-7870.0000878.

[248] R.A. Bini, R.F.C. Marques, F.J. Santos, J.A. Chaker, M. Jafelicci, Synthesis and

functionalization of magnetite nanoparticles with different amino-functional alkoxysilanes, J. Magn. Magn. Mater. 324 (2012) 534–539. https://doi.org/10.1016/j.jmmm.2011.08.035.

[249] M.C. Mascolo, Y. Pei, T.A. Ring, Room Temperature Co-Precipitation Synthesis of Magnetite Nanoparticles in a Large ph Window with Different Bases, Materials (Basel). 6 (2013) 5549–5567. https://doi.org/10.3390/ma6125549.

[250] S. Chandra, S. Mehta, S. Nigam, D. Bahadur, Dendritic magnetite nanocarriers for drug delivery applications, New J. Chem. 34 (2010) 648–655. https://doi.org/10.1039/b9nj00609e.

[251] P. Van De Watering, N.J. Zuidam, M.J. Van Steenbergen, O.A.G.J. Van Der Houwen, W.J.M. Underberg, W.E. Hennink, A mechanistic study of the hydrolytic stability of poly(2-(dimethylamino)ethyl methacrylate), Macromolecules. 31 (1998) 8063–8068. https://doi.org/10.1021/ma980689g.

[252] H. Dong, J. Huang, R.R. Koepsel, P. Ye, A.J. Russell, K. Matyjaszewski, Recyclable antibacterial magnetic nanoparticles grafted with quaternized poly(2-(dimethylamino)ethyl methacrylate) brushes, Biomacromolecules. 12 (2011) 1305–1311. https://doi.org/10.1021/bm200031v.

[253] A. Bratek-Skicki, Design of ultra-thin PEO/PDMAEMA polymer coatings for tunable protein adsorption, Polymers (Basel). 12 (2020). https://doi.org/10.3390/polym12030660.

[254] K.A. Gibney, I. Sovadinova, A.I. Lopez, M. Urban, Z. Ridgway, G.A. Caputo, K. Kuroda, Poly(ethylene imine)s as antimicrobial agents with selective activity, Macromol. Biosci. 12 (2012) 1279–1289. https://doi.org/10.1002/mabi.201200052.

[255] L.A.B. Rawlinson, S.M. Ryan, G. Mantovani, J.A. Syrett, D.M. Haddleton, D.J. Brayden, Antibacterial effects of poly(2-(dimethylamino ethyl)methacrylate) against selected gram-

positive and gram-negative bacteria, Biomacromolecules. 11 (2010) 443–453. https://doi.org/10.1021/bm901166y.

[256] L. Yang, Y. Zhan, R. Yu, J. Lan, J. Shang, B. Dou, H. Liu, R. Zou, S. Lin, Facile and scalable fabrication of antibacterial CO_2-Responsive cotton for ultrafast and controllable removal of anionic dyes, ACS Appl. Mater. Interfaces. 13 (2021) 2694–2709. https://doi.org/10.1021/acsami.0c19750.

[257] Attawapiskat First Nation, Attawapiskat First Nation - FYNE Membrane Pilot System Study, (2015) 8:75.

[258] J.R. Vanderveen, S. Burra, J. Geng, A. Goyon, A. Jardine, H.E. Shin, T. Andrea, P.J. Dyson, P.G. Jessop, Characterizing the Effects of a “Switchable Water” Additive on the Aqueous Solubility of Small Molecules, ChemPhysChem. (2018) 1–9. https://doi.org/10.1002/cphc.201701303.

[259] I.T. Cunha, H. Yang, P.G. Jessop, High pressure switchable water: an alternative method for separating organic products from water, Green Chem. (2021). https://doi.org/10.1039/d1gc01113h.

[260] A. Inada, T. Takahashi, K. Kumagai, H. Matsuyama, Morpholine derivatives as thermoresponsive draw solutes for forward osmosis desalination, Ind. Eng. Chem. Res. 58 (2019) 12253–12260. https://doi.org/10.1021/acs.iecr.9b01712.

[261] X. Lin, B. Shao, J. Zhu, F. Pan, J. Hu, M. Wang, H. Liu, In Situ Electromagnetic Induction Heating for CO_2 Temperature Swing Adsorption on Magnetic Fe_3O_4/N-Doped Porous Carbon, Energy and Fuels. 34 (2020) 14439–14446. https://doi.org/10.1021/acs.energyfuels.0c02699.

[262] Y. Inoue, H. Guo, T. Honma, R.L. Smith, Amino-functional biocarbon with CO_2-responsive property for removing copper(II) ions from aqueous solutions, Colloids

Surfaces A Physicochem. Eng. Asp. 616 (2021) 126304. https://doi.org/10.1016/j.colsurfa.2021.126304.

[263] Z. He, Q. Chen, Y. Luo, Y. He, Y. Zhang, T. Liu, W. Xu, J. Zhang, Y. Liu, L. Xiong, S. Wang, Z. Guo, Degradable CO_2-responsive microgels with wrinkled porous structure for enhanced, selective and recyclable removal of anionic dyes, Cr(VI) and As(V), Eur. Polym. J. 149 (2021) 110374. https://doi.org/10.1016/j.eurpolymj.2021.110374.

[264] T. Jun, C. Shixiong, J. Wang, CO_2-switchable Pickering emulsions: efficient and tunable interfacial catalysis for alcohol oxidation in biphasic systems, Chem. Commun. (2019) 11079–11083.

[265] Dow-Filmtec-Lenntech, FILMTEC™ BW30-4040 Membranes FILMTEC Fiberglassed Elements for Light Industrial Systems, (2020) 2. www.lenntech.com (accessed June 6, 2021).

[266] W. Li, Y. Shi, L. Gao, J. Liu, Y. Cai, Occurrence, fate and risk assessment of parabens and their chlorinated derivatives in an advanced wastewater treatment plant, J. Hazard. Mater. 300 (2015) 29–38. https://doi.org/10.1016/j.jhazmat.2015.06.060.

Appendix A
Instructions for Performing a DMO Measurement

In DMO, a solution and a pure solvent are placed in opposite sides of a membrane (Figure A1). Driven by the π gradient, water molecules try to enter the solution through the membrane but only a very small number can, as the solution chamber is completely filled with liquid and is sealed. This action causes pressure to build up in the solution chamber, which under ideal conditions is equal to π. Full details on the DMO, can be found in the paper "Fast membrane osmometer as alternative to freezing point and vapor pressure osmometry" (A. Grattoni, et al., Anal. Chem. 80 (2008) 2617–2622). Detailed instructions for the procedure on how to set up a DMO experiment are provided below, as well as conditions which cause the measured pressure to deviate from π. A discussion of the reported upper pressure limit of the RO membranes used in DMO is also included.

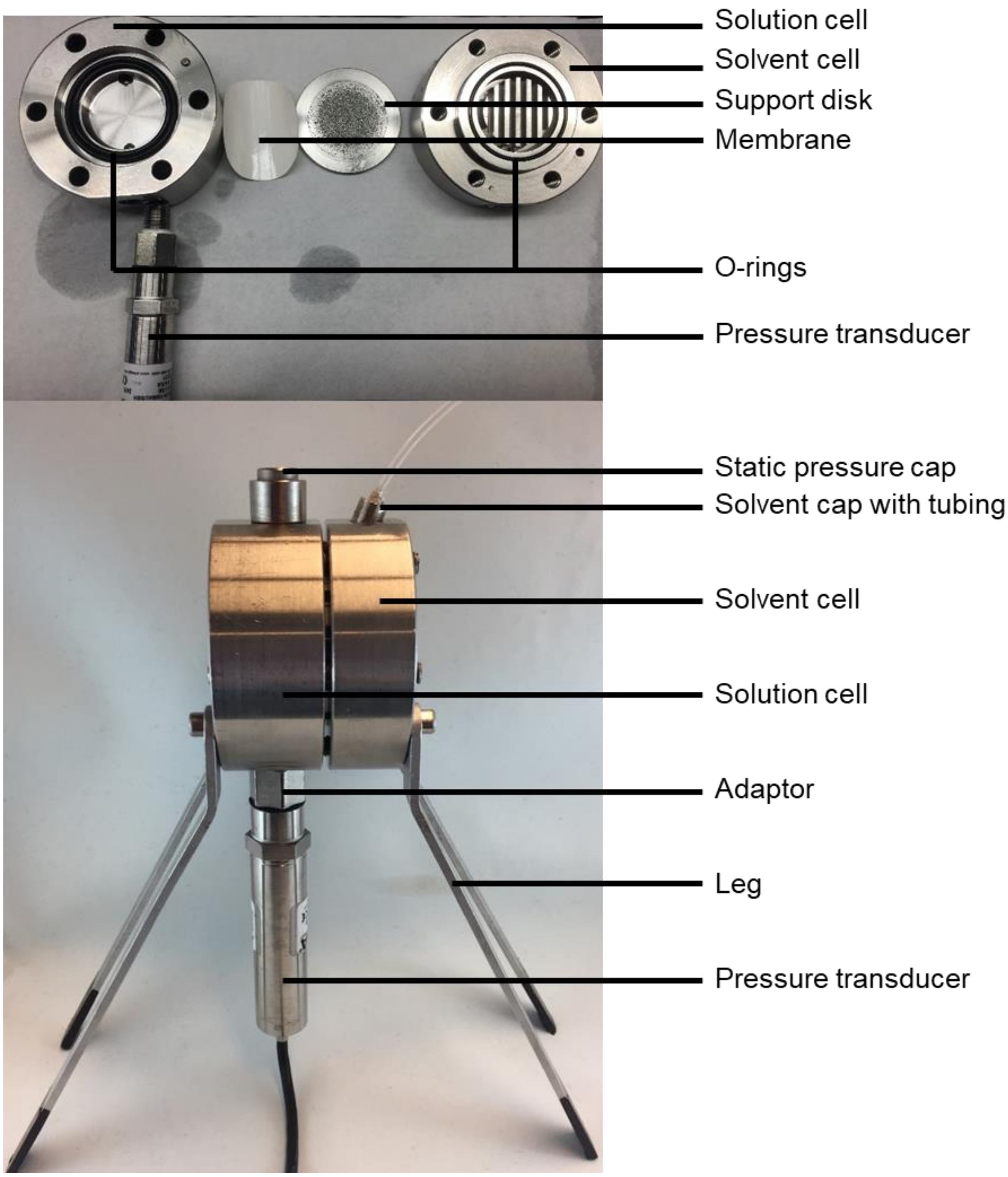

Figure A1. Labelled image of the DMO used in this work.

Performing an osmotic pressure measurement using a Grattoni DMO:

1. Thoroughly clean the osmometer before use.
    - Always wear new and clean gloves when handling the interior components of the DMO.
    - Rinse all parts of the DMO that will be in contact with the solvent or the solution thoroughly with deionized water obtained from a MilliQ purification system with a resistivity of 18.2 MΩ. These components include: the solvent and solution cells, O-rings, support disk, static pressure cap.
    - Carefully rinse the inside of the pressure transducer and shake out excess water. Be **extremely** careful to **not** touch the diaphragm (interior bottom) of the transducer. It is extremely sensitive. Puncturing or denting it will result in irreversible damage.
2. Plug in the transducer to the computer and open the Digital Transducer Application Software (available free from the Omega website).
3. Dry all components of the DMO that will be in contact with the solution. Use a wipe that will not leave a residue (e.g., Kimwipes).
4. Carefully fill a 12 mL syringe (4” G19 needle) with ca. 12 mL of the solution to be tested.
    - Draw the solution up slowly to avoid forming bubbles or decarbonating the solution. Take special care when pulling up viscous solutions.
5. Cover the screw of the transducer (or adaptor connected to the transducer) with Teflon tape.
6. **Carefully** fill the inside of the transducer with the solution to be tested. Insert the needle just inside the transducer and inject the solution along the sides to fill to avoid forming bubbles

- Dispense the solution slowly to avoid dispensing bubbles or building up pressure within the syringe. Take especial care when handling viscous solutions.

7. Screw the transducer into the solution cell of the osmometer and tighten it carefully with a wrench. Place it on a table.
8. Place the O-rings in each cell (2 in the solution cell, 1 in the solvent cell).
9. Put the needle of the syringe holding the solution through the top of the solution cell until the needle is firmly in place in the base of the solution cell.
    - Be extremely careful to not insert the needle into the transducer.
    - Ensure the point of the needle is pointing towards the solution cell, away from where the membrane will be. This will help avoid damaging the membrane when the syringe is removed.
10. The membrane should be soaked in water for at least 1 h prior to the experiment. Gently pat the active side of the membrane dry with a kimwipe. Place the membrane on top of the O-rings in the solution cell, with the active side facing the solution.
    - The active side of the membrane is shiny and the support side is matte.
    - Membranes are obtained in sheets from Sterlitech, and disks the size of the support disk are cut out of it using clean scissors.
    - Before using a membrane, inspect it for imperfections or holes, and discard it if there are any concerns.
11. Place the support disk on the membrane, with the more porous side facing away from the solution cell.
    - Ensure there is good contact between the support disk and the membrane, and there are no air bubbles trapped between them.
    - The support disk should be soaked in water prior to use, to ensure it does not contain any air bubbles.

12. Place the solvent cell on top of the solution cell, aligning the tops together.
13. Using both hands, flip the two cells around, ensuring the interior components remain in place. The exterior of the solution cell should now be on top.
14. Insert the 6 compression screws in the osmometer. Tighten the screws in a star pattern, tightening them in gradually with an Allen key.
15. Insert the legs on the osmometer and tighten the screw finger tight.
16. Start gathering data on the transducer software. Leave the instrument still for a few seconds to gather background readings.
    - Ensure the box for the transducer in use is selected on the plotting and logging tabs. Click “start” on each of these tabs to start gathering data.
17. With the osmometer standing up, fill the solution side of the osmometer to the brim with the syringe. Remove the syringe.
    - Dispense the solution slowly to ensure no bubbles are dispensed.
    - If necessary, tap the sides of the osmometer to dislodge any bubbles.
    - When removing the needle, be very careful not to touch or scratch the membrane.
18. Rapidly seal the solution side with the static pressure cap with an Allen key.
    - The pressure should begin to increase.
19. Using a new, clean 12 mL syringe, fill the solvent side with the solvent. Insert the solvent chamber cap with tubing attached. Using a long, flexible needle, fill the tubing with the solvent.
    - The purpose of this tubing is to monitor the water level during the experiment.
20. Leave the osmometer until the pressure has equilibrated (see Figure A2).
    - If the pressure equilibrates relatively quickly, let it equilibrate for 30 min.
    - If the pressure took a long time to equilibrate (> ca. 8 h) or there is a risk of solute flux, leave the solution for 45-60 min to equilibrate.

21. After the pressure has equilibrated, stop the data acquisition on the software, and save the data as both an image and an excel file.
22. Remove the solution cap and extract the solution with a syringe.
23. The DMO apparatus can be disassembled in the reverse order it was assembled.
24. Immediately clean the interior of the transducer.

Notes:

- Ensure that the measured pressure does not exceed the upper pressure limit of the transducer. Digital transducers with a range of upper pressure limits can be obtained from Omega.
- After opening the solution cell of the DMO, note if there are bubbles present. This can affect the accuracy of the measurement.
- If the measurement did not proceed as expected, inspect the membrane for imperfections or holes.
- The static pressure cap can measure up to 200 bar. For fast measurements, the dynamic pressure cap can be used as described in reference: Grattoni, et al. Anal. Chem. (2008). https://doi.org/10.1021/ac7023987..
- Solute flux: Small solutes may pass through the membrane into the solvent side. This decreases the π of the solution and contaminates the solvent. If a significant amount of solute flux occurs over the course of the measurement, the pressure will decrease with time or not reach the true π. Solute flux can be detected after the experiment by analyzing the composition of the liquid on the solvent and solution cells (e.g., NMR, conductivity) or by removing the solvent and weighing the residue (if there is significant solute flux). Solute flux may also be detected by the measured pressure decreasing over time. Solute

flux is not a concern with pure polymer solutions which have been dialyzed to remove low molecular weight material.

- Membrane compatibility: ensure that the solution to be measured and the desired solvent are compatible with the membrane (e.g., within the pH range specified by the manufacturer). RO membranes are typically used due to their high rejection rates and pressure resistance. Many different RO membranes are available, with a range of different chemical and physical properties.
- Stirring: To avoid concentration gradients, the solution can be stirred. As the DMO is left for as long as necessary until the pressure has equilibrated, concentration gradients are only of concern with highly viscous solutions. To stir the solution, a small (1 cm) magnetic stir bar can be added into the solution cell before the static pressure cap is inserted. The DMO can then be placed horizontally on a stir plate, and the desired stir rate can be set. The DMO can be orientated with the stir bar on the membrane or the back of the solution cell. The former configuration will more directly disperse concentration gradients, but also risks damaging the membrane.

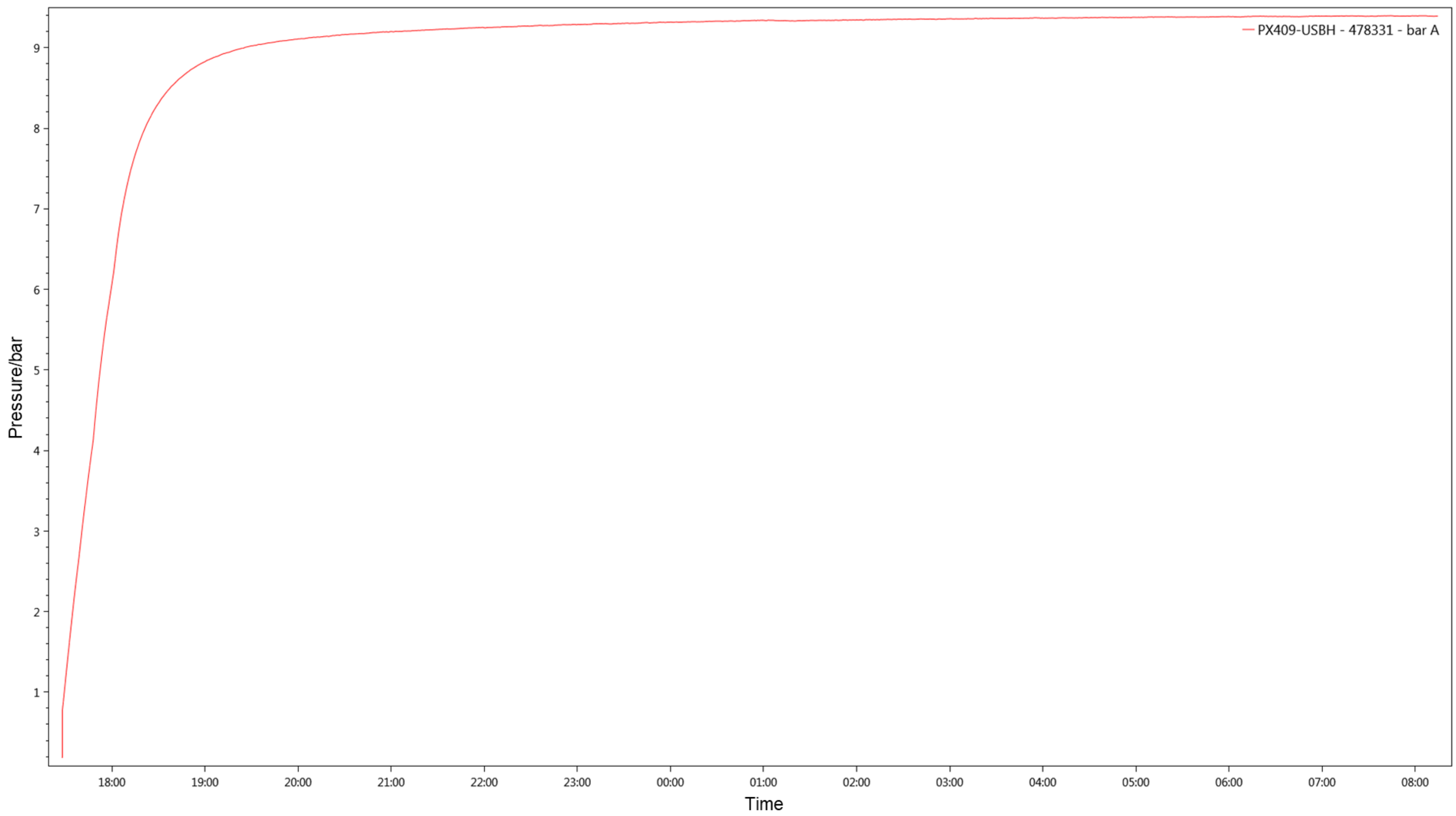

Figure A2. Sample of pressure-time curve obtained using DMO. Sample: b-PMEI, 20 wt.% under air.

Note on the Upper Membrane Pressure Limit:

As the pressure within the solution cell of the DMO increases, the membrane is compressed. At extreme pressures, the pores of the membrane may be so compressed that water can no longer pass across the membrane, causing the pressure within the DMO to plateau before π is reached. The steady pressure reading may cause a user to mistakenly believe that this pressure is the true π. The membranes used in this work (Dow BW30, obtained from Sterlitech) are used in RO modules with an upper pressure limit of 41 bar [265]. It was important to determine if the pressures measured by DMO in this work (<75 bar) were sufficient to damage the membrane and cause the measured pressure to differ from π.

The upper pressure limit of the module reported by the manufacturer is affected by several factors. First, it is important to emphasize that this value is the upper pressure limit of the RO module, not the membrane itself, and may be limited by the module's external casing, seals, or other internal components. Other factors which are considered when determining the upper pressure limit include maximizing the life span of the membrane and maintaining a high flux during RO. These factors are of lesser importance when the membrane is used in a DMO, as the membrane is only used once and the DMO measurements are left for as long as necessary until the pressure has equilibrated. In summary, the reported upper pressure limit is often not related to the membrane, or the point when water flux across the membrane has stopped.

To ensure that the pressures measured in this work (some of which were higher than the recommended upper pressure limit) were not compromising the membrane, solutions were run in the DMO with and without additional application of pressure on the solution side. If pressure-induced membrane compression is limiting water diffusion, application of higher pressures should cause the final pressure measured by DMO to differ from the pressure measured without an overpressure.

DMO experiments without an overpressure were obtained with the static pressure cap (as described previously in Appendix A). When using the static pressure cap, the solution cell of the DMO is sealed and the pressure within the solution cell increases from the initial 0 bar of gauge pressure as a small amount of water diffuses through the membrane from the solvent to the solution cell by osmosis. The pressure increases then plateaus to a steady final value (Figure A3.a, red curve). That steady pressure is assumed to be the equilibrium π but if the membrane pores have closed then it may instead be lower than the true π. DMO experiments with an overpressure were obtained with the dynamic pressure cap as described in the paper "Fast membrane osmometer as alternative to freezing point and vapor pressure osmometry" (A. Grattoni, et al., Anal. Chem. 80 (2008) 2617–2622). When using the dynamic pressure cap, the pressure within the solution cell of the DMO is manually increased to a pressure greater than the anticipated π. A small amount of water diffuses through the membrane from the solution cell to the solvent cell, decreasing the internal pressure until π is reached (Figure A3.a, blue curve).

Comparing the pressures measured by DMO of the same solution using the static and dynamic pressure caps will indicate whether pressure-induced membrane compaction is changing the equilibrium pressure. If the pores in the membrane remain open despite the overpressure, water diffusion will be maintained, and the final pressure measured will be the same if the dynamic or the static pressure cap are used (assuming only a modest overpressure is applied (10-20 bar)) (Figure A3.a). This pressure can therefore be assumed to be equal to π. If degradative pressure-induced membrane compaction is occurring, water will no longer be able to cross the membrane to equilibrate the pressure between the solution and solvent sides of the DMO. If the final pressure observed with the static pressure cap was caused by membrane pore closure rather than the attainment of equilibrium, then the true π should be higher than the observed pressure. Thus starting the experiment with a pressure greater than the purported osmotic pressure would give a different final value (Figure A3.b).

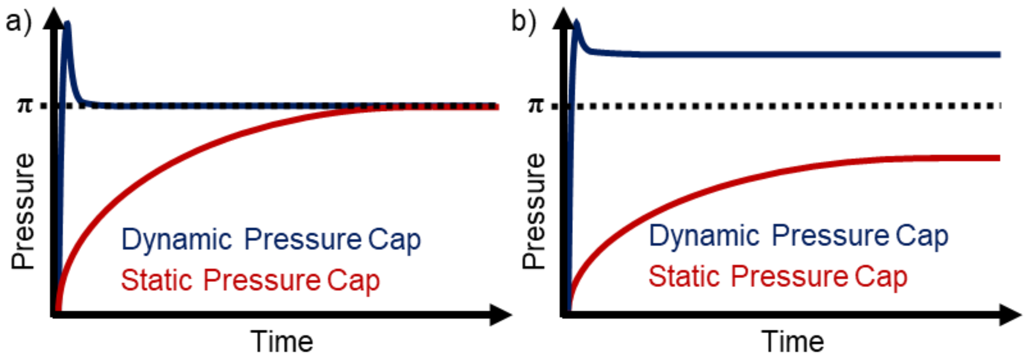

Figure A3. Idealized illustrations of the pressure versus time curves obtained by DMO using the dynamic and static pressure caps a) without pressure-induced membrane compaction (final pressure = π) and b) with pressure-induced membrane compaction (final pressure ≠ π). Note that pressure-induced membrane compaction may produce several different pressure vs time curves; for simplicity, only one situation is shown.

Solutions of sodium poly(acrylate) (PSA) (M_w = 1,200 g/mol, obtained from Sigma-Aldrich as a 45 wt.% aqueous solution) were used in the solution cell. The final measured π for various PSA solutions with and without overpressures are presented in Table S1. Modest overpressures did not greatly alter the measured π. This indicates that pressure-induced membrane compaction is not limiting water diffusion at the pressures measured in this work. Based on these successful results, it is recommended that a comparison between the pressures obtained with the dynamic and static pressure caps be used to determine if degradative membrane compaction is occurring in DMO in the future. This method may be used when measuring pressures above the nominal pressure ratings of new membranes, or with Dow BW30 membranes at pressures greater than 75 bar.

Table S1. Effect of application of overpressure on final pressure of DMO measurements.*

	Dynamic Pressure Cap		Static Pressure Cap
[PSA]/ wt.%	Applied pressure/ bar	Final pressure/ bar	Final pressure/ bar
27	68	52.0	52.3
30	80	70.7	69.4

* All pressures are gauge pressures

Appendix B

Soluble Polymer Supplementary Information

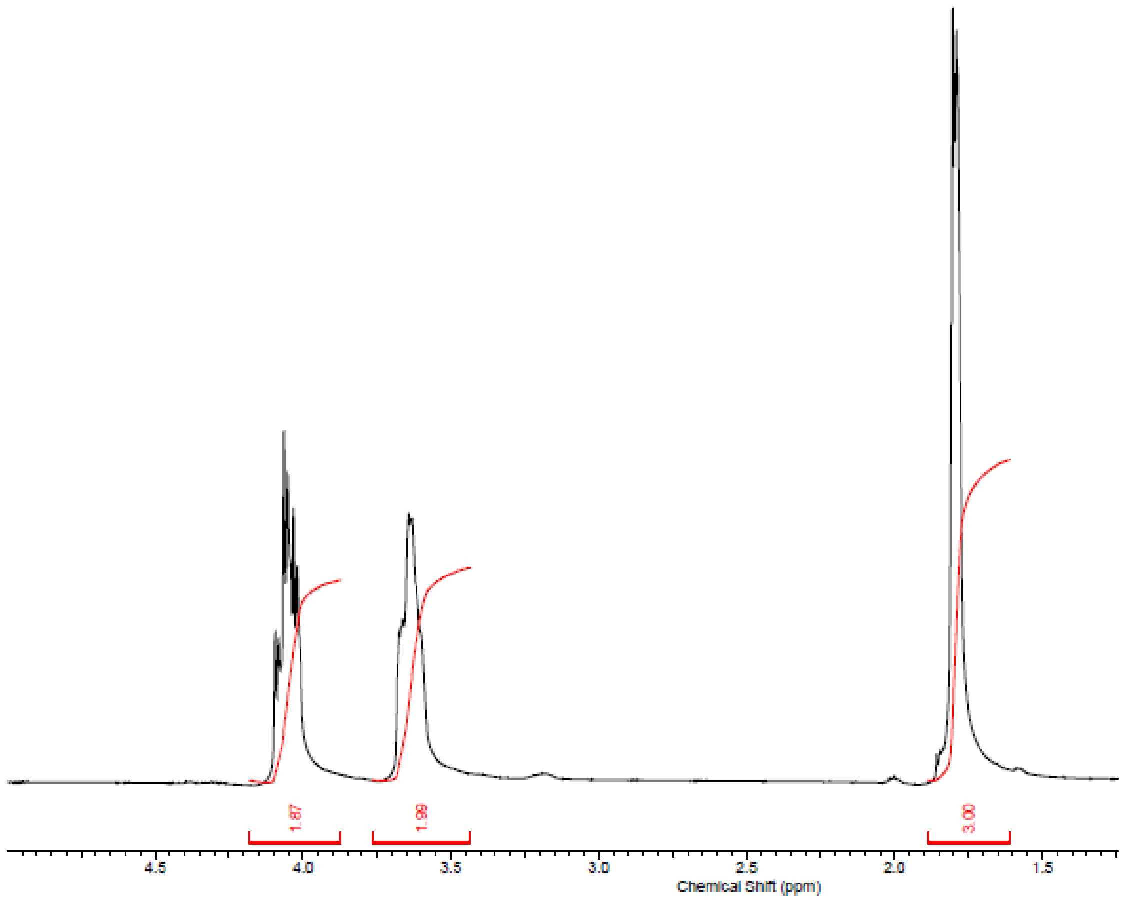

Figure B1. ^{1}H NMR spectrum of poly(2-methyl-2-oxazoline) in $CDCl_3$.

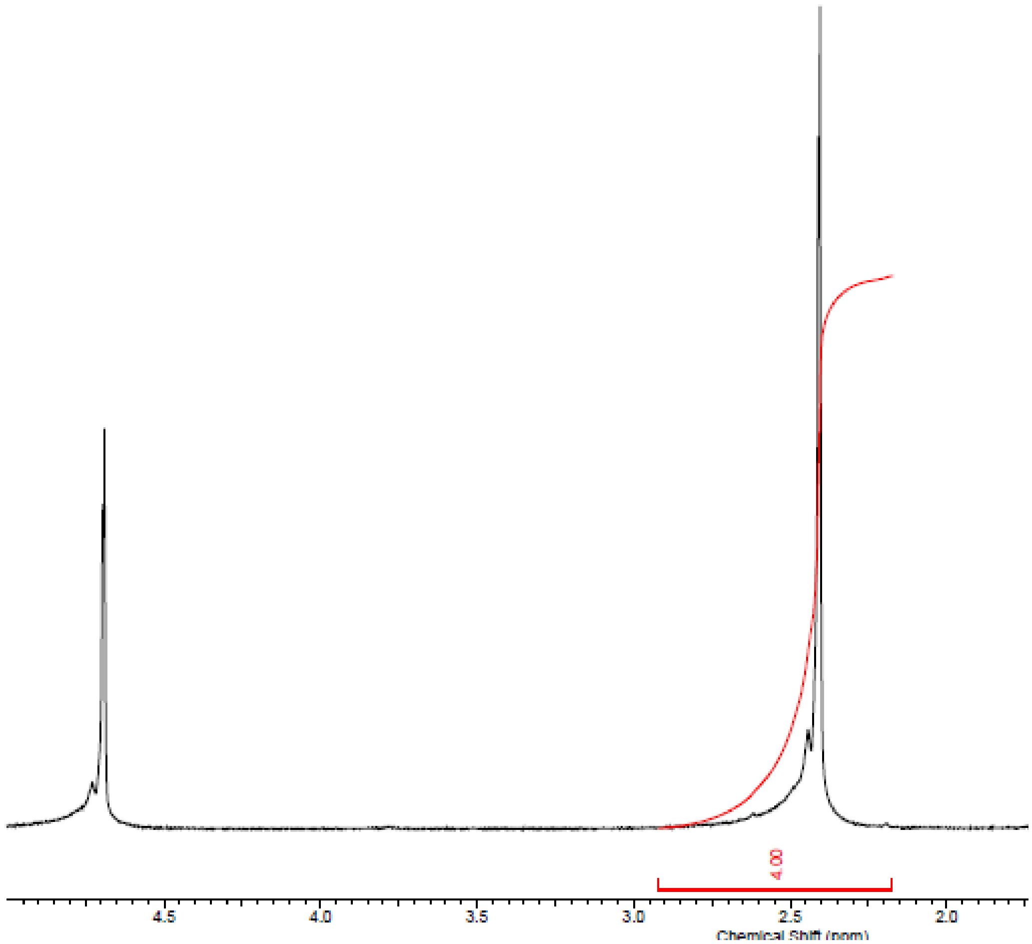

Figure B2. ^{1}H NMR spectrum of l-PEI in D_2O.

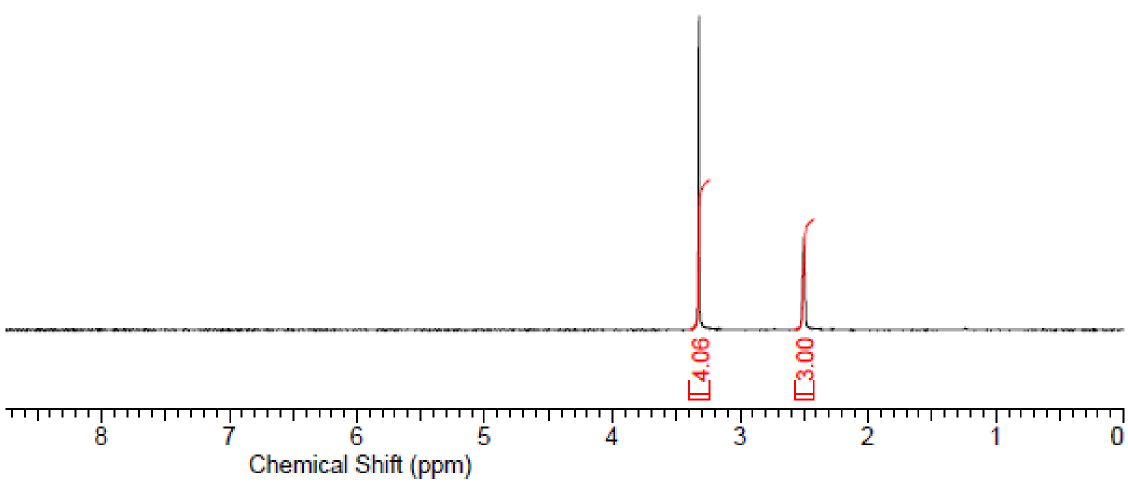

Figure B3. ^{1}H-NMR spectrum of l-PMEI in D_2O.

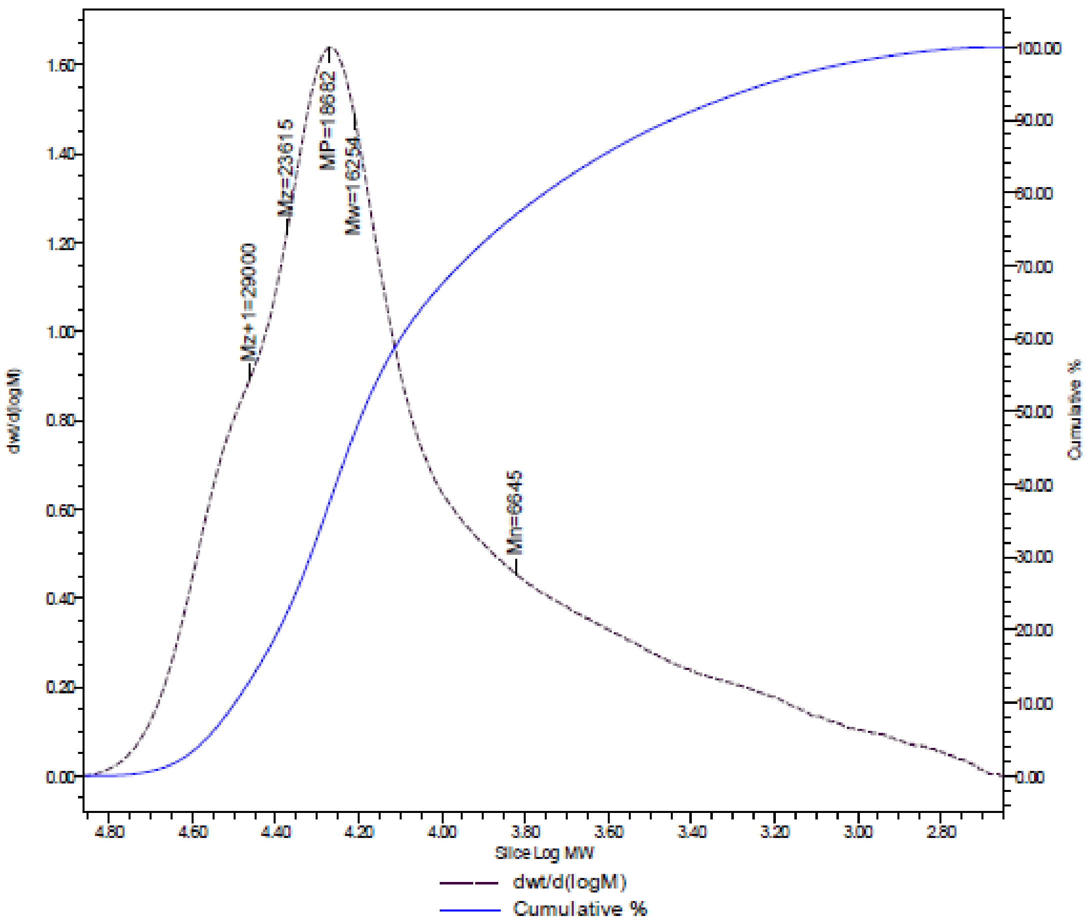

Figure B4. GPC trace of poly(2-ethyl-2-oxazoline).

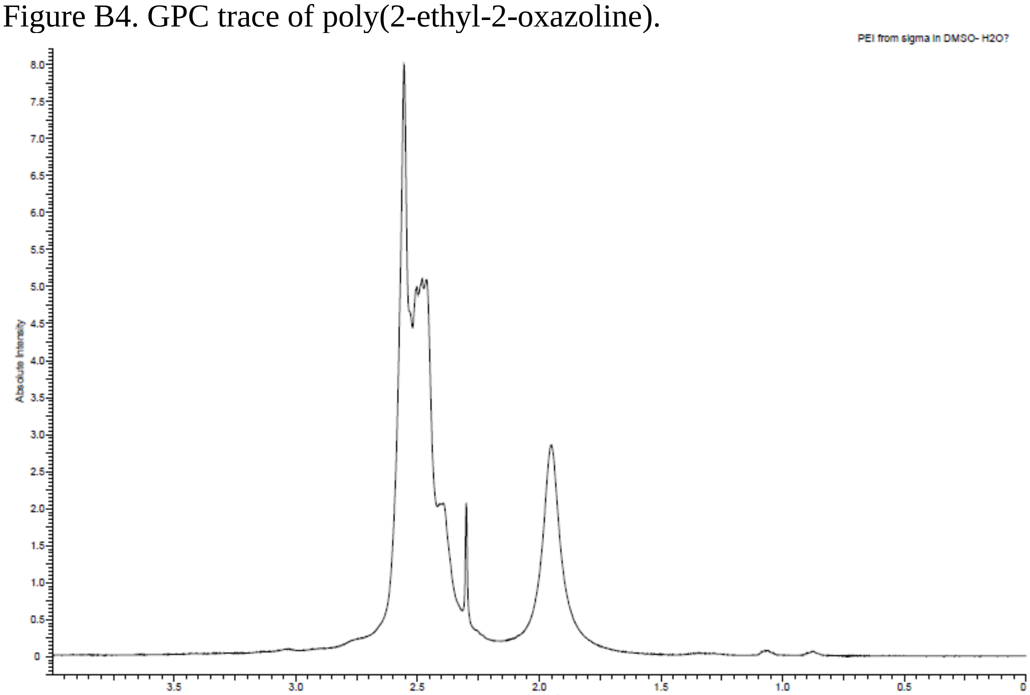

Figure B5. [1]H-NMR spectrum of b-PEI in DMSO-d_6.

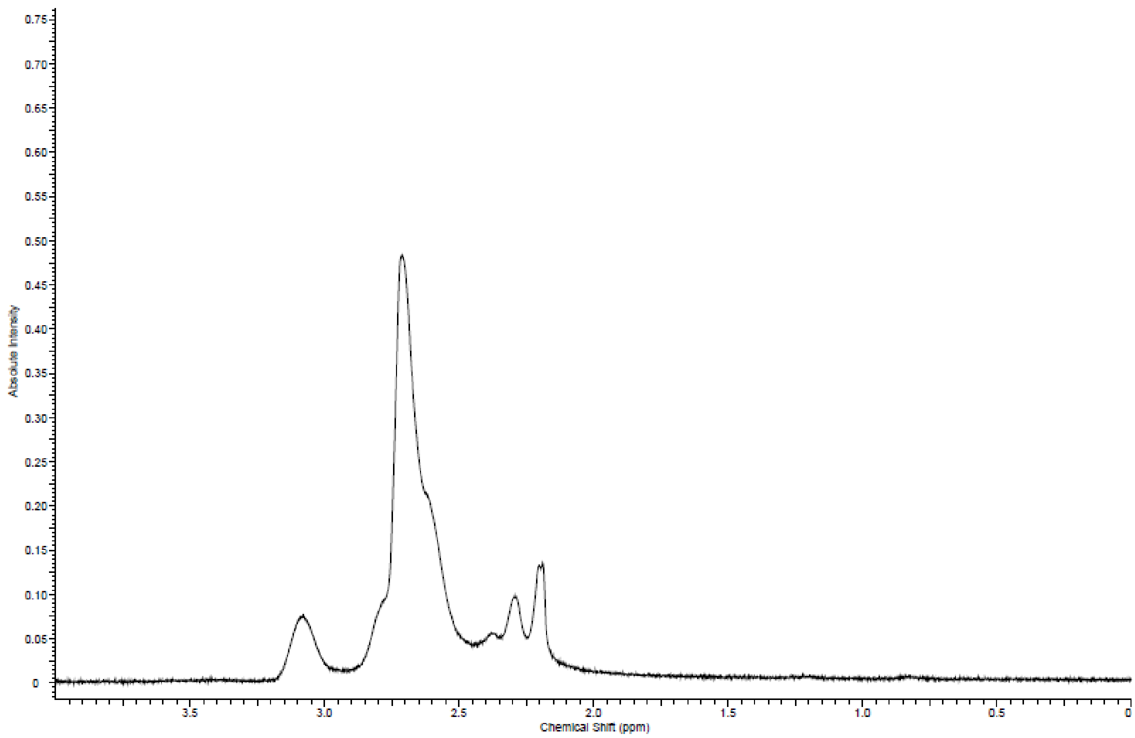

Figure B6. ^{1}H-NMR spectrum of b-PMEI in $CDCl_3$.

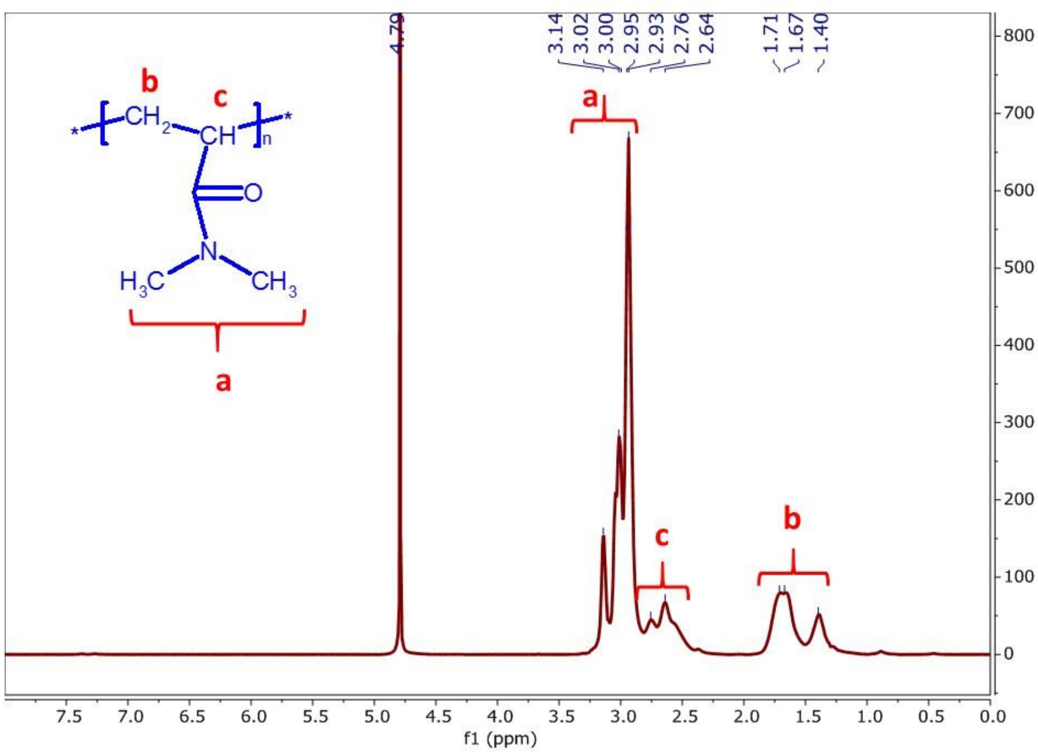

Figure B7. ^{1}H-NMR spectrum of poly(N,N-dimethylacrylamide) in D_2O.

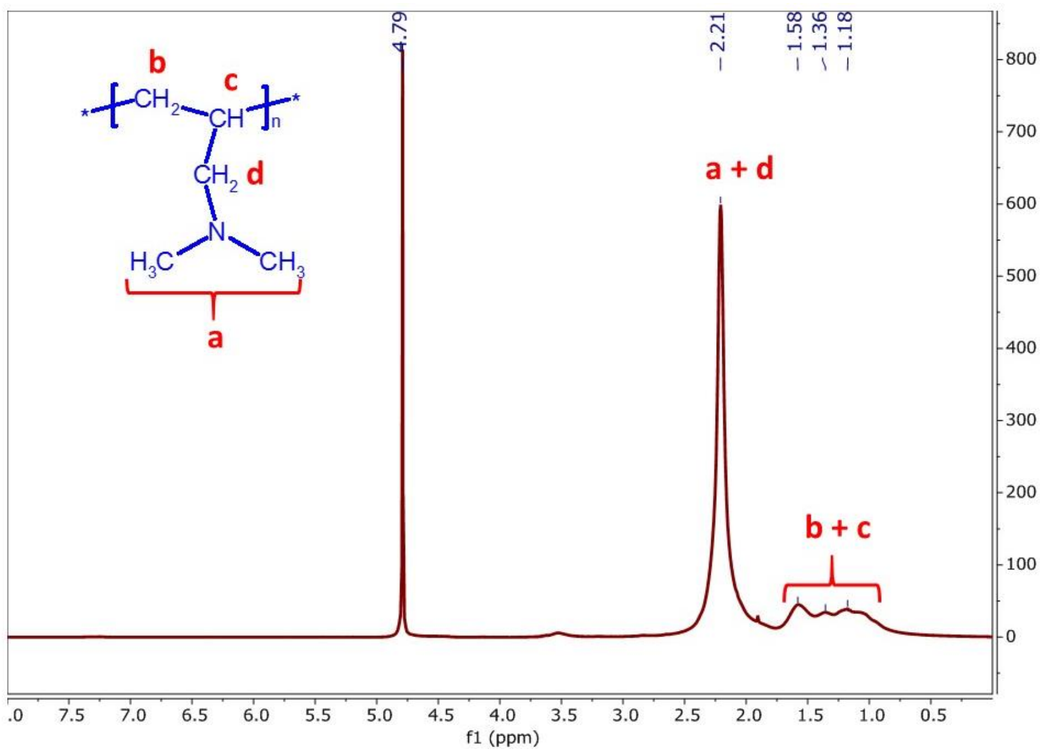

Figure B8. ^{1}H-NMR spectrum of poly(N,N-dimethylallylamine) in D_2O.

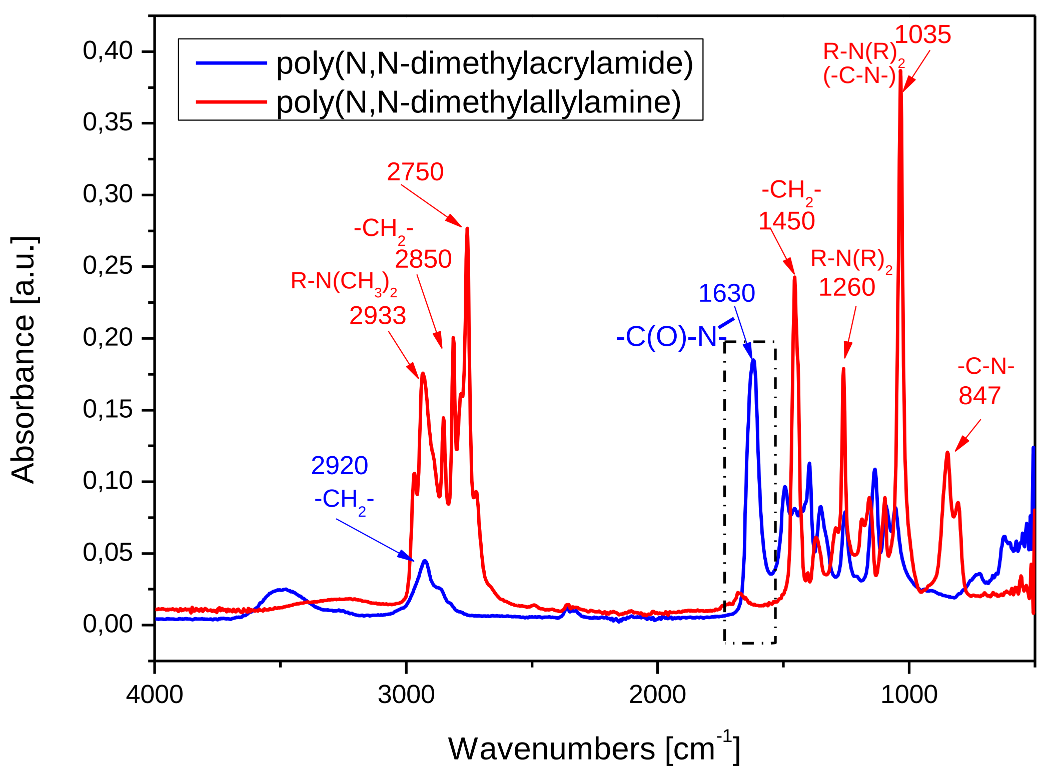

Figure B9. FT-IR spectra of poly(N,N-dimethylacrylamide) (red line) and poly(N,N-dimethylallyamine) (blue line).

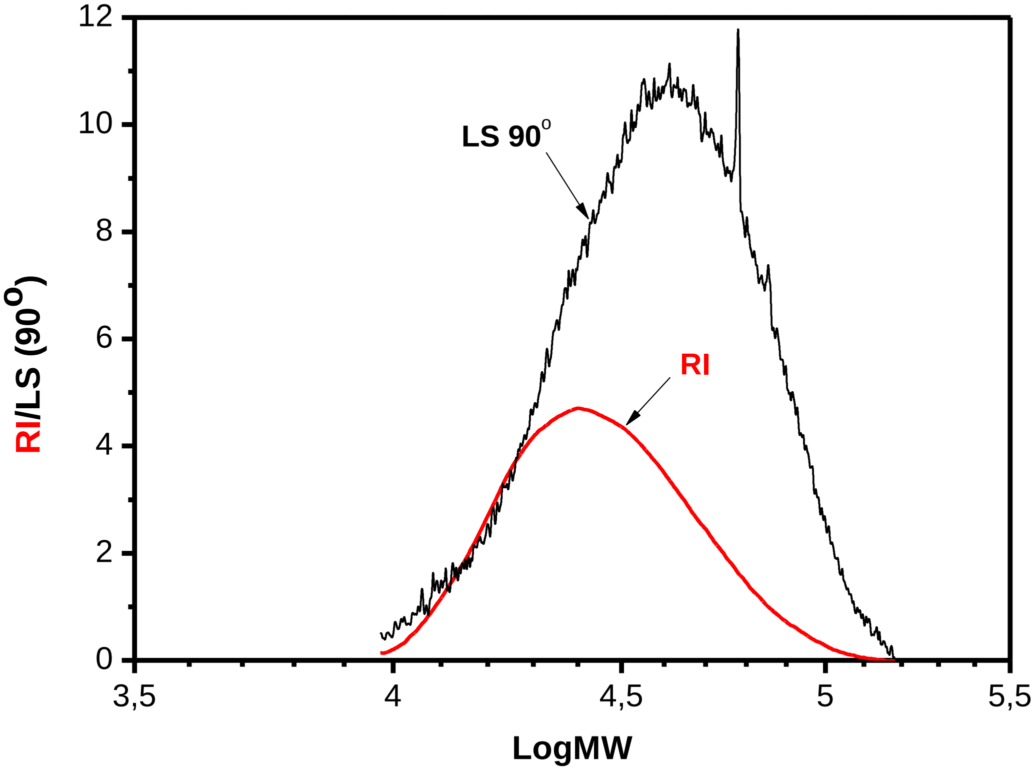

Figure B10. Size-exclusion chromatograms (RI detector response and LS 90° detector response vs. molecular weight) of poly(N,N-dimethylallylamine) polymer.

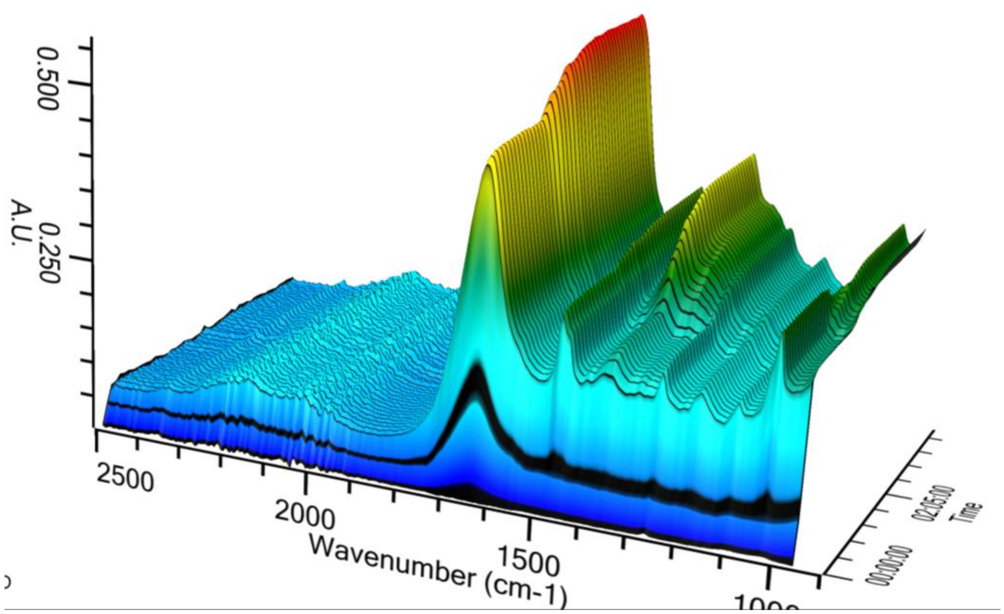

Figure B11. IR spectra of 25 wt./vol.% PDMAAm solution over the course of carbonation.

Table B1. Comparison of measured and calculated pHs of PDMAAm solutions

Concentration, wt.%	pH Under air		pH Under CO_2	
	Measured	Calculated	Measured	Calculated
20	11.0	11.0	7.6	7.8
30	11.3	11.1	7.8	7.9

Procedure for alternative synthesis of PDMAAm:

The following is an excerpt from "Forming a Treated Switchable Polymer and Use Thereof in a Forward Osmosis System" US patent 62/722,275. For full details, see the patent.

60 g of Allylamine was transferred to a 150 mL addition funnel that is connected to a 250 mL round bottom flask, which contains 86 mL of 12 M HCl. The round bottom flask was placed in a liquid nitrogen bath and with stirring the allylamine was added drop-wise to produce allylammonium chloride. The resulting allylammonium chloride solution was transferred to a 3-neck 250 ml round bottom flask equipped with a condenser and an addition funnel that contains 3.56 g of initiator VA-044 ((E)-1,2-bis(2-(4,5-dihydro-1H-imidazol-2-yl)propan-2-yl)diazene) dissolved in 10 mL of de-ionized water. Both the monomer solution (round bottom flask) and the initiator solution (addition funnel) were purged with nitrogen for 1 hr, using a 16G needle with an outer diameter of 1.651 mm and an inner diameter of 1.194 mm. After purging, the round bottom reaction flask temperature was set to 55 °C and the initiator (6.7 mL of the solution) was transferred to the monomer solution dropwise over 1h. After 22 h, a 5 mL sample was withdrawn from the reaction mixture using a syringe with a needle. This sample was analyzed by proton NMR to assess reaction conversion. The conversion was determined by integrating the signal from $-CH_2-$ (C') at 3.45 ppm from the monomer and the signal from $-CH_2-$ (c) at 3.00 ppm from the polymer. After this the remaining 3.3 mL of the initiator solution was added to the reaction

mixture and heating at 55 ˚C was continued. After 94 h the reaction was stopped by placing the 3-neck 250 ml round bottom flask into an ice bath.

Poly(N,N-dimethylallylamine) was synthesized using standard conditions for an Eschweiler-Clarke methylation with formaldehyde and formic acid [209]. Poly(allylamine) (15 wt.% in water, 20 g) was dissolved in formic acid (55 mL), and 37 % formaldehyde solution (110 mL). Resulting solution was refluxed for 48 h. Solvent was removed under vacuum, followed addition of concentrated hydrochloric acid (150 mL). Resulting solution was stirred for 30 min, then the solvent (water) was removed under vacuum. Resulting solid was dissolved in 30 wt. % sodium methoxide solution (100 mL). Salt was filtered off, and solvent (methanol) was removed under vacuum. The final product was purified by dialysis (3.5 kDa MWCO tubing), affording a polymer with a molecular weight of 24 kDa.

Appendix C
Hydrogel Supplementary Information

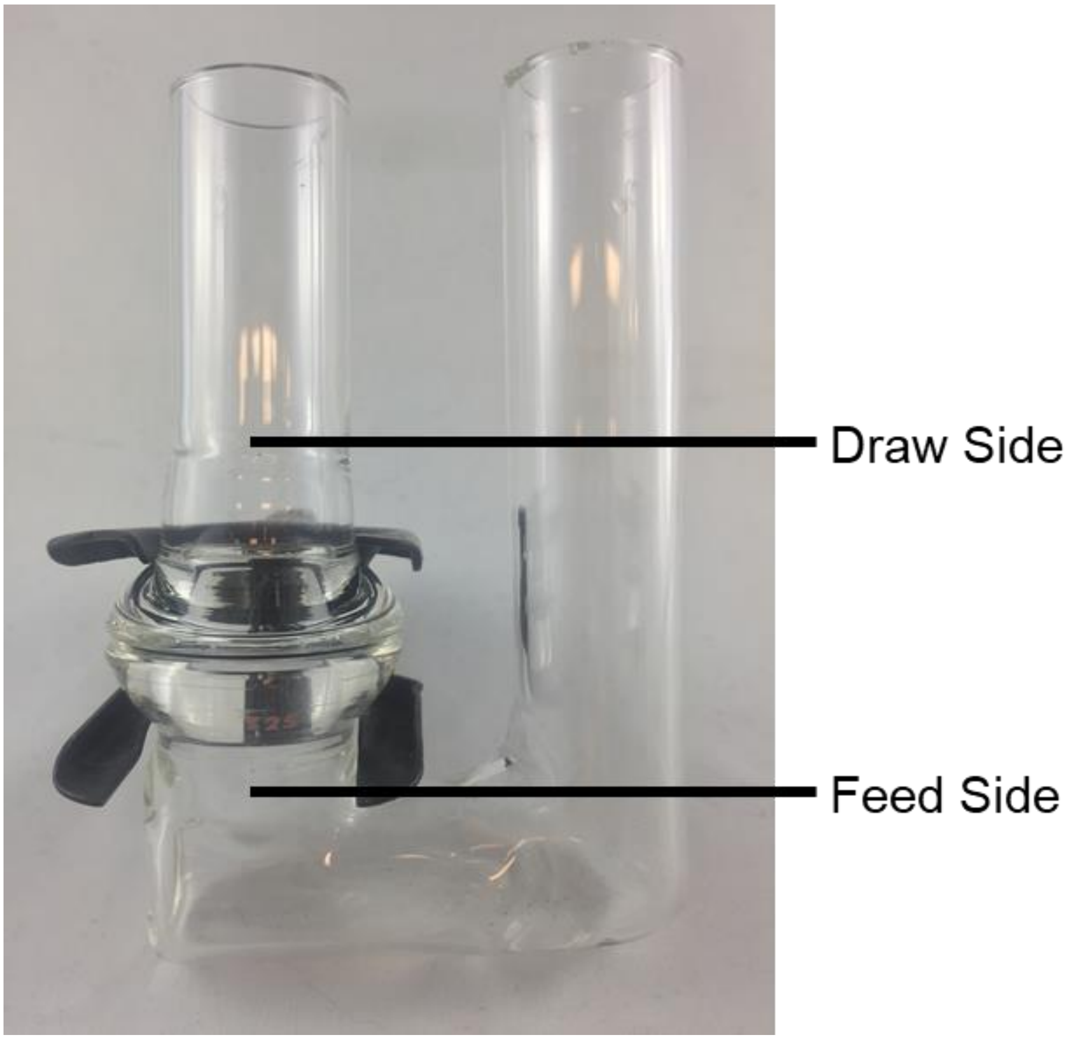

Figure C1. The glass U-tube used to measure the flux of g-PDMAAm.

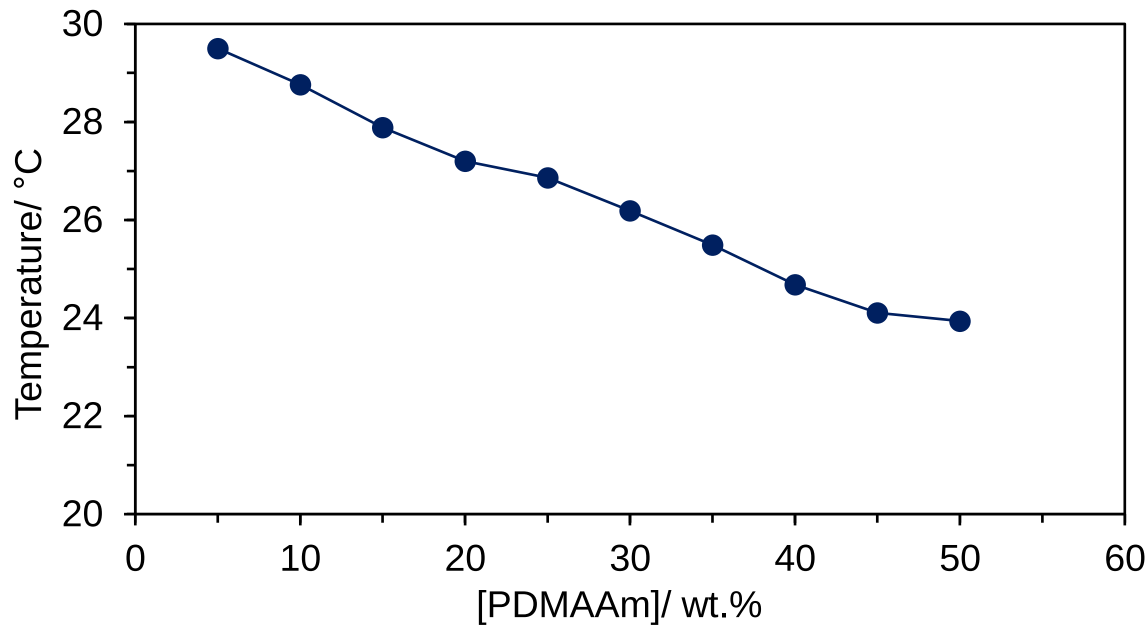

Figure C2. The cloud point of PDMAAm in water as a function of concentration.

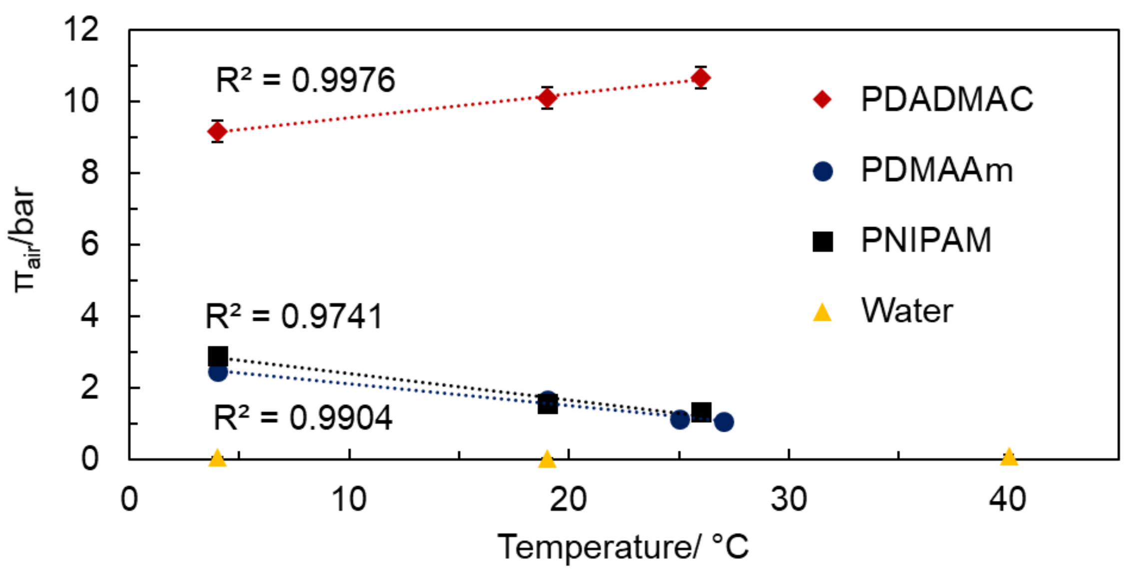

Figure C3. Osmotic pressure under air as a function of temperature for thermo-responsive (PDMAAm (17 wt.%) and PNIPAM (20 wt.%)) and non-thermo-responsive (PDADMAC (20 wt.%)) soluble polymers, including a blank of pure water.

Table C1. Osmotic Pressure of PMEMA under CO_2, at 20 wt.% and 25 °C*

Polymer	π_{air}	π_{CO2}
PMEMA**	0.2	1.2

* All pressures are gauge pressure.

** Cloud point = 50 °C, Kotsuchibashi, Y.; Ebara, M.; Aoyagi, T.; Narain, R. Recent Advances in Dual Temperature Responsive Block Copolymers and Their Potential as Biomedical Applications. *Polymers*. MDPI AG October 27, 2016. https://doi.org/10.3390/polym8110380.

Synthesis of PMEMA:

Materials: N-Morpholino-2-ethyl methacrylate (MEMA) was obtained from Sigma-Alrdich. Monomer was passed through a column of basic alumina to remove inhibitors. 2,2′-Azobis(2-methyl- propionitrile) (AIBN) was obtained from Millipore-Sigma and was recrystallized from ethanol. Anhydrous DMSO was obtained from EMD. All solvents were used as received. Water was deionized by a Synergy MilliQ system and had a resistivity of 18.2 MΩ/cm before exposure to air. Dialysis tubing (3.5 kDa molecular weight cut off) was obtained from Thermo Scientific.

Synthesis of PMEMA: A Schlenk flask was purged with argon three times. MEMA and DMSO (x3 volume of monomer) were added to the flask, which was heated to 65 °C with magnetic stirring (500 rpm). AIBN (1 mol% to monomer) was added to the flask, and the solution was stirred overnight. The solution was cooled to room temperature, then diluted with water, and the DMSO was removed from the polymer by dialysis (5 exchanges with 20-40x excess volume of water, minimum residence time of 4 h). After dialysis, water was removed by rotary evaporation. ^{1}H NMR (300 MHz, D_2O, δ ppm): 4.10 (1.9H, CH_2CO_2), 3.68 (4.0H, $(CH_2)_2O$), 2.65-2.5 (6.2H, $(CH_2)_2NCH_2$); 2.0-0.75 (5.0H, CH_2CCH_3). GPC (1 mM LiBr + 0.1 M formic acid in water): M_w= 153 kDa, Mn=41 kDa, Đ=3.7.

Characterization: Synthesis was confirmed by ^{1}H NMR spectroscopy, using a Bruker Avance 300.13 MHz NMR spectrometer. Molecular weight of PMEMA was determined by gel permeation chromatograph (GPC) with 0.3 wt.% LiBr and 0.3 M formic acid in HPLC grade water as eluent at 40 °C at 1 mL/min. A Agilent triple detection GPC equipped PSS NOVEMA Max Lux analytical and PSS NOVEMA Max Lux columns. The light scattering detector was calibrated using poly(2-vinyl-pyridine) standards.

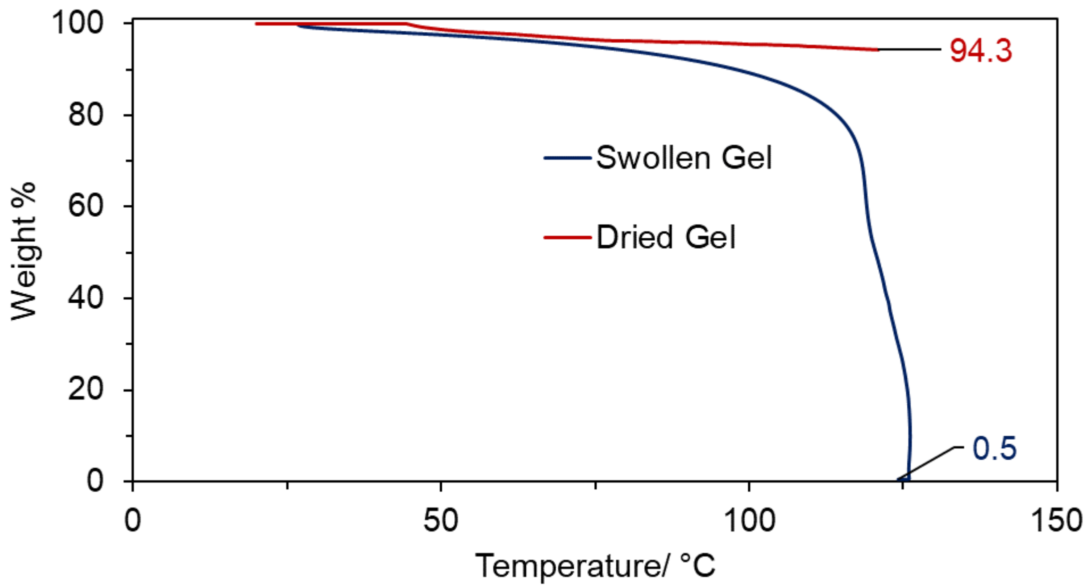

Figure C4. TGA thermogram of g-PDMAAm swollen in carbonated water at 20 °C, and g-PDMAAm deswollen under air at 60 °C.

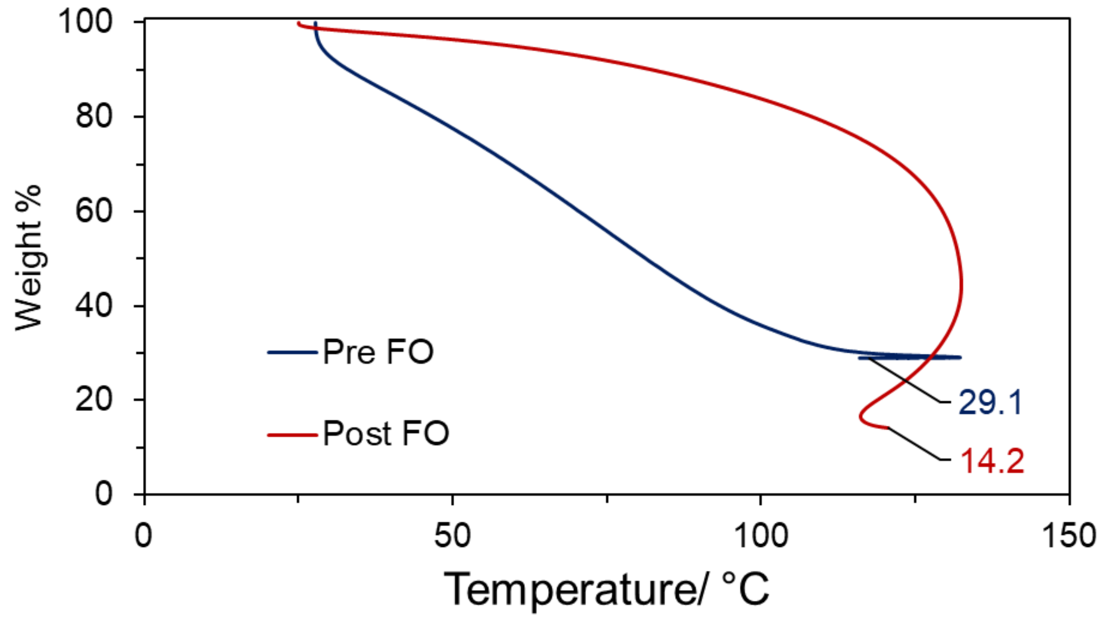

Figure C5. TGA thermogram of 30 wt.% g-PDMAAm before and after FO. The sample of g-PDMAAm after FO was taken from the membrane surface. Note that the wt.% of PDMAAm is slightly lower than 30 wt.% due to the addition of CO_2. The exact amount of CO_2 cannot be accurately determined by TGA as CO_2 desorbs from the gel during sample preparation.

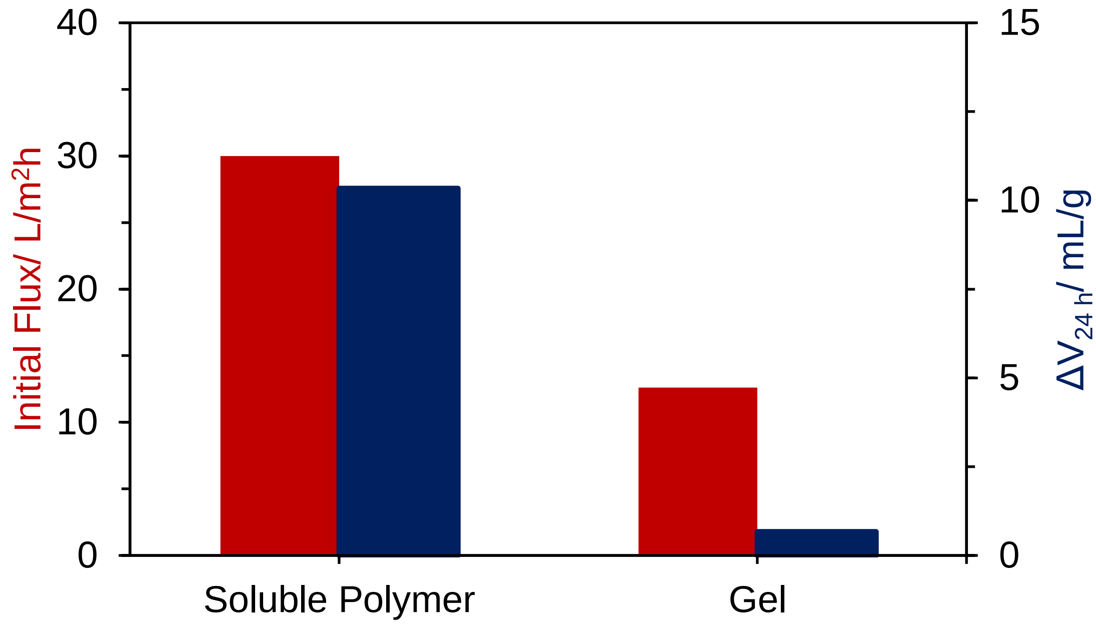

Figure C6. Comparison of the FO performance of soluble PDMAAm with g-PDMAAm (30 wt.%) vs 1.75 wt.% NaCl feed solution. $\Delta V_{24\ h}$ (blue bars) refers to the volume of water transferred from the feed to the draw in a 24 h period per gram of dry polymer.

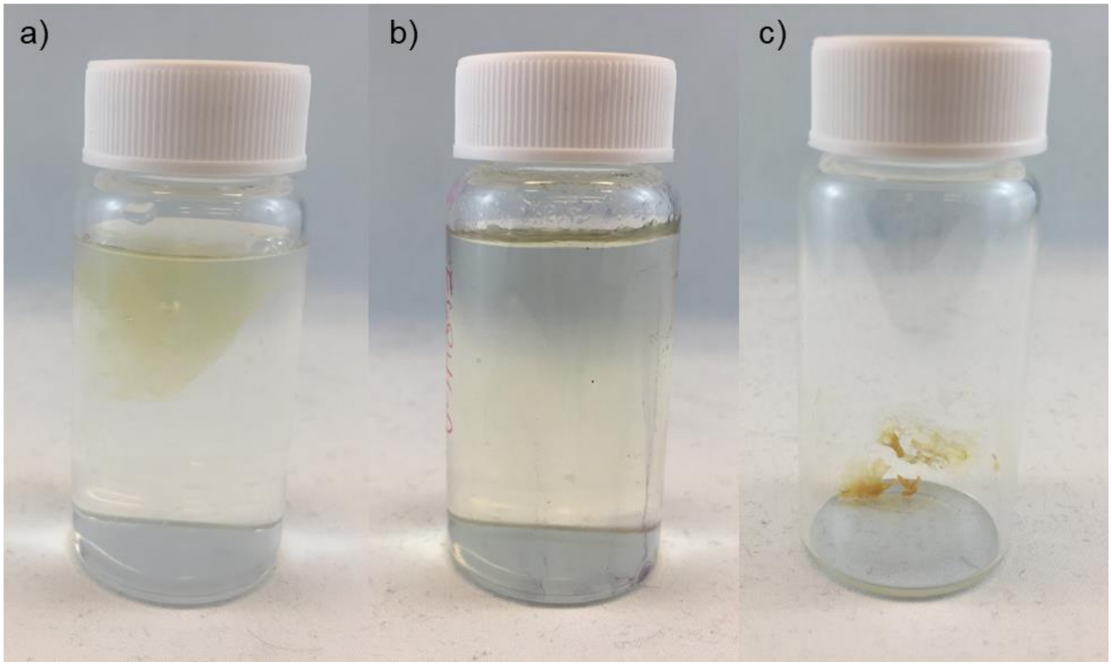

Figure C7. The swelling of g-PDMAAm under a) air at 20 °C, b) CO_2 at 20 °C, and c) air at 60 °C. g-PDMAAm is swollen by neutral water (a). When CO_2 is introduced the gel swells even more water, and fills the vial (a, note the yellow tinge). When the water is heated (60 °C) the gel shrinks and releases the water it has absorbed, which can be decanted (c).

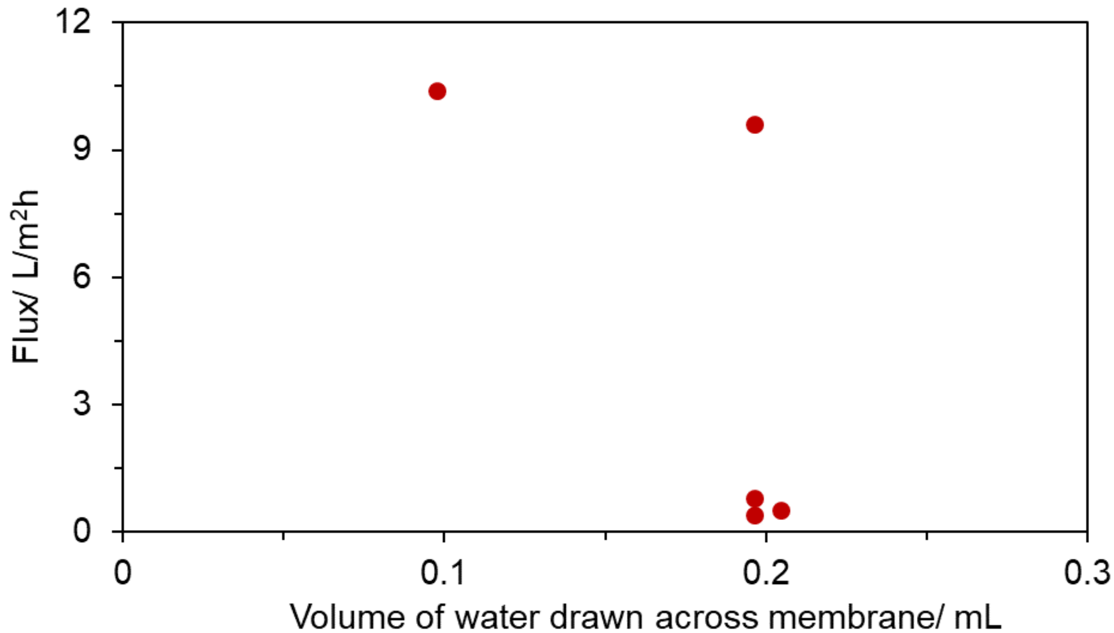

Figure C8. Flux as a function of volume water drawn across membrane (30 wt.% g-PDMAAm draw vs. 3.5 % NaCl feed).

Appendix D

Magnetic Particle Supplementary Information

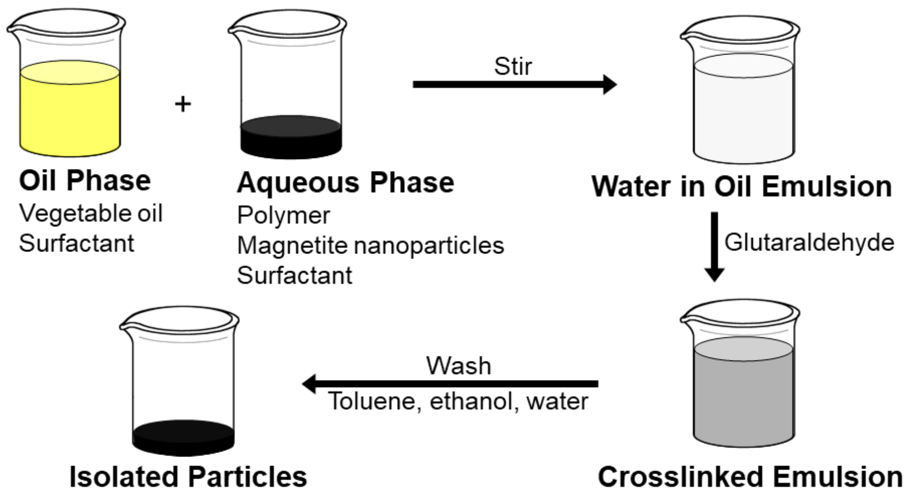

Figure D1. Simplified schematic of PDMAEMA-Fe_3O_4 microgel synthesis

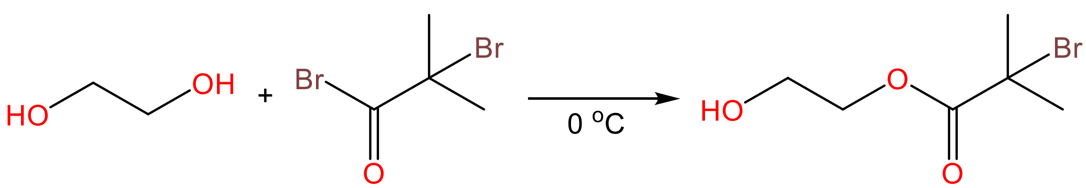

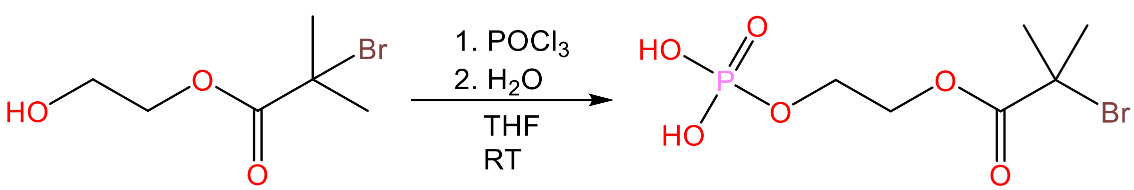

Figure D2. Synthetic pathway for ATRP initiator 2-(phosphonooxy)ethyl 2-bromo-2-methylpropanoate.

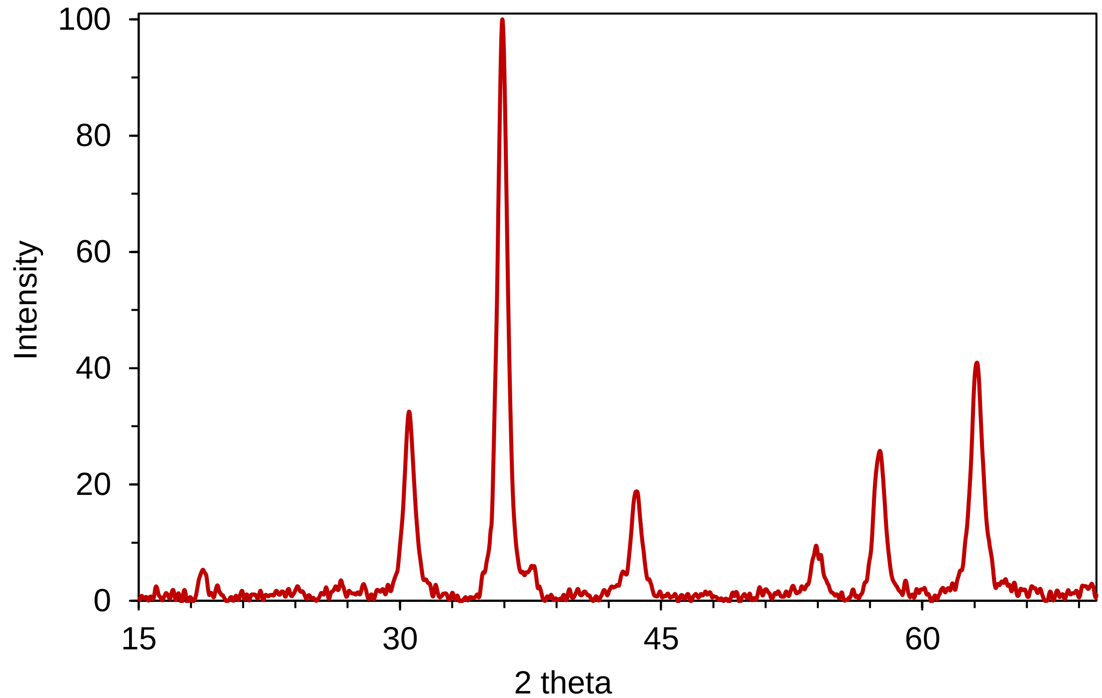

Figure D3. XRD spectrum of Fe_3O_4 nanoparticles.

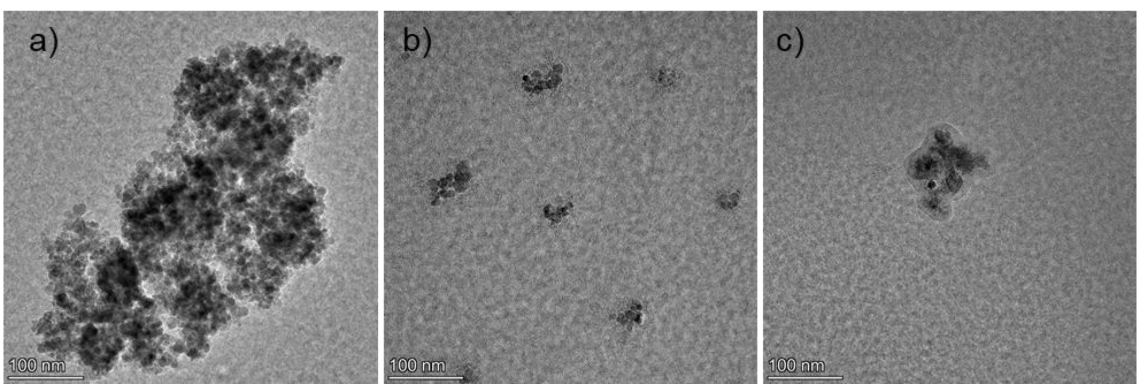

Figure D4. TEM images of a) magnetite nanoparticles, b) PDMAEMA-Fe_3O_4 nanoparticles, c) PDMAEMA·glycolic acid-Fe_3O_4 nanoparticles.

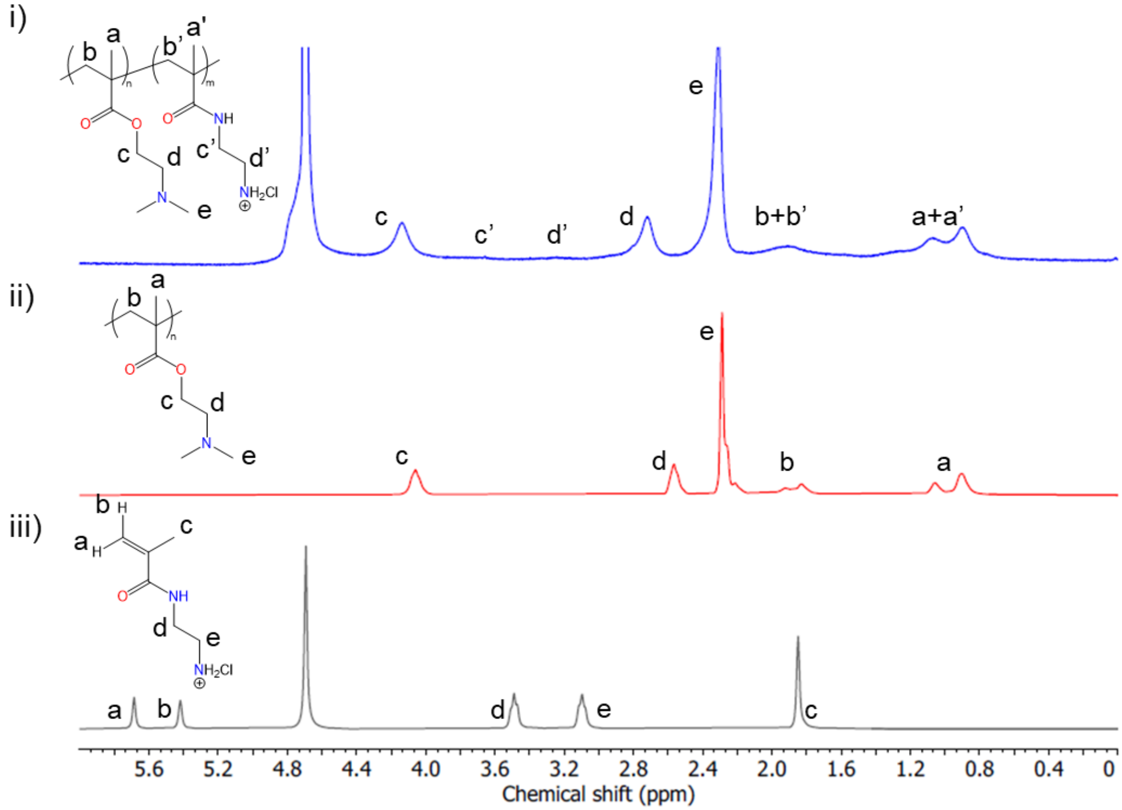

Figure D5. [1]H NMR spectra of i) P(DMAEMA-AEMA) (in D_2O), ii) PDMAEMA (in $CDCl_3$), and iii) AEMA·HCl (in D_2O).

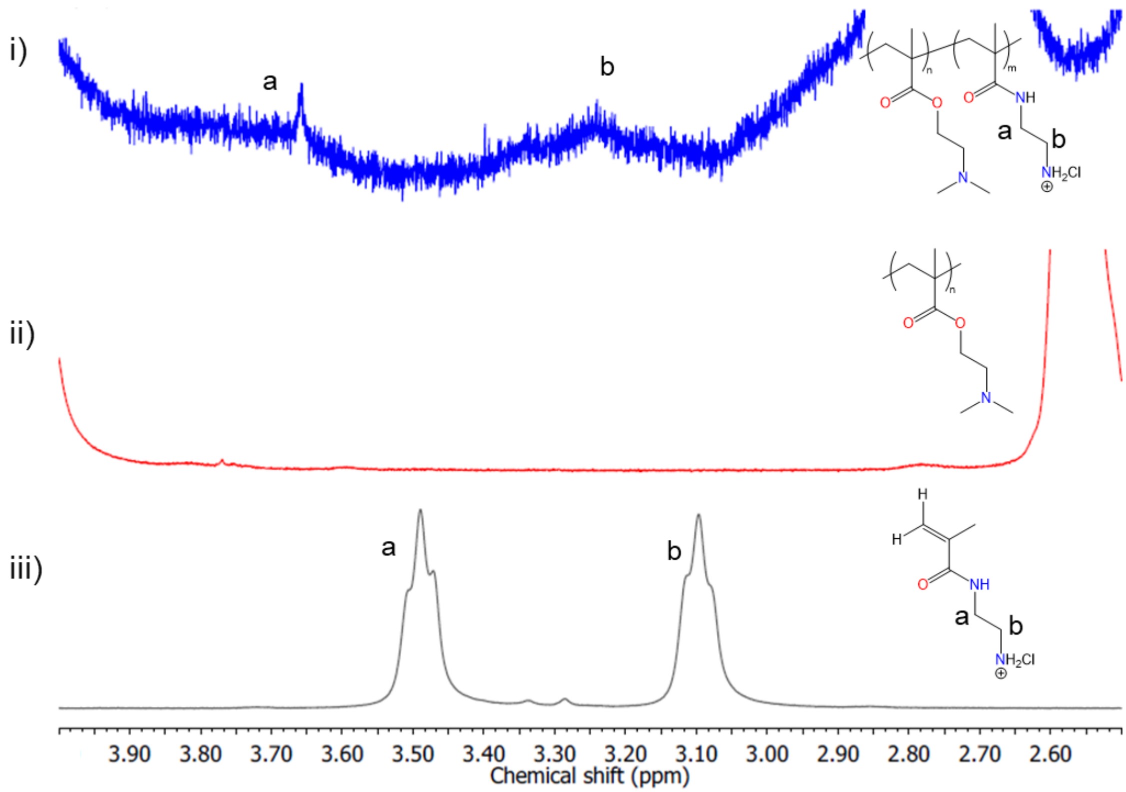

Figure D6. Expansion of the ^{1}H NMR spectra of i) P(DMAEMA-AEMA) (in D_2O), ii) PDMAEMA (in $CDCl_3$), and iii) AEMA·HCl (in D_2O), showing the presence of AEMA peaks in P(DMAEMA-AEMA).

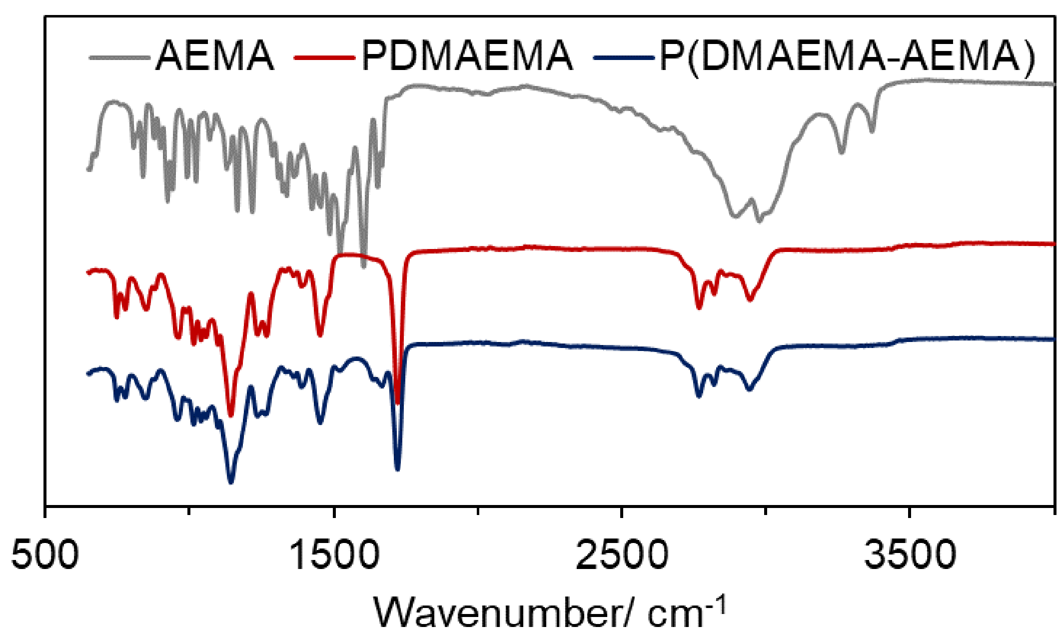

Figure D7. IR spectra of AEMA·HCl, PDMAEMA and P(DMAEMA-AEMA)

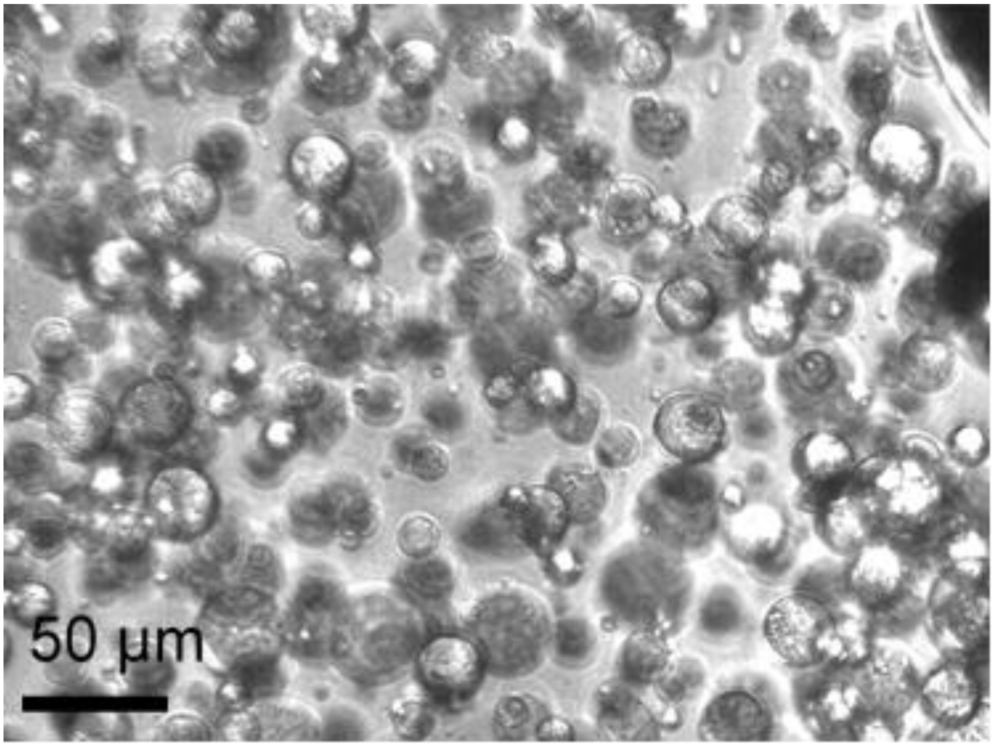

Figure D8. Optical microscope image of PDMAEMA/MNP water-in-oil emulsion prior to crosslinking.

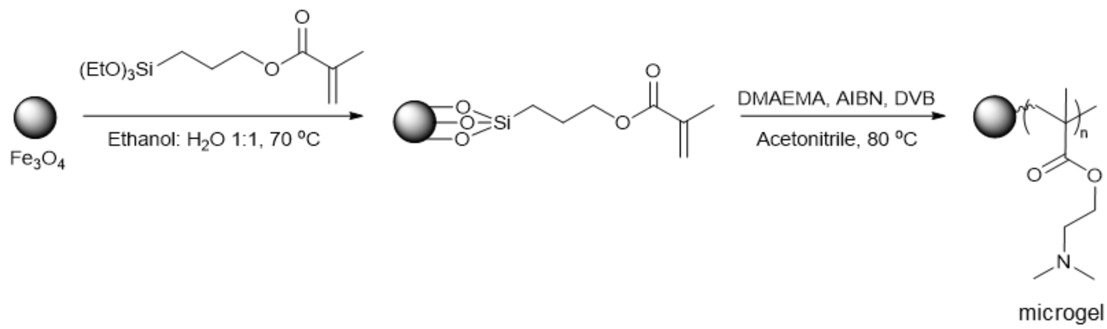

Figure D9. Alternative synthesis of PDMAEMA microgels with embedded MNP via surfactant free emulsion polymerization. (DVB= divinylbenzene crosslinker). (Che et al. 2015 Polym. Chem. DOI: 10.1039/c4py01800a.)

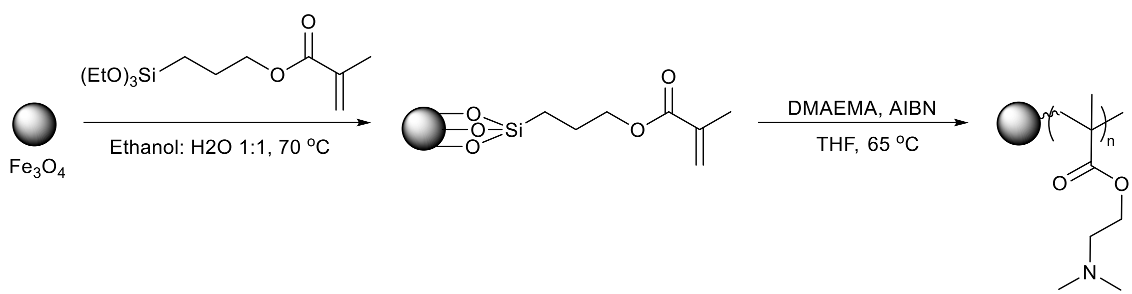

Figure D10. Alternative synthesis of PDMAEMA functionalized MNP via free radical polymerization.

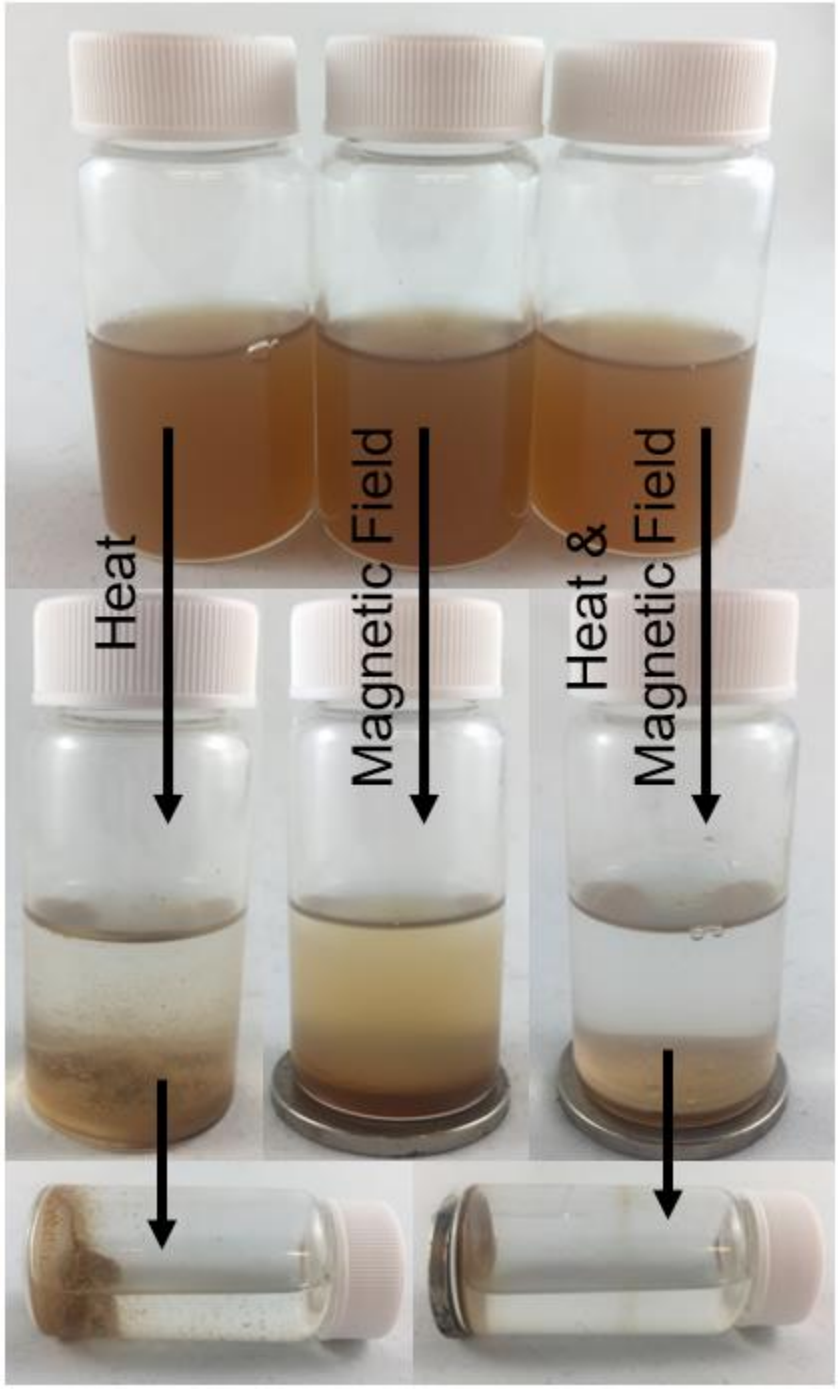

Figure D11. Images of CO_2-responsive-Fe_3O_4 microgels separated by application of heat (65 °C, time), magnetic field (time) and both heat and magnetic field. Note that the magnet used in these images had a low strength.

Appendix E

Alternative Applications of CO_2-Responsive Magnetic Microgels

Introduction

Incorporation of magnetic nanoparticles can facilitate the removal of CO_2-responsive materials. This can have advantages for many applications beyond forward osmosis draw agents. A potential alternative use includes reusable sorbents for toxic materials in water, such as heavy metals or parabens.

Amines' ability to bind to metals has led to their use as metal scavengers. The incorporation of CO_2-responsivity can provide an easy and benign pathway for their regeneration (Figure E1). Amines can readily draw metals out of contaminated water under air. The amines can then be removed and placed in a small volume of water. Upon bubbling of CO_2 the amine preferentially forms bicarbonate bonds over chelating to the metal, thereby releasing the metal into a more controlled and concentrated solution [29,262]. The amine can be decarbonated and then reused.

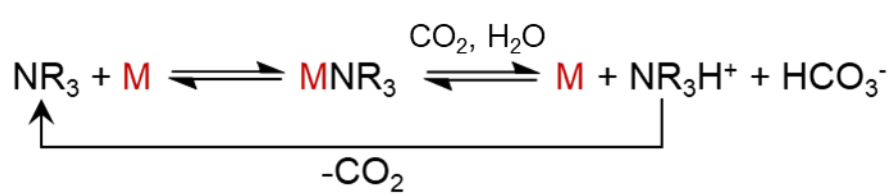

Figure E1. Reversible adsorption of metals (M) in water by a CO_2-responsive tertiary amine

Amines may also be used as reversible sorbents for specific weak acids (Figure E2). Amines can form salts with acidic contaminants in water. The acid loaded amine can then be removed and placed in small volume of water. If the acid is sufficiently weak (e.g., phenols), it can be protonated by CO_2 and returned to solution. The amine can be decarbonated as reused. Only acids with the appropriate pK_a could be used for this process. One such example is parabens, which are increasingly common in wastewater [266].

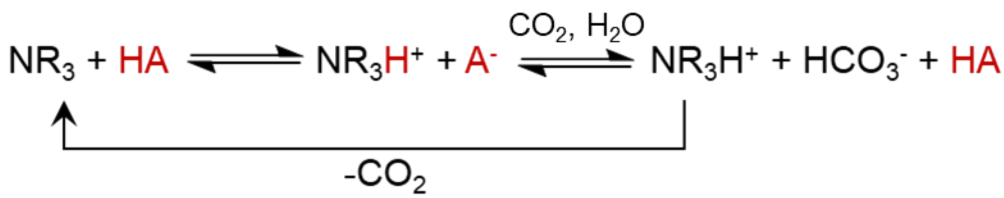

Figure E2. Reversible adsorption of weak acids (HA) in water by a CO_2-responsive tertiary amine.

A preliminary set of experiments were conducted to explore the performance of the CO_2-responsive magnetic particles synthesized in Chapter 4 as reversible sorbents for metals and parabens. The PDMAEMA-MNP microgels were selected over the PDMAEMA-functionalized magnetic nanoparticles, as they can be removed by magnetic separation under CO_2 as well as air.

Materials

Copper(II) nitrate trihydrate (≥99.0%), Pb(II) nitrate (≥99.0%), and methyl paraben (≥99.0%) were obtained from Sigma-Aldrich. PDMAEMA-Fe_3O_4 microgels were synthesized as described in section 4.2.4. Water (deionized) was obtained from a Synergy MilliQ system and had a resistivity of 18.2 MΩ/cm prior to exposure to air. Carbon dioxide (grade 3.0) was obtained from Praxair.

Methods

PDMAEMA magnetic particles (0.42 g of 8.3 wt.% slurry) were added to stock solution of copper, lead or methylparaben (1 mM, 20 mL) in 4 dram vials and shaken on a shaker plate for 2 h. The particles were isolated using a magnetic field. The supernatant was reserved for analysis. The particles were washed with water (3 x 10 mL), then redispersed in water (20 mL) and bubbled with CO_2 overnight. The particles were removed by magnetic separation followed by gravity filtration. The supernatant was reserved for analysis.

The concentration of metals in the water was determined by ICP-OES (Thermo Scientific, iCAP 7400), performed by Queen's Analytical Services Unit. The concentration of methylparaben was determined by UV-vis spectroscopy (Agilent 8453 spectrometer).

Results & Discussion

The amounts of methylparaben, Cu^{2+} and Pb^{2+} absorbed and released by the CO_2-responsive microgels are presented in Table E1. A ten-fold molar excess of amine to analyte was used. Despite this large excess, the microgels did not absorb large amounts of methylparaben but were able to reject nearly all they absorbed upon carbonation. Conversely, the microgels were able to absorb large amounts of the metals but were less efficient at releasing them upon exposure to CO_2.

The microgels were able to absorb ca. 25 mg of metal per gram of microgel, which is an order of magnitude lower than PDMAEMA-based alternatives reported in the literature [29,262]. Possible explanations for the poor performance include poor diffusion within the gels (especially when in the uncarbonated state) and pH. Previous reports conducted their experiments are pH 4.5-

6.0 (where PDMAEMA would be >95% protonated). As measuring the pH within a microgel is challenging, the pH was not altered in this work. This may be an area for future improvements.

Table E1. Reversible CO_2-triggerd absorption and release of analytes by CO_2-responsive magnetic microgel

Substrate	Absorbed		Released	
	Analyte Absorbed/%	Moles analyte/ moles nitrogen	Analyte Released/%	Moles analyte/ moles nitrogen
Methylparaben	16±5	0.016	85±15	0.014
Cu^{2+}	74±2	0.074	12±1	0.009
Pb^{2+}	75±1	0.075	2±1	0.001

Conclusions

Preliminary results demonstrate that the microgels have limited use for reversible absorption of analytes from water. However, further optimization may improve these results. The strong binding of metals demonstrated here may have other benefits as recyclable ligands in catalysis.